

Study of Film Formation in EHD Contacts Using a Novel Method Based on Electrical Capacitance

by

Marian Dumitru Furtuna

Submitted for the degree of Doctor of Philosophy

Department of Mechanical Engineering

Brunel University



**BRUNEL
UNIVERSITY
WEST LONDON**

2011

In memory of my grandfather

ABSTRACT

The elastohydrodynamic lubrication regime (EHD) is found in many machine elements, such as rolling element bearings, gears, cam/tappet, where a combination of hydrodynamic effect, elastic deformation of the surfaces and an increase of the lubricant's viscosity with pressure create a continuous lubricant film which is capable of supporting pressures of the order of tens of thousands of atmospheres. One of the most important features of these films is their thickness, as this determines whether the bounding surfaces are completely separated, thus avoiding premature wear and failure of the contact. Consequently for many years scientists were interested in finding methods for measuring the lubricant film thickness in elastohydrodynamic conditions.

One of the most versatile and widely used techniques for measuring lubricant film thickness in EHD contacts is the optical interferometry method. Apart from numerous advantages, this method has the limitation in the fact that one of the contacting surfaces must be transparent, usually glass or sapphire, thus it does not replicate real conditions found in machine elements contacts. On the other hand, the other group of methods used for studying the behaviour of elastohydrodynamic films includes a variety of electrical methods. Historically, these appeared before the optical methods, but gradually lost importance with the success of the later. Most capacitive, resistive, inductance methods developed so far use specially designed sensors for monitoring the lubricant film thickness. In the case of electrical techniques, both elements of the contact are metallic, which means that these can be used for measuring film thickness in real machine elements. One of the main disadvantages of electrical methods though, is the difficulty with which the calibration of various electrical quantities, against lubricant film thickness is obtained.

This thesis describes the work carried out by the author on the application of a capacitive method for studying lubrication of elastohydrodynamic contacts. The novelty of the method used consists in the calibration of the capacitance of the contact with optical interferometry. This project started from the premises that a thicker Chromium layer will supply the phase change needed to precisely measure the lubricant film thickness by eliminating the fragile silica layer, and it has been shown that an increase in Cr thickness results in a increase in reflection of the glass–Cr interface making the resulting images hard to process.

Modifications to the existing experimental rig were carried out in order to apply/collect an electrical signal from both the disc and the ball. Signal collection from the disc was quite straightforward and a graphite brush paired with a copper nut was used, as this is the oldest method of collecting/applying and electrical signal from a rotating element. Collecting an

electrical signal from the ball presented quite a challenge as the ball is submerged in oil. A number of brushes was designed, made and tested and the one that provided the most stable results chosen.

For calibration purposes a base oil and two additives were chosen, the additives were chosen in such a way that the improvement made to the lubrication process to be very different from one additive to the other. The chosen additives were a Viscosity Index Improver [VII] and an Organic Friction Modifier [OFM]. The VII is used by many researchers in order to obtain multigrade lubricants using the same base oil by varying its percentage in the mix. The OFM is used to provide protection between the two contacting bodies when EHD film fails and EHD lubrication is replaced by mixed lubrication by forming a boundary layer on the contacting surfaces.

Optical measurements were carried out on the base oil and the two resulting lubricants from the additive mixes using the Ultra Thin Film Interferometry [UTFI] method. The measurements were used as a benchmark against which the capacitive measurements were calibrated. Tests were conducted in a number of controlled conditions for speed, temperature, load and sliding conditions.

Results showed that the highest influence on the lubrication process was given by the speed, an increase in speed results in an increase in optically measured film thickness and a decrease in electrically measured film thickness. Phenomenon explained by a large amount of lubricant pushed into the contact. Another parameter that influenced the results quite significantly was temperature, a rise in temperature supplies a decrease in optically measured film thickness and an increase in capacitive measured film thickness which was explained by lubricant viscosity dropping with a rise in temperature.

Three different sliding conditions were employed and a small drop in optically measured film thickness followed by a small rise in electrically measured film thickness was recorded due to a local increase in contact temperature when sliding was employed.

The capacitive method developed in this project is precise enough to accurately measure lubricant film thickness down to 100nm; a model for thicknesses lower than 100nm was proposed.

Results from the optical and capacitive methods were compared and a good correlation was found, indicating that the developed capacitive method can be used as a tool for measuring metal on metal contacts without further calibration.

ACKNOWLEDGEMENTS

The author would like to thank the Engineering and Physical Sciences Research Council (EPSRC) for funding this project.

A special thanks goes to my supervisor Dr. Romeo P. Glovnea for his encouragement, guidance and support from the initial to the final level enabling me to develop and understand the subject.

I would like to show my gratitude to my good friend and distinguished colleague Dr. Colin Bell for his support and proofreading this thesis.

NOMENCLATURE

Roman letters:

<i>A</i>	cross sectional area of the capacitor plate [m ²];
<i>a, b</i>	radius of the contact area [m];
<i>C</i>	capacitance [pF];
<i>d</i>	distance between capacitor plates i.e. lubricant film thickness [m];
<i>E'</i>	reduced Young's modulus [Pa];
<i>h</i>	distance from the ball tip to the flat surface/film thickness [m];
<i>h_r</i>	central film thickness [m];
<i>h₀</i>	minimum film thickness [m];
<i>I</i>	light intensity;
<i>k</i>	the ellipticity parameter defined as: $k = a/b$, where <i>a</i> is the semiaxis of the contact ellipse in the transverse direction [m] and <i>b</i> is the semiaxis in the direction of motion [m];
	Ch 2.2.2
<i>k</i>	absorption index, where subscript refers to each layer starting from top;
<i>n</i>	refractive index, where subscript refers to each layer starting from top;
<i>n</i>	fringe number;
	Ch. 2.3.2
<i>N</i>	fringe order;
<i>p</i>	contact pressure (Hertzian pressure) [Pa];
<i>q</i>	fluid flow where the subscripts <i>x</i> , <i>y</i> and <i>z</i> refer to the corresponding axis;
<i>q</i>	pressure distribution;
	Ch. 2.2
<i>r</i>	fringe radius;
<i>R'</i>	reduced radius of curvature [m];
<i>R</i>	ball radius [m];
<i>s₁</i> = $4\pi h_1/\lambda$;	
<i>s₂</i> = $4\pi h_2/\lambda$;	
<i>S₀</i>	Roelands viscosity–temperature index;
<i>t</i>	temperature [°C];
<i>t</i>	time [s];
	Ch. 2.3
<i>U</i>	entraining surface velocity [m/s], i.e., $U = (U_A + U_B)/2$, where the subscripts <i>A</i> and <i>B</i> refer to the velocities of bodies <i>A</i> and <i>B</i> , respectively;
<i>V</i>	main entrainment velocity [m/s];
<i>W</i>	normal load [N];
<i>w</i>	surface deflection [m];
<i>w, u, v</i>	surface velocities on x, y and z axis [m/s];
	Ch. 2.1.1
<i>x</i>	silica thickness;
	Ch. 2.3.2

$x, y, z,$	axis coordinates;
Z_0	Roelands viscosity-pressure index;
z	depth under the surface where the maximum shear stress acts [m];

Greek letters:

α	the pressure-viscosity coefficient [m^2/N];
δ	total deflection at the centre of the contact (i.e., $\delta = \delta_A + \delta_B$; where δ_A and δ_B maximum deflections of body A and B [m]);
δ	phase difference; Ch. 2.3.1
Δ	path difference;
ε_0	absolute permittivity [$8.854 \cdot 10^{-12} \text{ pF}\cdot\text{m}^{-1}$];
ε_r	relative permittivity;
η_0	the viscosity at atmospheric pressure of the lubricant [$\text{Pa}\cdot\text{s}$];
η	dynamic viscosity [$\text{Pa}\cdot\text{s}$];
θ	scanning angle; Ch. 4.4
θ	angle of incidence;
λ	light wave length [nm];
μ	friction coefficient;
ρ	density;
σ	Poisson's ratio;
τ	shear stress [Pa];
ω	angular frequency [Hz];
*	nondimensional quantity.

FIGURES TABLE

Figure 1: Two generalised surfaces in contact.....	23
Figure 2: Equilibrium of an element [3]	24
Figure 3: Three components of the fluid velocity profile	26
Figure 4: Flow into column of fluid.....	27
Figure 5: Schematic diagram of changes in friction at the limits of hydrodynamic lubrication [3].....	30
Figure 6: Shear stress – Shear rate characteristic of a Newtonian fluid.....	31
Figure 7: Geometry of two contacting spheres [5].....	32
Figure 8: The geometry of the EHD contact inlet according to Grubin and Vinogradova	36
Figure 9: Grubin's model of an elastohydrodynamic contact.....	36
Figure 10: Geometry of the contact between two spheres.....	39
Figure 11: Contact between a sphere and a flat surface.....	41
Figure 12: Lubrication of two rigid rollers [12].....	43
Figure 13: Hydrodynamic pressure distribution in an elastohydrodynamic contact.....	44
Figure 14: A transversal sine wave expressed by Equation 86, at t = 0.....	46
Figure 15: Interference by amplitude division. Calculation of path difference	47
Figure 16: Principle of optical interferometry	49
Figure 17: Schematic representation of the ball on glass plate [18]	51
Figure 18: Ultra thin film interferometry technique	53
Figure 19: Light passing through a glass disc with a Chromium coating [27]	55
Figure 20: Schematic representation of the experimental setup [27].....	56
Figure 21: Multi-beam optical EHL interferometry [29]	57
Figure 22: Crook's disc machine [47].....	62
Figure 23: Calibration curves for film thickness versus capacitance [48]	63
Figure 24: Electrical resistance measurement setup and pattern of the recorded signal [49] ...	64
Figure 25: Film thickness in a cam/follower contact [54]	65
Figure 26: Arrangement of capacitive sensors for measurement of ring oil film thickness [56]	66
Figure 27: Experimental setup film thickness measurements between a piston and a cylinder [59].....	67
Figure 28: Lubrication control system for large two stroke marine diesel engine [61]	68
Figure 29: Wien's bridge used by Zheng to measure EHL oil thickness [65]	69
Figure 30: Zheng et al. experimental setup [65]	69
Figure 31: Steel–oil–mercury system [66].....	70
Figure 32: Diagram of the Capacitance Bridge and associated equipment [67].....	70
Figure 33: Schematic of Tallian's conductivity test circuit [71].....	71

Figure 34: Schematic of the electric circuit [74].....	72
Figure 35: Electrical circuit for measuring the degree of separation between specimens [80]	73
Figure 36: Schematic representation of an ultrasonic beam incident on a lubricated contact [85]	76
Figure 37: Experimental setup for ultrasonic lubricant measurements [88]	77
Figure 38: Schematic diagram of a profilometer scan of a calibration slide [90]	78
Figure 39: Calibration sample with a maximum wax thickness of 255 nm [90]	78
Figure 40: Experimental set-up	81
Figure 41: Smooth surfaces film thickness	82
Figure 42: Film thickness for glass disc, 20N load	83
Figure 43: Film thickness for sapphire disc, 30N load	83
Figure 44: Experimental setup	86
Figure 45: Schematic representation of the infrared spectrometer	86
Figure 46: Green light image of the contact before the tests using Di–urea grease.....	87
Figure 47: Fluorescence image of the contact before the tests using Di–urea grease.....	88
Figure 48: Di–urea grease pure state ne minute into the experiment.....	88
Figure 49: Di–urea grease pure state ten minutes into the experiment	88
Figure 50: Di–urea grease pure state twenty minutes into the experiment	88
Figure 51: Di–urea grease pure state forty minutes into the experiment	88
Figure 52: LiSt grease PAO 400 green light image taken before the tests.....	89
Figure 53: LiSt grease PAO 400 fluorescence image taken before the tests	89
Figure 54: LiSt grease PAO 400 first minute in the experiment.....	89
Figure 55: LiSt grease PAO 400 ten minutes in the experiment.....	89
Figure 56: LiSt grease PAO 400 twenty minutes in the experiment.....	90
Figure 57: LiSt grease PAO 400 forty minutes in the experiment.....	90
Figure 58: LiSt grease PAO 30 green light image taken before the tests.....	90
Figure 59: LiSt grease PAO 30 fluorescence image taken before the tests.....	90
Figure 60: LiSt grease PAO 30 first minute in the experiment.....	91
Figure 61: LiSt grease PAO 30 ten minutes in the experiment.....	91
Figure 62: LiSt grease PAO 30 twenty minutes in the experiment.....	91
Figure 63: LiSt grease PAO 30 forty minutes in the experiment.....	91
Figure 64: LiSt grease PAO 30 green light image of the disc track after the tests were finished.....	91
Figure 65: LiSt grease PAO 30 fluorescence light image of the disc track after the tests were finished.....	91
Figure 66: LiSt grease PAO 30 green light image of the ball track after the tests were finished.....	92

Figure 67: LiSt grease PAO 30 fluorescence light image of the ball track after the tests were finished.....	92
Figure 68: LiSt grease PAO 30 green light image of the disc track after the tests were finished.....	92
Figure 69: LiSt grease PAO 400 green light image of the disc track after the tests were finished.....	92
Figure 70: LiSt grease PAO 30 fluorescence image of the disc track after the tests were finished.....	93
Figure 71: LiSt grease PAO 400 fluorescence image of the disc track after the tests were finished.....	93
Figure 72: Di–urea grease PAO 30 green light image taken before the tests.....	93
Figure 73: Di–urea grease PAO 30 fluorescence image taken before the tests.....	93
Figure 74: Di–urea grease PAO 30 one minute into the experiment.....	94
Figure 75: Di–urea grease PAO 30 thirty minutes into the experiment.....	94
Figure 76: Di–urea grease PAO 30 Fifty minutes into the experiment.....	94
Figure 77: Di–urea grease PAO 30 Ninety minutes into the experiment.....	94
Figure 78: Di–urea grease PAO 30 Green light image of the disc track after the tests were finished.....	95
Figure 79: Di–urea grease PAO 30 Fluorescence image of the disc track after the tests were finished.....	95
Figure 80: Di–urea grease PAO 30 Green light image of the ball track after the tests were finished.....	95
Figure 81: Di–urea grease PAO 30 Fluorescence image of the ball track after the tests were finished.....	95
Figure 82: FTIR analysis of the sapphire disc track for the Di–urea grease.....	96
Figure 83: FTIR analysis of the sapphire disc track for the LiSt grease	96
Figure 84: Experimental set–up for static permittivity measurement.....	98
Figure 85: Experimental setup for EHD measurements	100
Figure 86: Film thickness measurements.....	100
Figure 87: Contact capacitance function of speed	101
Figure 88: Contact capacitance function of pressure	102
Figure 89: Lubricant permittivity function of pressure.....	102
Figure 90: Experimental setup for the classical Ultra Thin Film Interferometry method.....	104
Figure 91: Experimental setup for the modified Ultra Thin Film Interferometry method.....	105
Figure 92: Schematic representation of the PCS EHL test rig.....	107
Figure 93: Interferogram for Cr sputtered [10nm] and silica disc with a 20N load.....	108
Figure 94: Interferogram for Cr only disc with a thickness of ~25 nm with a 20N load.....	109
Figure 95: Interferogram for Cr only disc with a thickness of ~ 50 nm with a 20N load.....	109

Figure 96: 0. 02 m/s.....	110
Figure 97: 0. 075 m/s.....	110
Figure 98: 0. 126 m/s.....	110
Figure 99: 0. 36 m/s.....	110
Figure 100: 0. 606 m/s.....	110
Figure 101: 1. 03 m/s.....	110
Figure 102: Intensity curve values for images obtained using a 25 nm thick Cr sputtered disc	111
Figure 103: Intensity curve values for images obtained using a 25nm thick Chromium sputtered disc with the spectrometer grating stationary for all speeds.....	111
Figure 104: Interferogram for Cr only disc with a thickness of ~15nm with a 20N load.....	112
Figure 105: Computed intensity of the ray reflected by the chromium layer	113
Figure 106: Sphere on infinite flat surface [98].....	114
Figure 107: Experimental test rig for static capacitance measurements	115
Figure 108: Capacitance values compared with the theoretical values obtained using Hudlet's formula.....	116
Figure 109: Capacitance variation at a constant frequency of 10kHz.....	116
Figure 110: Experimental setup for capacitance measurement.....	117
Figure 111: Electronic schematics for the electronics box	118
Figure 112: Capacitance variation at constant frequency	119
Figure 113: Background capacitance measurements in different rolling conditions	120
Figure 114: Background capacitance variation with temperature.....	121
Figure 115: Capacitance measurements for PAO 40 at different temperatures using a Cr sputtered disc	122
Figure 116: Film thickness measurements using the capacitive method	123
Figure 117: Film thickness measurements for PAO 40 at 40°C using a Chromium sputtered disc	123
Figure 118: Film thickness measurements for PAO 40 at 60°C using a Chromium sputtered disc	124
Figure 119: Film thickness measurements for PAO 40 at 80°C using a Chromium sputtered disc	124
Figure 120: Film thickness measurements for PAO 40 at 100°C using a Chromium sputtered disc	124
Figure 121: Lubricant viscosities at different temperatures.....	125
Figure 122: Film thickness measurements for a PAO 40 lubricant at different temperatures in pure rolling conditions	126
Figure 123: Film thickness measurements for a PAO 40 lubricant at different temperatures in a 20% slide/roll condition.....	126

Figure 124: Film thickness measurements for a PAO 40 lubricant at different temperatures in a 60% slide/roll condition	127
Figure 125: Film thickness comparison for a PAO 40 at 40°C in different slide/roll conditions	127
Figure 126: Film thickness comparison for a PAO 40 at 60°C in different slide/roll conditions	128
Figure 127: Film thickness comparison for a PAO 40 at 80°C in different slide/roll conditions	128
Figure 128: Film thickness comparison for a PAO 40 at 100°C in different slide/roll conditions	128
Figure 129: Film thickness measurements for a PAO 40 lubricant with a 1% organic friction modifier [OFM] present in the mixture at different temperatures in pure rolling conditions .	130
Figure 130: Film thickness measurements for a PAO 40 lubricant with a 1% OFM present in the mixture at different temperatures in 20 % slide/roll condition	130
Figure 131: Film thickness measurements for a PAO 40 lubricant with a 1% OFM present in the mixture at different temperatures in 60 % slide/roll condition	131
Figure 132: Comparison of film thickness measurements for a PAO 40 lubricant with a 1% OFM present in the mixture at 40°C in different slide/roll conditions.....	131
Figure 133: Comparison of film thickness measurements for a PAO 40 lubricant with a 1% OFM present in the mixture at 60°C in different slide/roll conditions.....	132
Figure 134: Comparison of film thickness measurements for a PAO 40 lubricant with a 1% OFM present in the mixture at 80°C in different slide/roll conditions.....	132
Figure 135: Comparison of film thickness measurements for a PAO 40 lubricant with a 1% OFM present in the mixture at 100°C in different slide/roll conditions.....	132
Figure 136: Film thickness measurements for a PAO 40 lubricant with a 10 % viscosity index improver [VII] present in the mixture at different temperatures in pure rolling conditions ...	133
Figure 137: Film thickness measurements for a PAO 40 lubricant with a 10 % [VII] present in the mixture at different temperatures in 20 % slide/roll condition	134
Figure 138: Film thickness measurements for a PAO 40 lubricant with a 10 % [VII] present in the mixture at different temperatures in 60 % slide/roll condition	134
Figure 139: Comparison of film thickness measurements for a PAO 40 lubricant with a 10% VII present in the mixture at 40°C in different slide/roll conditions.....	135
Figure 140: Comparison of film thickness measurements for a PAO 40 lubricant with a 10% VII present in the mixture at 60°C in different slide/roll conditions.....	135
Figure 141: Comparison of film thickness measurements for a PAO 40 lubricant with a 10% VII present in the mixture at 80°C in different slide/roll conditions.....	135
Figure 142: Comparison of film thickness measurements for a PAO 40 lubricant with a 10% VII present in the mixture at 100°C in different slide/roll conditions.....	136

Figure 143: Film thickness comparison for a PAO 40 lubricant with different additives in the mixture at 40°C in pure rolling conditions.....	137
Figure 144: Film thickness comparison for a PAO 40 lubricant with different additives in the mixture at 60°C in pure rolling conditions.....	138
Figure 145: Film thickness comparison for a PAO 40 lubricant with different additives in the mixture at 80°C in pure rolling conditions.....	138
Figure 146: Film thickness comparison for a PAO 40 lubricant with different additives in the mixture at 100°C in pure rolling conditions.....	138
Figure 147: Contacting capacitor plates.....	139
Figure 148: Capacity measured values compared with the calculated values at 80°C.....	139
Figure 149: Capacitance measured values compared with the calculated ones for a range of temperatures.....	140
Figure 150: Capacitance variation at different speeds	141
Figure 151: Capacitance measurements for the base oil in pure rolling conditions.....	142
Figure 152: Capacitance measurements for the base oil when 20% sliding is present.....	142
Figure 153: Capacitance measurements for the base oil when 60% sliding is present.....	143
Figure 154: Film thickness measurements comparison between the optical and electrical method at a temperature of 40°C.....	143
Figure 155: Film thickness measurements comparison between the optical and electrical method at a temperature of 60°C.....	144
Figure 156: Film thickness measurements comparison between the optical and electrical method at a temperature of 80°C.....	144
Figure 157: Film thickness measurements comparison between the optical and electrical method at a temperature of 100°C.....	144
Figure 158: Film thickness comparison with capacitance measurements for the base oil at 40°C	145
Figure 159: Film thickness comparison with capacitance measurements for the base oil at 60°C	145
Figure 160: Film thickness comparison with capacitance measurements for the base oil at 80°C	146
Figure 161: Film thickness comparison with capacitance measurements for the base oil at 100°C.....	146
Figure 162: Capacitive measurements comparison in different sliding conditions at 40°C ...	147
Figure 163: Capacitive measurements comparison in different sliding conditions at 60°C ...	147
Figure 164: Capacitive measurements comparison in different sliding conditions at 80°C ...	147
Figure 165: Capacitive measurements comparison in different sliding conditions at 100°C .	148
Figure 166: Capacitance measurements for the base oil mixed with 1% OFM in pure rolling conditions.....	149

Figure 167: Capacitance measurements for the base oil mixed with 1% OFM in a 20% sliding condition	149
Figure 168: Capacitance measurements for the base oil mixed with 1% OFM in a 60% sliding condition	150
Figure 169: Film thickness measurements comparison between the optical and electrical method at a temperature of 40°C for a base oil mixed with 1% OFM.....	150
Figure 170: Film thickness measurements comparison between the optical and electrical method at a temperature of 60°C for a base oil mixed with 1% OFM.....	151
Figure 171: Film thickness measurements comparison between the optical and electrical method at a temperature of 80°C for a base oil mixed with 1% OFM.....	151
Figure 172: Film thickness measurements comparison between the optical and electrical method at a temperature of 100°C for a base oil mixed with 1% OFM.....	151
Figure 173: Capacitance values compared with film thickness for the base oil mixed with 1% OFM at a temperature of 40°C.....	152
Figure 174: Capacitance values compared with film thickness for the base oil mixed with 1% OFM at a temperature of 60°C.....	152
Figure 175: Capacitance values compared with film thickness for the base oil mixed with 1% OFM at a temperature of 80°C.....	153
Figure 176: Capacitance values compared with film thickness for the base oil mixed with 1% OFM at a temperature of 100°C	153
Figure 177: Capacitive measurements comparison in different sliding conditions at 40°C ...	154
Figure 178: Capacitive measurements comparison in different sliding conditions at 60°C ...	154
Figure 179: Capacitive measurements comparison in different sliding conditions at 80°C ...	154
Figure 180: Capacitive measurements comparison in different sliding conditions at 100°C .	155
Figure 181: Capacitance measurements for the base oil mixed with 10% VII in pure rolling conditions.....	156
Figure 182: Capacitance measurements for the base oil mixed with 10% VII when 20% sliding is present	156
Figure 183: Capacitance measurements for the base oil mixed with 10% VII when 20% sliding is present	157
Figure 184: Film thickness measurements comparison between the optical and electrical method at a temperature of 40°C for a base oil mixed with 10% VII.....	157
Figure 185: Film thickness measurements comparison between the optical and electrical method at a temperature of 60°C for a base oil mixed with 10% VII.....	158
Figure 186: Film thickness measurements comparison between the optical and electrical method at a temperature of 80°C for a base oil mixed with 10% VII.....	158
Figure 187: Film thickness measurements comparison between the optical and electrical method at a temperature of 100°C for a base oil mixed with 10% VII	158

Figure 188: Capacitance values compared with film thickness for the base oil mixed with 10% VII at 40°C	159
Figure 189: Capacitance values compared with film thickness for the base oil mixed with 10% VII at 60°C	159
Figure 190: Capacitance values compared with film thickness for the base oil mixed with 10% VII at 80°C	160
Figure 191: Capacitance values compared with film thickness for the base oil mixed with 10% VII at 100°C	160
Figure 192: Capacitive measurements comparison in different sliding conditions at 40°C ...	161
Figure 193: Capacitive measurements comparison in different sliding conditions at 60°C ...	161
Figure 194: Capacitive measurements comparison in different sliding conditions at 80°C ...	161
Figure 195: Capacitive measurements comparison in different sliding conditions at 100°C .	162
Figure 196: Capacitance measurements comparison for different lubricant mixtures at 40°C pure rolling.....	163
Figure 197: Capacitance measurements comparison for different lubricant mixtures at 60°C pure rolling.....	164
Figure 198: Capacitance measurements comparison for different lubricant mixtures at 80°C pure rolling.....	164
Figure 199: Capacitance measurements comparison for different lubricant mixtures at 100°C pure rolling.....	164
Figure 200: Capacitance measurements comparison for different lubricant mixtures at 40°C 20% sliding	165
Figure 201: Capacitance measurements comparison for different lubricant mixtures at 60°C 20% sliding	165
Figure 202: Capacitance measurements comparison for different lubricant mixtures at 80°C 20% sliding	166
Figure 203: Capacitance measurements comparison for different lubricant mixtures at 100°C 20% sliding	166
Figure 204: Capacitance measurements comparison for different lubricant mixtures at 40°C at 60% sliding	167
Figure 205: Capacitance measurements comparison for different lubricant mixtures at 60°C at 60% sliding	167
Figure 206: Capacitance measurements comparison for different lubricant mixtures at 80°C at 60% sliding	167
Figure 207: Capacitance measurements comparison for different lubricant mixtures at 100°C 60% sliding	168
Figure 208: Film thickness measurements comparison between Cr and Steel at 40°C for PAO 40	170

Figure 209: Film thickness measurements comparison between Cr and Steel at 60°C for PAO 40	170
Figure 210: Film thickness measurements comparison between Cr and Steel at 80°C for PAO 40	170
Figure 211: Film thickness measurements comparison between Cr and Steel at 100°C for PAO 40	171
Figure 212: Film thickness measurements comparison between Cr and Steel at 40°C 1% OFM mix	171
Figure 213: Film thickness measurements comparison between Cr and Steel at 60°C 1% OFM mix	172
Figure 214: Film thickness measurements comparison between Cr and Steel at 80°C 1% OFM mix	172
Figure 215: Film thickness measurements comparison between Cr and Steel at 100°C 1% OFM mix	172
Figure 216: Film thickness measurements comparison between Cr and Steel at 40°C 10% VII mix	173
Figure 217: Film thickness measurements comparison between Cr and Steel at 60°C 10% VII mix	173
Figure 218: Film thickness measurements comparison between Cr and Steel at 80°C 10% VII mix	174
Figure 219: Film thickness measurements comparison between Cr and Steel at 100°C 10% VII mix	174
Figure 220: Ball with artificial roughness features passing through a lubricated contact	179
Figure 221: Schematic representation of the specially designed glass disc	180

CONTENTS

Abstract.....	3
Acknowledgements.....	5
Nomenclature	6
Figures Table	8
Contents	17
1 Introduction.....	20
1.1 Preliminary	20
1.2 Background.....	20
1.3 Objectives and Scopes of Research	21
1.4 Thesis Outline.....	22
2 Basic Principles Of Lubrication.....	23
2.1 Hydrodynamic Lubrication.....	23
2.1.1 Reynolds equation.....	23
2.1.2 Solution to Reynolds equation	29
2.1.3 Limits of Hydrodynamic Lubrication	30
2.2 Elastohydrodynamic Lubrication	32
2.2.1 Geometry of EHD films	39
2.2.2 Film thickness equations	44
3 Literature Review On Experimental Techniques In Ehd Lubrication.....	46
3.1 Optical Techniques for Measuring Lubricant Film Thickness	46
3.1.1 Interference of light.....	46
3.1.2 EHD film thickness measurement by optical interferometry:.....	49
3.1.3 Variations of the classical optical interferometry method.....	52
3.1.4 Applications of optical interferometry to mixed lubrication.....	57
3.2 Electrical Methods for Evaluating Lubrication in EHD Contacts	61
3.2.1 Background	61
3.2.2 Measurement of lubricant film thickness	61
3.2.3 Detection of asperity contact in mixed regime.....	71
3.2.4 The effect of an electric field upon lubrication phenomena.....	73
3.3 Other Methods for Measuring Lubricant Film Thickness	75
3.3.1 Ultrasound	75
3.3.2 Laser induced fluorescence	77
4 Experimental Methods Explored By The Author	80
4.1 Optical Interferometry ^[92]	80
4.1.1 Introduction:	80
4.1.2 Experimental Set Up and Procedure:	80

4.1.3	Results and Discussion:.....	82
4.1.4	Conclusions:	83
4.2	Experiments on Grease Lubrication by Fluorescence	84
4.2.1	Introduction:.....	84
4.2.2	Experimental Set Up and Procedure:	84
4.2.3	Results and discussion.....	87
4.2.4	Conclusions	97
4.3	Electrical method ^[96]	98
4.3.1	Introduction:.....	98
4.3.2	Experimental Details:.....	98
4.3.3	Results and Discussion:.....	101
4.3.4	Conclusions:	103
5	Experiment.....	104
5.1	Rationale of the Experimental Work	104
5.2	The EHD Film Thickness Test Rig	107
5.3	Modifications to the Ultra Thin Film Interferometry [UTFI] Method	108
5.4	Static Measurement of the Capacitance between a Sphere and a Flat.....	114
5.5	Capacitive Dynamic Measurements of EHD Point Contacts	117
5.5.1	Modifications to the EHD Test Rig.....	117
5.5.2	Calibration of the Capacitance of EHD Contacts.....	122
6	Results And Discussion	125
6.1	Film Thickness Measurement by the Optical Method.....	125
6.1.1	Base Oil	126
6.1.2	Film Thickness of Organic Friction Modifier Solution.....	130
6.1.3	Film Thickness of Viscosity Index Improver Solution	133
6.1.4	Thickness Measurements Comparison Film Using Different Lubricant Solutions.....	137
6.2	Limitations of the Capacitive Method	139
6.3	Capacitance Measurements Results for EHD Point Contacts	142
6.3.1	Base Oil.....	142
6.3.2	Organic Friction Modifier Solution.....	149
6.3.3	Viscosity Index Improver Solution	156
6.4	Capacitance Measurements Comparison for Base Oil and Different Oil Mixtures	163
6.5	Comparison between Chromium-coated glass and Steel discs Capacitive Measurements	169
7	Conclusions.....	175
	Recommendations For Future Work.....	179
	Appendix.....	181

List Of Published Papers.....	181
Modification To The Existing Experimental Rig	182
Bibliography	196

1 INTRODUCTION

1.1 Preliminary

Tribology deals with friction, wear and lubrication. Those phenomena occur in the contact of many machine components. The performance of the components involves many variables such as tribological conditions, materials and surface conditions, and environment. Many efforts have been made in order to understand the influence of these variables and interaction between them. The aim of tribology research is to understand the friction and wear processes and their mechanisms. It is also aiming to improve the life span of such components and to fulfil the need of working under conditions of harsh environments such as higher load, speed and temperature. Previous attempts produced a considerable knowledge about failure modes and mechanisms. It is generally well known that wear of materials is a complicated phenomenon. Therefore, the need for knowledge to fill the understanding gap in this field is still remaining.

1.2 Background

The definition states that Tribology is the science and technology of interactive surfaces in relative motion; it studies the principles of friction, lubrication and wear. The phenomena considered in Tribology are among the most fundamental and most common of those encountered by humans in interaction with their largely solid environment.

Motion and ultimately power is transmitted between the components of any machine or mechanism through direct contact. When relative motion exists in those contacts, wear and possible failure can occur if the contacting surfaces are not protected by a lubricant film. In the case of liquid-lubricant films, there are three main mechanisms of lubrication: hydrodynamic (HD), elastohydrodynamic (EHL) and hydrostatic (HS). Hydrodynamic lubrication is a special case of fluid film lubrication which occurs when the lubricant is able to support the load without external pressure, through hydrodynamic forces alone, which deform the shape of the interposing lubricant film into a wedge shape and drags the lubricant into the film, so that the externally applied load can be supported.

In case of elastohydrodynamic lubrication, two additional mechanisms, apart from the hydrodynamic lift, play a crucial role in the formation of a lubricant film, the elastic deformation of the surfaces and the variation of the lubricants' viscosity with pressure. As the lubricant film thickness is very small (anything between ten nanometres and one micrometer) and is established in the inlet of the contact, where the pressure is low, the film thickness is very sensitive to changes of the geometry due, for instance, to passing of asperities or other features through the contact.

A lubricant primarily controls friction and wear, but it can also perform other functions, which vary with the application, but which can include vibration insulation, corrosion inhibition and heat convection.

The importance of Tribology has greatly increased during its long history, [1] it is known that tribological issues affect the performance and life span of all mechanical systems and provides solutions for a higher reliability, accuracy and precision. Energy loss through friction in tribo-elements is a major factor that limits the energy efficiency of any system, by using strategic materials; many tribo-elements obtain the required performance. Research in Tribology dedicated to elastohydrodynamic lubrication has resulted in industry developing better and more efficient oil seals, improved design of rolling elements, bearings and gears, improvement on lubricant replenishment to the EHD contact in grease lubricated contacts, improved surface finish, better materials, filtering systems to prevent lubricant contamination, additives designed for target applications [2].

1.3 Objectives and Scopes of Research

The main objective of this research is to develop and calibrate the capacitive method for measuring EHD film thickness.

Other objectives, which are subordinates to the main objective, are:

- Changes to the Ultra Thin Film Interferometry technique (UTFI) technique to allow measurement of the film thickness without a silica spacer layer.
- Changes to a PCS-Instruments EHD film thickness test rig to allow capacitance measurement.
- Evaluate the suitability of the capacitive method for measuring very thin lubricant films.

1.4 Thesis Outline

The first chapter of the thesis includes a brief introduction to the object of study of Tribology and the objectives of the present research programme.

The second chapter gives an account of the principal problems of the fluid film lubrication and its basic principals. The main equations of the hydrodynamic lubrication regime are presented in this chapter. The main mechanisms involved in the elastohydrodynamic lubrication regime are also discussed in this chapter.

Third chapter includes detailed analysis of the optical interferometry techniques for measuring thin lubricant film thickness. The physical phenomena involved in this technique are described and the evolution of this method over the years is also added.

This chapter also includes a literature review of the electrical methods used in lubrication, with the focus on EHD regime. The principles of these methods and typical applications are discussed, with a focus on electrical capacitance. Other methods for the study of elastohydrodynamic films are debated here.

The fourth chapter is dedicated to methods explored by the author in published papers including results obtained when different optical and electrical techniques are experimented with.

The fifth chapter describes the experimental setup, the modifications made to the EHD test rig and the calibration of the capacitance method. Both static and dynamic experimental set-ups are described in detail.

Chapter six contains results obtained using the optical and the capacitive methods and a comparison between them.

Chapter seven is dedicated to conclusions, while the final chapter includes suggestions for future work.

2 BASIC PRINCIPLES OF LUBRICATION

2.1 Hydrodynamic Lubrication

2.1.1 Reynolds equation

The serious appreciation of hydrodynamics in lubrication started at the end of the 19th century, when Beauchamp Tower, an engineer, noticed that the oil in a journal bearing always leaked out of a hole located beneath the load. The leakage of oil was a nuisance, so the hole was plugged first with a cork, which still allowed oil to squeeze out, and then with a hard wooden bung. The hole was originally placed to allow oil to be supplied into the bearing to provide lubrication. When the wooden bung was slowly forced out of the hole by the oil, Tower realized that the oil was pressurized by some yet unknown mechanism. Tower then measured the oil pressure and found that it could separate the sliding surfaces by a hydraulic force [3]. At the time of Beauchamp Towers' discovery, Osborne Reynolds and other theoreticians were working on a hydrodynamic theory of lubrication. By a most fortunate coincidence, Tower's detailed data was available to provide experimental confirmation of hydrodynamic lubrication, almost at the exact time when Reynolds needed it. The result of this was a theory of hydrodynamic lubrication, published in the Proceedings of the Royal Society by Reynolds in 1886 [3]. Reynolds provided the first analytical proof that a viscous liquid can physically separate two sliding surfaces by hydrodynamic pressure, resulting in low friction and theoretically zero wear.

Reynolds equation describes the pressure field set up in a fluid between two solid surfaces when the surfaces slide or are squeezed together, Figure 1 shows a general situation.

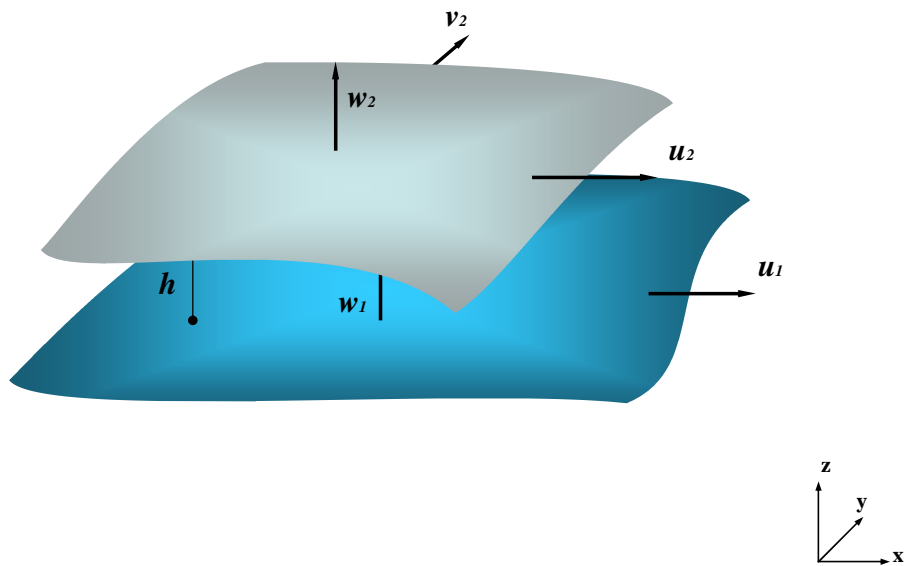


Figure 1: Two generalised surfaces in contact

In this generalised case, the fluid pressure, $p = f(x, y, h, u_1, u_2, w_1, w_2, \eta, v_1, v_2)$ where u, v and w are the velocities of the surfaces in the x, y and z direction. Surface separation, h and fluid dynamic viscosity, η can vary over x and y .

The Reynolds equation can be derived by an appropriate simplification of the full Navier–Stokes equation or by combining a fluid element of equilibrium with flow continuity.

Assumptions made in deriving Reynolds equation:

1. Body forces negligible
2. Pressure constant through film
3. No slip at the boundaries
4. Newtonian lubricant
5. Laminar flow
6. Negligible inertia
7. Fluid
8. Constant density
9. Constant viscosity through film

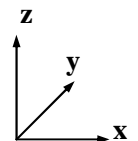
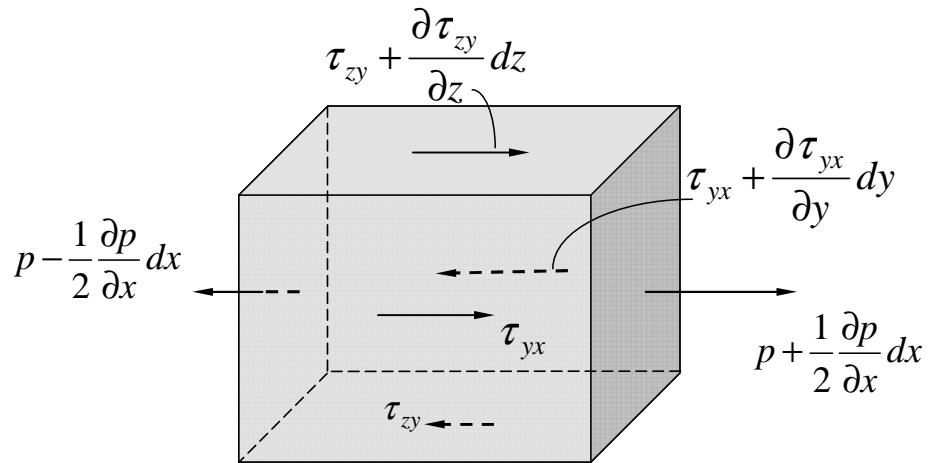


Figure 2: Equilibrium of an element [3]

If we consider the equilibrium of forces in x -direction we get:

$$\left(p - \frac{1}{2} \frac{\partial p}{\partial x} dx \right) dy dz + \left(\tau + \frac{\partial \tau}{\partial z} dz \right) dy dx = \tau dx dy + \left(p + \frac{1}{2} \frac{\partial p}{\partial x} dx \right) dy dz \quad (1)$$

Simplifying the terms yields:

$$\frac{\partial \tau}{\partial z} dx dy dz = \frac{\partial p}{\partial x} dx dy dz \quad (2)$$

Since $(dx dy dz)$ is an arbitrary, non-zero volume, we can write:

$$\frac{\partial \tau}{\partial z} = \frac{\partial p}{\partial x} \quad (3)$$

From Newton's viscosity hypothesis, using assumptions 4 and 5.

$$\tau = \eta \frac{\partial u}{\partial z} \quad (4)$$

Replacing this expression of the shear stress into Equation 3 the pressure gradient becomes:

$$\frac{\partial p}{\partial x} = \frac{\partial}{\partial z} \left(\eta \frac{\partial u}{\partial z} \right) \quad (5)$$

Similar expression can be derived for the flow in y direction:

$$\frac{\partial p}{\partial y} = \frac{\partial}{\partial z} \left(\eta \frac{\partial v}{\partial z} \right) \quad (6)$$

And from assumption 2:

$$\frac{\partial p}{\partial z} = 0 \quad (7)$$

On both surfaces $\frac{\partial v}{\partial x} = \frac{\partial u}{\partial y} = 0$, so shear forces on $(dx dz)$ faces are small. $\frac{\partial u}{\partial z}$ is of the order of

U_S/h

Velocity Profiles

From Equation 1, since $p \neq f(z)$ and $\eta \neq f(z)$ (from assumptions 2 and 8)

$$\eta \frac{\partial u}{\partial z} = \int \frac{\partial p}{\partial x} dz = \frac{\partial p}{\partial x} z + C_1 \quad (8)$$

and

$$\eta u = \int \left(\frac{\partial p}{\partial x} z + C_1 \right) dz = \frac{\partial p}{\partial x} \frac{z^2}{2} + C_1 z + C_2 \quad (9)$$

Boundary conditions are $z = 0$ at $u = U_1$ and $z = h$ at $u = U_2$ (from assumption 3). These give:

$$C_2 = \eta U_1 \quad (10)$$

$$C_1 = (U_2 - U_1) \frac{\eta}{h} - \left[\frac{\partial p}{\partial x} \frac{h}{2} \right] \quad (11)$$

Consequently:

$$\eta u = \frac{\partial p}{\partial x} \frac{z^2}{2} + \eta (U_2 - U_1) \frac{z}{h} - \frac{\partial p}{\partial x} \frac{hz}{2} + \eta U_1 \quad (12)$$

And

$$u = \frac{\partial p}{2\eta \partial x} (z^2 - zh) + (U_2 - U_1) \frac{z}{h} + U_1 \quad (13)$$

$$v = \frac{\partial p}{2\eta \partial y} (z^2 - zh) + (V_2 - V_1) \frac{z}{h} + V_1 \quad (I) \quad (II) \quad (III) \quad (14)$$

Equations 13 and 14 represent velocity profiles across the film and consist of three super imposed terms, (I), (II) and (III).

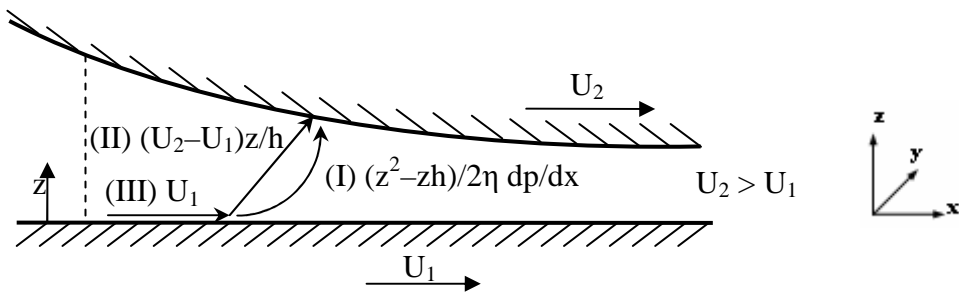


Figure 3: Three components of the fluid velocity profile

Continuity of flow in a column

Consider the column of lubricant between the solid surfaces. Flow in the x and y directions comes from integrating the velocity profile over the film thickness, h .

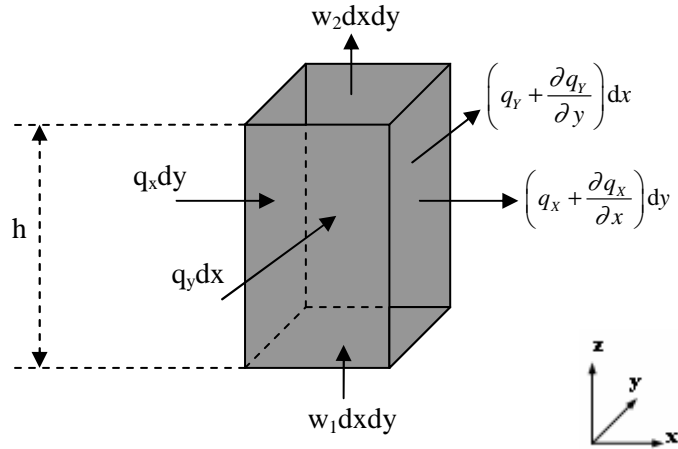


Figure 4: Flow into column of fluid

Flow per unit width in the y and x directions respectively;

$$q_x = \int_0^h u dz \quad (15)$$

$$q_y = \int_0^h v dz \quad (16)$$

$$q_x = \left[\frac{\partial p}{2\eta \partial x} \left(\frac{z^3}{3} - \frac{hz^2}{2} \right) + (U_2 - U_1) \frac{z^2}{2h} + zU_1 \right]_0^h \quad (17)$$

The flows in both x and y directions are:

$$q_x = -\frac{h^3}{12\eta} \frac{\partial p}{\partial x} + (U_2 + U_1) \frac{h}{2} \quad (18)$$

$$q_y = -\frac{h^3}{12\eta} \frac{\partial p}{\partial y} + (V_2 + V_1) \frac{h}{2} \quad (19)$$

Apply continuity of volume flow to the column above Figure 4 [3]. Mass flow can also be used but is more complicated, so by taking assumption 7 we get.

$$q_x dy + q_y dx + w_1 dx dy = \left(q_x + \frac{\partial q_x}{\partial x} dx \right) dy + \left(q_y + \frac{\partial q_y}{\partial y} dy \right) dx + w_2 dx dy \quad (20)$$

Hence:

$$\frac{\partial q_x}{\partial x} + \frac{\partial q_y}{\partial y} + (w_2 - w_1) = 0 \quad (21)$$

Substituting in Equations 16 and 17,

$$\frac{\partial}{\partial x} \left\{ -\frac{h^3}{12x} \frac{\partial p}{\partial x} + (U_2 + U_1) \frac{h}{2} \right\} + \frac{\partial}{\partial y} \left\{ -\frac{h^3}{12\eta} \frac{\partial p}{\partial y} + (V_2 + V_1) \frac{h}{2} \right\} + (w_2 - w_1) = 0 \quad (22)$$

Rearranging and putting $U = \frac{U_1 + U_2}{2}$ and $V = \frac{V_1 + V_2}{2}$ (the main entrainment velocities):

$$\frac{\partial}{\partial x} \left\{ \frac{h^3}{12\eta} \frac{\partial p}{\partial x} \right\} + \frac{\partial}{\partial y} \left\{ \frac{h^3}{12\eta} \frac{\partial p}{\partial y} \right\} = \frac{\partial(Uh)}{\partial x} + \frac{\partial(Vh)}{\partial y} + (w_2 - w_1) \quad (23)$$

Assuming $U \neq f(x)$ and $V \neq f(y)$

$$\frac{\partial}{\partial x} \left\{ \frac{h^3}{\eta} \frac{\partial p}{\partial x} \right\} + \frac{\partial}{\partial y} \left\{ \frac{h^3}{\eta} \frac{\partial p}{\partial y} \right\} = 12 \left\{ U \frac{\partial h}{\partial x} + V \frac{\partial h}{\partial y} + w_2 - w_1 \right\} \quad (24)$$

Equation 22 is the Reynolds Equation in two dimensions.

In hydrodynamics, (as opposed to elastohydrodynamic) one of the two surfaces is always stationary with respect to the contact, so $U = \frac{U_1 + U_2}{2} = \frac{U_1}{2}$ (arbitrarily assigning suffix 1 to moving surface). Then Equation 22 will become:

$$\frac{\partial}{\partial x} \left\{ \frac{h^3}{\eta} \frac{\partial p}{\partial x} \right\} + \frac{\partial}{\partial y} \left\{ \frac{h^3}{\eta} \frac{\partial p}{\partial y} \right\} = 6 \left\{ U_1 \frac{\partial h}{\partial x} + V_1 \frac{\partial h}{\partial y} + 2(w_2 - w_1) \right\} \quad (25)$$

Simplifying:

$$\frac{\partial}{\partial x} \left\{ \frac{h^3}{\eta} \frac{\partial p}{\partial x} \right\} + \frac{\partial}{\partial y} \left\{ \frac{h^3}{\eta} \frac{\partial p}{\partial y} \right\} = 12 \left\{ U \frac{\partial h}{\partial x} + V \frac{\partial h}{\partial y} \right\} + 12(w_2 - w_1) \quad (26)$$

2.1.2 Solution to Reynolds equation

Reynolds Equation is too complex for algebraic solution, and a number of simplifications are commonly made to aid its solution. Although these are less important than they used to be, since computational methods have made it quite easy to solve the full equation, they are still significant since one, they save a lot of computing time and two, they provide insight into the form of the solution and how operating parameters, such as film thickness and friction are related.

It is almost always possible to choose axes so that $V = 0$ in which case:

$$\frac{\partial}{\partial x} \left\{ \frac{h^3}{\eta} \frac{\partial p}{\partial x} \right\} + \frac{\partial}{\partial y} \left\{ \frac{h^3}{\eta} \frac{\partial p}{\partial y} \right\} = 12 \left\{ U \frac{dh}{dx} + (w_2 - w_1) \right\} \quad (27)$$

If there is no vertical flow of oil i.e. bearings are not porous, surfaces are not coming together (*squeeze film effects*) then $w_2 - w_1 = 0$, in which case:

$$\frac{\partial}{\partial x} \left\{ \frac{h^3}{\eta} \frac{\partial p}{\partial x} \right\} + \frac{\partial}{\partial y} \left\{ \frac{h^3}{\eta} \frac{\partial p}{\partial y} \right\} = 12U \frac{dh}{dx} \quad (28)$$

This can be a wrong assumption in bearings because most of them, regardless of the application, vibrate. If there are no significant thermal effects, then η will be constant over the film, in which case:

$$\frac{\partial}{\partial x} \left\{ h^3 \frac{\partial p}{\partial x} \right\} + \frac{\partial}{\partial y} \left\{ h^3 \frac{\partial p}{\partial y} \right\} = 12U\eta \frac{dh}{dx} \quad (29)$$

If the bearing can be regarded as infinitely long, i.e. there are no side edge effects, and then $\frac{\partial p}{\partial y} \approx 0$ in which case, assuming also that $h \neq f(y)$ we have the one-dimensional expression:

$$\frac{d}{dx} \left\{ h^3 \frac{dp}{dx} \right\} = 12U\eta \frac{dh}{dx} \quad (30)$$

This can be integrated with respect to x , to yield:

$$h^3 \frac{dp}{dx} = 12U\eta h + C \quad (31)$$

If $\frac{dp}{dx} = 0$ at $h = \bar{h}$, then

$$\frac{dp}{dx} = 12U\eta \left(\frac{h - \bar{h}}{h^3} \right) \quad (32)$$

2.1.3 Limits of Hydrodynamic Lubrication

As has been implied throughout this chapter, hydrodynamic lubrication is only effective when an appreciable sliding velocity exists [3]. A sliding velocity of 1m/s is typical of many bearings. As the sliding velocity is reduced, the film thickness also declines, to maintain the pressure field. This process is very effective, as pressure magnitudes are proportional to the square of the reciprocal of film thickness. Eventually, the film thickness will have diminished to such a level that the high points or asperities on each surface will come into contact. Contact between asperities causes wear and elevated friction. This condition, where the hydrodynamic film still supports most of the load but cannot prevent some contact between the opposing surfaces, is known as “*partial hydrodynamic lubrication*”. When the sliding speed is reduced further still the hydrodynamic lubrication fails completely and solid contact occurs. A lubricant may still, however, influence the coefficient of friction and wear rate to some degree. Original research into the limits of hydrodynamic lubrication was performed early in the 20th century by Stribeck and Gumbel [3]. The limits of hydrodynamic lubrication are summarized in a graph shown in Figure 5.

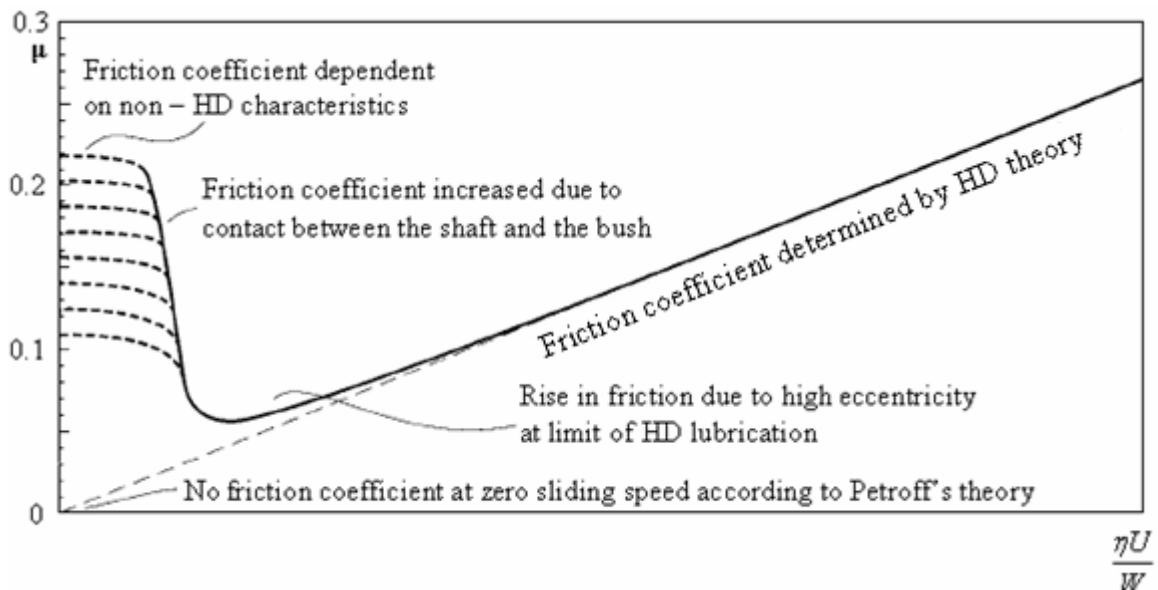


Figure 5: Schematic diagram of changes in friction at the limits of hydrodynamic lubrication [3]

When the friction measurements from a journal bearing were plotted on a graph against a controlling parameter defined as $\eta U/W$, it was found that, for all but very small sliding speeds, friction μ was proportional to the above parameter, which is known as the “*Stribeck number*”. When a critically low value of this parameter was reached, the friction increased from values of about 0.01 to much higher levels of 0.1 or more. The rapid change in the coefficient of friction represents the termination of hydrodynamic lubrication. Later work revealed that hydrodynamic lubrication persists until the largest asperities are separated by only a few nanometres of fluid. It was found that a minimum film thickness of more than twice the

combined roughness of the opposing surfaces ensures full hydrodynamic lubrication of perfectly flat surfaces [3]. Tests carried out by the authors were done on a Newtonian fluid, Figure 6 presents the Shear stress – Shear rate characteristics for a Newtonian fluid.

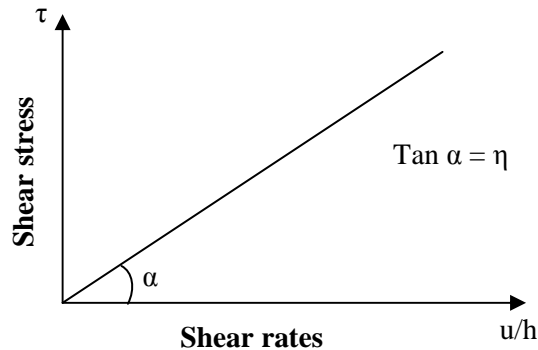


Figure 6: Shear stress – Shear rate characteristic of a Newtonian fluid

With the level of surface roughness attainable today on machined surfaces, a minimum film thickness of a few micrometers could thus be acceptable. In fact, for small bearings, i.e. a journal bearing of 80mm diameter, it is possible to use twice the combined roughness as a minimum limit for film thickness. On the other hand, for large hydrodynamic bearings, larger clearances are usually selected because of the great difficulty in ensuring that such a small minimum film thickness is maintained over the entire bearing surface. Even if the bearing surfaces are machined accurately, elastic or thermal deflection would almost certainly cause contact between the bearing surfaces. If contact between sliding surfaces occurs then, particularly at high speeds of 10m/s, the dramatic increase in frictional power dissipation can cause overheating of the lubricant and possibly seizure of the bearing.

Most hydrodynamic bearings, particularly the larger bearings, are designed to operate at film thicknesses well above the estimated transition point between fully hydrodynamic lubrication and wearing contact because of two factors:

- The transition loads and speeds are difficult to specify accurately,
- Bearing failure is almost inevitable if the hydrodynamic film is allowed to fail even momentarily.

2.2 Elastohydrodynamic Lubrication

Many machine elements and mechanisms transmit relative motion and forces between surfaces which make theoretical contact in a point or along a line. In practice, the contact takes place on a very small surface, which makes the contact pressure considerably large, even at relatively low loads. Assuming elastic bodies in contact, which is often the case with steel components, under typical loads, the deflection of these surfaces is predicted by the Hertz theory of elastic contact [4]. The elastic deflection of the contacting surfaces is one of the three most important phenomena which are involved in the elastohydrodynamic lubrication.

Elastic deformation of the contacting bodies is the first mechanism required to obtain elastohydrodynamic lubrication. Let us consider two spheres in contact. If the two spheres are originally just touching under zero load the separation at radius a , can be written $(a^2/2)(1/R_1+1/R_2) = a^2/2R$, where $1/R = 1/R_1+1/R_2$ for a much smaller than R [5].

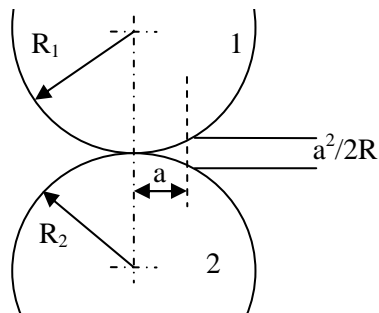


Figure 7: Geometry of two contacting spheres [5]

After loading, the gap at radius a is now zero, as this now is the radius of the contact area, the total deflection at radius a is:

$$w_1 + w_2 = \left(\frac{1-\sigma_1^2}{E_1} + \frac{1-\sigma_2^2}{E_2} \right) \pi p_{\max} \frac{a}{4} \quad (33)$$

Where subscripts 1 and 2 refer to the two contacting spheres 1 and 2 thus

$$\frac{a^2}{2R} = \left(\frac{1-\sigma_1^2}{E_1} + \frac{1-\sigma_2^2}{E_2} \right) \pi p_{\max} \frac{a}{4} \quad (34)$$

$$a = \left(\frac{1-\sigma_1^2}{E_1} + \frac{1-\sigma_2^2}{E_2} \right) \pi p_{\max} \frac{R}{2} \quad (35)$$

When total load ($W = (2\pi/3)p_{\max}a^2$) is introduced in the formula we get:

$$a^3 = \left(\frac{1-\sigma_1^2}{E_1} + \frac{1-\sigma_2^2}{E_2} \right) \frac{3RW}{4} \quad (36)$$

If the materials are similar then

$$a^3 = \left(\frac{1-\sigma^2}{E} \right) \frac{3RW}{4} \quad (37)$$

These results can now be combined to obtain the distorted surface of sphere outside the contact area.

$$w = \frac{1-\sigma^2}{2E} ap_{\max} \left\{ \left(2 - \frac{r^2}{a^2} \right) \sin^{-1} \frac{a}{r} + \left(\frac{r^2}{a^2} - 1 \right)^{1/2} \right\} \quad (38)$$

Now if the surface started off as being spherical, the distance, z , of the surface above the plane is $z = r^2/2R$ and $r = a$ then

$$w = \frac{1-\sigma^2}{E} \pi p_{\max} \frac{a}{4} = \frac{a^2}{2R} \quad (39)$$

And

$$\frac{r^2}{2R} = \frac{a^2}{2R} \frac{r^2}{a^2} = \frac{1-\sigma^2}{4E} \pi p_{\max} a \left(\frac{r^2}{a^2} \right) \quad (40)$$

Hence

$$h = w + \frac{r^2}{2R} - \frac{2a^2}{2R} = w - \frac{1-\sigma^2}{4E} ap_{\max} \frac{\pi}{2} \left(2 - \frac{r^2}{a^2} \right) \quad (41)$$

Or

$$h = \frac{1-\sigma^2}{2E} ap_{\max} \left\{ \left(2 - \frac{r^2}{a^2} \right) \sin^{-1} \frac{a}{r} + \left(\frac{r^2}{a^2} - 1 \right)^{1/2} \right\} - \frac{1-\sigma^2}{2E} ap_{\max} \frac{\pi}{2} \left(2 - \frac{r^2}{a^2} \right) \quad (42)$$

And

$$\sin^{-1} \left(\frac{a}{r} - \frac{\pi}{2} \right) = -\cos^{-1} \left(\frac{a}{r} \right) \quad (43)$$

Hence

$$h = \frac{1-\sigma^2}{2E} ap_{\max} \left\{ - \left(2 - \frac{r^2}{a^2} \right) \cos^{-1} \frac{a}{r} + \left(\frac{r^2}{a^2} - 1 \right)^{1/2} \right\} \quad (44)$$

If both surfaces are elastic as they must be, then

$$h = \left(\frac{1-\sigma_1^2}{2E_1} + \frac{1-\sigma_2^2}{2E_2} \right) ap_{\max} \left\{ -\left(2 - \frac{r^2}{a^2} \right) \cos^{-1} \frac{a}{r} + \left(\frac{r^2}{a^2} - 1 \right)^{1/2} \right\} \quad (45)$$

If both materials have the same elastic constant, then

$$\left(\frac{1-\sigma_1^2}{2E_1} + \frac{1-\sigma_2^2}{2E_2} \right) = \frac{1-\sigma}{E} \quad (46)$$

And finally, the film thickness is given by

$$h = \frac{1-\sigma^2}{E} ap_{\max} \left\{ -\left(2 - \frac{r^2}{a^2} \right) \cos^{-1} \frac{a}{r} + \left(\frac{r^2}{a^2} - 1 \right)^{1/2} \right\} \quad (47)$$

Another mechanism which contributes to the formation of an EHD film is the hydrodynamic effect, which is responsible for the “*lift*” or load carrying capacity of the bearing and it is described by the Reynolds Equation (26).

Finally the third mechanism required is the variation of the fluid’s viscosity with pressure. The normal way of describing the variation of viscosity with pressure [5] is by means of the exponential plot developed by Barus. The relation is:

$$\eta_p = \eta_0 e^{\alpha p} \quad (48)$$

Where: η_p – is the viscosity at pressure p ;

η_0 – is the viscosity at atmospheric pressure;

α – is the pressure viscosity coefficient.

When this pressure–viscosity relation is employed [6], the integrated Reynolds Equation takes the form:

$$\exp(-\alpha p) \frac{dp}{dx} = 12\eta_0 u \left[\frac{h-h_m}{h^3} \right] \quad (49)$$

However, Cameron [5] found that α fluctuates with temperature; after a number of experimental measurements on a wide variety of oils, he concluded that α varied with temperature in such a way that $\alpha(t + \theta)$, where t is the temperature and θ is approximately constant. The value of θ varies between 80 and 90 with a mean of 85.

Barus approach to the variation of α with temperature Equation 50 is followed by Roeland Equation 51. Barus’ model:

$$\eta = \eta_0 \exp[\alpha p - \gamma(t - t_0)] \quad (50)$$

Roelands' model:

$$\eta = \eta_0 \exp \left[(\ln \eta_0 + 9.67) \left\{ -1 + (1 + 5.1 * 10^{-9})^z \right\} - \gamma(t - t_0) \right] \quad (51)$$

In another paper Kaneta et al. [7] adopted viscosity–pressure–temperature relationship proposed by Roeland. The relation used by the authors can be expressed as:

$$\eta(p, t) = \eta_0 \exp \left\{ (\ln \eta_0 + 9.67) \left[-1 + (1 + 5.1 * 10^{-9})^{Z_0} \left(\frac{t - 138}{t_0 - 138} \right)^{-S_0} \right] \right\} \quad (52)$$

Where

$$Z_0 - \text{Roelands viscosity-pressure index, dimensionless: } Z_0 = \frac{\alpha}{1.5 * 10^{-9} (\ln \eta_0 + 9.67)}$$

$$S_0 - \text{Roelands viscosity-temperature index, dimensionless: } S_0 = \frac{\beta(t_0 - 138)}{(\ln \eta_0 + 9.67)}$$

Stadler [8] uses the Roelands' Equation 53 to assess the correlation of pressure viscosity on the cavity length. This time the author does not take into account the viscosity variation with temperature therefore the equation used was

$$\eta(p) = \eta_0 \exp \left\{ \frac{\alpha p_0}{z} \left[-1 + \left(1 + \frac{p}{p_0} \right)^z \right] \right\} \quad (53)$$

He also uses the Dowson & Higginson equation for density and pressure relation (Equation 54)

$$\rho(p) = \rho_0 \left(1 + \frac{5.8 * 10^{-10} p}{1 + 1.7 * 10^{-9} p} \right) \quad (54)$$

The conclusion for these tests, after a formula to predict the length of the cavity, was that the equation is only valid for enclosed type cavities; and cavity length is dominated by the viscosity, sum velocity, cavity pressure, and geometry of the contact.

Combining these three phenomena in an analysis of an exquisite simplicity and elegance, Grubin and Vinogradova were able to reveal the mechanisms of elastohydrodynamic lubrication [9] of linear contacts (this is also attributed to Ertel [10]). They considered that the film is completely flat and that the shape of the deformed surfaces in the inlet of the contact is given by the Hertz theory. It follows that the separation between the surfaces in the convergent inlet is the sum of the constant lubricant film thickness and the Hertzian elastic deformation (h_s), as seen in Figure 8.

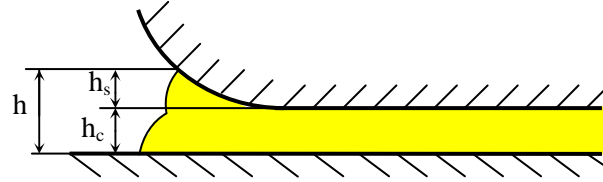


Figure 8: The geometry of the EHD contact inlet according to Grubin and Vinogradova

Assuming the Barus exponential law for the dependence of the viscosity on the pressure and that the pressure remains Hertzian inside the contact, the Reynolds equation can be integrated to give, after some manipulations, the thickness of the EHD film.

$$h_c = 1.93(\alpha\eta_0 U)^{3/4} R^{3/8} W^{-1/8} E'^{1/8} \quad (55)$$

Where R is the reduced radius of curvature in the direction of flow ($R=[(1/R_1)+(1/R_2)]^{-1}$), W is the load per unit length of contact and E' is the reduced elastic modulus of the materials ($E'=[(1-n_1^2)/E_1+(1-n_2^2)/E_2]^{1/2}$), as defined earlier in Hertz's solution of the contact of elastic bodies.

Although approximate, Grubin's solution gives an insight into the physics of the elastohydrodynamic lubrication and has been fully supported by exact numerical solutions [11]. Grubin determined the value of h_0 , which produced an infinite pressure at the inlet edge of the Hertzian zone [6], due to allowance being made for the influence of pressure on viscosity. Grubin's model of an elastohydrodynamic contact is presented in Figure 9.

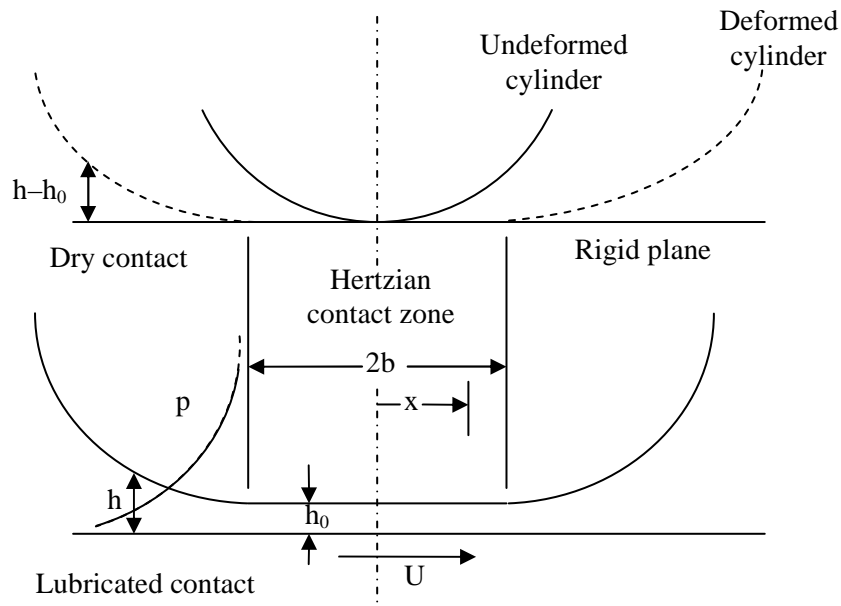


Figure 9: Grubin's model of an elastohydrodynamic contact

Grubin produced an expression for the film thickness h_0 which can be written:

$$\frac{h_0}{R} = 1.95 \frac{(\eta_0 u \alpha)^{8/11} E^{1/11}}{R^{7/11} P_y^{1/11}} \quad (56)$$

The derivation rests on two simplifying assumptions [6]:

1. the deformed shape of the cylinders will be the same as that in the dry contact
2. a high pressure is developed in the entry region to the Hertzian zone.

The Hertzian displacement outside the contact zone is given by

$$H - H_0 = \frac{h - h_0}{R} = \frac{4W}{\pi} \left[X \left(X^2 - 1 \right)^{1/2} - \ln \left(X + \left[X^2 - 1 \right]^{1/2} \right) \right] \quad (57)$$

Where $X = x/b$ and $W = w/(E'R)$ is the load parameter R is the effective radius of the roller contact. In terms of the reduced pressure the integrated form of Reynolds equation is

$$\frac{dq}{dx} = 12\eta_0 u \left[\frac{h - h_0}{h^3} \right] \quad (58)$$

If $Q = q/E'$ and $b/R = 4(W/2\pi)^{1/2}$, then Equation 58 takes dimensionless form

$$\frac{dQ}{dX} = 48 \left(\frac{W}{2\pi} \right)^{1/2} U \frac{H - H_0}{H^3} \quad (59)$$

The pressure developed at the inlet edge of the Hertzian zone will therefore be

$$Q_{x=-1} = 48 \left(\frac{W}{2\pi} \right)^{1/2} U \int_{-\infty}^{-1} \frac{H - H_0}{H^3} dX \quad (60)$$

Grubin evaluated this integral numerically for a range of values for H_0 and found an expression that gave a good fit over the range of practical importance. His variables were different to those used by Dowson and Higginson [6] such that they wrote

$$\int_{-\infty}^{-1} \frac{H - H_0}{H^3} dX = \left(\frac{\pi}{2W} \right)^2 * \text{Grubin's integral} \quad (61)$$

Grubin's integral was fitted by

$$0.0986 \left(\frac{\pi H_0}{2W} \right)^{-11/8} \quad (62)$$

Thus giving

$$Q_{x=-1} = 48 \left(\frac{W}{2\pi} \right)^{1/2} U \left(\frac{\pi}{2W} \right)^2 * 0.0986 \left(\frac{\pi H_0}{2W} \right)^{-11/8} \quad (63)$$

Dowson and Higginson approach the theory of Grubin in three steps:

1. The integration of Reynolds equation to give the pressure distribution for a known geometry
2. The inverse solution of the Reynolds equation giving the geometry which will provide a specified pressure distribution
3. Calculation of surface displacements

The integration of Reynolds equation

The numerical integration is quite straightforward. For an incompressible lubricant, all the terms for reduced pressure are known, and Simpson's rule is used by the author.

$$\frac{dq}{dx} = \frac{12\eta_0 u}{h^2} \left(1 - \frac{\rho_m h_m}{\rho h} \right) \quad (64)$$

In the first three terms Dowson and Higginson use a Taylor expansion giving

$$\frac{d^2 q}{dx^2} = \frac{12\eta_0 u}{h^2} \left[\frac{1}{h} \frac{dh}{dx} (1 - 3r) + \frac{1}{\rho} \frac{d\rho}{dx} (1 - r) \right] \quad (65)$$

Where:

$$r = \left(1 - \frac{\rho_m h_m}{\rho h} \right) \quad (66)$$

ρ is expressed in terms of p and $d\rho/dx$ is replaced by $d\rho/dp$ and dp/dx .

The inverse solution of the Reynolds equation

The inverse solution of the Reynolds equation obtained for an incompressible fluid by Dowson and Higginson is:

$$h^3 \frac{d}{dx} \left(\frac{1}{\eta} \frac{dp}{dx} \right) - \frac{dh}{dx} \left(12u - \frac{3h^2}{\eta} \frac{dp}{dx} \right) = 0 \quad (67)$$

The inclusion of compressibility in the calculation makes a very little difference; therefore the Reynolds equation with variable fluid density is:

$$\frac{d}{dx} \left(\frac{\rho h^3}{\eta} \frac{dp}{dx} \right) = 12u \frac{d}{dx} (\rho h) \quad (68)$$

Calculation of surface displacements

After a number of calculation for surface displacements by dividing the pressure curve into suitable blocks, not of equal size, and representing each block by appropriate values, Dowson and Higginson conclude on a dimensionless form for the displacement

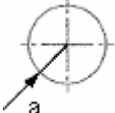
$$V = \frac{v}{R} = \frac{8P_0}{\pi} \sum AF + Constant \quad (69)$$

2.2.1 Geometry of EHD films

Contact between two spheres

The contact area between two spheres is enveloped by a circle [3]. The formulas for the main contact parameters of two spheres in contact, shown in Figure 10, are summarized in Table 1.

Table 1: Formulas for contact parameters between two spheres

Contact area dimensions	Maximum contact pressure	Average contact pressure	Maximum deflection	Maximum shear stress
$a = \left(\frac{3WR'}{E'} \right)^{\frac{1}{3}}$ 	$p_{max} = \frac{3W}{2\pi a^2}$ Hemispherical pressure distribution	$p_{average} = \frac{W}{2a^2}$	$\delta = 1.0397 \left(\frac{W}{E'^2 R'} \right)^{\frac{1}{3}}$	$\tau_{max} = \frac{1}{3} p_{max}$ at a depth of $z = 0.638a$

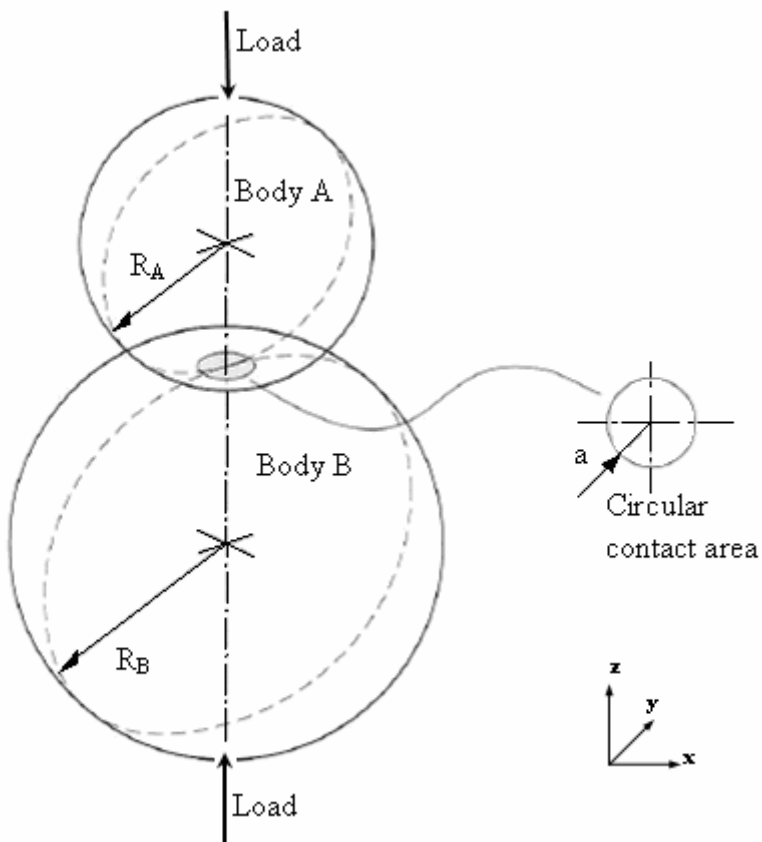


Figure 10: Geometry of the contact between two spheres.

The reduced Young's modulus is defined as:

$$\frac{1}{E'} = \frac{1}{2} \left[\frac{1 - \sigma_A^2}{E_A} + \frac{1 - \sigma_B^2}{E_B} \right] \quad (70)$$

Where: σ_A and σ_B are the Poisson's ratios and E_A and E_B are the Young's modules of the contacting bodies A and B respectively.

For spheres:

$$R_{ax} = R_{ay} = R_A \quad (71)$$

$$R_{bx} = R_{by} = R_B \quad (72)$$

Where R_A and R_B are the radii of the spheres A and B . The reduced radius of both contacting bodies can be given by Equation 73.

$$\frac{1}{R'} = \frac{1}{R_x} + \frac{1}{R_y} = \frac{1}{R_A} + \frac{1}{R_B} + \frac{1}{R_A} + \frac{1}{R_B} = 2 \left(\frac{1}{R_A} + \frac{1}{R_B} \right) \quad (73)$$

Contact between a Sphere and a Plane Surface:

The contact area between a sphere and a plane surface, as shown in Figure 11, is also circular, this being a special case of two spheres in contact, but one of them has an infinite radius of curvature [3]. The contact parameters for this configuration can be calculated according to the formulas summarized in Table 1. The radii of curvature of a plane surface are infinite and symmetry of the sphere applies, so that $R_{bx}=R_{by}=\infty$ and $R_{ax}=R_{ay}=R_A$. The reduced radius of curvature is therefore given by:

$$\frac{1}{R'} = \frac{1}{R_x} + \frac{1}{R_y} = \frac{1}{R_A} + \frac{1}{\infty} + \frac{1}{R_A} + \frac{1}{\infty} = \frac{2}{R_A} \quad (74)$$

Where:

$$R_x = R_y = R_A \quad (75)$$

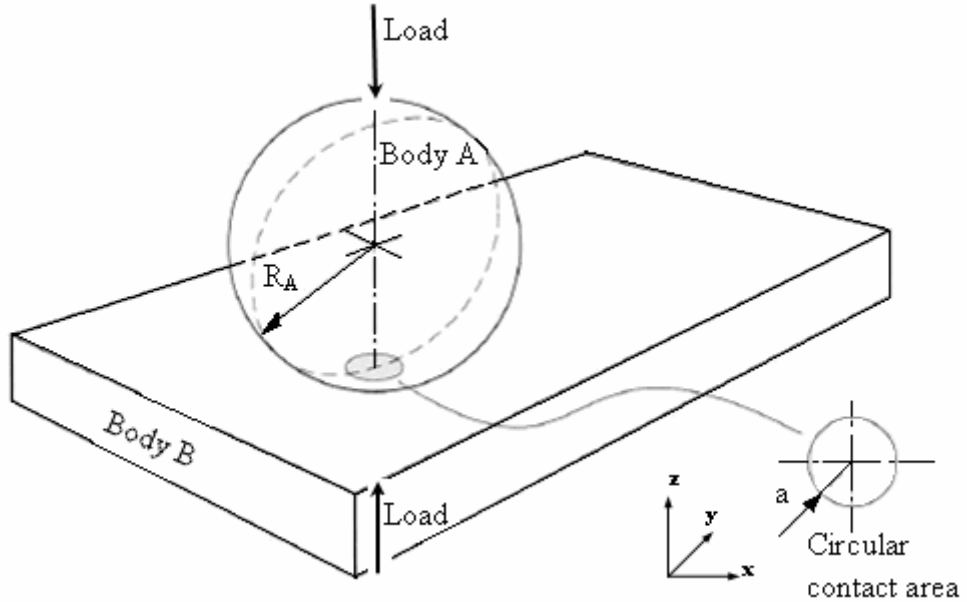


Figure 11: Contact between a sphere and a flat surface.

In a paper dedicated to Grubin–Ertel theory of elastohydrodynamic lubrication, Greenwood [12] looks in the importance of the combined effects of elastic deformation and increased viscosity under pressure, which results in a continuous oil film for heavily loaded rolling or sliding contacts.

The simple concept from Grubins' theory is that in order to carry a very high load, the pressures must be high, and so the viscosity, by virtue of the Barus relation $\eta_p = \eta_0 e^{\alpha p}$ must be enormous. Thus making the Reynolds equation

$$\frac{dp}{dx} = 12\eta U \left(\frac{h - h^*}{h^3} \right) \quad (76)$$

Where U is the main velocity of the contacting surfaces, h the film thickness and h^* an integration constant, the film thickness must be almost equal to h^* , and so be almost constant, over an appreciable distance. The author states that if we take the surfaces to have the deformed shape of an non-lubricated contact, as given by Hertz's theory, but moved apart by a fixed displacement h^* , we shall get a good approximation to the actual conditions in a lubricated contact.

Grubin calculated the film thickness on the above assumptions and obtained values very much greater than the classical ones, and agreeing reasonably well with the numerical solutions that have appeared subsequently.

For a constant viscosity in a lubrication condition between two rollers that rotate with speeds U_1 and U_2 having a central film thickness of h_0 , then for a distance x from the centre line film thickness will approximately be

$$h = h_0 + \frac{x^2}{2R} \quad (77)$$

Where:

$$\frac{1}{R} = \frac{1}{R_1} + \frac{1}{R_2}$$

And:

$$U = \frac{(U_1 + U_2)}{2}$$

The Reynolds condition used is that pressure returns to zero at a point where $h=h^*$ for preservation of continuity of flow between the pressurised film and the unpressurised outlet. The pressure in Greenwoods' experiments reaches a maximum of $2.1508\eta UR^{1/2} / h_0^{3/2}$ at $h = 1.22575 h_0$.

When the viscosity is variable with pressure according to Barus $\eta_p = \eta_0 e^{\alpha p}$, Grubins' substitution gives

$$\alpha q = 1 - e^{-\alpha p} \quad (78)$$

Transforming the Reynolds equation in

$$\frac{dq}{dx} = 12\eta U \left(\frac{h - h^*}{h^3} \right) \quad (79)$$

In Grubin's theory, the film shape corresponding to a central flat region with an added constant separation h^* is substituted into the Reynolds equation, and the equation integrated to find the maximum pressure. The pressure then remains at this constant value across the flat. However, the interest is in pressures such that αp is very large, and for all such values the reduced pressure q Equation 78 must be very nearly equal to $1/\alpha$. Thus the varying hertzian pressure distribution can be achieved with negligible variations in q , and so the approximation that the film thickness is exactly h^* is acceptable [12]. If this analysis is repeated using the film shape associated with an off-centre flat setting q_{max} equal to $1/\alpha$, he finds

$$\frac{1}{\alpha} = 12\eta_0 U \int_{h=\infty}^{h=h^*} \frac{h - h^*}{h^3} dx = 12\eta_0 U \int_{\xi=-\infty}^{\xi=-1} \frac{\left(\frac{b^2}{4R} \right) a(\xi) b}{\left[h^* + \left(\frac{b^2}{4R} \right) a(\xi) \right]^3} d\xi \quad (80)$$

To evaluate the integral he sets $\xi = -\cosh \theta$ and $H_0 = 4Rh^*/b^2$

$$\frac{b^3}{8\alpha\eta_0 UR^2} = 24 \int_0^{\infty} \frac{A(\theta) \sinh(\theta)}{[H_0 + A(\theta)]^3} d\theta \quad (81)$$

Where

$$A(\theta) = \sinh 2\theta - 2\theta + 4\mu (\sinh \theta - \theta)$$

Numerical values were extracted for given value to H_0 and μ

Consider now the outlet. If the Reynolds boundary condition applies, we must have $q=0$ when h returns to h^* after the constriction. Accordingly we also have

$$\frac{b^2}{8\alpha\eta_0 UR^2} = 24 \int_0^{\theta^*} \frac{B(\theta) \sinh(\theta)}{[H_0 - B(\theta)]^3} d\theta \quad (82)$$

Where

$$B(\theta) = 4\mu (\sinh \theta + \theta) - (\sinh 2\theta - 2\theta)$$

θ^* – is the value at which the film thickness returns to h^* where $B(\theta^*) = 0$.

In conclusion, the author specifies that a convenient analytical theory reproducing most of the features of elastohydrodynamic lubrication has been achieved. Figure 12 presents a graphical representation of the lubrication of two rigid rollers used by Greenwood [12].

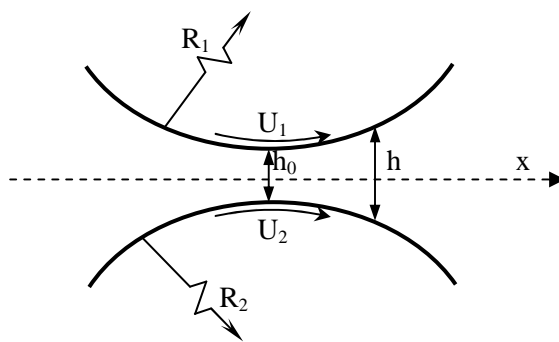


Figure 12: Lubrication of two rigid rollers [12]

2.2.2 Film thickness equations

The exact analysis of elastohydrodynamic lubrication by Hamrock and Dowson provided the most important information about EHL [3]. The results of this analysis are the formulae for the calculation of the minimum film thickness in elastohydrodynamic contacts. The formulae derived by Hamrock and Dowson apply to any contact, such as point, linear or elliptical, and are now routinely used in EHL film thickness calculations. They can be used with confidence for many material combinations, including steel on steel, even up to maximum pressures of 3–4GPa [3]. The numerically derived formulae for the central and minimum film thicknesses, as shown in Figure 13, are in the following form [3]:

$$\frac{h_c}{R} = 2.69 \left(\frac{U\eta_0}{E'R} \right)^{0.67} (\alpha E')^{0.53} \left(\frac{W}{E'R^2} \right)^{-0.067} \left(1 - 0.61 e^{-0.73k} \right) \quad (83)$$

$$\frac{h_0}{R} = 3.63 \left(\frac{U\eta_0}{E'R} \right)^{0.68} (\alpha E')^{0.49} \left(\frac{W}{E'R^2} \right)^{-0.073} \left(1 - e^{-0.68k} \right) \quad (84)$$

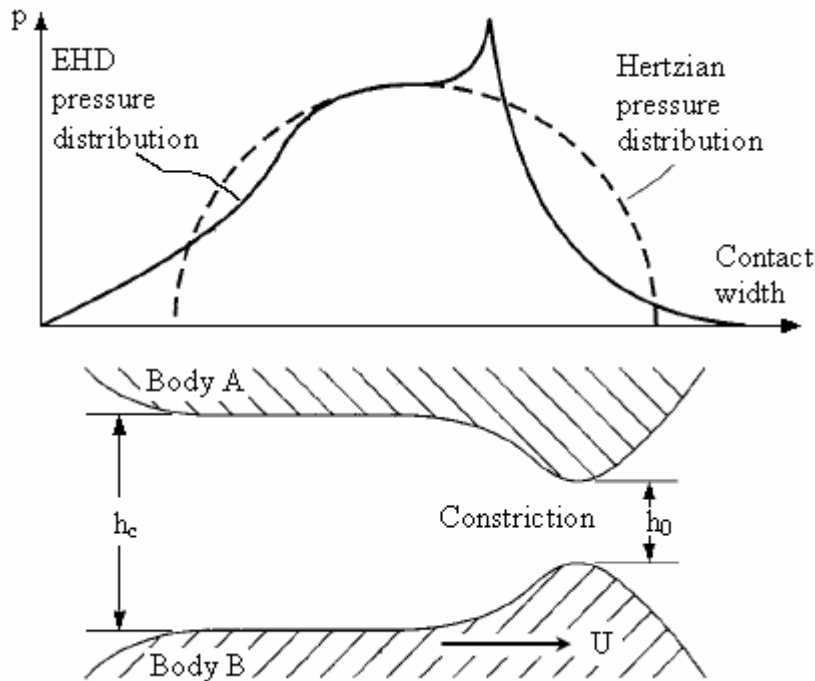


Figure 13: Hydrodynamic pressure distribution in an elastohydrodynamic contact

The approximate value of the ellipticity parameter can be calculated with sufficient accuracy from:

$$\bar{k} = 1.0339 \left(\frac{R_y}{R_x} \right)^{0.636} \quad (85)$$

The non-dimensional groups in Equations 83 and 84 are frequently referred to in the literature as:

The non-dimensional film parameter

$$H = \frac{h}{R'}$$

The non-dimensional speed parameter

$$U = \left(\frac{U\eta_0}{E'R'} \right)$$

The non-dimensional materials parameter

$$G = (\alpha E')$$

The non-dimensional load parameter

$$W = \left(\frac{W}{E'R'^2} \right)$$

The non-dimensional ellipticity parameter

$$k = \frac{a}{b}$$

3 LITERATURE REVIEW ON EXPERIMENTAL TECHNIQUES IN EHD LUBRICATION

3.1 Optical Techniques for Measuring Lubricant Film Thickness

3.1.1 Interference of light

Many phenomena specific to light, reflection, refraction, interference, etc., can be satisfactorily explained by the classical wave theory. Some of these phenomena make light a very useful tool for experimental research in a wide number of fields. In this chapter, some terms and concepts characteristic to physical optics will be briefly defined. A light wave can be represented by a sine or cosine function, as in Equation 86.

$$y = A \sin \frac{2\pi}{\lambda} (x - vt) \quad (86)$$

This is the equation of a transverse wave, which moves at velocity v in direction x , [13]. A is the amplitude and λ the wavelength of the light, as seen in Figure 14. It is convenient to express the equation of simple harmonic waves in terms of the angular frequency ‘ ω ’.

$$y = A \sin \left(\omega t - \frac{2\pi}{\lambda} x \right) \quad (87)$$

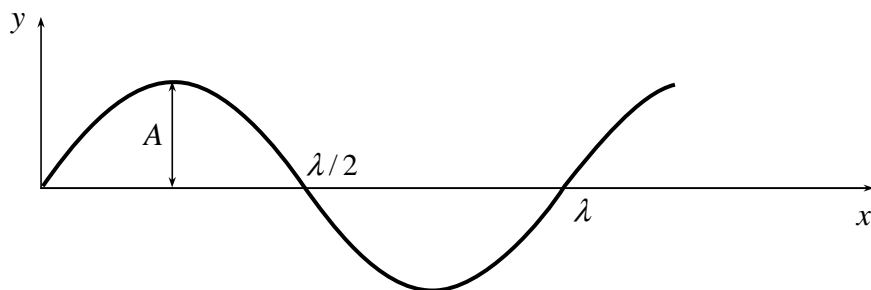


Figure 14: A transversal sine wave expressed by Equation 86, at $t = 0$

In Equation 86 $(x-vt)$ is known as *phase* and expresses the position of the wave at a certain time t . In practice, what is important is the phase difference δ between two beams of light when they reach the point of interest.

$$\delta = \frac{2\pi}{\lambda} \Delta \quad (88)$$

Where Δ is the path difference, when light is travelling through different media, the velocity of the light waves is altered according to the refractive indexes of the media. The *optical path* is therefore defined as the product between the geometrical path and the refractive index of the medium. It means that the phase difference can be written as:

$$\text{Phase difference } \delta = \frac{2\pi}{\lambda} \times \text{Optical path difference} = \frac{2\pi}{\lambda} \Delta$$

Whenever a beam of light travelling through a medium with a certain refractive index arrives at the boundary with another medium with different refractive index, it is partly *reflected* and partly transmitted (*refracted*). It is important to mention that the reflection of light at any boundary surface is accompanied by a phase change.

When two beams of light of equal wavelength, arrive at a certain point in space, a phenomenon of superposition (combination) takes place, with the net result being a change of the amplitude and intensity of the resulted light.

Thomas Young was the first one to state the interference of light thus establishing the wave character. In the region of crossing two beams of light at once we are lead to believe the resultant is the sum of these two beams; in reality the resultant is the two beams interfered and is very different than the sum of their intensity. This modification in intensity is called interference [13]. If the resultant intensity is null or less than the expected result the interference is called *destructive interference*, if the resultant intensity is higher than the intensity of each separate beam we have *constructive intensity*.

In practice, interference can be obtained from a single beam, by *wave front* or *amplitude division* [14]. Amplitude division takes place when a beam of light arrives at the interface between two media, being both reflected and transmitted. As this is the phenomenon used to accurately measure thin elastohydrodynamic films, it will be briefly explained in the following paragraphs. Consider a beam of light which hits a thin plate of thickness h , at a certain angle of incidence θ . The refractive index of the material, of which the plate is made, is n . At the interface between air and the plate, the beam will be partly reflected, path ADF , and partly transmitted, path AB , as seen in Figure 15. At C , the beam is transmitted, path CF' , and reflected. This internal reflection can take place several times; a phenomenon known as *multiple reflections*. It should be noted that the amplitudes of the reflected rays become negligible after the second internal reflection. Moreover, for the purpose of the calculation of the path difference only the first two rays are needed.

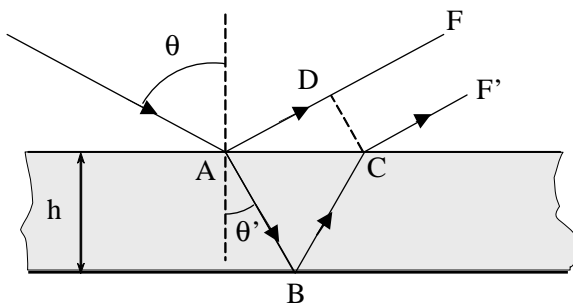


Figure 15: Interference by amplitude division. Calculation of path difference

As seen by division of amplitude, the initial ray results in two rays: AF and CF' . There is a phase difference between these two rays resulting from the path difference between them and from the advance in phase produced by the reflection at A . The latter is equal to $\lambda/2$, for air–glass reflection. The former is the difference between the path ABC , travelled by the transmitted ray, in the medium with index of refraction n and the path AD travelled, in air, by the reflected ray. D is the foot of the perpendicular from C to the reflected beam.

$$\Delta = 2nAB - AD + \frac{\lambda}{2} \quad (89)$$

Distances AB and AD are found from simple geometrical considerations.

$$AB = \frac{h}{\cos \theta'} AD = AC \sin \theta = 2h \sin \theta \tan \theta'$$

The path difference becomes:

$$\Delta = 2nh \cos \theta' + \frac{\lambda}{2} \quad (90)$$

The intensity of the light at a point on the surface of the plate is given, up to a constant, by:

$$I \approx \cos^2 \frac{\delta}{2} \quad (91)$$

Replacing the phase difference according to expression (88) the intensity becomes:

$$I \approx \cos^2 \frac{\pi \Delta}{\lambda} = \cos^2 \left[\pi \left(\frac{2nh}{\lambda} \cos \theta' + \frac{1}{2} \right) \right] \quad (92)$$

It is obvious that what an observer will see are bright and dark fringes. Assuming that the refractive index of the medium is constant, the path difference depends only on the thickness of the plate. The condition to obtain a bright fringe is given by:

$$\frac{2nh}{\lambda} \cos \theta' + \frac{1}{2} = N \quad (93)$$

Where $N = 0, 1, 2, \dots$ is the fringe order. A dark fringe is obtained for:

$$\frac{2nh}{\lambda} \cos \theta' = N \quad (94)$$

For normal incidence, $\cos \theta' = 1$, and a dark fringe corresponds to a thickness $h = N\lambda/2n$. Whenever a transition was made from a dark fringe to another, the thickness of the plate changes by $\lambda/2n$.

3.1.2 EHD film thickness measurement by optical interferometry:

Developed in the early sixties, this method employs a flat, transparent disc (usually glass or sapphire), loaded against a shiny steel ball or roller. The contacting flat surface is coated with a semi-reflective metallic layer (Chromium), such that any incident light shone onto the contact (usually monochromatic) is twice reflected, firstly at the glass–metal layer interface and secondly, at the ball/roller surface as seen in Figure 16.

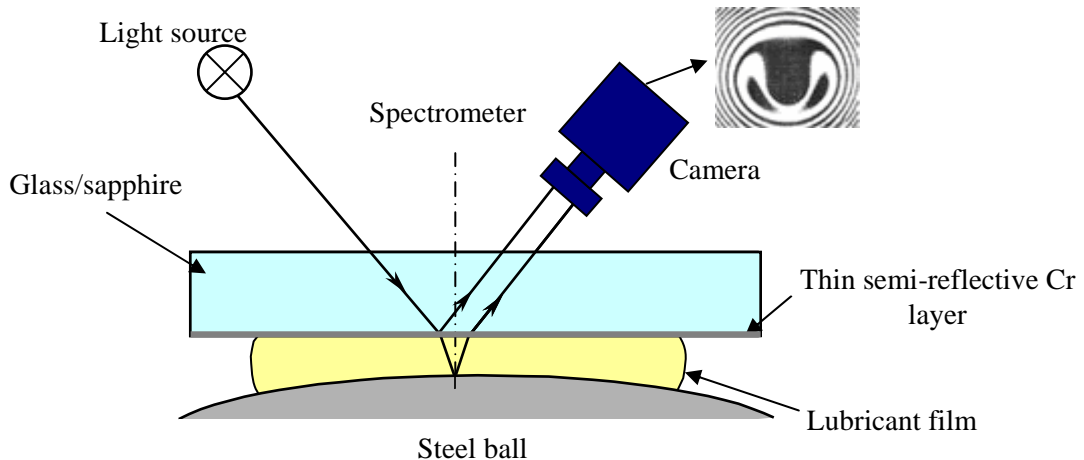


Figure 16: Principle of optical interferometry

Upon recombination, the path difference between the reflected rays results in either constructive or destructive interference. This interference depends on the thickness of the semi-reflective metallic layer.

One of the early encountered problems was choosing the transparent media and the reflective media. In the first paper [15] Westlake & Cameron are opting for a transparent media that will give them the reflection needed to measure the film thickness; the problem with this option was that the fringes were not very clear and thus an improvement had to be made. The first solution was to deposit a Chromium layer on the transparent surface. After a 20 percent Chromium deposit on the glass surface, the quality of the obtained images was again diminished as a large part of the light was absorbed in the Chromium layer. The obtained interference in this case was a two beam and followed a (\cos^2) intensity distribution. To overcome this issue a Titanium Dioxide layer is employed, this giving a much lower absorption of 0.5 percent in comparison to 20 percent of the Chromium deposit. The TiO_2 layer supplies much better images with clearer and sharper fringes, thus giving multiple beam interference. Authors also states that for the setup they are using, in this report, the limitation of the method is that the first order fringe occurs at a lubricant film thickness of about 2000\AA [$1\text{\AA} = 0.1\text{nm}$]. His results were quite accurate for the time and the pictures obtained with the technology at hand are relatively good.

In another report Wedeven and Cameron [16] developed a device to observe the contact in a thrust bearing by isolating the contact area of a given rolling element. They used an interesting way to cope with the automatic triggering system, employing a phototransistor to trigger the high speed flash camera. This method is not very different to what is being used today. However the novelty comes with positioning the phototransistor beneath the point of observation. Today the camera is triggered when certain position on the disc connected to the other end of the shaft that moves the disc is reached. The pictures taken show the oil film shape in the contact, the scratches on the ball surface and the condition of the elastohydrodynamic contact i.e. starved/flooded, a very big accomplishment for the time.

The classical method was limited to films thicker than a quarter of the wavelength, what meant that films thinner than 900Å could not be measured. In [17] an improvement of the method was reported. For the first time optical crown glass was used for the transparent media; as for the reflective coating, a TiO₂, with a thickness of a quarter of the wave length of the light employed for the actual experiments, was used. Silicon monoxide was deposited on optical crown glass after the titanium dioxide layer. This silicon layer permits the appearance of the first fringe, before the film thickness is a quarter of the wavelength, due to the silicon layer, having the same refractive index as the oil, and it has a abrasive resistance. Equation 95 gives us the approach the authors took to accurately measure the film thickness from the fringe radii.

$$r = \sqrt{\left(\frac{R}{2} \left\{ \left(\frac{\lambda(2n-1)}{\mu} \right) - 4x \right\} \right)} \quad (95)$$

Where r is the radius of the n^{th} fringe, R is the radius of the ball used in the experiments, n is the fringe, x is the depth of the silica and λ is the wavelength of the light used.

Another thing worth mentioning is that the authors actually tried a ball coated with silica and they state that the results obtained are similar to coating the disc. The pictures obtained by the authors show the fringe migration at no silica and different silica thicknesses.

This method is still largely being used today; only the Titanium layer has been replaced with Chromium instead and the formula that is being used is different.

Cameron and Gohar [18] take another approach in measuring and observing the formation of elastohydrodynamic lubrication between a steel ball and a glass plate. An isometric representation is presented in Figure 17. Using monochromatic light as a source, a chosen load and oil, the fringe pattern was observed at zero speed; the central region was dark initially, due to the phase change on reflection. Upon increasing the speed from zero, as soon as the centre

of the dark region turned light, the thickness of the film at this point was one-quarter of the wavelength in oil. As soon as the light had turned into dark, the thickness was half a wavelength of the light in oil. In this manner the authors managed to plot speed against film thickness at decent intervals.

The captured images confirm that the film thickness is constant just inside the leading edge of the contact, as required by the approximate theory [18]. Successful oil film thicknesses measurements were done in the order of 500Å to 1000Å (1nm = 10Å). Also observed by the authors was that the higher the speed the more the arms of the horseshoe shape constriction extend forward. The constriction at the exit demonstrated in line contact is found to be of a horseshoe shape, in these conditions, the film is smallest at the edges.

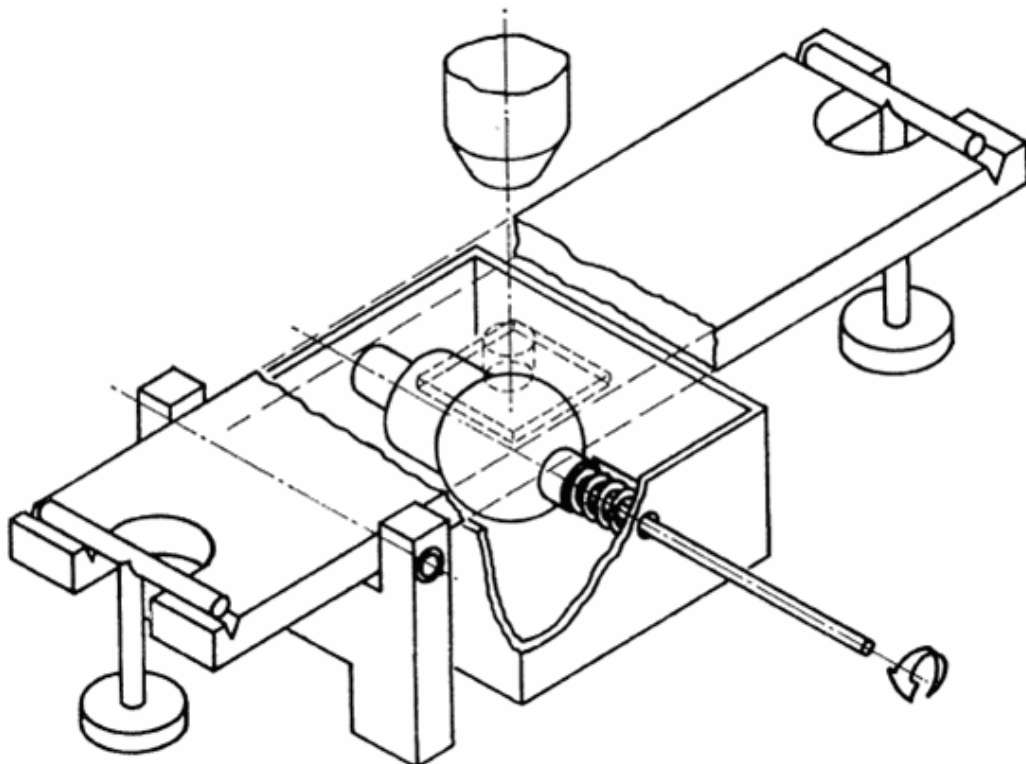


Figure 17: Schematic representation of the ball on glass plate [18]

Gohar and Cameron [19] give a comparison between the shape and thickness of the elastohydrodynamic oil film formed between a rotating ball loaded against a diamond, sapphire, or glass plate, and a rotating roller loaded against a glass plate. The authors found that the shape and film thickness are dependent on speed and load. Their paper describes film thicknesses at different loads, speeds and using a steel ball or a steel roller. Of particular interest in this paper is the way the surfaces tend towards their undeformed shape at high speeds. This phenomenon is well known today because at high speeds the film thickness is large and the contacted surfaces tend to return to their initial shape.

In 1968 Foord et al. [20] using a similar setup as Cameron, a steel ball loaded against a glass disk coated with a thin chromium layer under conditions of pure rolling, carries out a large number of experimental determinations using a variety of lubricants and additives. His conclusion was that for most fluids, except the polymer thickened oils and silicones, the fluid structure influences the film thickness primarily through its effect on viscosity and pressure viscosity coefficient.

Also Kaneta & Yang [21] discovered an interesting phenomenon that takes place under pure-sliding conditions i.e. multi-dimple, which occurs at slow sliding speeds; stable dimples can be generated in the contact. However, at higher sliding speeds, dimples become stable again, but two dimples become single dimple, or three become two. Their conclusion was that simple dimple phenomena and multiple dimple are produced by the mechanism of the temperature viscosity wedge which was proposed by Cameron [19].

3.1.3 Variations of the classical optical interferometry method

The main limitation of the method in this form is that it cannot distinguish between films thinner than approximately a quarter of the wavelength of the light used. The refinement that overcame this limitation was the addition of a solid spacer layer on top of the semi-reflective chromium layer. In the same year and approaching the same method as Westlake [17], Wedeven [22] deposited a silicon monoxide layer on optical crown glass after the titanium dioxide layer. This silicon layer permits the appearance of the first fringe before the film thickness is a quarter of the wavelength because the silicon layer has the same refractive index as the oil. The pictures obtained by the authors show the fringe migration at different silicon thicknesses.

Johnston et al. [23] tries to overcome two of the greatest limitations of the classical method: first, it cannot easily be used to accurately measure films less than one quarter the wavelength of visible light; second, only certain, discrete thickness, spaced at least 50 nm apart can be determined. His approach was to use a fixed thickness spacer layer (silica) deposited on top of the 20 nm thick chromium layer. This spacer layer has a refractive index close to that of mineral oils, which makes it act as a “*solid oil*”, increasing the separation between the surfaces of the contact and thus allowing measurements of films theoretically of any thickness. The benefits of the spacer layer were fully exploited in ultra-thin film optical interferometry method (UTFI), which uses white light and a spectrometer to disperse it into its component wavelengths as shown in Figure 18. The resolution of this technique is in the order of nanometres [24, 32].

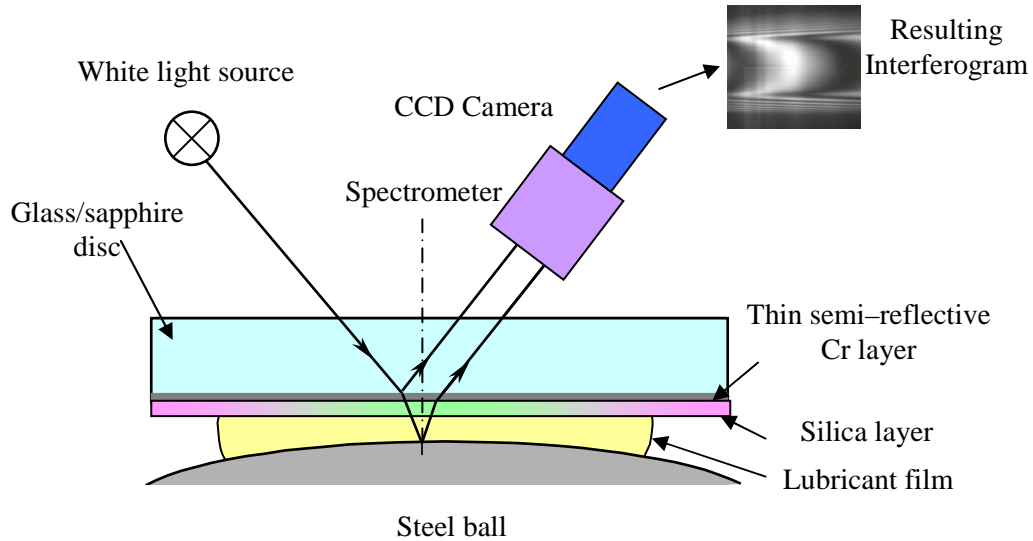


Figure 18: Ultra thin film interferometry technique

The UTI technique was further refined by Glovnea et al. [25] allowing reliable measurement of lubricant films thinner than one nanometre. This method employs a much bigger number of points used to determine the intensity–wavelength curve, unlike the classical UTI method of using just the data points around the maximum of the curve. This modified technique has been applied to study the film-forming properties of three fluids, hexadecane, a dilute solution of surfactant in hexadecane, and cyclohexane with which the author is able to measure film thicknesses down to 0.3 nm with a standard deviation of 0.15nm. The main advance with this method is that it replaces two-beam interference analysis with multiple-beam in finding of the wavelength of maximum constructive interference. Equation 96 gives the intensity of the reflected light [25].

$$I = \frac{A}{B} \quad (96)$$

Where A and B are given by Equations 97 and 98. In these equations the subscript of the refractive indexes (n) and absorption indexes (k) refers to the following layers:

- 0 glass
- 1 chromium
- 2 silica and lubricant
- 3 steel

The extinction coefficient known as the absorption index (k) is the parameter defining how strongly a substance absorbs light at a given wavelength.

To be noted that n and k depend on the wavelength λ .

Whilst: $s_1 = 4\pi h_1/\lambda$;

$$s_2 = 4\pi h_2/\lambda.$$

$$\begin{aligned}
 A = & (2(k_1^2 + (n_0 + n_1)^2)((k_3^2 + n_2^2)(k_1^2 + n_1^2 + n_2^2) - 4n_1n_2^2n_3 + (k_1^2 \\
 & + n_1^2 + n_2^2)*n_3^2 - (4k_1k_3n_2^2 + k_1^2(k_3^2 - n_2^2 + n_3^2) + (n_1 - n_2)(n_1 + n_2) \\
 & (k_3^2 - n_2^2 + n_3^2))*\cos(n_2s_2) + 2n_2(k_1^2k_3 + k_3(n_1 - n_2)(n_1 + n_2) - k_1 \\
 & (k_3^2 - n_2^2 + n_3^2))*\sin(n_2s_2)) + 2\exp(2k_1s_1)(k_1^2 + (n_0 - n_1)^2)((k_3^2 \\
 & + n_2^2)(k_1^2 + n_1^2 + n_2^2) + 4n_1n_2^2n_3 + (k_1^2 + n_1^2 + n_2^2)n_3^2 - (-4k_1k_3n_2^2 \\
 & + k_1^2(k_3^2 - n_2^2 + n_3^2) + (n_1 - n_2)*(n_1 + n_2)(k_3^2 - n_2^2 + n_3^2))*\cos \\
 & (n_2s_2) + 2n_2(k_1^2k_3 + k_3(n_1 - n_2)(n_1 + n_2) + k_1(k_3^2 - n_2^2 + n_3^2)) \\
 & *\sin(n_2s_2)) + 4\exp(k_1s_1)*\cos(n_1s_1)((-k_1^2 + n_0^2 - n_1^2)*(k_1^2 \\
 & + n_1^2 - n_2^2)(k_3^2 + n_2^2) - 8k_1^2n_0n_2^2n_3 - (k_1^2 - n_0^2 + n_1^2)(k_1^2 + n_1^2 \\
 & - n_2^2)*n_3^2 + (8k_1k_3n_0n_1n_2^2 + k_1^4(k_3^2 - n_2^2 + n_3^2) - k_1^2(n_0^2 - 2n_1^2 \\
 & - n_2^2)(k_3^2 - n_2^2 + n_3^2) - (n_0 - n_1)(n_0 + n_1)(n_1^2 + n_2^2)(k_3^2 - n_2^2 \\
 & + n_3^2))*\cos(n_2s_2) - 2n_2(k_1^4k_3 - k_3(n_0 - n_1)(n_0 + n_1)(n_1^2 + n_2^2) \\
 & + k_1^2k_3(-n_0^2 + n_1^2 + n_2^2) - 2k_1n_0n_1(k_3^2 - n_2^2 + n_3^2))*\sin(n_2s_2)) \\
 & + 2\sin(n_1s_1)*(k_1(- (n_0(k_1^2 + n_1^2 - n_2^2)(k_3^2 + n_2^2) + 2(k_1^2 - n_0^2 \\
 & + n_1^2)*n_2^2n_3 - n_0(k_1^2 + n_1^2 - n_2^2)*n_3^2 + (-2k_1^2k_3n_1n_2^2 + 2k_3 \\
 & (n_0 - n_1)n_1(n_0 + n_1)n_2^2 + k_1^3)n_0*(k_3^2 - n_2^2 + n_3^2) + k_1n_0 \\
 & (n_1^2 + n_2^2)(k_3^2 - n_2^2 + n_3^2))*\cos(n_2s_2) - n_2(2k_1^3k_3n_0 + 2k_1k_3n_0 \\
 & (n_1^2 + n_2^2) + k_1^2n_1(k_3^2 - n_2^2 + n_3^2) + n_1(-n_0 + n_1)(n_0 + n_1) \\
 & (k_3^2 - n_2^2 + n_3^2))**\sin(n_2s_2)))) \\
 \end{aligned} \tag{97}$$

$$\begin{aligned}
 B = & (2(k_1^2 + (n_0 - n_1)^2))*((k_3^2 + n_2^2)(k_1^2 + n_1^2 + n_2^2) - 4n_1n_2^2n_3 + (k_1^2 \\
 & + n_1^2 + n_2^2)*n_3^2 - (4k_1k_3n_2^2 + k_1^2(k_3^2 - n_2^2 + n_3^2) + (n_1 - n_2)(n_1 + n_2) \\
 & (k_3^2 - n_2^2 + n_3^2))*\cos(n_2s_2) + 2n_2(k_1^2k_3 + k_3(n_1 - n_2)(n_1 + n_2) - k_1 \\
 & (k_3^2 - n_2^2 + n_3^2))*\sin(n_2s_2)) + 2\exp(2k_1s_1)(k_1^2 + (n_0 + n_1)^2) \\
 & *((k_3^2 + n_2^2)(k_1^2 + n_1^2 + n_2^2) + 4n_1n_2^2n_3 + (k_1^2 + n_1^2 + n_2^2)n_3^2 - \\
 & (-4k_1k_3n_2^2 + k_1^2(k_3^2 - n_2^2 + n_3^2) + (n_1 - n_2)*(n_1 + n_2)(k_3^2 - n_2^2 + n_3^2)) \\
 & *\cos(n_2s_2) + 2n_2(k_1^2k_3 + k_3(n_1 - n_2)(n_1 + n_2) + k_1(k_3^2 - n_2^2 + n_3^2)) \\
 & *\sin(n_2s_2)) + 4\exp(k_1s_1)*\cos(n_1s_1)*((-k_1^2 + n_0^2 - n_1^2)*(k_1^2 \\
 & + n_1^2 - n_2^2)(k_3^2 + n_2^2) + 8k_1^2n_0n_2^2n_3 - (k_1^2 - n_0^2 + n_1^2)(k_1^2 + n_1^2 - n_2^2) \\
 & *n_3^2 + (-8k_1k_3n_0n_1n_2^2 + k_1^4(k_3^2 - n_2^2 + n_3^2) - k_1^2(n_0^2 - 2n_1^2 + n_2^2) \\
 & *(k_3^2 - n_2^2 + n_3^2) - (n_0 - n_1)(n_0 + n_1)(n_1^2 + n_2^2)(k_3^2 - n_2^2 + n_3^2))*\cos \\
 & (n_2s_2) - 2n_2(k_1^4k_3 - k_3(n_0 - n_1)*(n_0 + n_1)(n_1^2 + n_2^2) + k_1^2k_3(-n_0^2 \\
 & + n_1^2 + n_2^2) - 2k_1n_0n_1(k_3^2 - n_2^2 + n_3^2))*\sin(n_2s_2)) + 2\sin(n_1s_1) \\
 & *(k_1(n_0(k_1^2 + n_1^2 - n_2^2)(k_3^2 + n_2^2) + 2(k_1^2 - n_0^2 + n_1^2)*n_2^2n_3 + n_0 \\
 & (k_1^2 + n_1^2 - n_2^2)*n_3^2) - (2k_1^2k_3n_1n_2^2 + 2k_3n_1(-n_0^2 + n_1^2)n_2^2 + k_1^3n_0 \\
 & (k_3^2 - n_2^2 + n_3^2) + k_1n_0(n_1^2 + n_2^2)(k_3^2 - n_2^2 + n_3^2)\cos(n_2s_2) - n_2 \\
 & (2k_1^3k_3n_0 + 2k_1k_3n_0(n_1^2 + n_2^2) - k_1^2n_1(k_3^2 - n_2^2 + n_3^2) - n_1(-n_0 + n_1) \\
 & (n_0 + n_1)(k_3^2 - n_2^2 + n_3^2))*\sin(n_2s_2)))) \\
 \end{aligned} \tag{98}$$

Wang et al. [26] develop a new method of measuring the optical characteristics of thin film coatings. They use this technique to also find the refractive index of the thin film and the phase change of the light beam which is being reflected from the coated surface. In this paper he eliminates the fragile spacer layer of silicon and as an alternative uses a thicker Chromium layer that gives him the necessary phase change (falls between the reasonable range of 0 and π) needed to overcome the first big problem of the optical method, the quarter wave length film thickness, for his experiments. A schematic of the experimental setup is shown in Figure 19. The analysis carried out by the author is purely theoretical, stating that a new optical technique for measuring phase change and interference was developed. As this theses was partially embracing this theoretical statement, it will be explained why a thicker Cr layer does not solve the problem of providing a larger phase change needed to measure film thicknesses smaller than a quarter of the light wave length used to examine the contact.

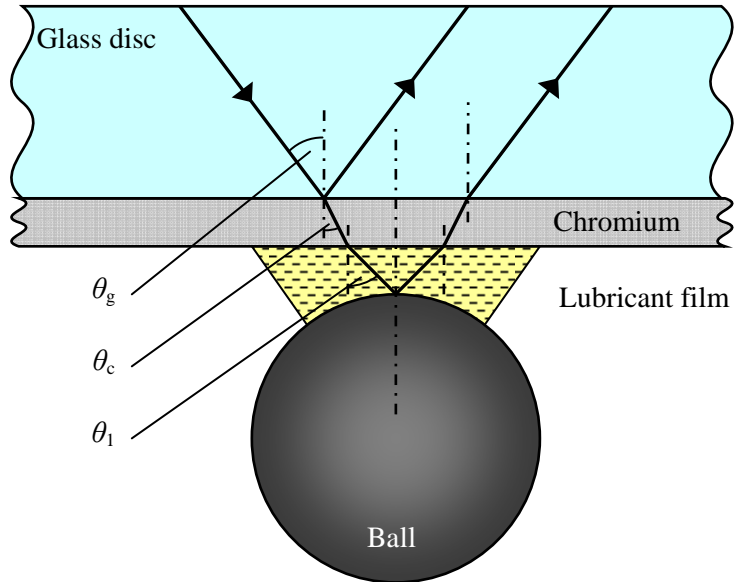


Figure 19: Light passing through a glass disc with a Chromium coating [27]

Another new developed method by Hartl et al. [27] uses an automatic program for the real-time evaluation of EHD film thickness and shape by using special software. This software coordinates the data acquisition and instrument control and also provides real-time data processing and photo displaying. The software uses colorimetric interferometry, which overcomes the conventional optical interferometry limitations. Even though the author still uses the fragile silica layer, he is able to get very thin lubricant films measured around 3nm thick. A schematic representation to the experimental setup used by Hartl is presented in Figure 20.

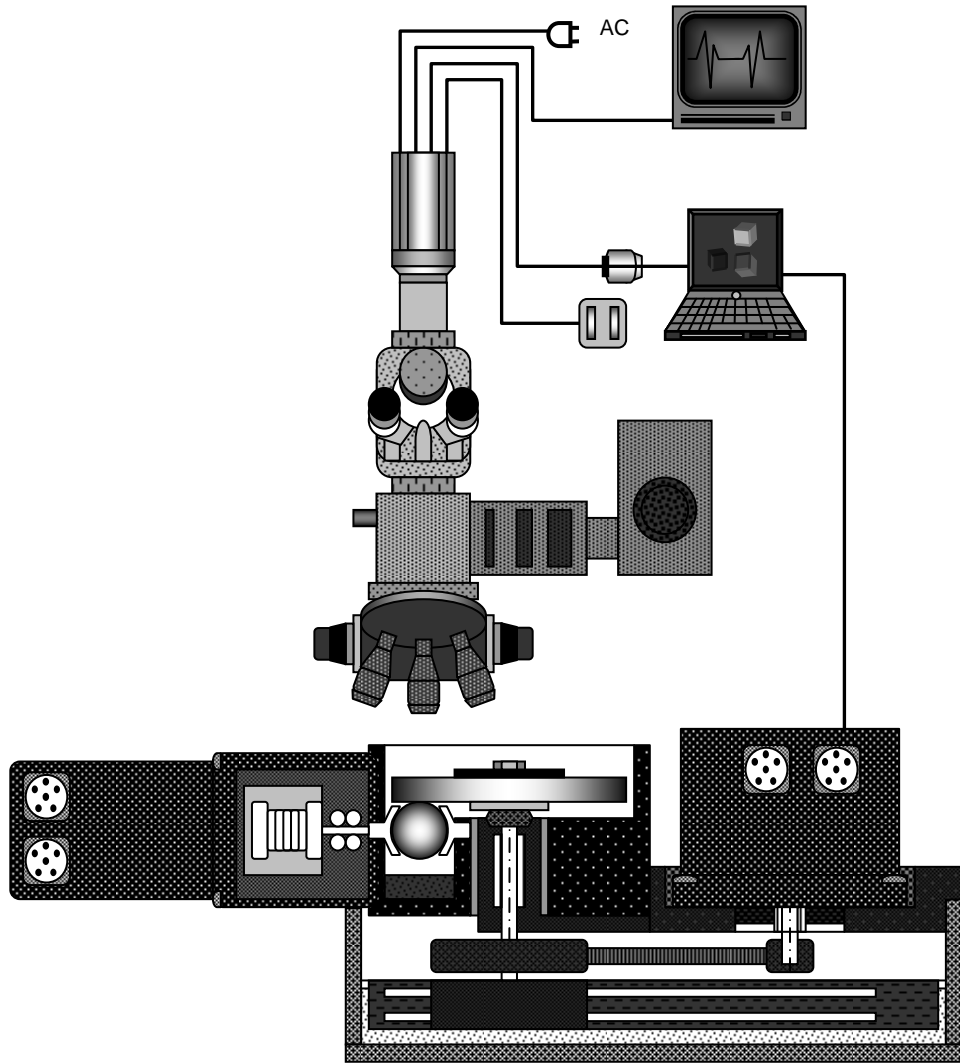


Figure 20: Schematic representation of the experimental setup [27]

In addition Krupka, et al. [28] studies the influence of high contact pressure using thin film colorimetric interferometry to examine the behaviour of thin EHD lubricant films under very high contact pressures in the order of 0.5–3GPa. He uses a Chromium coated sapphire disc and a steel or ceramic ball to obtain a circular EHD contact. The change in the film thickness–speed dependence indicates that lubricant flow and hydrodynamic action behave differently from expectation of the classical EHD theory. For higher contact pressures, this transition point tends to occur at higher critical rolling speeds.

Guo & Wong [29] develop a method called *multi-beam intensity* (MBI) which is actually a modification to a normal EHD test rig. The researchers wrote a program to aid them in the measurement of the film thicknesses. By using the fringe counting technique, the results obtained from this approach are acceptable, measuring from 1nm to 2.5 μ m, with a standard deviation of 0.9nm. A schematic representation of the contact is presented in Figure 21.

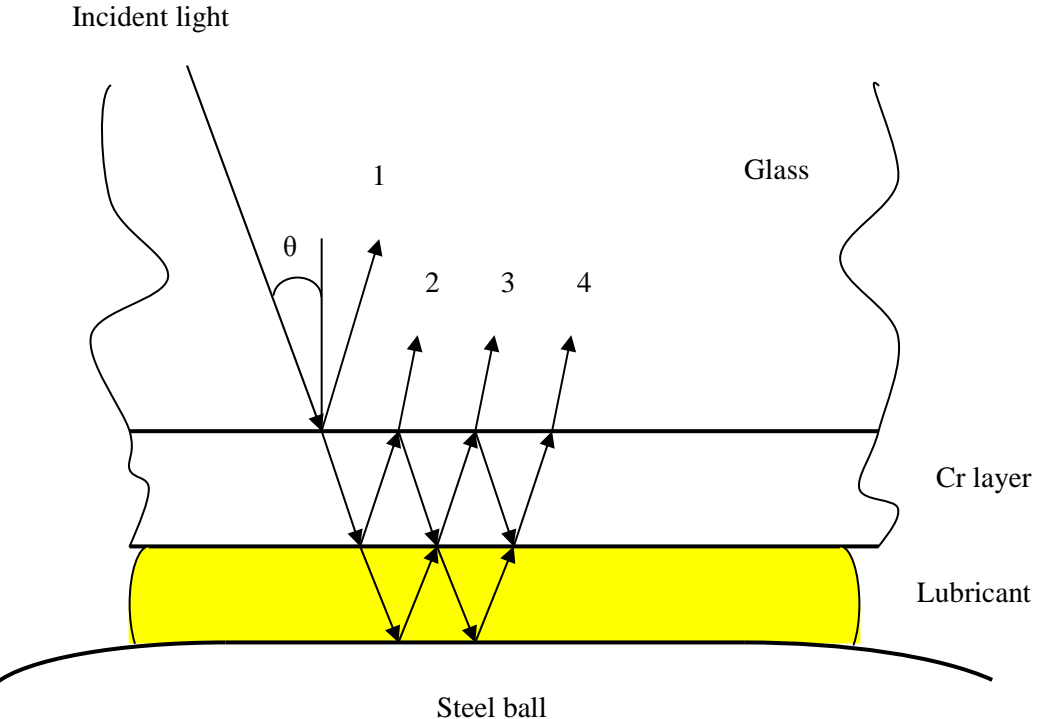


Figure 21: Multi-beam optical EHL interferometry [29]

Chapcov et al. [30] in his paper contributes to the understanding of the behaviour of a smooth point EHL contact with a generalized Newtonian lubricant under pure rolling. He also utilizes a numerical simulation to determine the film thickness. The author uses in this case a point contact in an optical ball-on-disc device for predicting film thicknesses incorporating a shear-thinning rheological model. The EHL film thickness values predicted by the model were compared to experimental measurements and a good agreement was obtained.

3.1.4 Applications of optical interferometry to mixed lubrication

A great deal of research has been done over a number of years regarding the effect of roughness in EHD lubrication. The reason for such a wide interest in this feature and the way it influences the EHL film thickness is that machine elements over long periods of time develop scratches, dimples and other features that tend to interfere with normal lubricating conditions. Very often the roughness is modelled by artificial features deposited onto the contacting surfaces.

Guangteng et al. [31] use a well known method for observing behaviour of artificial roughness in EHD mixed lubrication. Using a number of artificial features such as dimples and ridges at different orientations, the detailed shape of the EHD film varies with each artificial roughness feature. For longitudinal ridges there is a deep minimum at the sides of each ridge, giving a slow development of the EHD film with speed. On the other hand, for transverse ridges there is a minimum film thickness at the edge of the ridge, closest to the contact inlet. For the

circular bumps each asperity forms an individual circular horseshoe shape film almost behaving like an independent contact, with minimum film thickness towards the sides and end of the bump i.e. the contact inlet.

Glovnea et al. [32] publishes a study on boundary film forming using a viscosity modifier. In his measurements the author uses ultra thin film interferometry (UTFI) for determining the actual film thickness in the contact. In addition, measurements of film thickness with isotropic rough surfaces were made using the “*spacer layer imaging method*” [SLIM]. This is able to map the film thickness over the whole contact and is thus suited to study the influence of roughness that varies in both directions. Authors found that the polymer is able to form a boundary film in rough surface rolling contact just as it does in smooth surface contact; the formation of a viscous boundary film by a polymer produces a major reduction in friction on both smooth and rough surface rolling/sliding contact and therefore has an important practical implication in lubricant design.

The same SLIM method was used by Choo et al. [33] to observe the influence of transverse roughness in thin film mixed EHD lubrication. They use chromium sputtered balls of three different heights of 60, 165 and 270nm to simulate the boundary lubrication often encountered in real life machine components. The amplitude ratio of the ridges does not appear to depend on their uncompressed height, all ridges, regardless of their shape step-like (60nm) or sinusoidal like shape (165 and 270 nm), recover their height when entrainment speed and film thickness is increased. The taller ridges, was found by the authors, to give higher average central film thickness compared to that in a smooth contact.

In another paper, but on the same subject, Choo et al. [34] was to observe the influence of another type of artificial roughness i.e. circular bumps, using spacer layer imagining system (SLIM). The use of three different bump heights were employed by the authors, the peak to base height used was 65, 129 and 260nm. The classical constriction was viewed for each experiment in addition a micro-elastohydrodynamic lubricant (EHL) film formed at every bump within the contact, as found previously by [33]. The orientation of the micro-EHL film at each bump was parallel to the vector joining the contact center to the point at which that bump originally entered the contact. In conclusion the authors found that the film thickness of the bump decreased as the bump height increased, in thin film conditions, the height of the bumps recovered at an increasing rate as the speed and film thickness increased; for thicker films, this rate reduced until the uncompressed height was recovered.

In another interesting paper that uses SLIM for observing the EHL contact A.V. Olver [35] uses a micro-pit i.e. as very small indentation in the contacting surface of a roller to observe its influence on the lubrication process and the contact. Different rolling sliding conditions have

been tested and the results show a remarkable interaction between the micro-pit, the direction of sliding and the elastohydrodynamic film. Under negative slide-roll ratio (pit on slower surface), there is a large region of thin film present; positive sliding (pit on faster surface) leads to both the closure of the crack (reducing or removing the leakage path) and to the obscuring of any residual starvation by the defect itself. Fluid expulsion into the cavitated region was observed by the author as the micro-pit emerges from the contact.

Kaneta & Nishikawa [36] also study the influence of artificial roughness on EHD contacts; the interesting approach that they take is using oblique orientated bumps at an angle of 45^0 to the direction of fluid flow. In testing conditions the authors use slide-roll ratios of minus one, zero and plus one. The effects of surface roughness on EHL film were examined using model irregularities. The results obtained for a single defect, like a circular bump, transverse bump, circular dent and transverse groove, agree well with numerical simulations. For multiple irregularities, however, numerical simulations do not have the same level of agreement with the present experimental results. No big difference in film thickness between the transverse orientated bumps and the oblique ones has been observed by the authors.

Krupka & Hartl [37] approach the artificial roughness issue on a steel ball and coated glass disc type contact. They observed that even very thin viscous boundary films can significantly reduce direct asperity interactions. That was confirmed through the qualitative chromium layer wear test. Thin viscous boundary films can also provide some rubbing surface protection even under the operating conditions, when thick viscous boundary films are no longer formed on rubbing surfaces. In another paper, the same author [38] studies the effect of surface texturing on EHD films and the influence of micro-dents of various depths in the contact using colorimetric interferometry. The depth of the micro-dents has been observed to have significant effect on lubricant film formation for positive slide-to-roll ratio, when the disc is moving faster than the micro-textured ball. The presence of deep micro-dents within lubricated contact results in film thickness reduction downstream. As the depth of micro dents is reduced, this effect diminishes and mostly beneficial effect of micro-dents on film thickness formation has been observed. No significant influence of micro-dents depth on lubricant film shape has been observed in case of negative slide-to-roll conditions.

Glovnea et al. [39] in 2003 study the experimental behaviour of a 100nm high transversely oriented ridge in an elastohydrodynamic (EHD) contact using, ultra thin film interferometry, they measure accurately from few nanometres up to nearly one micron. In pure rolling, the authors found that the film constriction near the ridge, recovered to about 90 percent of its undeformed height at a main film thickness of 1mm. In contrast, when the slide/roll ratio was

one, the surfaces near the ridge remained almost fully deformed, with a high local pressure, even when the mean film thickness was as much as twice the height of the original ridge.

Another interesting technique to monitor artificial roughness in EHD contacts was approached by Nishikawa et al. [40] by using a thermal camera and analyzing captured images. The choice of roughness is strange, as most researchers opt for transversal roughness. Nishikawa uses longitudinal roughness and the results discovered are as surprising as the choice of ridge orientation. They show a higher temperature at the valley of the longitudinal roughness than the peak. This phenomenon was explained by the authors by the short wavelength and low amplitude of the roughness and by the moderate entrainment velocities depending on the slide roll ratio.

Another important step that revolutionised the machine elements industry was the addition of different chemicals that improve the various qualities of lubricants, such as viscosity index improvers [VII], organic friction modifiers [OFM] and others that give users the freedom to experiment in various conditions.

Smeeth et al. [41, 42] study the effects of a range of polymers on the EHD lubrication, observing a 15 to 3nm layer deposited between the two contacting surfaces. By trying different polymers and different solutions of oils and using UFTI they detected absorbed layers up to 10nm. A much higher viscosity was observed for these absorbed layers, and the behaviour of these layers is very different to the bulk oil solution, the polymers are behaving as boundary lubricant additives forming boundary films. Using different additives Smeeth et al. [42] show the effects of viscosity index improvers [VII] on the EHD lubrication using the same optical method. They explore the effects of VII solutions at different temperatures, observing a much thicker film than predicted for the VII that have polar molecular groups. The behaviour seems to result from the adsorption of polymer molecules on the rolling surfaces to form an enhanced viscosity layer of about 5 to 15nm, under thin film conditions the contact operates within this viscous material resulting in a much larger film thickness.

3.2 Electrical Methods for Evaluating Lubrication in EHD Contacts

3.2.1 Background

Historically, electrical methods, such as voltage discharge, resistance and capacitance preceded optical methods for studying film formation in lubricated contacts. The main advantage of electrical methods is the fact that the elastohydrodynamic contact can be formed between two steel bodies, which is identical to the contacts found in the machine components that work in the elastohydrodynamic regime. Theoretically, they can also be used to directly evaluate the lubrication of real machine components during operation. There, are however, some disadvantages to electrical methods: the resistance and capacitance of the contact depend on the shape of the bodies, which can only be presumed inside the contact, where large local deformations occur; they are very sensitive to the purity of the lubricant and can be difficult to calibrate. Additionally, these methods only give average values over the contact area and offer no direct indication of the local shape of the film.

Usually, electrical methods have been used to investigate lubrication phenomena in three different ways:

1. Film thickness measurement of studied lubricants;
2. Full-film detection conditions of asperity contacts in rough surfaces;
3. Performance evaluation of lubricated contacts under the effect of an electric field.

3.2.2 Measurement of lubricant film thickness

The problem of the lubrication mechanisms of gears and rollers was a subject of intense debate among researchers and scientists throughout the first half of the twentieth century. This debate was based around the theoretical work of Martin [43] in 1916, who considered the contacting bodies' rigidity and the viscosity of the lubricant independently of the pressure, to develop a relationship for the oil film thickness, based on the hydrodynamic theory. About three decades later Ertel-Grubin came with their solution to the problem [9, 10], as shown in the previous chapter. These theories needed to be experimentally validated, which was accomplished through the use of electrical methods.

Experiments carried out by Siripongse et al. [44, 45], using voltage discharge, and Crook [46, 47], using electrical resistance, proved that a continuous lubricant film can form even under extremely large pressures generated in nominally line and point contacts. Siripongse et al. focused their study on the relationship between the voltage/current characteristics and film thickness in line contacts [44] and point contacts [47]. The main obstacle for getting reliable results was in the calibration of their technique, as the content and size of impurities in the oil significantly changed the slope of the breakdown voltage/film thickness dependence. They concluded that the variation of breakdown voltage with film thickness is linear, while the

variations of speed or load have little or no effect on it. They also established that the standard concepts of hydrodynamic lubrication and elasticity, together with the variation of viscosity with pressure, can alone explain the behaviour of the lubricant in heavily loaded contacts.

In a series of papers intended to elucidate the mechanisms of lubrication of concentrated contacts, Crook [47] evaluated the lubricant film thickness formed between lubricated discs, with parallel axes, using a capacitive method. In order to avoid the uncertainty introduced by the true shape of the deformed contacting surfaces and by the variation of the dielectric constant of the oil with pressure, Crook opted to measure the capacitance between a disc and a stationary, unloaded pad. A schematic of this apparatus is shown in Figure 22. The calibration equation, which relates the capacitance of the pads to the film thickness, in the case of undeformed discs, is given by the relation:

$$C_D = 2.38(h_{0D}^*)^{-\frac{1}{2}} \quad (99)$$

Where h_{0D}^* is the minimum separation between discs and 2.38 is a coefficient calculated by the author that takes into account lubricant properties i.e. dielectric constant.

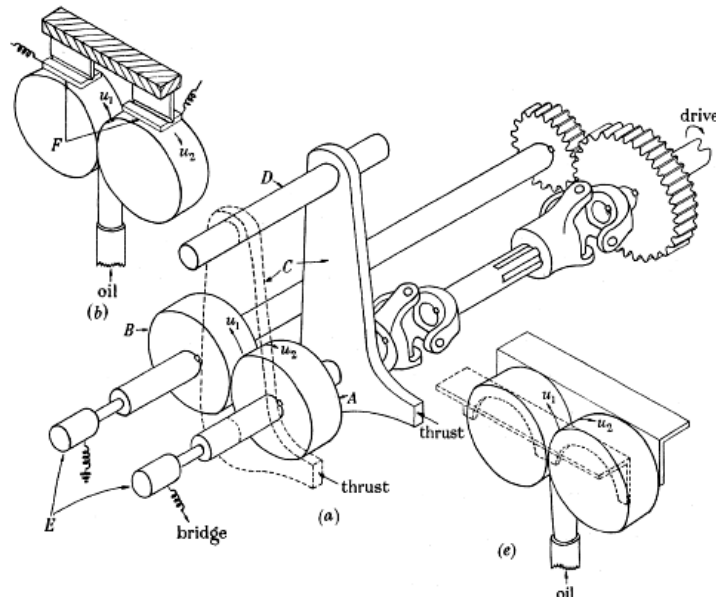


Figure 22: Crook's disc machine [47]

Figure 23 shows a comparison of the calibration curves obtained, in similar conditions, with Equation 99 and the more accurate relation found by Dyson et al. [48]. This graph shows how sensitive the electrical methods are to the calibration procedures.

Crook's results showed that at low loads, the film thickness is proportional to the speed and inversely proportional to the load, as predicted by Martin's original equations, but the absolute value detected was half of the theoretical value. At large loads, however, the measured film thickness exceeds the theoretical values. Crook also highlighted the importance of the variation of the viscosity with pressure and of the elastic deformation of the surfaces.

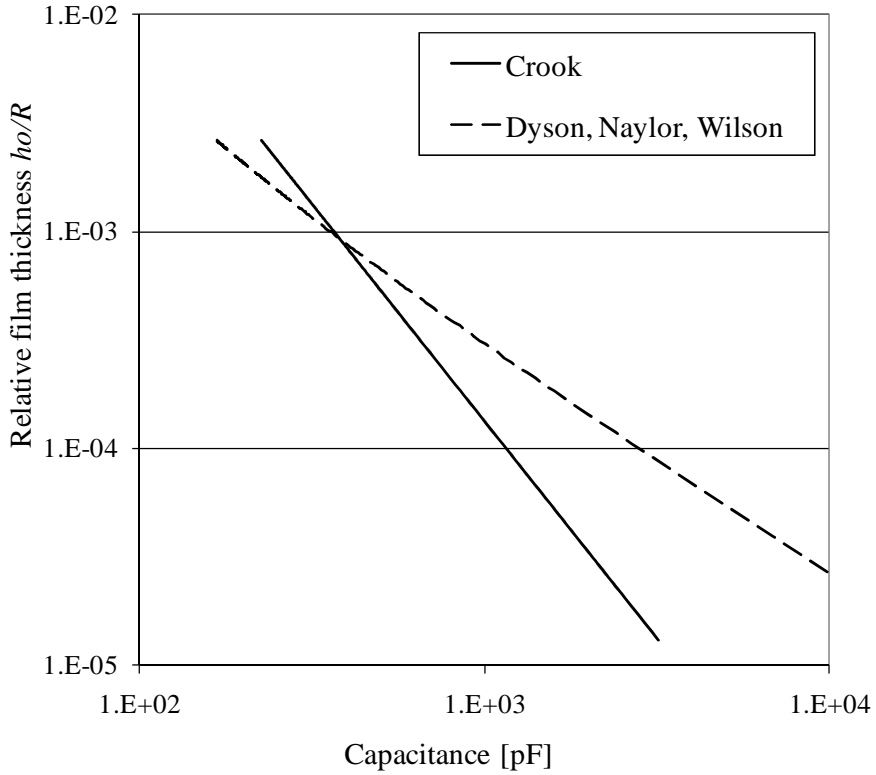


Figure 23: Calibration curves for film thickness versus capacitance [48]

Further experimental evidence was given by Archard and Kirk [49] who measured both the resistance and the capacitance of the contact between cross axes cylinders. Electrical circuit schematic of their apparatus is shown in Figure 24. They showed that the electric resistance of the contact indicates a film thickness far greater than that corresponding to the thickness calculated by the hydrodynamic theory for rigid surfaces and iso-viscous lubricants. The results indicated the existence of a hydrodynamic film at loads which would be capable of causing plastic deformation to the hardened steel specimens. Capacitance measurement of the contact over a wide range of loads, surface velocities and lubricant viscosities led Archard and Kirk to the conclusion that the thickness of the elastohydrodynamic film is proportional to the lubricant viscosity, surface velocity and radius of the contacting surfaces, according to the relation:

$$h \propto (\alpha\eta)^{0.57} V^{0.55} R^{0.62} \quad (100)$$

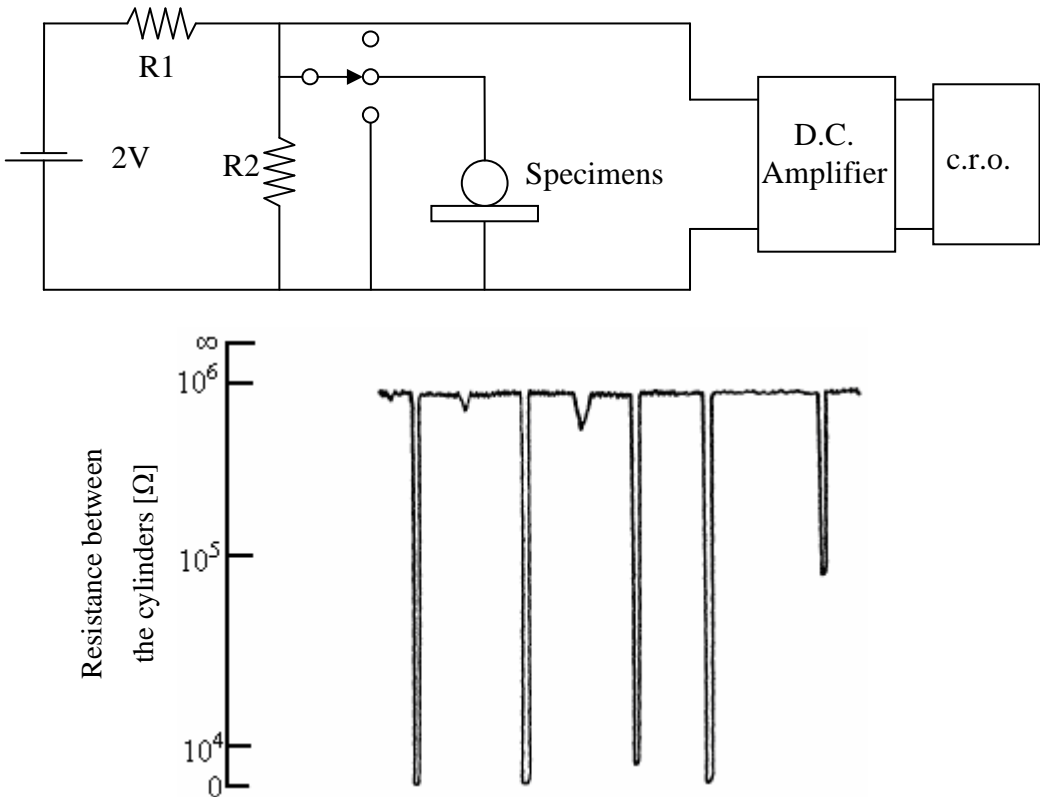


Figure 24: Electrical resistance measurement setup and pattern of the recorded signal [49]

Apart from fundamental studies on the lubrication of rollers, electrical methods have also been used to estimate the film thickness in systems, where optical interferometry is impracticable, such as gears, cams/tappets, the contact between piston–ring cylinder of internal combustion engines and plain hydrodynamic bearings.

MacConochie and Cameron [50] started their study on electrical resistance from the premise that it cannot yield quantitative measurements for elastohydrodynamic film thicknesses. Instead, they used the discharge voltage to measure the thickness of the lubricant film formed between straight spur gears' teeth. The electric circuit employed was quite simple, using a cathode–ray oscilloscope to detect the discharge voltage for a certain pair of teeth, detected by a magnetic marker. A constant current was obtained by connecting a battery with a variable resistance. They studied the effect of load and oil viscosity on the film thickness variation in various points of the meshing cycle. The results showed a considerably thick film at the pitch line, and also that the film thickness varies only a little with the viscosity of the oil and rather more strongly with the load. Later, Ibrahim and Cameron [51] use the same experimental arrangement to study the scuffing phenomena in gears.

Cameron and Chu [52] showed that when the lubrication regime is not mixed and there is a lubricant film between the two contacting surfaces, the resistance of the oil film can vary from

10^4 ohms down to 1 ohm. At higher resistances, the voltage discharge shows the presence of a quite sizeable lubricant film.

Similar to gears, cam/tappet contacts are characterized by a large variation of load, velocity and geometry. This makes it near-impossible to investigate their contacts using optical methods. Instead, electrical resistance and capacitance of the contact have been quite intensively used by various researchers to evaluate the lubricant film thickness in such systems. A comprehensive study of the transient elastohydrodynamic lubrication involving both entrainment and squeeze, with application to cam/tappet mechanisms was conducted by Vichard [53]. The study used the capacitive method in order to experimentally validate theoretical results obtained previously by Dyson et al. [48].

Van Leeuwen et al. [54] also studied the cam/follower lubrication in a specially designed experimental set-up which employed resistance in order to detect full film conditions and capacitance measurements to estimate the film thickness, while the local temperature in the contact was also measured using sub-surface transducers. In order to measure the capacitance they used a modified SKF Lubcheck instrument. For their particular testing conditions and lubricant, a film thickness variation of between 0.8 and 1.8 micrometers was detected, as shown in Figure 25.

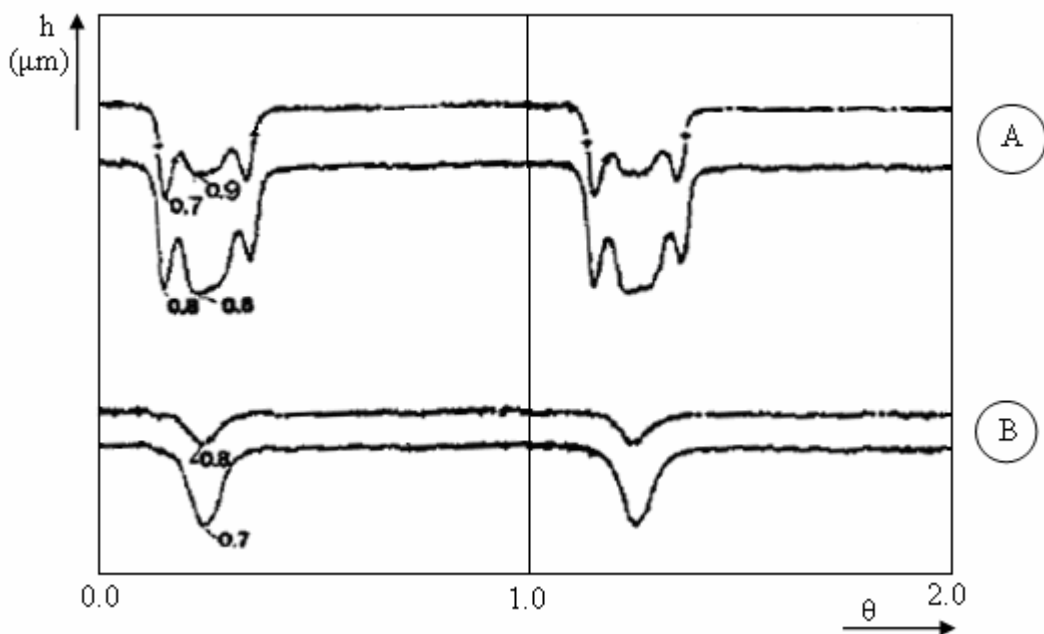


Figure 25: Film thickness in a cam/follower contact [54]

A great deal of research effort has been put into the measurement of the lubricant film thickness in the contact between the piston ring and cylinder liner of internal combustion engines. Furukama and Sumi [55] use two methods to evaluate oil film thickness of the piston-ring. One is to measure the electrical resistance/capacitance of the contact between the

cylinder and the piston ring, and the second is to measure the circumferential displacement of the gap of the piston ring. They concluded that estimation of the film thickness by direct measurement of the electric resistance and capacitance between the cylinder and ring is very difficult, due to metallic contacts between these components. Despite this, the second method did allow the authors to successfully evaluate the film thickness, with the results showing minimum film thickness at top dead centre (TDC) and bottom dead centre (BDC) and maximum at mid stroke. They also showed that the film thickness is proportional to $\mu U/W$, where μ is the viscosity of the oil, U is the speed and W the load.

Hamilton and Moore [56, 57] were able to overcome the difficulties Furukama and Sumi had encountered by employing a flat capacitive probe of a very small diameter (1.25mm), and by doing so, were successfully able to use capacitance measurements to evaluate the film thickness between piston ring and cylinder. The arrangement used by Hamilton and Moore is shown in Figure 26.

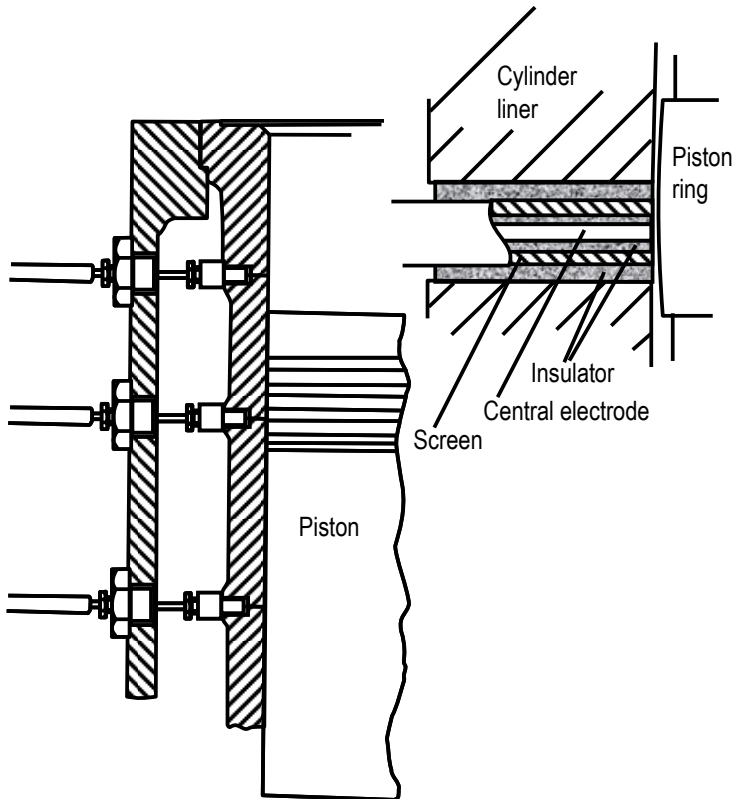


Figure 26: Arrangement of capacitive sensors for measurement of ring oil film thickness [56]

The capacitance is calibrated against a separation between plates, which is measured using a surface profilometer. The film thickness detected was in the range of 0.4mm to 2.5mm, and they concluded that the lubrication mechanisms in piston/ring systems are essentially hydrodynamic.

Sherrington et al. [58] describe the principle of operation of a novel capacitance based transducer which is employed in a bench mounted turbocharger to identify oil leakage from the “*piston–ring*” type seal at the turbine end of the shaft. The transducer developed by Sherrington et al. [59] is used to accurately measure and monitor lubricant film thickness in an internal combustion engine and is presented in Figure 27.

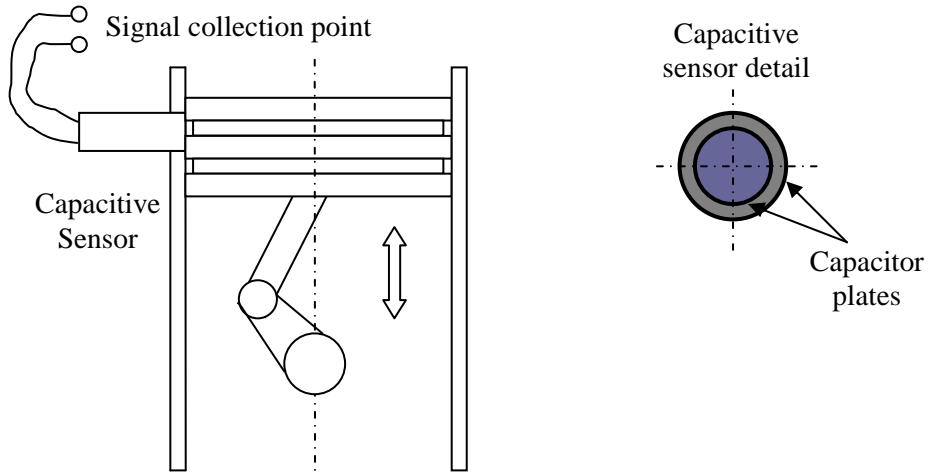


Figure 27: Experimental setup film thickness measurements between a piston and a cylinder [59]

Later research conducted by Grice, Sherrington et al. [60] described the designing and testing of a capacitance transducer to accurately measure hydrodynamic oil films over the range of $0.5\mu\text{m}$ to $20\mu\text{m}$. The transducer is based on the parallel plate capacitor theory which states that:

$$C = \frac{\epsilon_0 \epsilon_r A}{d} \quad (101)$$

Film thickness measurements were obtained by measuring the capacitance between the liner surface and the ring profile under investigation. They observed that the oil film thickness remained constant, regardless of the transducer position phenomenon, as observed by Hamilton and Moore [56, 57]. Accuracy was verified by employing different types of piston rings, a parallel faced compression ring and a tapered ring. The obtained results showed that the method is precise enough to observe different geometries of piston rings.

A review paper on multiple methods for measuring oil film thickness between piston rings and cylinder liners was again written by Sherrington [61]. Among the many electrical methods described by the author, worth mentioning is electrical resistance (which involves electrically insulating a ring or portion of a ring, connecting a small DC voltage and using a bridge arrangement to measure changes in resistance), or the inductance method (that uses some of the most responsive sensors to measure film thickness and temperature). The capacitance

method described there is similar to the one used in [59] to measure the film of oil between a piston ring and a cylinder liner.

Figure 28 gives a more detailed view of a capacitive transducer mounted in the cylinder liner of an internal combustion engine with the added benefit that that the amount of lubricant can now be controlled by using a ring pack lubrication system.

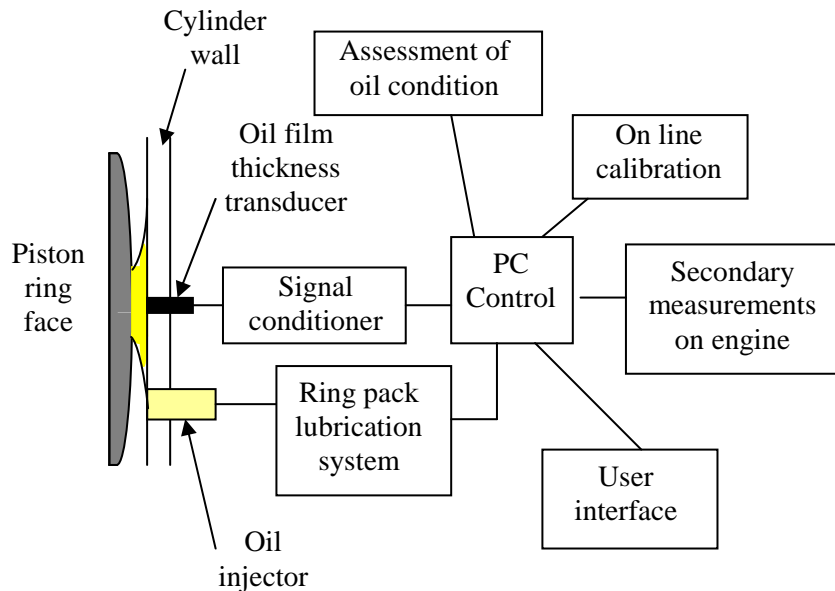


Figure 28: Lubrication control system for large two stroke marine diesel engine [61]

In their paper in 2001, Ducu et al. [62] developed a new type of capacitive probe for measuring film thickness between a piston ring and a cylinder for internal combustion engines. Before starting the tests, the authors knew that the measuring region needed to be flooded and the dielectric constant of the oil had to be known. After trying different types of probe shapes, they concluded that a rectangular shaped probe gave the best results. The research focuses on designing the capacitive probe; hence a lot of attention was given to insulating, eliminating and optimising the capacitive probe, rather than testing in multiple conditions.

In 1974 Karastelev et al. [63] measured the film flow through a 20mm tube by inserting a 0.2mm diameter needle in the tube and measuring the capacitance using a low frequency amplifier. They claimed that the accuracy of measuring the thin film thickness increased with an increase in frequency and voltage, but the largest film thickness which could be measured decreased appreciably. The method was sufficiently accurate to measure film thicknesses higher than 0.5mm.

Severens et al. [64] presented a new approach in measuring a thin film by measuring the phase shift of a capacitive transmission line. Although the authors used amorphous–hydrogenated silicon, the method is interesting because no wires were attached to either of the capacitor plates. They focused mostly on the design of the method and the results were based on different electrode dimensions. They concluded that the electrode width must be significantly larger than the measured gap.

In their paper Zheng et al. [65] optimised the electric parameters of the capacitance–resistance oscillation and developed an instrument for measuring EHL oil film thickness. The results found, agreed with the theoretical results derived from calculations, with an increase in film thickness, leading to a decrease in the measured capacitance. Figure 29 and Figure 30 present the electrical and experimental setup representation utilized by Zheng.

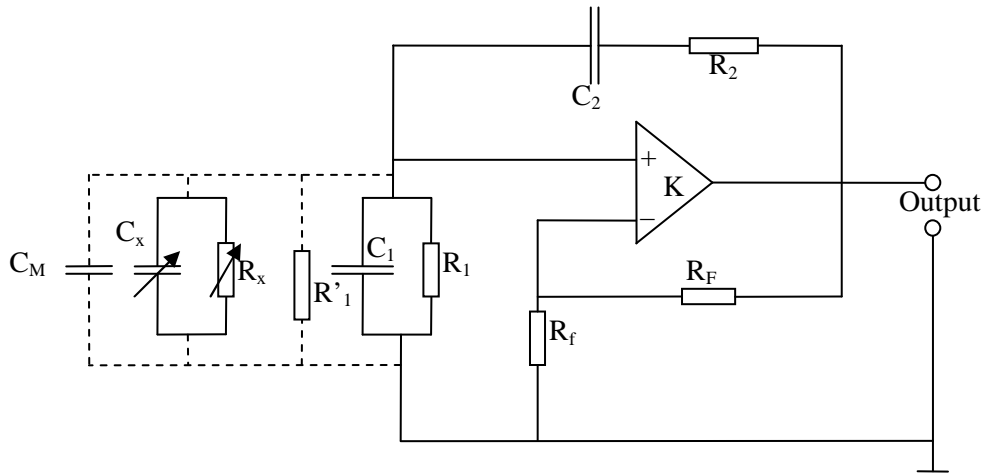


Figure 29: Wien's bridge used by Zheng to measure EHL oil thickness [65]

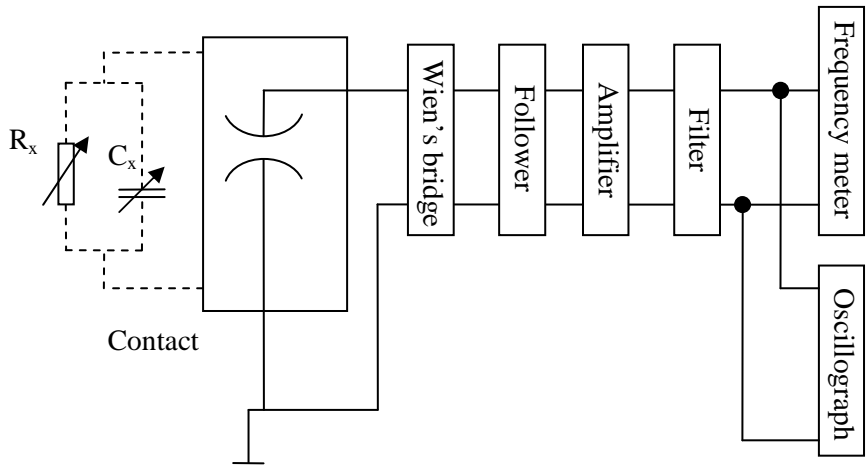


Figure 30: Zheng et al. experimental setup [65]

Nakano and Akiyama [66] developed a new inductive method for measuring oil film thickness for loaded boundary film between metal surfaces, by employing a metal surface and a mercury bath to minimize the effects of surface roughness of the two contacting bodies, as shown in Figure 31. Oil is squeezed between the two surfaces and the time evolution of lubricant film

thickness and coverage was recorded using complex impedance analysis. The authors found that the coverage is proportional to the film thickness squared in a range of 2nm to 40nm.

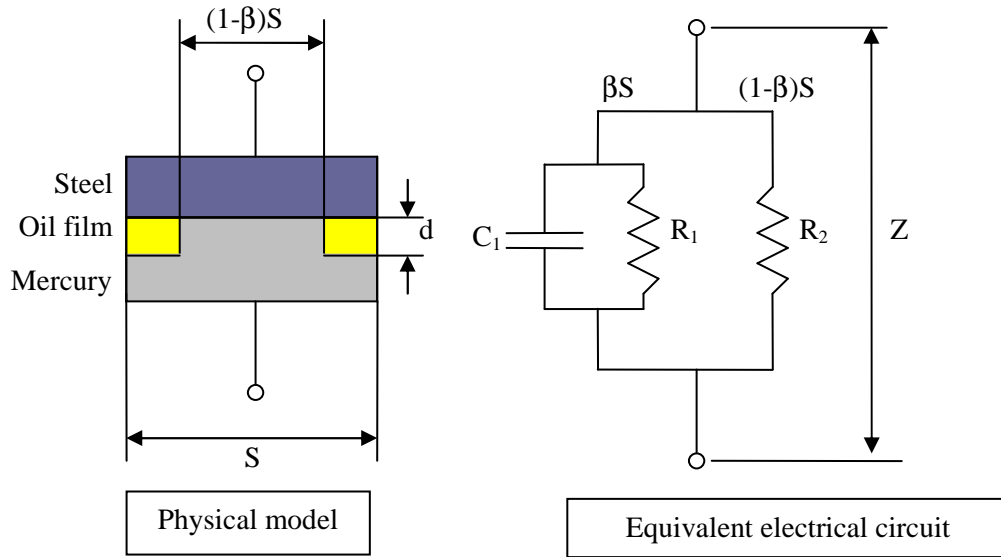


Figure 31: Steel–oil–mercury system [66]

Wilson [67] uses a new capacitive method to measure the grease film thickness in an entire bearing. The aim of the Wilson's research is to develop a method for measuring the thickness of grease films between rollers and rings, to compare the thicknesses of films formed by a grease over a range of speeds and temperatures, with those predicted for its base oil and to ascertain whether grease films become thinner with time, in bearings that were lubricated only at the start of a prolonged period of running time. In bearings plentifully supplied with grease, Wilson found that the lubricating films were about 20–25 percent thicker than predictions. When not replenished, the grease films rapidly became thinner than predictions for the base oil and for the same speed and temperature, bearings flooded with the base oil ran hotter than grease–lubricated bearings affected by starvation. The setup used by the author is presented in Figure 32.

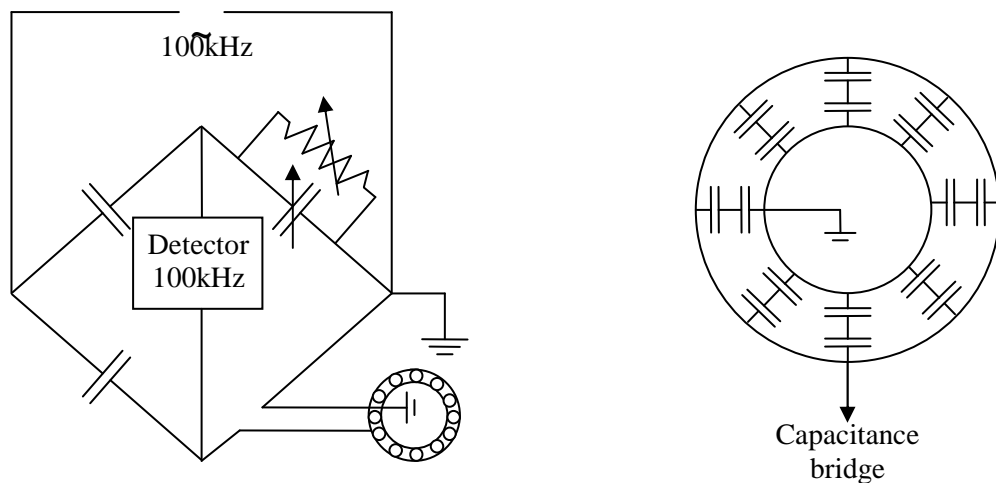


Figure 32: Diagram of the Capacitance Bridge and associated equipment [67]

Iulius and Dusulita [68] measured the oil film thickness in an anti-friction bearing, using a capacitive method. They concentrated more on the actual method of measuring the film thickness and did not show any actual results obtained with their method. However, the main conclusion of their tests was that high values of capacitance that correspond to very thin film thicknesses cannot be measured using the experimental method developed by them.

3.2.3 Detection of asperity contact in mixed regime

Due to its simplicity, the electrical resistance method was also used relatively considerably for the study of the mixed lubrication regime. The first notable work on resistance was conducted by Furey [69]. He used a test rig in which the instantaneous and average resistance of a contact formed between a fixed ball and a rotating cylinder are measured. The resistance of the contact was found to oscillate rapidly between very low and very high values, suggesting metallic contacts and full film conditions, typical to the mixed lubrication regime. Frictional force was also recorded simultaneously. These experiments allowed Furey to investigate the lubrication regime in a wide range of film thickness, i.e. from 0–100% metallic contact, which correspond to hydrodynamic and boundary regimes respectively. He stated a value of 104 ohms as a criterion of fluid film lubrication, which is considered by Chu and Cameron [70] as arbitrary.

Tallian et al. [71] modified and refined Furey's technique to accommodate the measurement of electric conductivity of the elastohydrodynamic contacts in a four-ball tester as shown in Figure 33.

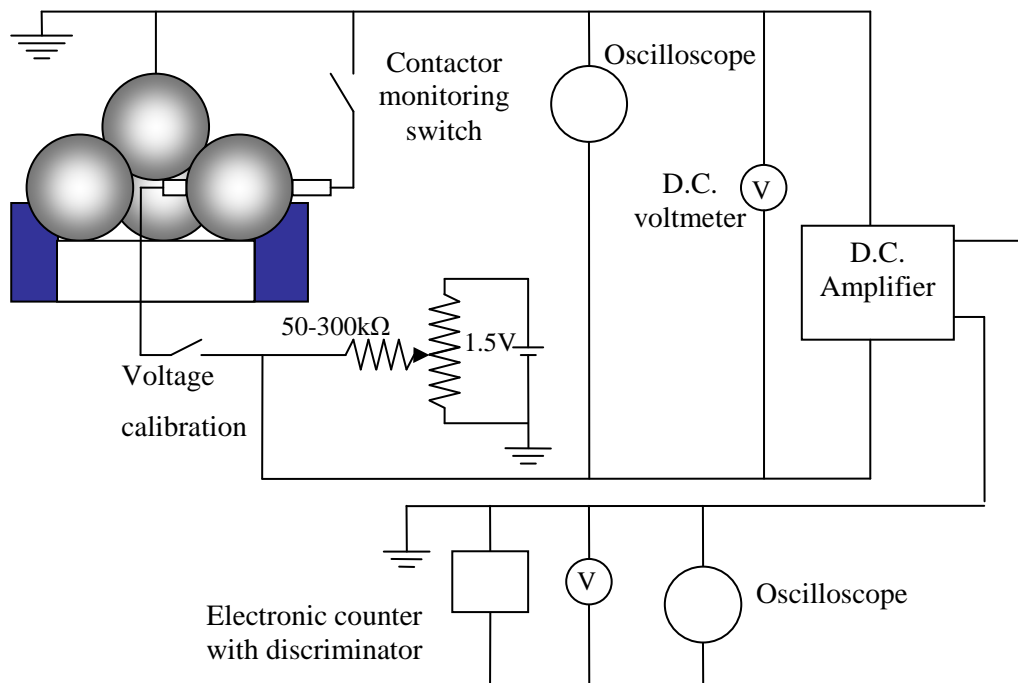


Figure 33: Schematic of Tallian's conductivity test circuit [71]

They compared, measured and computed values of the duration and frequency of electrical contacts between specimens and extracted estimates of the average film thickness as a function of speed and load. Palacios [72] also evaluated the occurrence of metallic contacts in a four-ball tester using the electrical resistance technique. He correlated the out-of-contact roughness with the number of contacts per unit time and monitored their evolution during the running-in process.

Napel and Bosma [73] studied the effect of the surface roughness upon the measurement of elastohydrodynamic film thickness using a capacitive method. They tested a linear contact and observed that there is a marked deviation of the measured film thickness and theoretical values predicted by the Dowson and Higginson formula. The error was attributed to the calibration of the film thickness against the capacitance estimated for a capacitor with perfectly smooth surfaces.

Guanteng et al [74] correlated electrical resistance with the lubricant film thickness and the friction force generated in a mixed lubrication regime EHD contact. They used optical interferometry to map the film thickness across the contact and directly interpret the electrical contact resistance in terms of film thickness distribution. A schematic of their electrical circuit is shown in Figure 34.

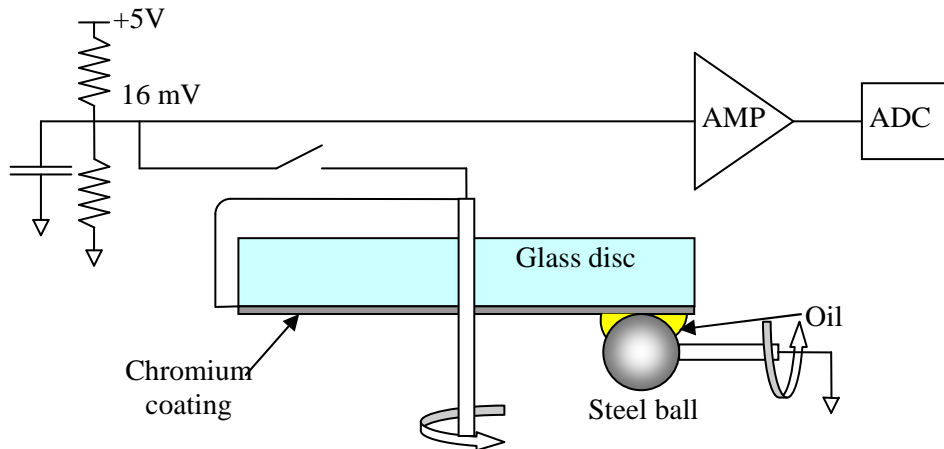


Figure 34: Schematic of the electric circuit [74]

They found that there is a threshold film thickness below which asperity contact occurs inside an EHD contact, dependent on the lubricant properties and the roughness parameters.

Lord and Larson [75] explored the film formation of base and fully formulated gear oils in mixed lubrication regime, by measuring the impedance of the contact. Their method automatically supplied simultaneous values of the resistance and the capacitance of the contact, the former describing the amount of metallic contact and the latter showing the separation between the surfaces.

3.2.4 The effect of an electric field upon lubrication phenomena

The application of electrical methods for the study of film thickness in lubricated systems has led to detailed studies on the behaviour of lubricating films subjected to an electrical field and those aimed at the evaluation of the dielectric properties of lubricants. All these approaches are related to each other, as it seems that the electric field can change the frictional behaviour of lubricated contacts, which in turn modifies the heat generated through friction, the viscosity of the lubricant and consequently the film thickness.

Studies on the effect of the electric field upon the life of rolling elements bearings have long been researched [76–79]. These studies have focused on the occurrence of pitting stimulated by the passage of the electric current through the bearings of electrical machines. Kure and Palmetshofer [78] stated that the risk of damage occurs when the voltage exceeds 0.5V or the current flow is more than 0.1A/mm^2 , whilst Prashad [79] has found that voltages as low as 200mV can cause failure of the rolling elements.

Yamamoto et al. [80] studied the effect of the applied voltage upon friction and wear characteristics in the mixed lubrication regime. They used a ball-on-pin arrangement, focusing on the friction characteristics of elastohydrodynamic contacts in various regimes of lubrication, in the presence of an electric field. A schematic of the electric circuit used to detect the film thickness is shown in Figure 35. They found that the presence of the electric field caused an oxide film to form at the anode side, which changes the friction and wear pattern on the specimens, whilst the element connected to the cathode showed abrasive wear. These findings can actually help to obtain favourable running-in.

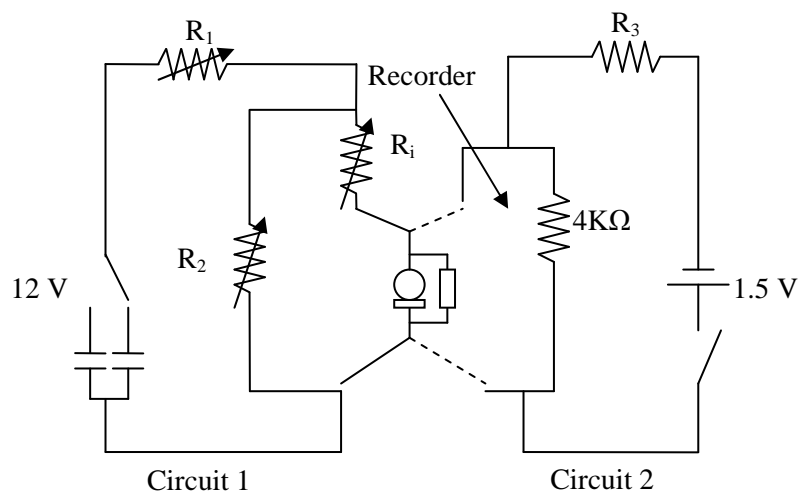


Figure 35: Electrical circuit for measuring the degree of separation between specimens [80]

They also concluded that the presence of an electric field promotes the breakdown of the EHD film in full film conditions, whilst in mixed and boundary regimes frictional characteristics can be improved by the presence of an electric field.

Luo et al. [81] have investigated the formation of ordered layers in elastohydrodynamic contacts subjected to an external electric field. They found that film thickness and friction coefficient are related to the voltage applied. A stronger electric field will produce thicker films in pure rolling conditions, while increasing the friction coefficient under pure sliding. Xie et al. [82] studied the lubrication phenomena in the bearings of electrical motors, (which are inherently subjected to an electric field) and reported the formation of gas bubbles in EHD film.

Carey [83] analysed the effects of additive presence in lubricants and the influence of additives on the dielectric constant of oils. He concluded that by constantly monitoring the dielectric constant of lubricants in operating systems, the quality of oils, presence of different contaminants, and therefore the lubrication regime can be continuously checked.

Rococea et al. [84] presented the effects of an electrical current passing through angular bearings. They tested several grease lubricants in different conditions, such as normal load and speed in order to determine which has the largest influence on the passing of electricity through the bearings. For different types of lubricants, the electrical resistance varied considerably due to the different chemical compositions of the grease. By testing a wide range of loads, Rococea et al. concluded that with an increase in load, (and implicitly in contact diameter), the discharge voltage decreases and when speed is varied the discharge voltage increases with an increase in speed, due to an increase in lubricant film thickness.

3.3 Other Methods for Measuring Lubricant Film Thickness

3.3.1 Ultrasound

A new method based on the reflection of the ultrasound from a liquid layer situated between two solid bodies makes possible the deduction of lubricant film thickness by comparing the frequency spectrum of the reflected pulse with that of the incident pulse [85]. This reflection depends on the ultrasonic frequency, the acoustic properties of the liquid and solid, and the layer thickness. If the wavelength is much greater than the liquid–layer thickness, then the response is governed by the stiffness of the layer. If the wavelength and layer thickness are similar [85], then the interaction of ultrasound with the layer is controlled by its resonant behaviour. The EHD lubricant film that forms between a ball sliding on a flat surface was also measured ultrasonically. The measured results agree well with theoretical predictions, taking into account the greatly increased speed of sound through the lubricant when it is under high pressure. Equation 102 presents Dwyer–Joyce et al [85] approach to measure lubricant film thickness.

$$R = \frac{z_1 - z_2}{z_1 + z_2} \quad (102)$$

Where:

$$T = 1 - R$$

R – reflection coefficient

T – transmission coefficient

z – acoustic impedance of the media

A big similarity between the optical method and the ultrasonic method is obvious, as the light intensity is equal to one and the sum of both reflection and transmission coefficient, i.e.

$$I = R + T \quad (103)$$

But $I = 1$, therefore:

$$T = 1 - R$$

I – intensity

R – reflection coefficient

T – transmission coefficient

The methodology used by Dwyer–Joyce et al. [85] was capable of measuring films in the range 50–500nm. Figure 36 shows an ultrasonic beam on a typical lubricated contact which represents the three layer system consisting of steel–lubricant–steel. An ultrasonic transducer was mounted on the bearing raceway and the pulse reflected from the lubricant layer as the ball passes was recorded. Again the measured results agreed well with what was predicted theoretically.

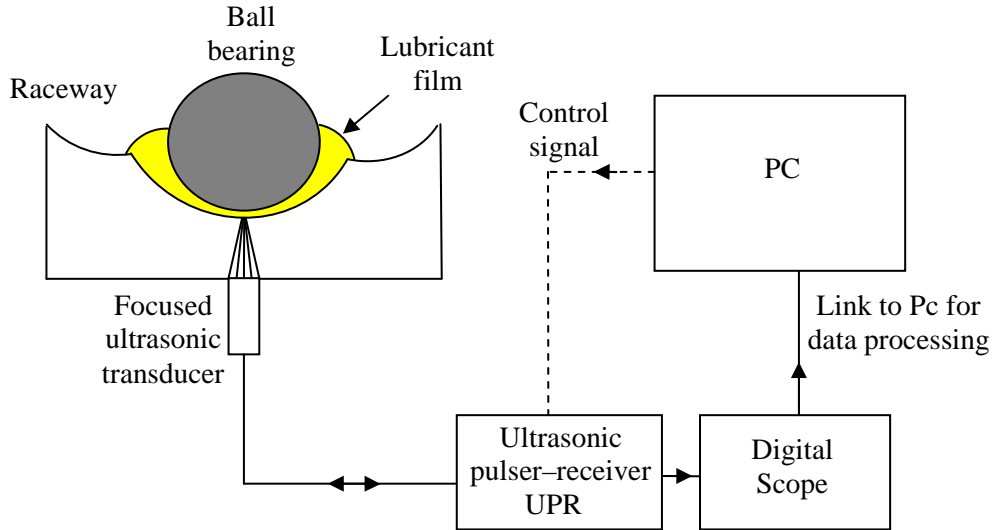


Figure 36: Schematic representation of an ultrasonic beam incident on a lubricated contact [85]

A lubricant-film monitoring system for a conventional deep groove ball bearing is described in [86]. A high-frequency ultrasonic transducer is mounted on the static outer raceway of the bearing. The transducer is focused on the ball-raceway interface and used to measure the reflection coefficient of the lubricant in the “contact” ellipse between bearing components. The reflection coefficient characterizes the lubricant film and can be used to calculate its thickness. An accurate triggering system enables multiple reflection measurements to be made, as each lubricated contact moves past the measurement location. Three contaminant materials (acetone, water, sand) were separately added to the lubricant to initiate failure of the bearing. These contaminants simulated common failure mechanisms that can occur in real life conditions. The ultrasonic reflection coefficient, vibration, and temperature were recorded under these three failure scenarios. The ultrasonic reflection coefficient measurements were shown to provide useful diagnostic information on the failures, as well as an early warning signal.

J. Zhang et al. [87] describe an experimental apparatus and procedure for the calibration of the ultrasonic lubricant-film thickness measurement technique. The calibration apparatus is demonstrated on a three layer steel–mineral–oil–steel system. In industrial bearings systems the lubricant-film thickness typically ranges from $0.1\text{--}100\mu\text{m}$. The calibration apparatus uses a high precision piezoelectric displacement translator to controllably displace one of the steel surfaces relative to the other and hence alter the lubricant-film thickness by a known amount. The response of a lubricant film to an ultrasonic pulse can be predicted using either a spring-layer model or a resonance-layer model. Practical guidelines for use of the calibration are then defined and calibration is demonstrated experimentally over the range $0.5\text{--}1.3\mu\text{m}$.

Reddyhoff et al. [88] uses three methods for measuring the oil film thickness between a mechanical seal and glass/steel disc. They use piezoelectric transducers mounted on the seal ring equally spaced at 120° to provide some redundancy of the test sensors. The ultrasonic measurements were compared with known optical and capacitive measurements and were found to give good results and even predict seal failure. A schematic representation of the setup used by Reddyhoff et al. [88] is shown in Figure 37.

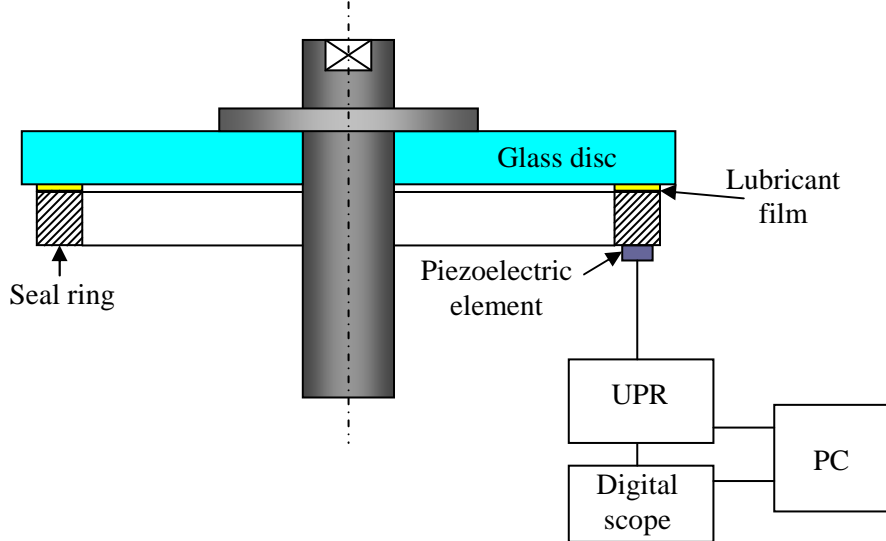


Figure 37: Experimental setup for ultrasonic lubricant measurements [88]

3.3.2 Laser induced fluorescence

Another optical method used for monitoring and measuring the lubricant film is Laser Induced Fluorescence (LFI) method, which was studied thoroughly by [89–92].

The measurement of liquid films from 10–60 μm thick, have been studied using photo-chromic dye activation by F. E. Hoge [89]. The method utilizes the change of the dye from a colourless form to a coloured form when irradiated with a specific wavelength. Based on the characteristics of the photo-chromic dye, when a thicker liquid film is irradiated with a beam of a fixed intensity, the colour will be darker because the number of dye molecules increases at a fixed dye mass fraction. The results show that the best wavelength to be used with this dye is 340nm, since at this wavelength the dye gives the optimum excitation and absorbance. Successful film thickness measurements were obtained for the proposed oil types. The results obtained show that for a highly absorbent oil the maximum absorbance happened at a oil film thickness of 100 μm whereas for a lower absorbance the max film thickness goes up to 1mm.

Another laser method [90] describes the calibration of a technique allowing quantitative measurements of industrial coatings with thicknesses as small as 10–20nm. Wax films doped with a fluorescent rhodamine dye were deposited by an electro-spray method onto an optically

flat surface of aluminium-coated glass, as shown in Figure 38. The films were of 220–450nm peak thickness, which were measured with an optical profilometer using laser triangulation. Fluorescence emitted from the samples was measured using a fibre-coupled probe with laser excitation and spectral detection (Figure 39). The fluorescence emission was shown to be reduced by a factor of ten by the presence of the aluminium layer. The calibration yielded thicknesses of industrial foil release coatings determined by on-line fluorescence measurement that were in agreement with thicknesses estimated from bulk measurement of the take-up of solution in the coating process.

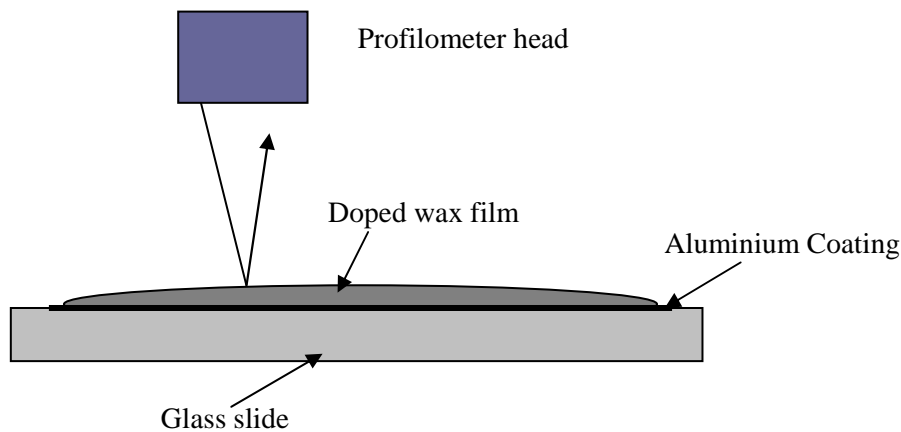


Figure 38: Schematic diagram of a profilometer scan of a calibration slide [90]

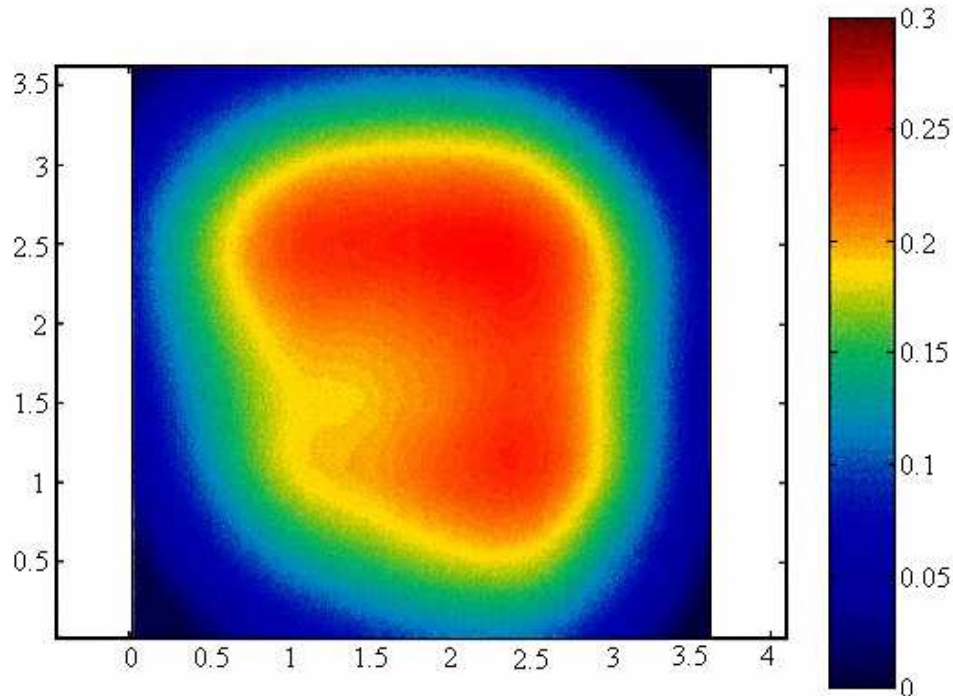


Figure 39: Calibration sample with a maximum wax thickness of 255 nm [90]

In order to allow quantitative determination of temperature and film thickness in internal combustion engines (ICE), Ostroski used of a fluorescent dopant molecule to enhance the natural fluorescence of motor oils [91]. Measurements of the fluorescence as a function of temperature were made with unaltered Mobil 1, and solutions of the dopant BTBP in mineral oil and Mobil 1. It was found that the fluorescence of Mobil 1 varied by up to 30% with temperature, but the spectral characteristics were unaffected. This made the direct determination of the temperature, which would allow a temperature correction to be made to the fluorescence, impossible. A solution of BTBP in mineral oil exhibited a marked increase in fluorescence yield with temperature. Additionally, the spectral content was found to change with temperature, allowing a direct determination of the oil temperature for temperatures above 40°C.

4 EXPERIMENTAL METHODS EXPLORED BY THE AUTHOR

4.1 Optical Interferometry [92]

4.1.1 Introduction:

The lubrication of rough surfaces has been a focus of researchers in the field for many years now. A good deal of work has been carried out either on the experimental or on the theoretical sides of the research. From the experimental point of view it is obviously more convenient to study the lubrication of artificial roughness features such as ridges, bumps or dents rather than real, random roughness. The advantage of model roughness features is that they are well individualized, located, and characterized, thus a comparison of the surfaces geometry inside and outside an elastohydrodynamic contact can be made. The studies carried out so far have focused on the effect of the geometry of the features and that of the entrainment speed. No detailed experimental work on the effect of the lubricant properties on the behaviour of the EHD films has been performed, to the authors' knowledge. The present study uses the optical interferometry method to measure the EHD film thickness between a flat disc and a ball on which artificial ridges have been sputtered. Two lubricants, with different viscosity and pressure/viscosity coefficient are used in a range of pressures and entrainment speeds.

4.1.2 Experimental Set Up and Procedure:

The method used in the present study, for measuring the elastohydrodynamic film thickness, is the optical interferometry. A schematic of the experimental set-up is shown in Figure 40. The contact is formed between a transparent, flat disc and a steel ball, on which the roughness features are deposited. A number of six ridges, whose length extends well beyond the diameter of the contact and one very short, were sputtered on the surface of the ball. This will allow locating exactly the position of the each feature inside the contact, for comparison with its geometry outside the contact. The maximum height of the asperities is 85 nanometres and they are approximately of sinusoidal shape.

[92] M. D. Furtuna, R. P. Glovnea "An Experimental Investigation into the Effect of Lubricant on the Local Film Thickness of Artificial Roughness Features" Proceedings of the STLE/ASME IJTC 2008, Miami, Florida

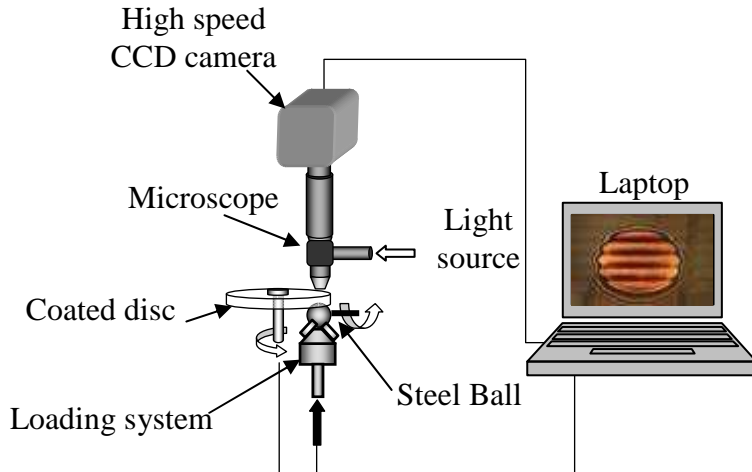


Figure 40: Experimental set-up

The disc is coated with a thin, semi-reflective chromium layer and a spacer layer made out of silica, approximately 135 nanometres thick. White light is used in this technique, which means colour interferometric patterns are analyzed according to calibration curves, which relate RGB of each pixel of the image to the separation between the ball surface and the chromium layer. Two discs were employed in this study, one made of glass, with elastic modulus about 75GPa, and the other of sapphire, with an elastic modulus of about 370GPa. Loads of 20N and 30N were employed, which gave, with the two glass and sapphire discs, pressures of 0.5GPa and 1.1GPa respectively.

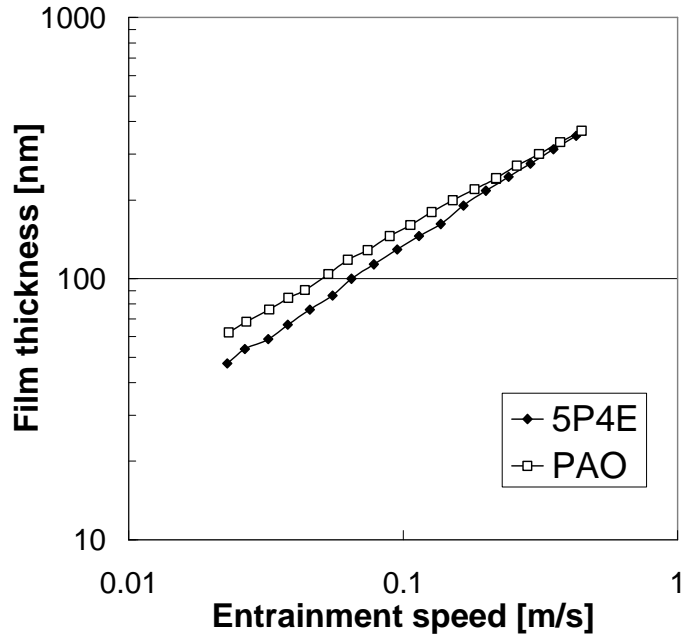
Both the disc and the ball are driven by DC controlled motors at desired speeds such that a combination of rolling and sliding rolling conditions can be set.

The lubricants used are a polyalphaolefin (PAO) and a polyphenyl ether (5P4E), with the relevant properties, at the temperature of the tests, listed in Table 2. The pressure/viscosity coefficient was estimated from film thickness tests, as suggested in [93].

Table 2. Lubricant properties

Lubricant	η [Pa•s]	α [GPa $^{-1}$]
PAO	0.121	19.5
5P4E	0.068	26

The tests were carried out at 60°, temperature at which both lubricants gave similar smooth ball film thickness, at low values of the entrainment speed, as seen in Figure 41.

**Figure 41: Smooth surfaces film thickness**

4.1.3 Results and Discussion:

Figure 42 shows the profile of the separation between the ball and the glass disc, for both 5P4E and PAO, at a speed of 40mm/s, in pure rolling conditions. The striking difference between the two oils is the amplitude of the film thickness variation. For the high pressure/viscosity coefficient oil, the 5P4E, the amplitude is about that of the undeformed height of the asperities, while for the low pressure/viscosity oil, PAO, the amplitude is about 70 percent of the undeformed height. A possible explanation of this behaviour is fluid leakage from the valleys. The high pressure/viscosity coefficient of 5P4E results in a very large effective viscosity, which make it very difficult to escape at the peripheries. At the same time PAO has an effective viscosity inside of the contact of more than ten times lower, thus is more likely to leak away from the contact.

The results for pure rolling and similar entrainment speed, but with a sapphire disc, are shown in Figure 43. The trend observed for glass, i.e. the compression of the asperities is greater for the low pressure/viscosity coefficient oil, is maintained for this new conditions. On the other hand, both oils show greater compression of the asperities, than was the case of the glass disc, which can be expected, as in the case of sapphire disc, the pressure is at least double in comparison to glass.

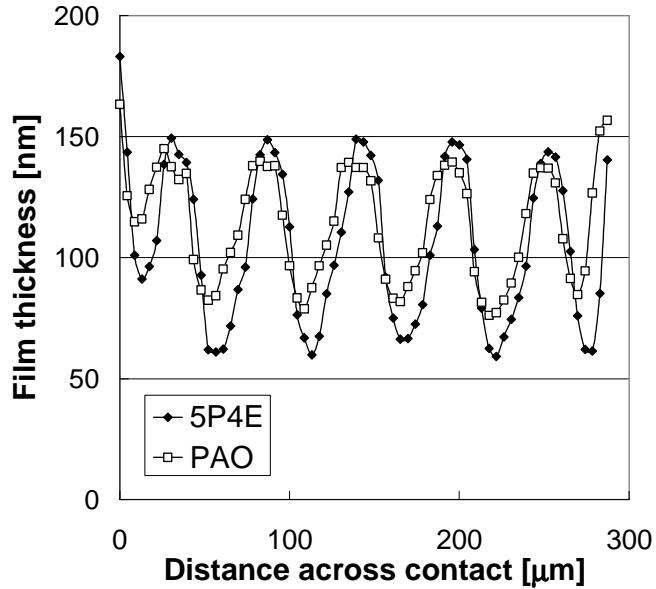


Figure 42: Film thickness for glass disc, 20N load

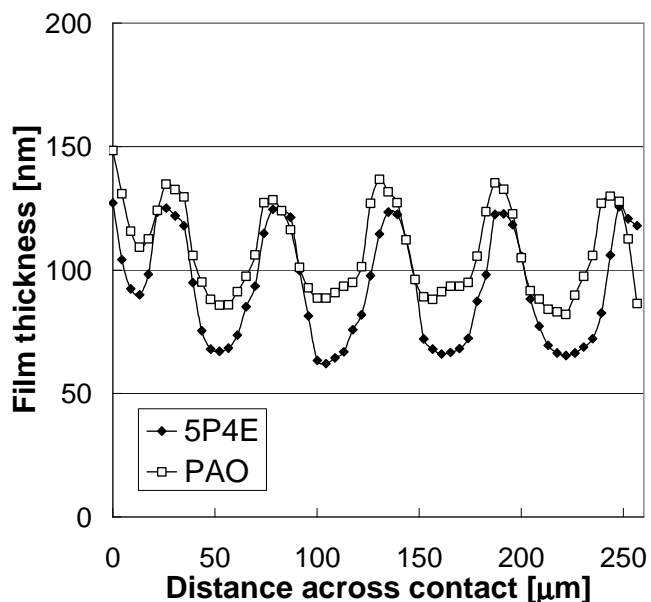


Figure 43: Film thickness for sapphire disc, 30N load

4.1.4 Conclusions:

Optical interferometry has been used to investigate the effect of lubricant properties upon the behaviour of the elastohydrodynamic film in the presence of artificially created ridges, transversally oriented relative to the rolling direction. It has been found that, in pure rolling conditions, the lubricant with lower pressure/viscosity coefficient shows the amplitude of the asperities, inside the contact, about 70 percent of that measured for the high pressure/viscosity lubricant. This can be attributed to side leakage of the lubricant through the valleys separating the ridges.

4.2 Experiments on Grease Lubrication by Fluorescence

A number of experiments have been carried out by the author on an exchange program between Brunel University and Kyushu University in Japan under the supervision of Professor Joichi Sugimura. The results obtained in this exchange program are being analysed and will be published in a paper.

The main objective of this investigation was to obtain an alternative method, to optical interferometry, for the calibration of the electrical capacitive method.

4.2.1 Introduction:

It is important to be able to observe and measure lubricating films in order to understand the mechanism of film formation and breakdown in the mixed and thin film regimes. Many methods have been developed over the years starting with electrical and going to optical methods, the ultra thin film interferometry method is one of the most used today due to its precision to measure accurately film thicknesses down to one nanometre thick.

The disadvantage of the UTFI method is that the contacting surface has a semi-reflecting coating sputtered on it to provide the necessary phase change, this reflecting layer is fragile and it worn down quite fast when sliding conditions and very thin lubricant film are measured. The alternative to this optical method is to use fluorescence, where a thin film even smaller than the light wavelength can be visually detected if it emits fluorescence light [94].

The great advantage of the fluorescence technique is that it does not require a coating of the specimens in contact, making it ideal to employ sever sliding conditions.

4.2.2 Experimental Set Up and Procedure:

A fluorescent substance absorbs radiation at a certain wavelength and re-radiates some of the absorbed energy at a lower wavelength [95], these wavelengths depend on the electrochemical properties of the substances. In most cases the optimum absorption is the wavelength in the ultraviolet region. Contact between a sapphire disc and a steel ball was employed.

The resulting track on the sapphire disc was analysed using Fourier Transform Infrared (FTIR) spectroscopy. The setup for this stage of the tests is being presented in Figure 45.

Figure 44 shows a schematic representation of the test rig. A sapphire disc is being span by an AC servomotor, which is controlled to have constant speed. A steel ball specimen with the diameter of 15 mm is pressed against the sapphire surface; the ball is also driven by an AC servomotor to achieve controlled pure rolling and sliding conditions. The contact is being lubricated using fluorescent grease described in Table 3.

In order to illuminate the contact surface and obtain fluorescence from the fluorescent substance in the ultraviolet region, a 100W high-pressure mercury lamp has been used. The microscope is also equipped with a filter unit that consists of an exciter filter, a dichroic mirror and a barrier filter. The filter unit allows only part of the light to pass, which is strongly

absorbed by the fluorescent substance, while allowing only fluorescent light that has a longer wavelength than the absorbed light wavelength, to be viewed by the observer.

The contact is observed using a B&W CCD camera; the recorded images will be analyzed using a piece of software. The test speeds have been kept constant throughout the measurements the test conditions are presented in Table 4. The experiments were carried out in a clean room where the temperature was kept at a constant of 22°C.

Table 3: Grease properties

Grease	Base oil	Viscosity of base oil [cSt] @ 40°C	Thickener	Consistency [% wt]
1.	Poly-alpha-olefin	30	di-urea	13.4
2.	Poly-alpha-olefin	30	LiSt	12
3.	Poly-alpha-olefin	400	LiSt	12

Table 4: Test conditions

Speed [m/s]	Slide/roll ratio
0.05	Pure rolling
	0.2
	0.4

The test pieces were cleaned in hexane and acetone in an ultrasonic bath and air dried. A new grease sample was used every time for each test, the FTIR tests were run several times to check repeatability.

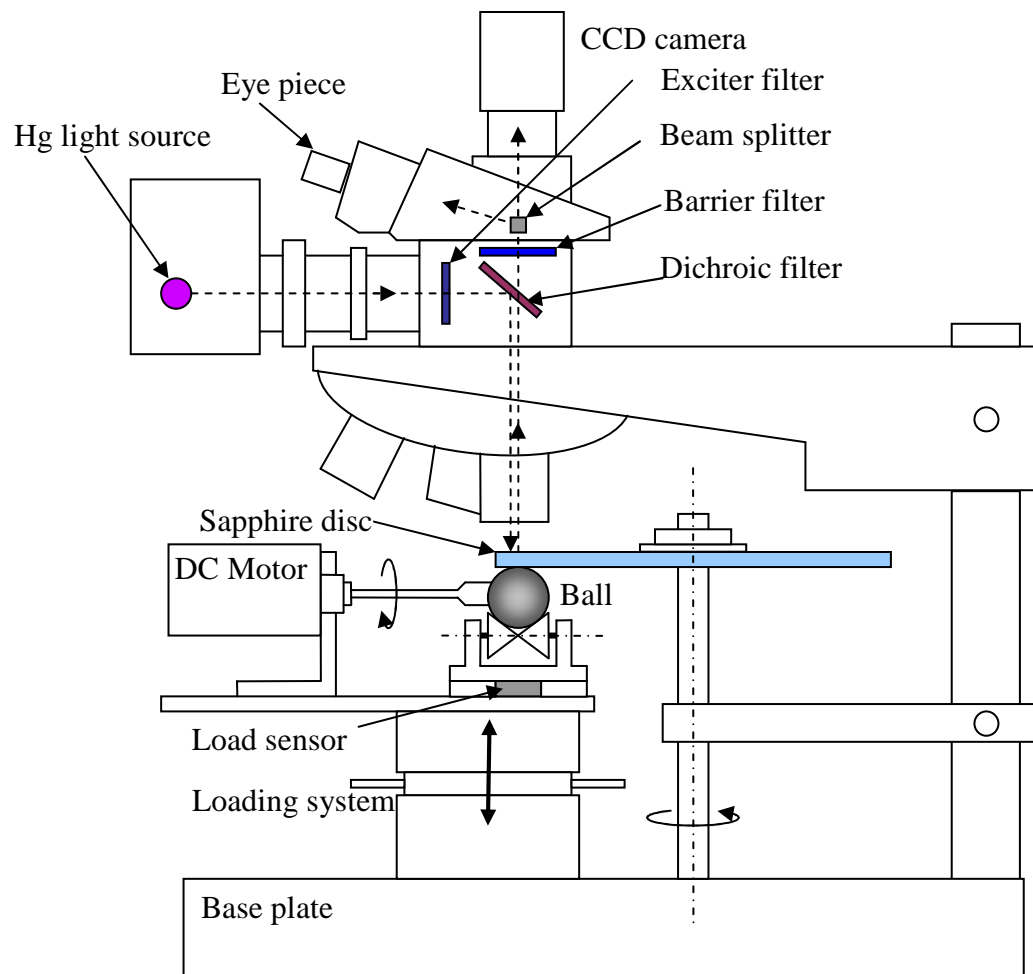


Figure 44: Experimental setup

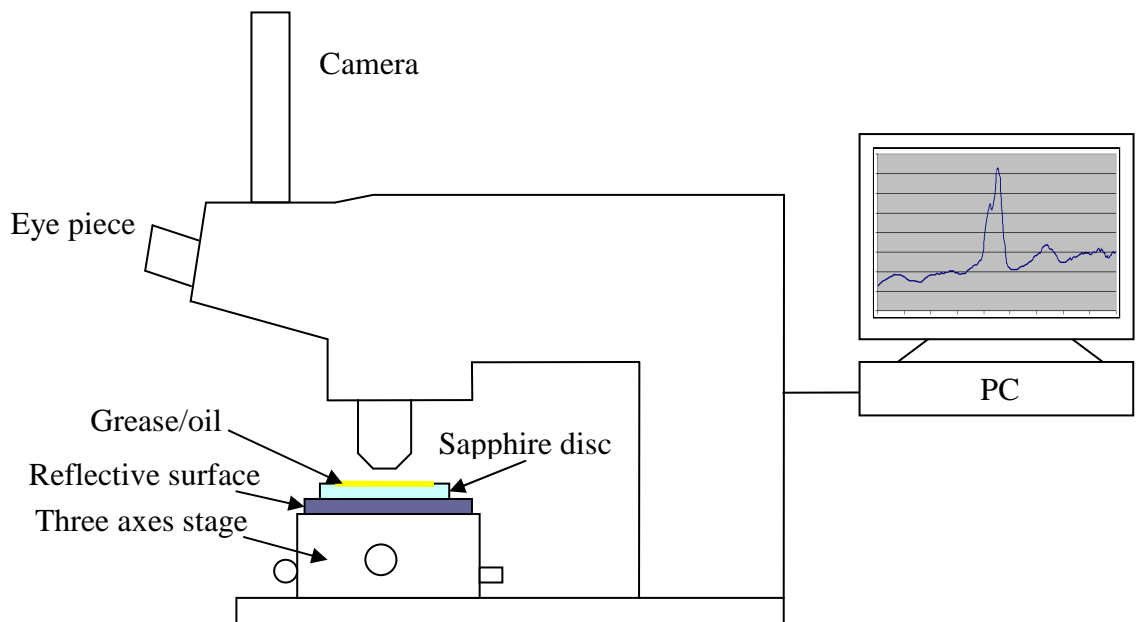


Figure 45: Schematic representation of the infrared spectrometer

4.2.3 Results and discussion

The grease supplier states that the thickener used i.e. Di–urea has fluorescence properties. The aim of the entire research was to see if film thickness measurements can be obtained without any additional mixes with various chemicals that have fluorescence capabilities. Figure 46 and Figure 47 present the images captured for the Di–urea grease in static conditions. As it can be observed from the Figures 48–51 the image quality needed to measure film thickness is not very good compared to work done by previous researchers [94–95] the conclusion was that an additional chemical with fluorescence properties was needed, therefore Pyrene was employed as a fluorescence “booster”. After this conclusion was reached the entire project was overturned and a different approach was needed. The new aim of the research was to see the influence of the thickener on the contact oil replenishment and the influence of different oil viscosities on the lubrication process.

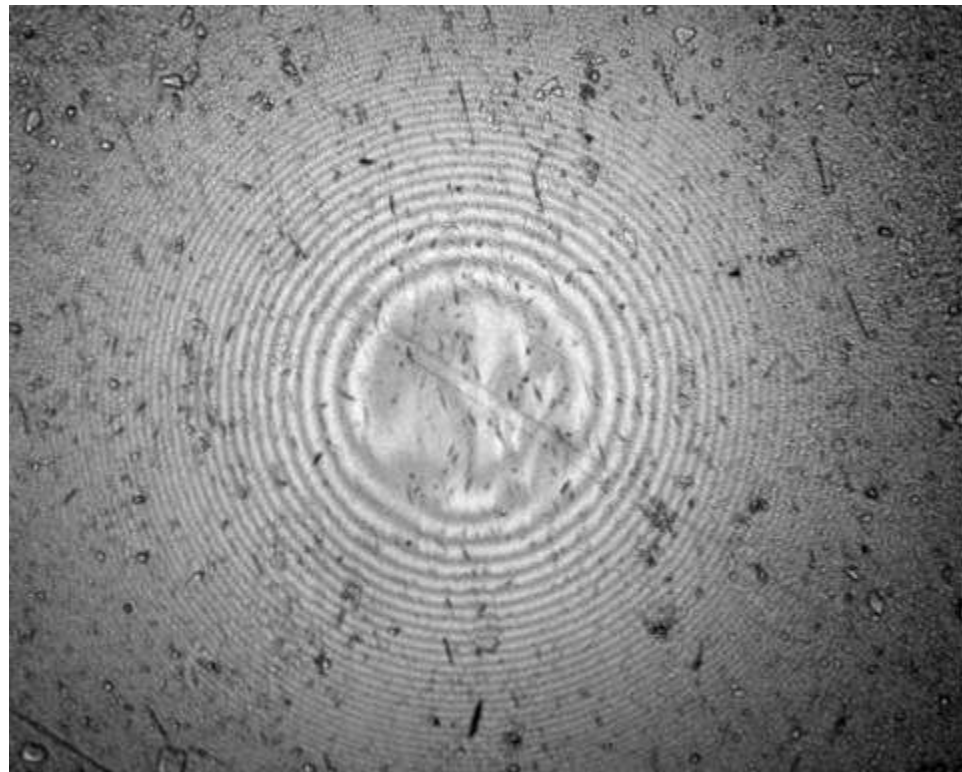


Figure 46: Green light image of the contact before the tests using Di–urea grease



Figure 47: Fluorescence image of the contact before the tests using Di-urea grease

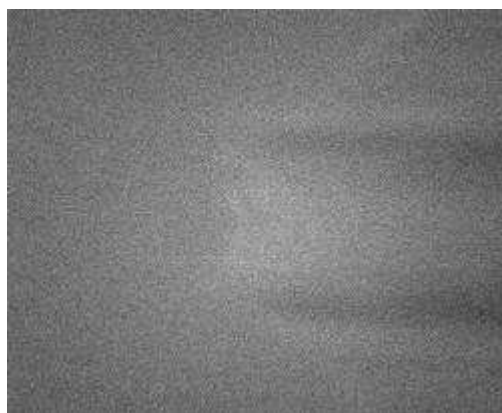


Figure 48: Di-urea grease pure state
One minute into the experiment



Figure 49: Di-urea grease pure state
Ten minutes into the experiment

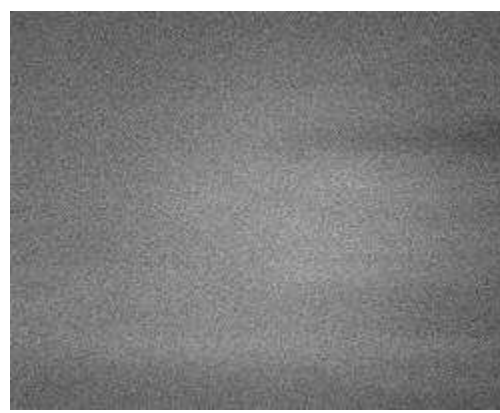


Figure 50: Di-urea grease pure state
Twenty minutes into the experiment

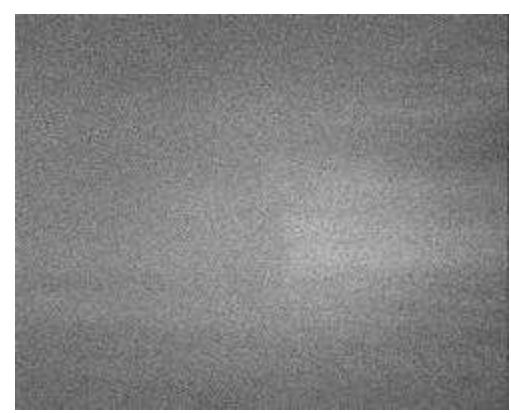
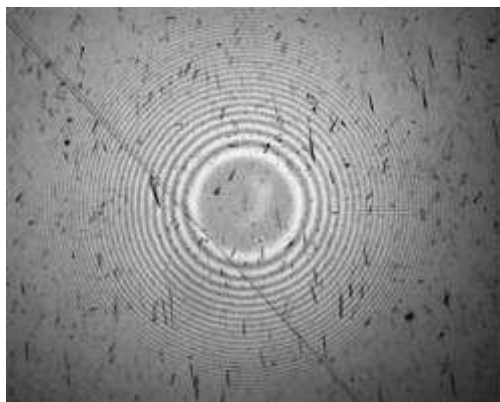


Figure 51: Di-urea grease pure state
Forty minutes into the experiment

The di-urea grease used in the initial tests does not provide normal fluorescence photos to analyze the film thickness; the reason behind this phenomenon is that only the thickener has fluorescence properties not the oil thus making impossible the measurement of lubricant film thickness between the two contacting bodies.

In order to overcome these problems, a new grease had been developed. The grease was mixed with a special chemical, Pyrene. This chemical had very good fluorescence properties and provided good images for observing the lubrication process. The Pyrene concentration used in the grease was 1% wt. The new aim of the research was to see the influence of the thickener on the contact oil replenishment and the influence of different oil viscosities on the lubrication process.

The pictures taken for Lithium Stearate grease with PAO base oil that has a viscosity of 400cSt at a temperature of 40°C and thickener concentration of 12% wt are presented in Figures 52–57. The problem encountered here is that the oil viscosity is so high, that even after over one hour of running, there was no noticeable difference between the captured images. This phenomenon can be observed in Figures 54–57.



**Figure 52: LiSt grease PAO 400
Green light image taken before the tests**

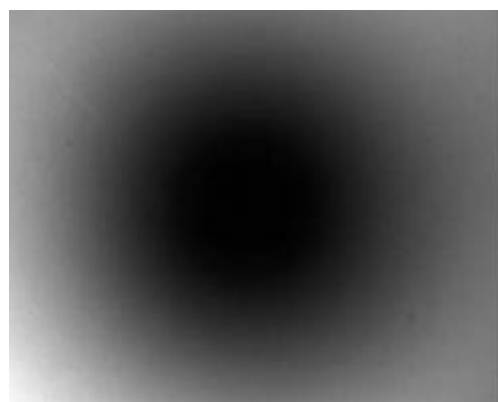


**Figure 53: LiSt grease PAO 400
Fluorescence image taken before the tests**

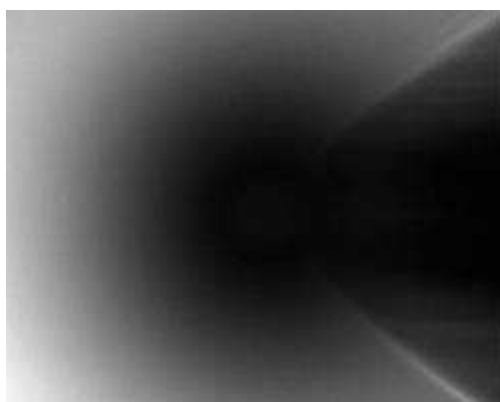


**Figure 54: LiSt grease PAO 400
First minute in the experiment**

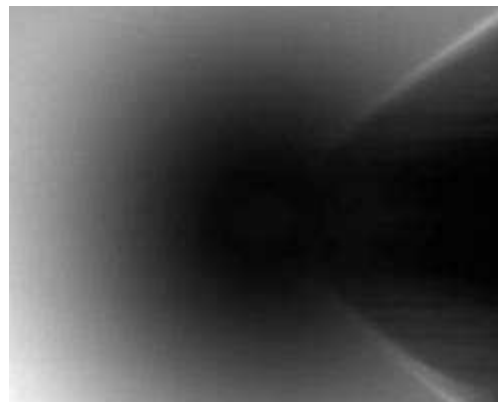


**Figure 55: LiSt grease PAO 400
Ten minutes in the experiment**

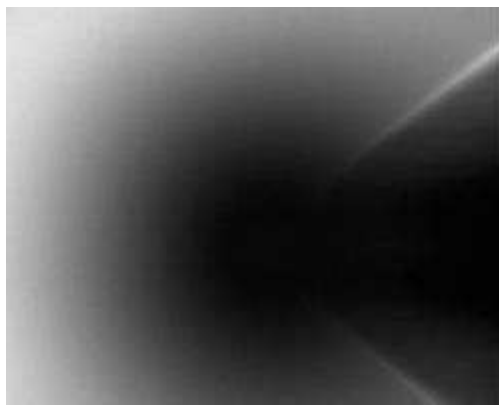


**Figure 56: LiSt grease PAO 400
Twenty minutes in the experiment**

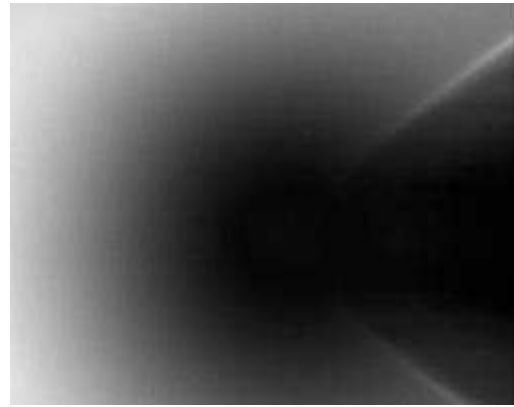


**Figure 57: LiSt grease PAO 400
Forty minutes in the experiment**

Grease with a base oil that has a smaller viscosity was employed to see if the lack of difference between the captured images is due to the base oil or due to the thickener. The grease used in the next batch of tests is also Lithium Stearate and has a PAO base oil with a viscosity of 30cSt, at a temperature of 40°C and thickener concentration of 12%wt. Again no difference can be observed for images captured at a certain time frame. The photos taken for a static contact are presented in Figures 58 and 59.

Contact fringes can very well be seen for the green light image, but not very clear for the fluorescence one; fringes are much better observed for a moving contact than for a static one in the fluorescence setting. This phenomenon is attributed to a thicker film thickness trapped in the static contact. The captured images show the contact fringes indicating a thinner lubricant film, caused by a much smaller viscosity of the base oil and are presented in Figures 60–63.



**Figure 58: LiSt grease PAO 30
Green light image taken before the tests**

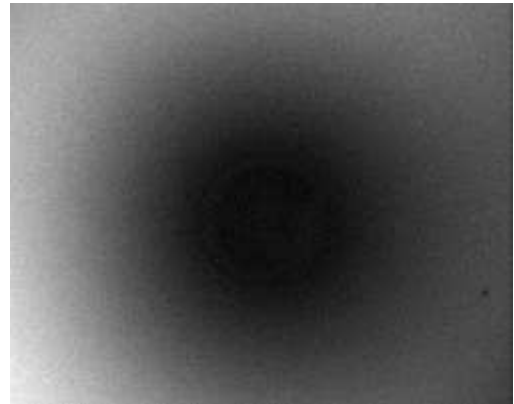


**Figure 59: LiSt grease PAO 30
Fluorescence image taken before the tests**

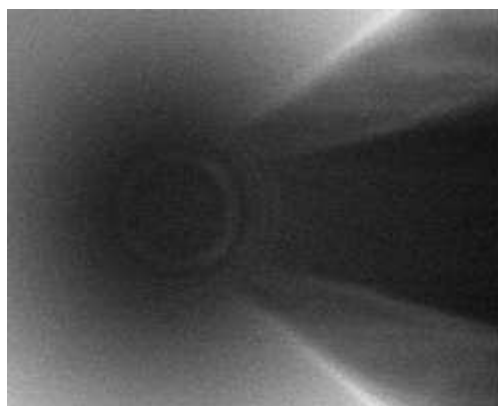


Figure 60: LiSt grease PAO 30
First minute in the experiment

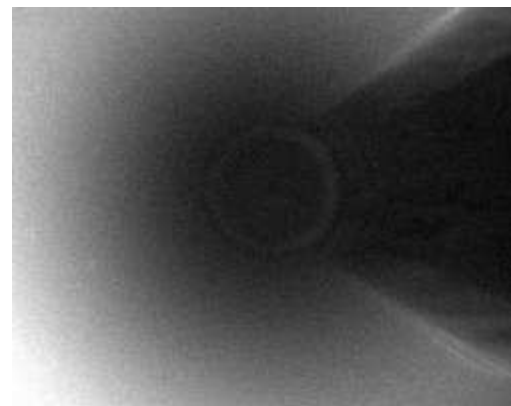


Figure 61: LiSt grease PAO 30
Ten minutes in the experiment

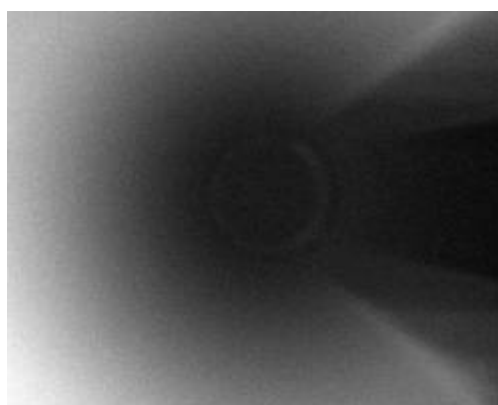


Figure 62: LiSt grease PAO 30
Twenty minutes in the experiment

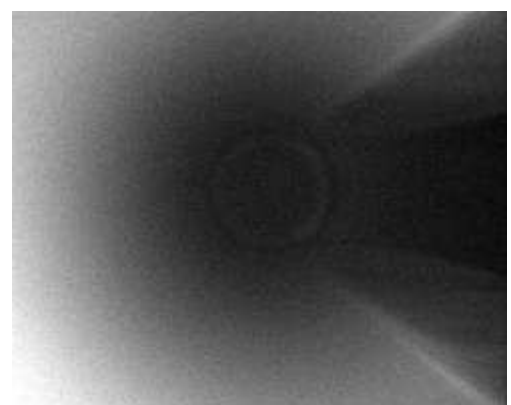


Figure 63: LiSt grease PAO 30
Forty minutes in the experiment

Images from the disc and the ball using green and ultraviolet light were taken for analysis after the tests were finished and are presented in the Figures 64–67. It can be observed that the track left on the disc surface, as well as the one left on the ball surface, is prominent; the edges of the track give us a better understanding of the lubricant replenishment mechanism that takes place during the contact.

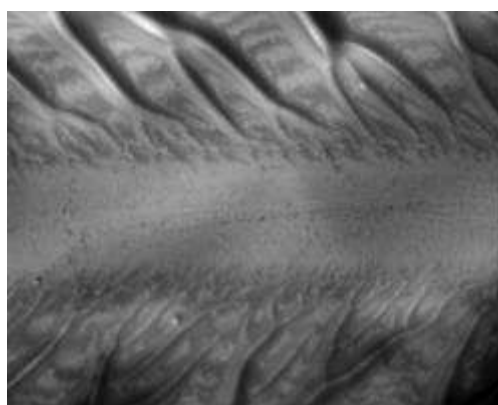


Figure 64: LiSt grease PAO 30
Green light image of the disc track
after the tests were finished



Figure 65: LiSt grease PAO 30
Fluorescence image of the disc track
after the tests were finished

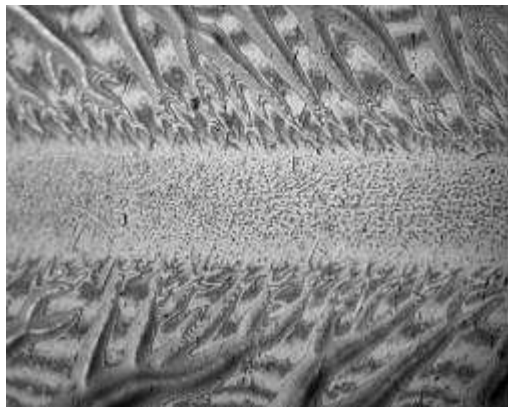


Figure 66: LiSt grease PAO 30
Green light image of the ball track
after the tests were finished

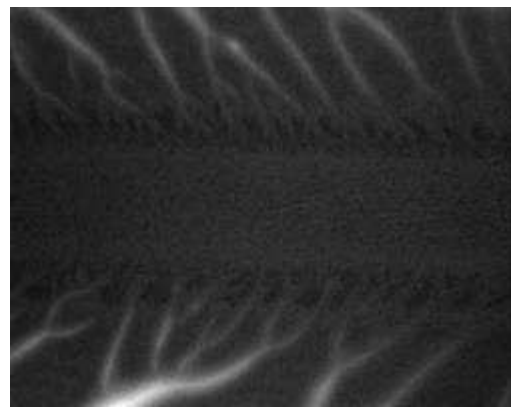


Figure 67: LiSt grease PAO 30
Fluorescence image of the ball track
after the tests were finished

The “*river*” like shape of the track edges shows the way the lubricant and thickener make their way back into the contact area. The high concentration of thickener and oil can be observed in both images, but the fluorescence image shows a low lubricant thickness just at the edge of the track, represented by a darker band on each side of the track.

A comparison has been done between the greases that use the same thickener, same base oil with different viscosities; images are presented in Figures 68–71.

It can be observed that the thicker i.e. the more viscous base oil, gives us a much better lubrication replenishment mechanism, as it can be seen in both Figures 69 and 71. There is a much thicker lubricant film on the track as compared to the oil with a lower viscosity, observed in Figures 69 and 70. The lubricant film, after the track was examined, shows to be clearly thicker for the grease with the base oil that has a higher viscosity.

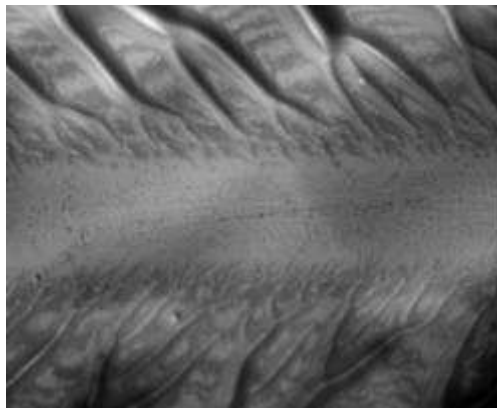


Figure 68: LiSt grease PAO 30
Green light image of the disc track
after the tests were finished

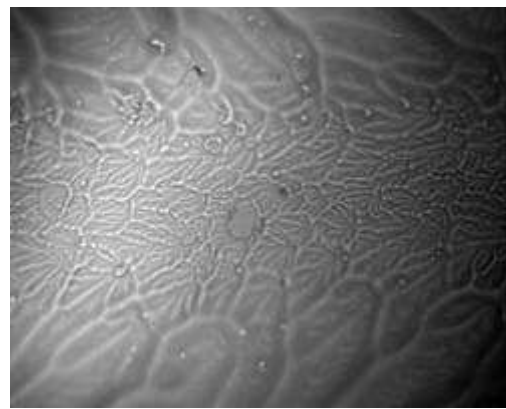


Figure 69: LiSt grease PAO 400
Green light image of the disc track
after the tests were finished



Figure 70: LiSt grease PAO 30
Fluorescence image of the disc track
after the tests were finished

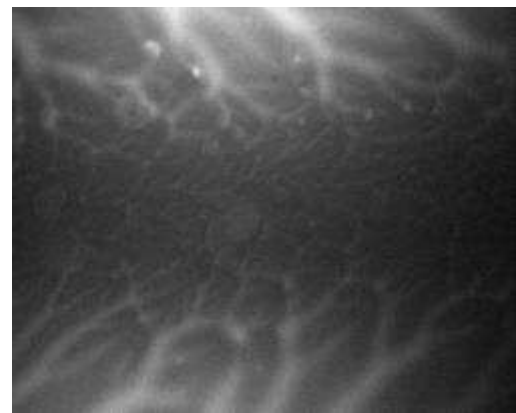


Figure 71: LiSt grease PAO 400
Fluorescence image of the disc track
after the tests were finished

Another approach had to be taken after tests showed that Di–urea thickener did not provide the necessary fluorescence for the lubrication mechanism to be analysed. To overcome this problem, a special chemical with fluorescent properties was employed. The grease was mixed with a 1% wt Pyrene, as for previous LiSt greases.

After the grease was mixed with the Pyrene, static images were captured to see if the fluorescent “booster” has the same effect on the Di–urea grease as for the LiSt grease. Images are presented in Figures 72 and 73.

Captured pictures clearly show a higher concentration of UV light in certain points on the images. This phenomenon can be explained either due to a cluster of thickener in the grease or a high concentration of Pyrene in the contact area.

Due to an impossibility to accurately measure the film thickness using the fluorescence method, a new study was employed to see the influence of the thickener on the lubrication mechanism.

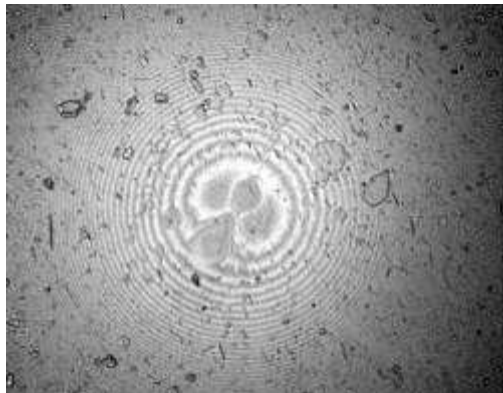


Figure 72: Di–urea grease PAO 30
Green light image taken before the tests

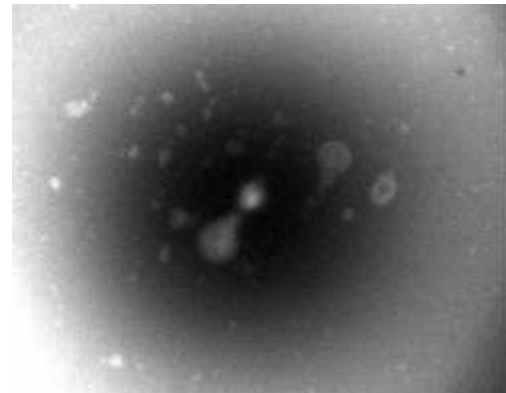


Figure 73: Di–urea grease PAO 30
Fluorescence image taken before the tests

A detailed analysis of the photos was made with the conclusion that the LiSt grease using the same base oil gives a much better lubrication than the Di-urea grease. Figures 74–77 present the contact lubrication at different time intervals. The brighter spot in the centre of the contact area can be attributed to a oil/thickener build-up, as experiment running time increases. This build-up decreases, resulting in contact film thickness diminishing. The development of a rolling track is much more prominent for the Di-urea grease than for the LiSt and can be clearly seen in Figures 76 and 77.



Figure 74: Di-urea grease PAO 30
One minute into the experiment

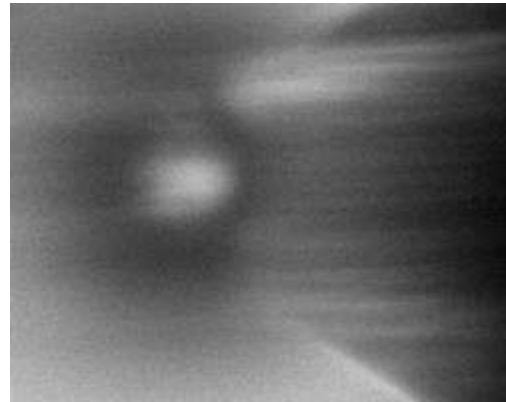


Figure 75: Di-urea grease PAO 30
Thirty minutes into the experiment

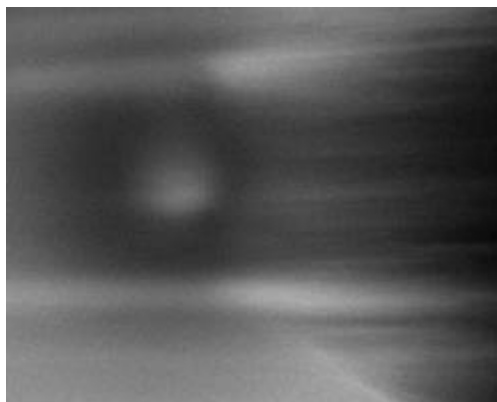


Figure 76: Di-urea grease PAO 30
Fifty minutes into the experiment



Figure 77: Di-urea grease PAO 30
Ninety minutes into the experiment

Images were captured both for the disc and the ball track after tests were conducted. From their analysis it can be clearly seen that the track left by the grease with the Di-urea thickener is much wider and the grease does not have such an accentuated presence in the outside of the track. Another thing that stands out to the viewer is that the inside of the track has a bigger concentration of lubricant/thickener.

This can be explained either by the fact that this thickener does not provide the oil replenishment needed to the contact, or it can be due to the fact that the contact between the sapphire disc and the steel ball is too close to the edge of the disc, resulting in a loss of grease due to spinning forces, but the radius of the sapphire disc is the same for both greases.

Images for the disc and ball track taken after the tests were completed are presented in Figures 78–81.

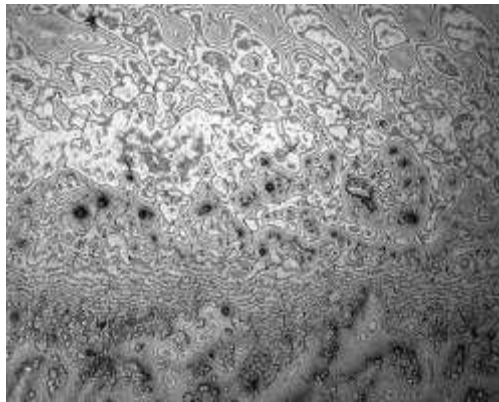


Figure 78: Di-urea grease PAO 30
Green light image of the disc track
after the tests were finished

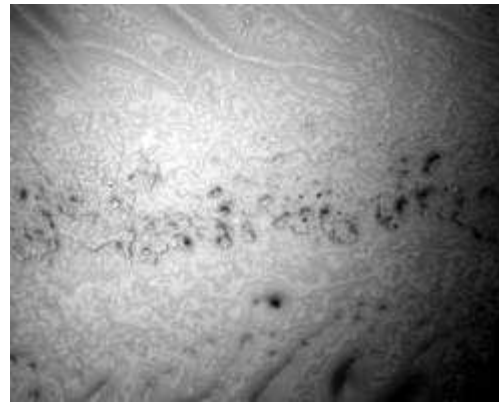


Figure 79: Di-urea grease PAO 30
Fluorescence image of the disc track
after the tests were finished

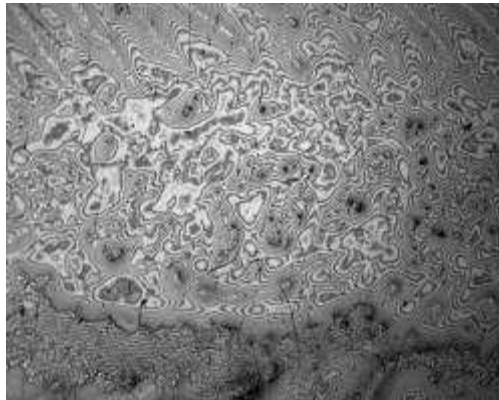


Figure 80: Di-urea grease PAO 30
Green light image of the ball track
after the tests were finished



Figure 81: Di-urea grease PAO 30
Fluorescence image of the ball track
after the tests were finished

Tests with two different slide/roll ratios were done and no big difference was observed for the greases that employ LiSt as a thickener, as opposed to the Di-urea grease that shows a much wider track on the disc. Analysis using the infrared spectroscopy was used to deduce the influence on oil viscosity, thickener and different slide/roll ratios on the lubrication mechanism. A lack of thickener can be observed in Figure 82 after infrared analysis. The difference in thickener presence in track is due to a variation in pure rolling and sliding condition.

The infrared spectroscopy tests carried out on the LiSt grease did not provide the needed accuracy to draw any relevant conclusion regarding thickener presence in the aftermath track or even contamination with different chemical elements, as it can be observed in Figure 83.

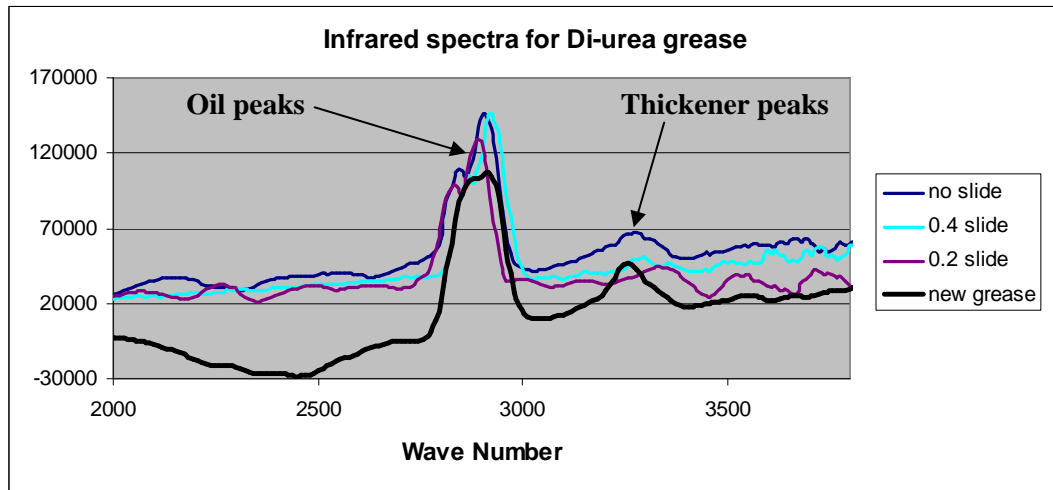


Figure 82: FTIR analysis of the sapphire disc track for the Di–urea grease

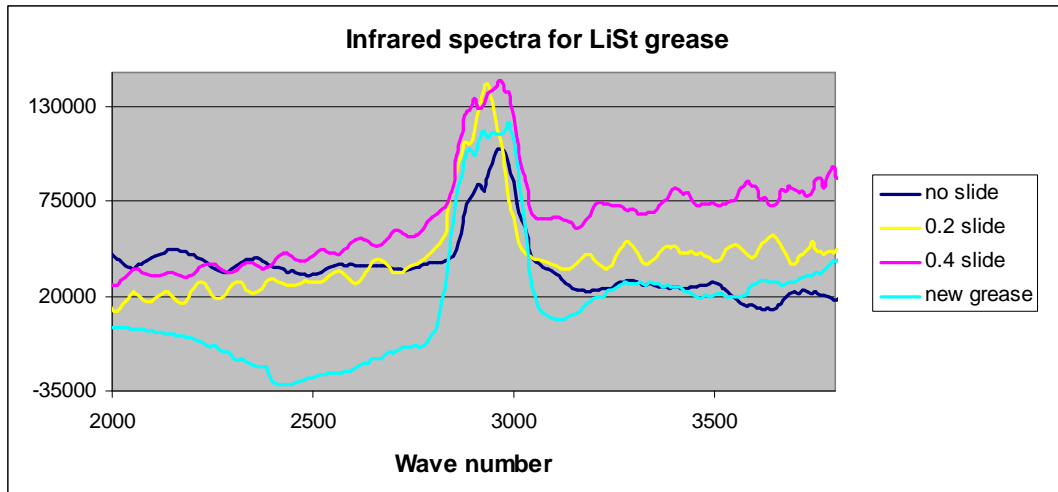


Figure 83: FTIR analysis of the sapphire disc track for the LiSt grease

The FTIR analysis of the sapphire tracks was irrelevant, except for the Di–urea grease, where as the sliding is more accentuated the thickener concentration in the track is lower. This is due to the fact that the grease is a fair distance from the reflective surface of the spectrometer i.e. the thickness of the sapphire disc; it is this researchers' opinion that this is the reason why the FTIR tests were inconclusive.

4.2.4 Conclusions

The optical method used in these tests, fluorescence, provides us with an excellent tool for observing in real time the process of lubrication.

The fluorescence method does not provide us with the resolution needed to measure contact film thicknesses.

The FTIR tests do not provide the resolution needed to observe oil presence in the disc track. After tests, no big difference can be viewed in the oil peaks, but they show, in the Di–urea grease, the presence or absence of thickener in the track.

The presence of a nearly white spot near the outlet of the contact is yet to be explained; in the authors point of view it is a mix of oil and thickener. This conclusion has been extracted after analyzing the pictures taken without Pyrene present in the grease mix. Although the clarity of the pictures is quite bad, something can still be distinguished.

This spot has been under discussion and additional tests were done to see if the presence of it is due to any sort of anomaly in the recording gear. For this reason PAO 400 oil with Pyrene present in its composition has been subjected to the same test conditions as the Di–urea grease mixed with Pyrene. The result was quite clear; the pictures do not show the presence of the white spot toward the outlet of the contact.

Another argument raised was the difference in track wideness at the end of the tests, the LiSt grease had a narrower track than the Di–urea grease. This phenomenon was attributed to the high viscosity of the base oil in the LiSt grease. This was tested by repeating the tests using a grease with the same base oil as the Di–urea grease. The conclusion after analyzing the photos was that for both LiSt greases (400cSt and 30cSt), the track width is similar, but for the grease with the higher viscosity base oil, the track has a higher concentration of oil.

Another phenomenon observed after tests was the influence of the slide roll ratio on the different grease:

- ↗ For the Di–urea grease, a difference in the thickener presence in the track after tests was observed using FTIR microscopy; the results were very different for each test (no slide, 0.2, 0.4 slide/roll ratio); as the slide/roll ratio increases, the thickener is being pushed out of the contact. Also the times for which the tests were run differs for each sliding condition, because the grease was being pushed out of the contact area due to sliding.
- ↗ For the LiSt (400cSt) grease this phenomenon cannot be observed for neither of the two methods employed; this can be attributed to the high viscosity of the base oil in the LiSt (400cSt) grease.

4.3 Electrical method [96]

4.3.1 Introduction:

The film thickness in elastohydrodynamic contact is accurately measured using optical interferometry technique. This method allows thicknesses below five nanometres to be measured and also allows the thickness over the whole contact area to be mapped. One of the disadvantages of this method however, is that one of the bodies in the contact must be a transparent material, such as glass or sapphire, which is not the case in real machine elements. One way of avoiding this limitation is to evaluate the film thickness by measuring the capacitance of the contact. This kind of measurement requires knowledge of the dielectric properties of the lubricant, and its function of temperature, pressure and shear strain. The results shown in this paper are aimed at developing a method of evaluating the elastohydrodynamic (EHD) films thickness based on the electric capacitance. The electric permittivity of two, commonly used lubricating oils, is evaluated via the measurement of the electric capacitance of the contact. The electric permittivity is first measured separately in a standard plate-capacitor arrangement. The permittivity of the same lubricants is subsequently measured in a ball-on-flat arrangement and the effect of entrainment speed and pressure are evaluated.

4.3.2 Experimental Details:

❖ Static Measurements:

Before measuring the dielectric permittivity of the lubricants in elastohydrodynamic contacts, the value of this parameter at ambient pressure and temperature in static conditions was determined. For this purpose, a simple experimental set-up was devised, as shown in Figure 84.

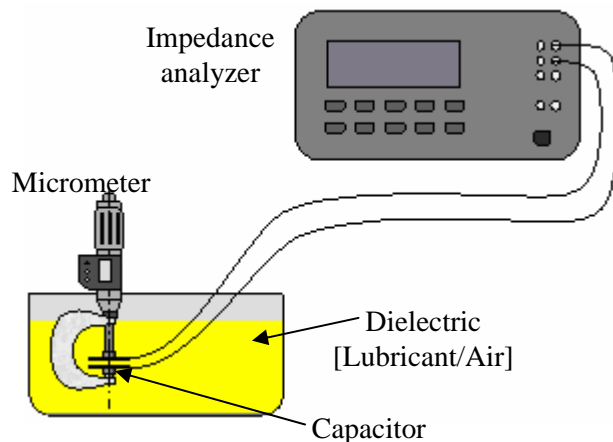


Figure 84: Experimental set-up for static permittivity measurement

[96] Y. Nagata, M. Furtuna, C. Bell and R.Glovnea “Evaluation of Electric Permittivity of Lubricating Oils in EHD Conditions” 2nd International conference on Advanced Tribology, 3–5 Dec 2008, Singapore

A simple capacitor was formed by two brass discs of 20mm diameter, fixed on the jaws of a micrometer, such that the gap between the plates can be accurately set. The two plates of this capacitor are connected to an impedance phase–gain analyzer device which is able to measure the capacitance at frequencies between 0.1Hz and 100MHz. The capacitance of this system is first evaluated using air as dielectric, and then for the studied oils (polyalphaolefin (PAO) and a mineral oil) with dynamic viscosities seen in Table 5.

Table 5: Dynamic viscosity [Pa•s]

Oil	40°C	100°C
PAO	0.021	0.004
Mineral oil	0.021	0.0042

The dielectric permittivity of the oils is found as the ratio between the capacitance of the system measured for oil and for air. The dielectric permittivity can also be determined from the Equation 104 of the capacitance of plane capacitors:

$$C = \epsilon_0 \epsilon_r \frac{A}{d} \quad (104)$$

Where $\epsilon_0 = 8.854 \cdot 10^{-12}$ F/m is the permittivity of free space, ϵ_r is the relative static permittivity of the dielectric between the plates, A is the area and d is the separation. The gap between the plates was kept constant at 0.2mm. The ratio between the capacitance of air and that of the oils indicate the relative static permittivity of the oils to be 2.2 at ambient pressure and temperature.

❖ Dynamic Measurements In EHD Conditions:

In order to measure the dielectric permittivity of the oils in elastohydrodynamic conditions, a PCS Instruments optical interferometry film thickness measurement rig has been adapted. A schematic of the experimental set-up is shown in Figure 85.

The elastohydrodynamic contact under study is formed between a steel disc and ball. The disc and the ball are driven independently by electrical motors, such that the entrainment speed and the sliding/rolling ratio can be set as required. The film thicknesses for the two oils as a function of entrainment speed were first measured using the optical ultra–thin film interferometry technique (UTFI) with a load of 20N and a temperature of 25°C.

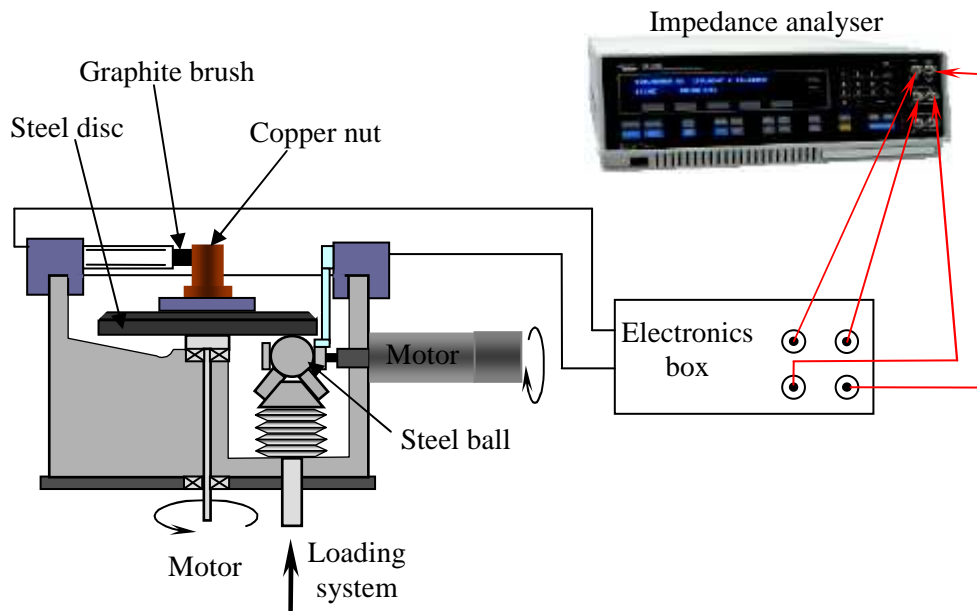


Figure 85: Experimental setup for EHD measurements

The variation of the film thickness with entrainment speed is shown in Figure 86.

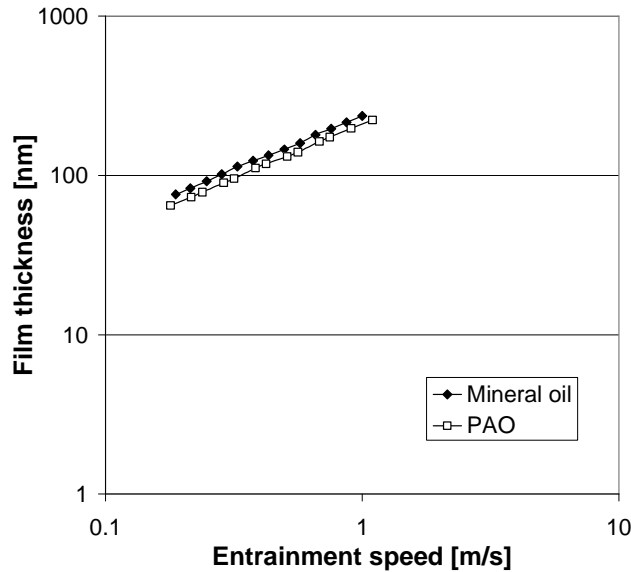


Figure 86: Film thickness measurements

Two kinds of capacitance tests were then carried out: constant load with a variable speed and constant speed with variable load. In the former case, the load was set to 10N instead of 20N to take into account the larger elastic modulus of the steel disc in comparison to the glass one. This gives a Hertzian pressure of 0.7GPa and a contact radius of 85 micrometers. The entrainment speed was varied between 0.2 and 1.1m/s.

Constant speed tests were carried out at 0.3 and 0.9m/s, with the load varying from 10N to 50N. The temperature of the tests was 25°C, as in the static measurement tests.

4.3.3 Results and Discussion:

After allowing for the contribution of background capacitance, the capacitance of the contact as a function of film thickness is shown in Figure 87.

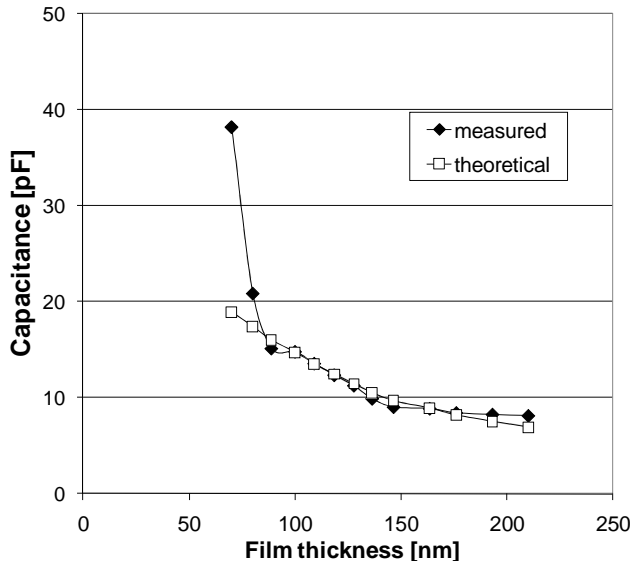
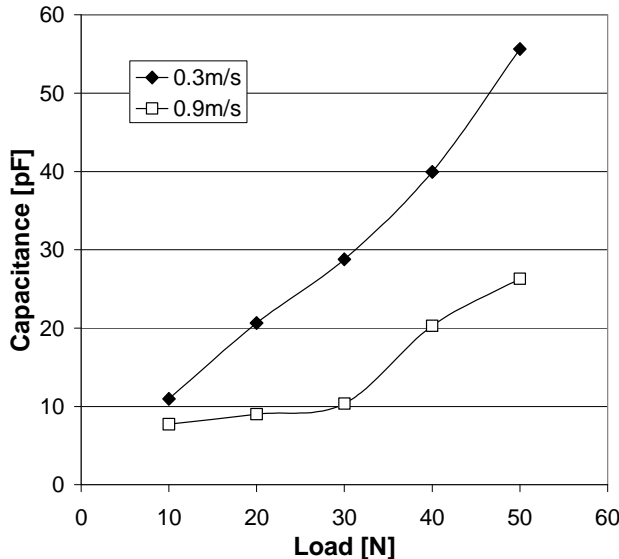
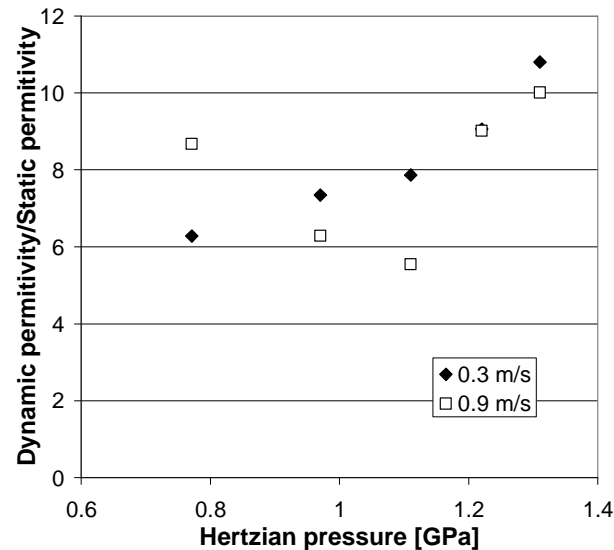


Figure 87: Contact capacitance function of film thickness

The theoretical capacitance shown has been calculated for an equivalent parallel plate capacitor, of circular shape, with an area equal to that of the Hertzian contact. To allow the theoretical data to best fit the measured capacitance, the relative permittivity of the oil must be 7, which is approximately 3 times larger than the value measured statically. This increase could be attributed to the larger pressure inside of the contact. At the lowest entrainment speed the measured capacitance departs substantially from the theoretical value. It is believed that this difference is due to the approximation of the contact with a flat surface. It is known that although an elastohydrodynamic film has a constant thickness over most of the contact; it exhibits regions of minimum film thickness towards the exit and sides of this area. At lower speeds, and hence thinner films, this effect is more pronounced than at larger thickness, thus a greater discrepancy is observed.

Figure 88 shows the capacitance variation of the contact with load, at two different entrainment speeds, for the PAO. Similar variation has been found for the mineral oil.

**Figure 88: Contact capacitance function of pressure****Figure 89: Lubricant permittivity function of pressure**

From the capacitance values in Figure 88, using Equation 104, the relative permittivity of the lubricant was extracted as a function of the contact pressure. The calculated permittivity, at 0.3m/s and 0.9m/s is shown in Figure 89.

The value obtained for 10N load is consistent with that observed before, in the constant load/variable speed test. As seen, the permittivity increases with pressure and is reasonably similar for the two speeds, as expected. If the two peculiar values at 0.9m/s are discarded, the variation of the permittivity with pressure is close to linear, for both speeds. This is consistent with the results obtained in static measurements for heptanol isomers by Vij et al. [97]. It is difficult to make a direct comparison between these results and those reported in [97], as the fluids are different, however a striking similarity can be observed.

The slope of the variation of the permittivity with pressure is about 8.4 in the current results and 8.5 in [97]. Gilchrist et al [98] also have found an increase of the dielectric constant of glycerol and 1-propanol with pressure, but in their case the slope of this variation decreased with pressure.

4.3.4 Conclusions:

The dielectric permittivity of two lubricants, a polyalphaolefin and a mineral oil, in elastohydrodynamic conditions has been evaluated, by measuring the capacitance of the contact. The contact under study was formed between a steel ball and disc.

Tests carried out at constant pressure and variable entrainment speed, revealed a relative permittivity similar for the two oils, of about 7.

The relative permittivity varies nearly linearly with pressure, from about 7 at 0.6GPa to about 10 at 1.3GPa, independent of the film thickness.

5 EXPERIMENT

5.1 Rationale of the Experimental Work

There are currently two main limitations of the optical interferometry method, Ultra Thin Film Interferometry (UTFI) as shown in Figure 90.

- One limitation is that it cannot measure very thin films when sliding is employed. Under such conditions the spacer layer, made of silica, is destroyed due to the high frictional forces present in the contact caused by a local rise in temperature of the contact region when sliding is introduced [101].

This means that very thin films can only be measured in pure rolling conditions. Several lubricant additives have been used over the years by different researchers and it was found that only boundary films are formed between the two solid surfaces in contact. There is thus a need to overcome this problem to be able to measure very thin films, characteristic of boundary and mixed lubrication regimes in sliding contacts.

- The other major limitation of the UTFI technique is that one of the two contacting surfaces is not steel but coated glass or sapphire.

For glass this leads to a much lower contact pressure than for steel on steel but the main concern is that lubricant additives will behave differently in a glass on steel tribopair than a steel-on-steel one, as is present in real machine elements.

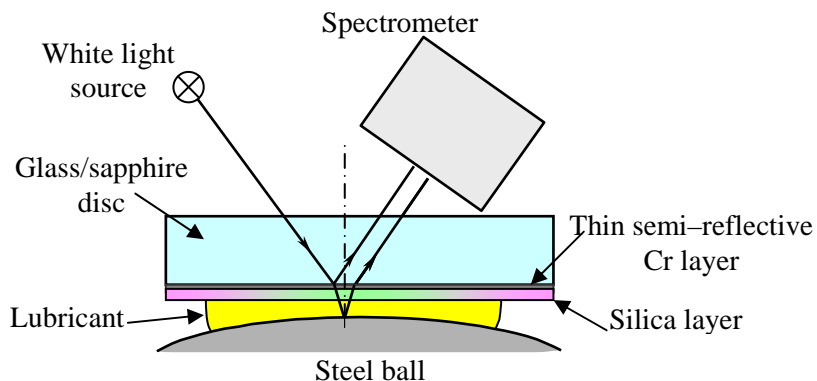


Figure 90: Experimental setup for the classical Ultra Thin Film Interferometry method

One of the proposed solutions in this project is to eliminate the fragile silica layer currently employed by the classical UTFI method, and use a higher Chromium layer thickness sputtered on the glass disc, as showed in Figure 91. A thicker Cr layer is believed to provide a higher phase shift corresponding to the spacer layer used in the classical UTFI method. This, together with a spectral analysis of the resulting interferograms, will facilitate measurements of very thin lubricant films. It is supposed that a thicker Cr is much tougher and more resilient than silica, thus tolerating various sliding conditions, allowing thin films to be measured accurately.

The optimum Cr thickness that will deliver the necessary phase change is unknown, but this will be established by experimenting with several different thicknesses, finding the equilibrium between the layer transmittance and its durability.

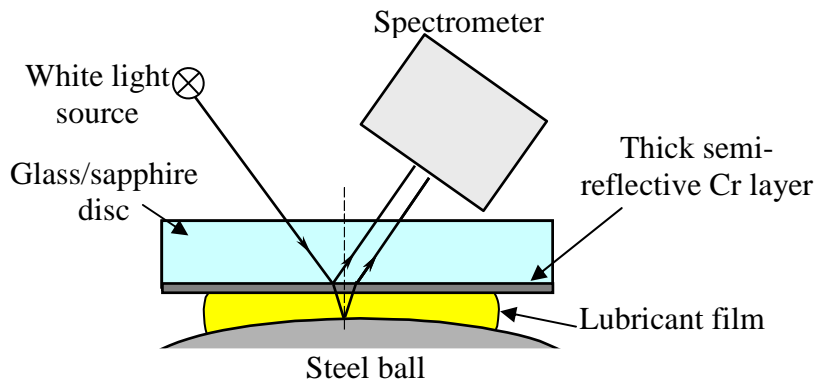


Figure 91: Experimental setup for the modified Ultra Thin Film Interferometry method

As explained in previous chapter (3.2) capacitive methods are quite often used to measure film thickness in lubrication research but these are confined to applications where the lubricant film thickness is relatively large, such as hydrodynamic bearings, or some piston–ring contacts [47, 58–61].

The electrical capacitance of EHD contacts has also been used in the past to estimate the film thickness in elastohydrodynamically lubricated contacts [47]. However, those studies have been largely abandoned with the development of optical interferometry and the success the method had in accurately measuring film thickness down to a few nanometres. A comprehensive, comparative study of film thickness by electrical capacitance and optical interferometry, the method which has proven to be the most accurate in determining film thickness, has never been attempted.

There appear to be two main problems with applying the capacitance technique when looking at very thin lubricant films.

- ❖ Film thickness determination depends on the dielectric constant of the film, which can vary considerably depending on the chemical nature of the film used, unlike optical interference which depends on the refractive index, which varies relatively little with chemical composition.
- ❖ For very thin films in the nanometre range it is not known if the conventional inverse relationship between capacitance and separation would supply good values.

The main issue this project will overcome are the two limitations summarized above. This will be done by using thin film optical interferometry to *calibrate* capacitance measurements. In the ball–on–disc optical interference method, the conducting chromium surface can be used as one

plate of a capacitor and the contacting ball as the other. If the other armature is the Hertzian flat on the ball surface, the capacitance of this system can be measured and correlated to the film thickness determined by optical interferometry in the same experiment. The lubricated Hertzian contact of interest is several hundred microns across and less than one micron thick and thus can be approximated to a parallel plate capacitor. Part of the project investigations were conducted to estimate the influence of the lubricant composition upon the capacitance of the contact. Tests were carried out with base oil and two solutions: one organic friction modifier and one a viscosity index improver polymer, both of which are known to form boundary films [41, 42]. Once the correlation between the capacitance of the contact and the EHD film thickness was established, the next phase of the project consists in measuring film thickness in steel-on-steel contacts. This was accomplished by replacing the glass/sapphire disc with a steel one and evaluating the influence the Cr/steel had on the resulting values.

5.2 The EHD Film Thickness Test Rig

The lubricant film thickness was measured by optical interferometry, using a test rig designed and manufactured by PCS Instruments. The contact between the glass disc and the steel ball is illuminated by a white light source, directed down a microscope through the disc, to give the necessary phase change and an additional silica layer, to give a higher accuracy. Part of the light is reflected from the Cr layer on the disc and part travels through the silica layer and lubricant film and is reflected back from the steel ball surface. A schematic representation of the test rig is presented in Figure 92. The recombining light paths form an interference image, which is then passed into a spectrometer and then into a high resolution B&W CCD camera. The camera image is captured by a video frame grabber and analysed by the control software, to determine film thickness.

The lubricant film thickness at any point in the captured image can be accurately calculated by measuring the light wavelength. The software measures the wavelength of the light returned from the centre of the contact, and therefore calculates the central film thickness of the contact.

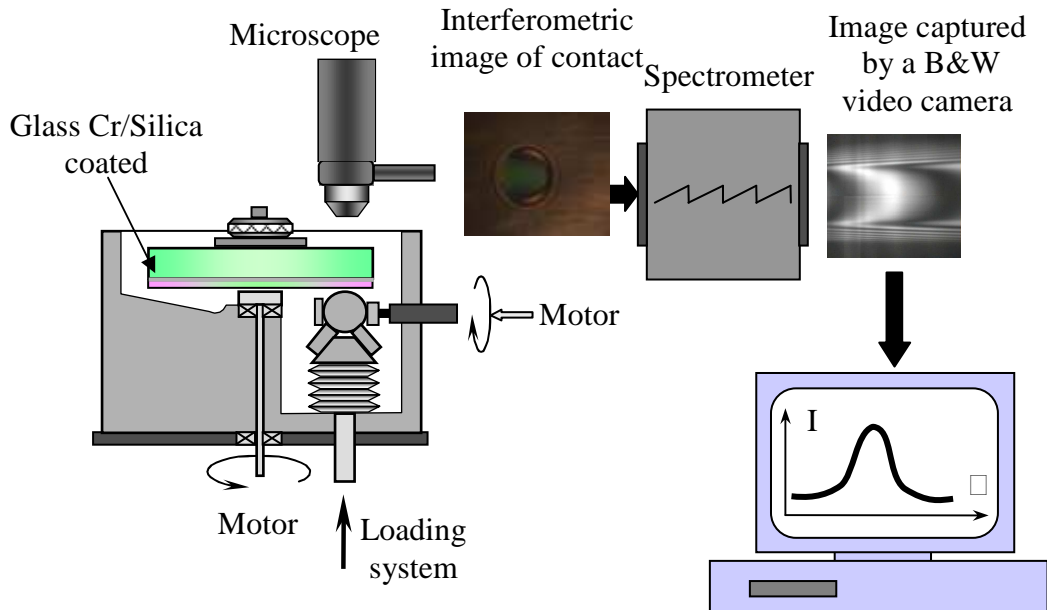


Figure 92: Schematic representation of the PCS EHL test rig

Technical specifications for the PCS EHL rig are presented in Table 6.

Table 6 Technical Specifications

Film Thickness	1 to approx. 1000 nm, ± 1 nm
Speed	0 to 5 m/s
Slide/roll ratio	0 to 100%
Load	0 to 50 [N]
Temperature	Ambient to 150°C

5.3 Modifications to the Ultra Thin Film Interferometry [UTFI] Method

As explained in chapter 5.1, a modified version of the UTFI method was needed to eliminate the fragile film of silica (SiO_2) and to calibrate the capacitive method against the modified optical method. The contact photos were captured after the interfered image was passed through a spectrometer.

In the first stages of the research, different discs with Chromium sputtered on them were used. The discs were supplied by Imperial College Electrical Department and the available Cr thicknesses were 10nm, 25nm and 50nm. Pictures were taken to assess if the actual contact can be observed. The images showed a rapid increase in reflection of the Cr surface; as the Cr film thickness becomes larger, this resulted in a change in interference from constructive leading to destructive interference, for the thickest Cr layer.

Figures 93–95 show the way the Cr layer influences the interference of light when it passes through the sputtered glass disc. A big difference between the images can be observed; whilst for the 10nm layer we can clearly see the shape of the contact, as the Cr film thickness increases, the image becomes much brighter and contact details are lost.

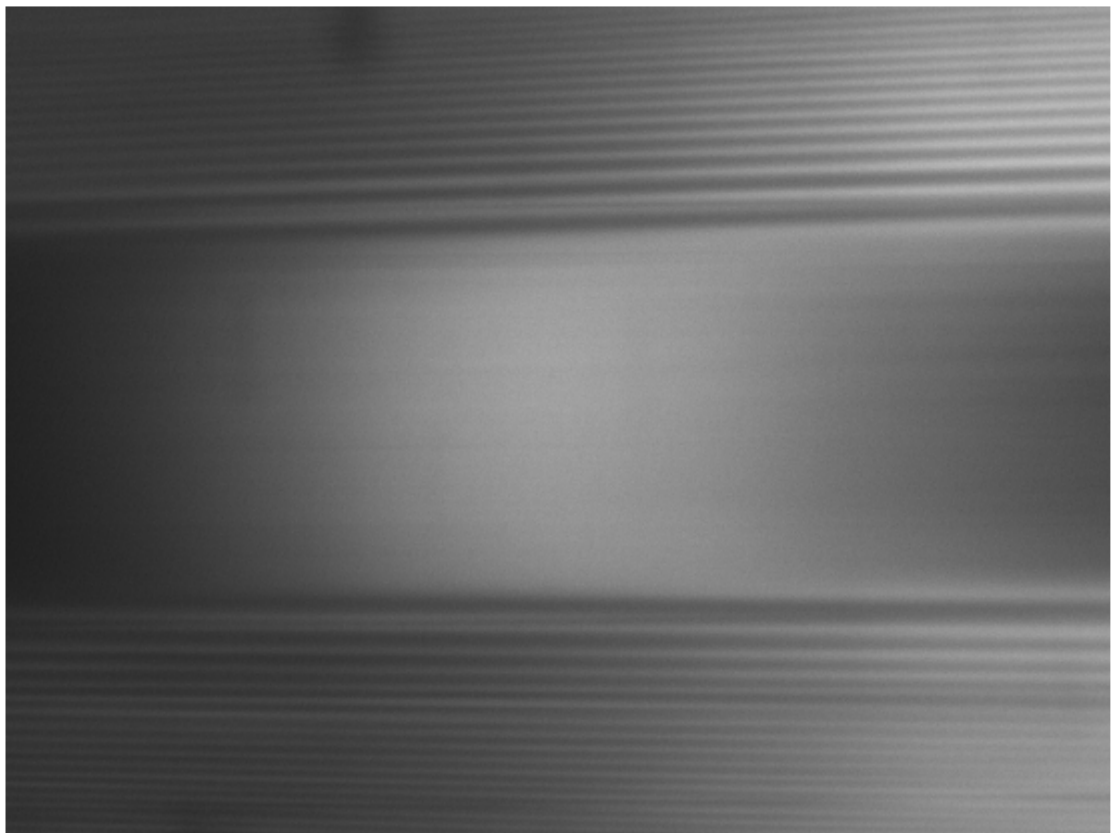


Figure 93: Interferogram for Cr sputtered [10nm] and silica disc with a 20N load

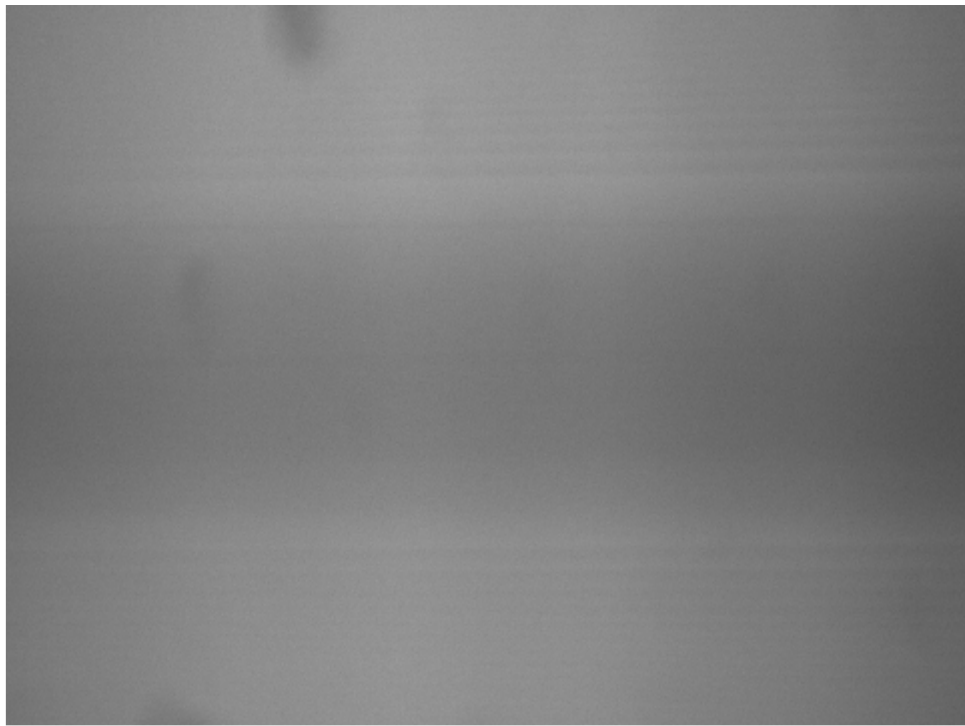


Figure 94: Interferogram for Cr only disc with a thickness of ~25 nm with a 20N load



Figure 95: Interferogram for Cr only disc with a thickness of ~ 50 nm with a 20N load

For this test a ruled diffraction grating with 150 grooves per mm and a designed wavelength of 300 nm has been used. The white shadows observed on captured images represent the grating grooves.

The actual light that passes through the Chromium layer decreases significantly with an increase in metal film thickness. The special software developed to analyse the images also confirms that the thicker Chromium does not allow film thickness analysis.

The following sequence of images represents, a test carried out using a mineral oil at room temperature, with a Chromium thickness of 25nm. Figures 96–101 present the images captured at different speeds, throughout the specified test. It might be assumed that the brighter part of the image represents the centre of the contact, and implicitly the central film thickness.

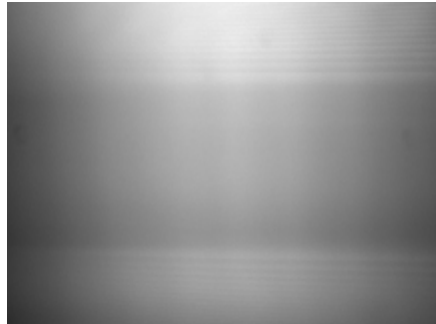


Figure 96: 0. 02 m/s



Figure 97: 0. 075 m/s

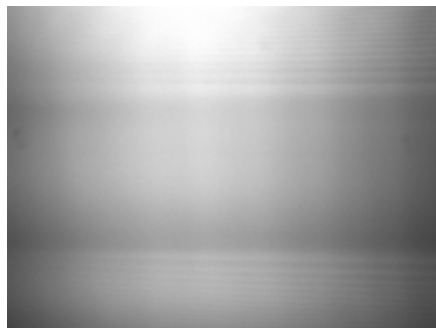


Figure 98: 0. 126 m/s

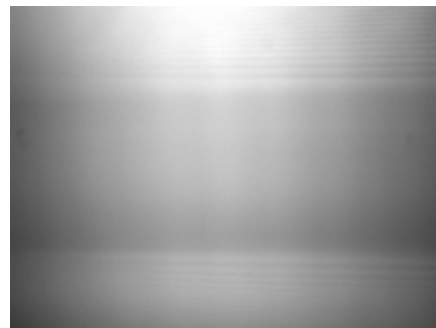


Figure 99: 0. 36 m/s



Figure 100: 0. 606 m/s

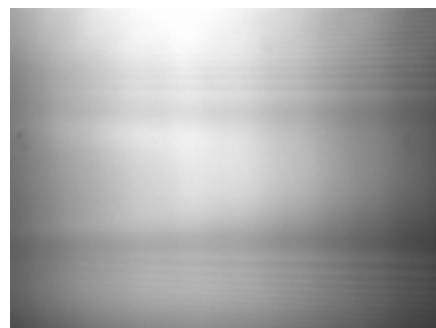


Figure 101: 1. 03 m/s

In reality, the brighter part in the centre of the contact represents the first reflection that takes place at the chromium/glass interface.

In Figure 101 the contact constriction can be observed more clearly, however even so, after analysis using the software an accurate film thickness measurement could not be obtained.

Exact values for a reliable measurement with the modified ultra thin film interferometry method that employs a thicker Chromium disc than the usual method (which uses silica layer in addition to a very thin Cr layer) could not be obtained.

Interferogram curves for the captured images in Figures 96–101 are presented in Figure 102. These were analysed using a specially written program.

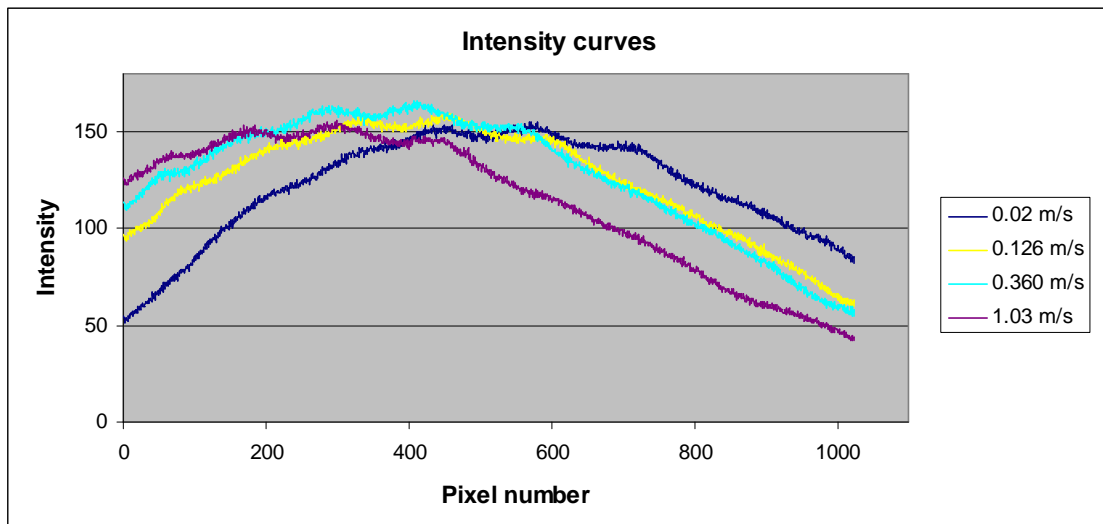


Figure 102: Intensity curve values for images obtained using a 25 nm thick Cr sputtered disc

The ridges that appear in both Figure 102 and Figure 103 represent the grooves on the spectral diffracting grating used in the spectrometer. The difference in these figures comes from the fact that the spectrometer grating was moved to keep the brighter part of the image central in Figure 102. The grating is connected to a micrometer head, which allows it to move with the contact position; in the case of the modified interferometry method, the movement of the grating only moves the peak of the intensity curve to the left of the graph. If the grating would have been stationary, all of the intensity curves could have been superimposed on each other. Figure 103 shows a more graphic representation of this phenomenon.

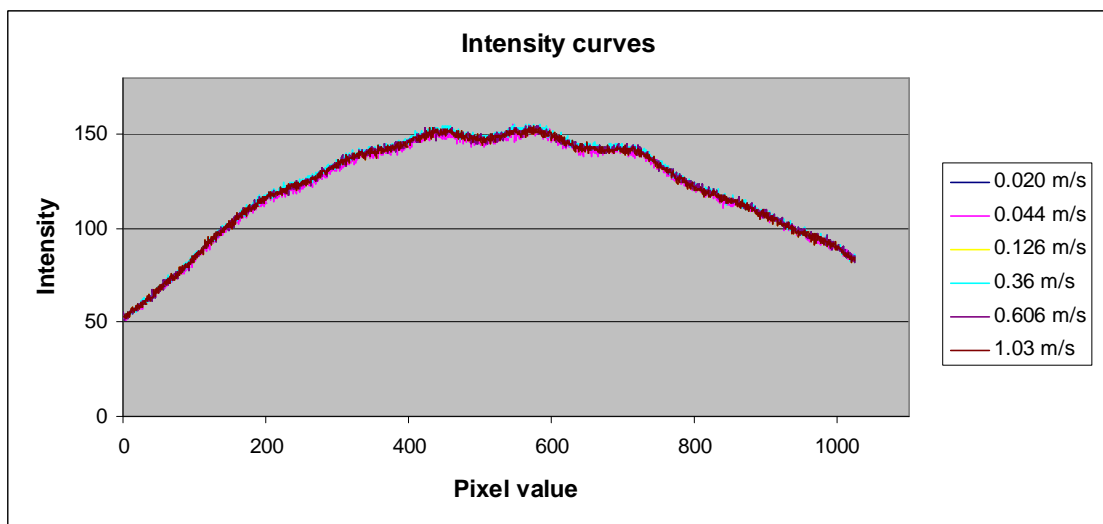


Figure 103: Intensity curve values for images obtained using a 25nm thick Chromium sputtered disc with the spectrometer grating stationary for all speeds

This superimposition of intensity values is attributed to a very high reflection of the Cr surface, this causes a low interference between the two reflected beams and the contact constriction cannot be observed.

To overcome this problem, a disc with thinner Cr layer was used. However when a thin Cr layer is being used, the phase change is very small. This means, a silica layer has to be employed, otherwise the original limitation of the optical interferometry method still applies, which is that no film thickness lower than a quarter of the wave length can be measured.

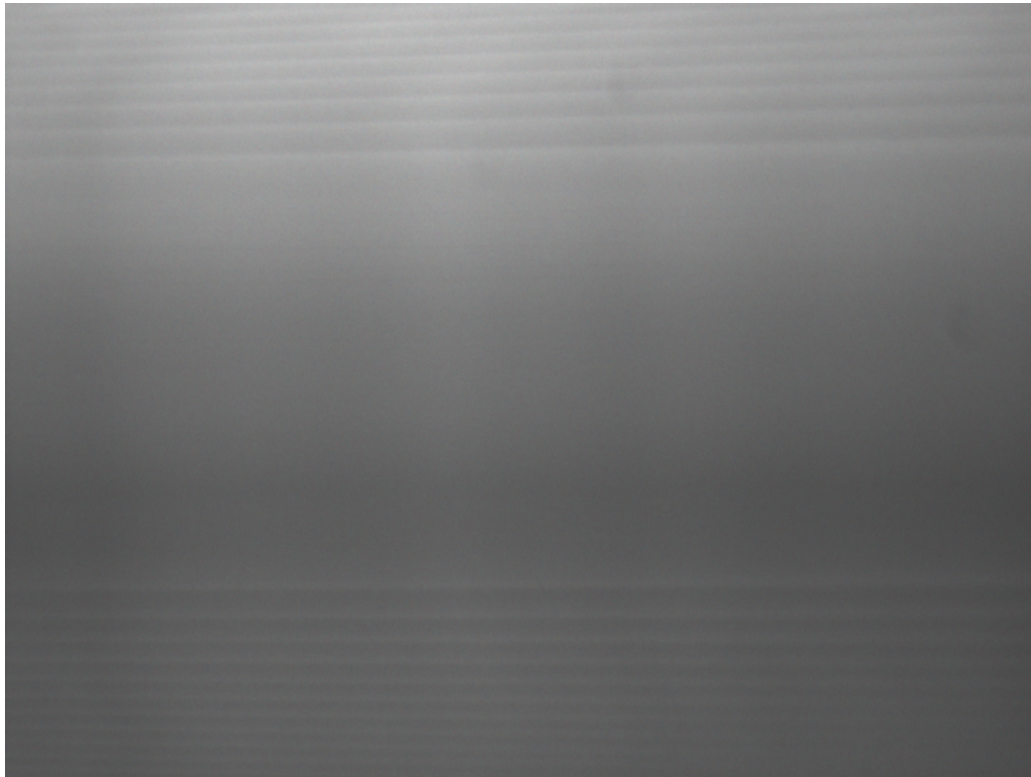


Figure 104: Interferogram for Cr only disc with a thickness of ~15nm with a 20N load

Since the 25nm and 50nm thick Chromium disc did not supply a good image to be analysed, another disc was manufactured, with a thickness of 15nm. This specially made disc was used to measure the capacitance values. Calibration using the 15nm thick Cr disc is not possible without using a silica layer sputtered on the disc. Therefore calibration of the capacitive method will be achieved in two stages: first the film thickness was measured using a PCS Instruments supplied glass disc that has a Cr layer of ~10nm followed by a Silica layer of ~550nm. The second stage was to use the ~15nm specially made disc to measure capacitance in the same experimental conditions as applied to the optical technique.

Initially, it was believed that a thicker Cr layer will provide a larger phase change and aid in the elimination of the fragile silica layer according to [26]. However, it was found that thicker chromium layer increases too much the intensity of the reflected rays at the chromium surface, thus the interference with the rays reflected from the ball surface becomes difficult.

Figure 105 presents the results of a theoretical analysis of the influence of Chromium thickness on the light intensity reflected by the Cr–glass interface. The intensity of the reflected rays is calculated with Equations (96), (97) and (98). The Cr film thickness is taken into account by the parameter s_1 ($s_1 = 4\pi h_1/\lambda$).

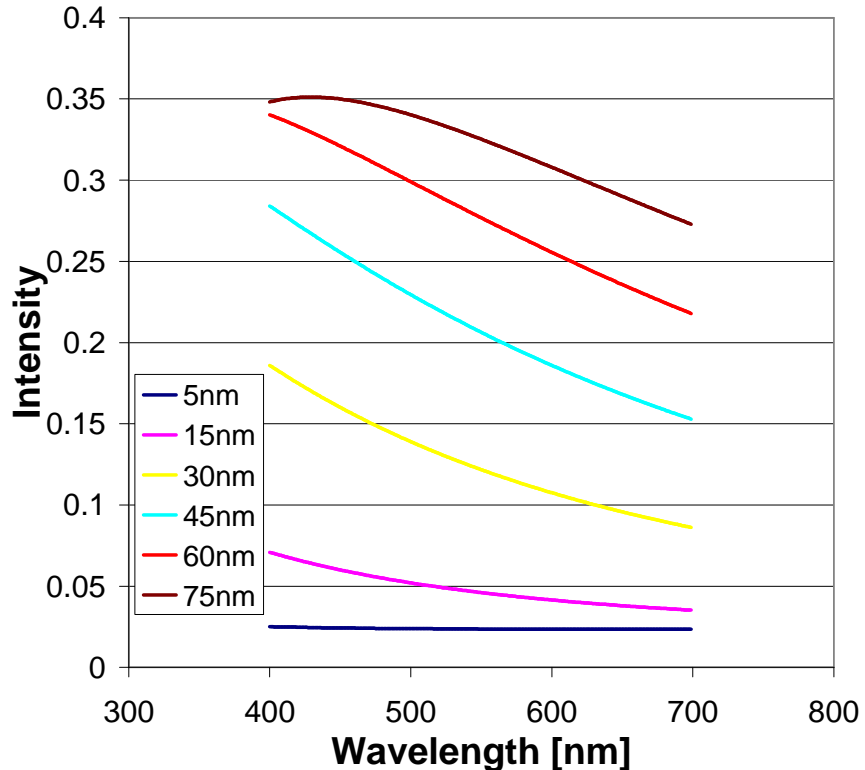


Figure 105: Computed intensity of the ray reflected by the chromium layer

It can clearly be seen from the graph that an increase in Cr thickness is theoretically followed by an increase in reflected light intensity. This phenomenon has a much higher influence on the image quality than initially believed, resulting in a destructive interference of the reflected rays from both the Cr surface and the ball interface.

Other researchers like Jenkins and White [13] do not even take into account the thickness of the Cr for the first reflection of the Cr–glass interface.

5.4 Static Measurement of the Capacitance between a Sphere and a Flat

In a 1997 paper, Hudlet et al. [98] proposes a very simple method to determine the electrical tip–surface force in Atomic Force Microscopes, which are used to study the electrical properties of metallic or insulating materials. To validate his experiments he used a sphere–infinite plane system as a reference. When a potential is applied between the tip and the underlying metallic surface, the system forms an axially symmetric capacitor. Figure 106 shows a sphere on an infinite flat surface setup used by [98].

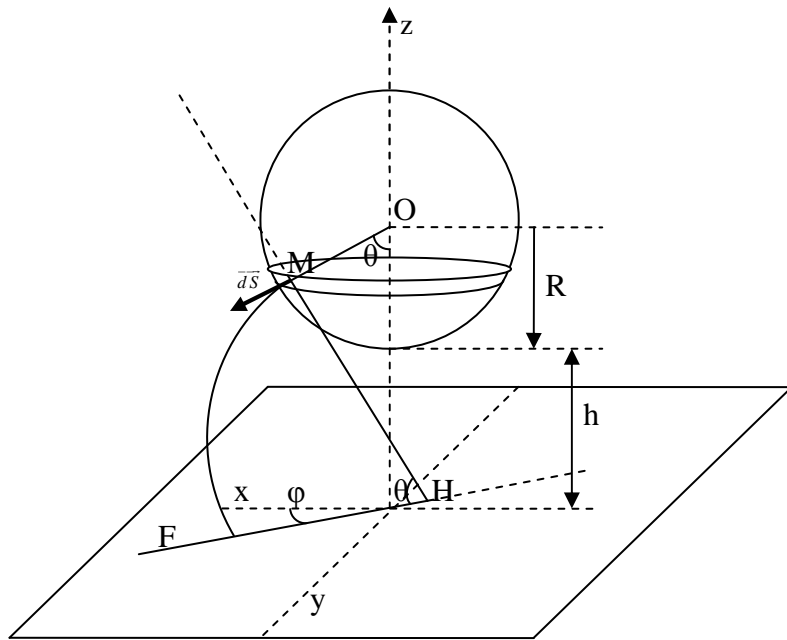


Figure 106: Sphere on infinite flat surface [98]

Since the sphere and the infinite plane are in total influence, it was more convenient for Hudlet to calculate the sphere–plane capacitance to determine this force. The capacitance expression used by Hudlet [98] is as follows:

$$C(z) = 2\pi\epsilon_0 R \int_0^\pi \frac{\sin^2 \theta}{\theta \left[\frac{h}{R} + 1 - \cos \theta \right]} d\theta \quad (105)$$

For testing the accuracy and the viability of the formula put forward by Hudlet, a special rig has been designed and build. This can be used for accurate measurements of capacitance between a flat surface and a ball. A schematic representation of the rig is presented in Figure 107.

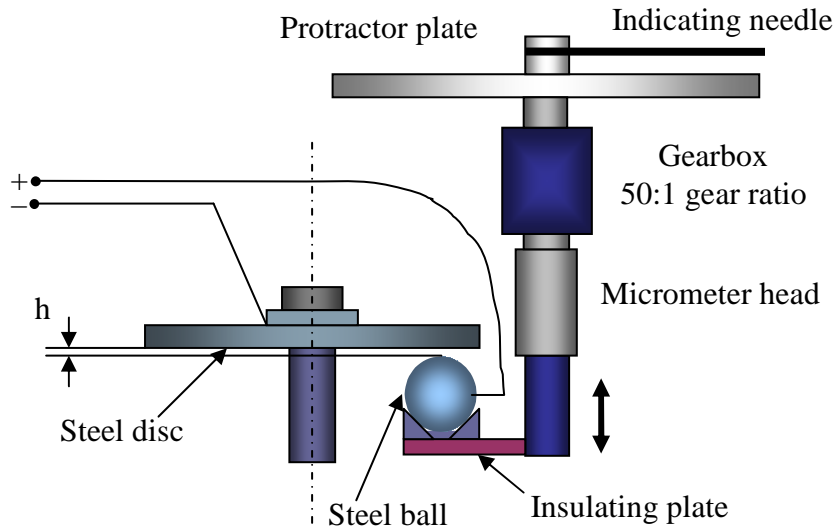


Figure 107: Experimental test rig for static capacitance measurements

Tests were carried out at different gaps between a steel ball and a steel disc with the purpose of observing the influence of the electrical field on the two employed surfaces. Test conditions are displayed in Table 7.

Table 7 Test parameters

Frequency (Hz)	10.000
AC Level (V)	1
DC Level (V)	0
Temperature (°C)	24 [room temp]

A gear box was used to give very small displacements of a wide range of distances; one degree on the protractor plate resulting in a ball movement of $7.7 \cdot 10^{-11}$ m. Capacitance measurements were done and are presented in Figure 108. The measurements follow the same trend as the theoretical ones obtained using Hudlet's capacitance formula.

A small difference between the measured values and the ones extracted from theory can be observed for both the air and oil measurements. This difference can be explained by the capacitance variation measured during the tests. Variation could be attributed to the fact that the apparatus used to measure capacitance actually measures impedance that varies with frequency.

Even in static conditions, the capacitance varies at a fixed frequency, as shown in Figure 109. This may be due to the physical structure of the material, to chemical processes within it or a combination of both.

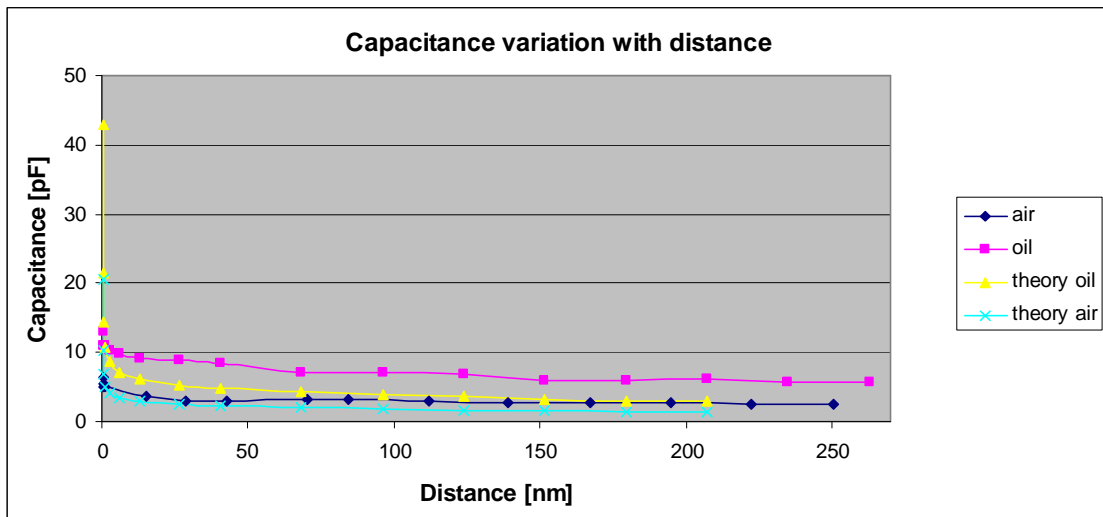


Figure 108: Capacitance values compared with the theoretical values obtained using Hudlet's formula

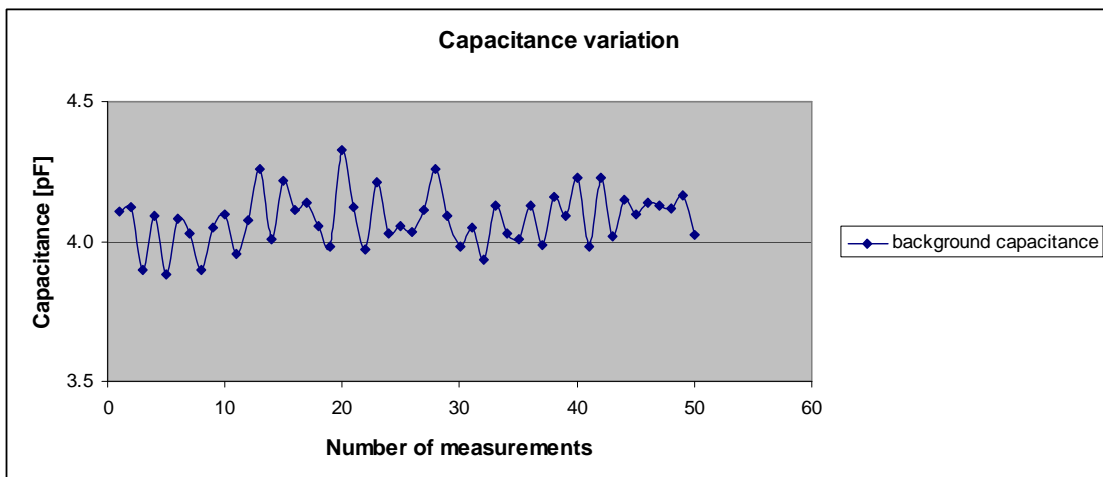


Figure 109: Capacitance variation at a constant frequency of 10kHz

5.5 Capacitive Dynamic Measurements of EHD Point Contacts

5.5.1 Modifications to the EHD Test Rig

For the electrical measurements, the experimental setup was designed in such a way to allow the capture of the electrical signal both from the ball and the disc. Figure 110 gives us a schematic representation of the whole assembly.

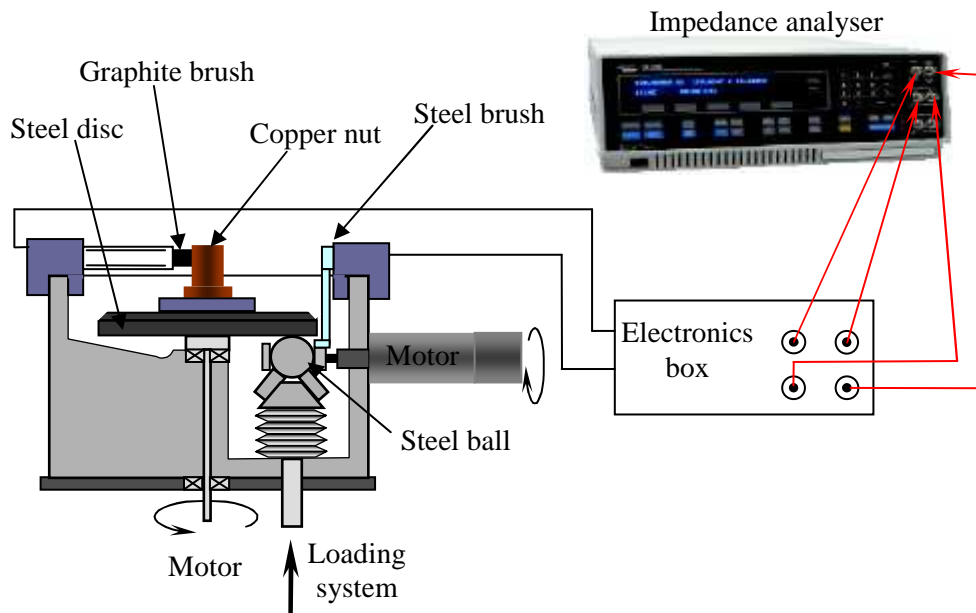
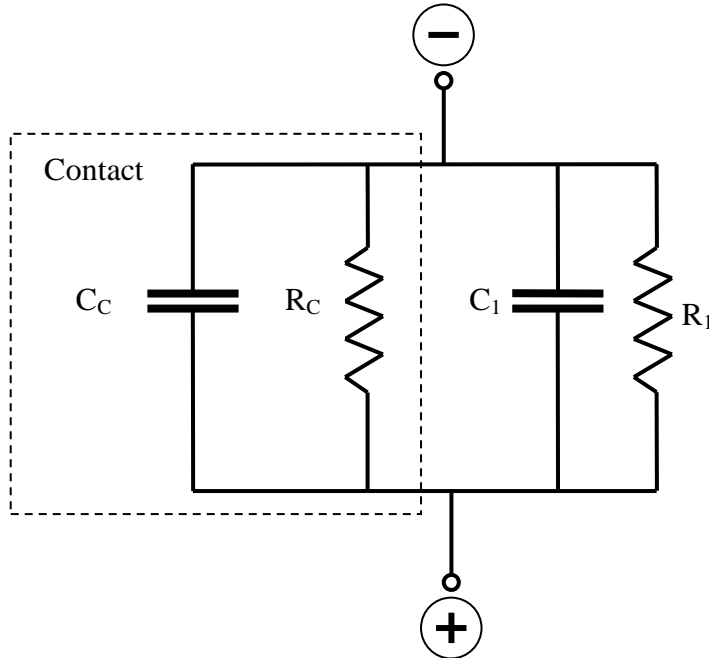


Figure 110: Experimental setup for capacitance measurement

The impedance phase shift analyser was supplied by Solartron Analytical. The device offers a very wide frequency range from $10\mu\text{Hz}$ up to 32MHz , it has a very good accuracy of 0.1 % making possible measurement of even the most subtle change in the setup. This device provides a noise free analysis by using a single sine correlation technique [100].

Virtually every liquid and solid is able to pass current when a voltage is applied to it. If a variable (AC) voltage is applied to the material, the ratio of voltage to current is known as the impedance. The measured impedance varies with the frequency of the applied voltage in a way that is related to the properties of the liquid or solid. This may be due to the physical structure of the material, to chemical processes within it or a combination of both.

**Figure 111: Electronic schematics for the electronics box**

C_C – contact capacitance

R_C – contact resistance

R_1 – resistance 2 k Ω

C_1 – capacitor 22 pF

Different configurations for the electronic box have been tried. Settings like the C_1 capacitor connected in series or parallel have been explored and no big difference in measured capacitance was observed. Different values for the R_1 resistor have been employed, an increase in resistance value results in a significant decrease in measured capacitance and implicitly, a decrease in resistance will give a bigger capacitance. This phenomenon is attributed to a decrease/increase in current flow through the elastohydrodynamic contact. The additional resistance R_1 and capacitor C_1 are needed in order to see if the current actually flows through the contact or is lost in any of the connections.

The criteria for establishing the test parameters are presented below:

A scan using frequency limits was done, this implies using a low and high frequency value. The impedance varies with frequency and from the tests it was found that for a 35kHz frequency, the resulting variation in capacitance is the smallest.

The AC level was set at 1V as for this level a wide range of thicknesses can be measured, anything higher than 1V gives a short circuit between the capacitor plates; at small film thicknesses if a lower AC level is used, then bigger film thicknesses cannot be measured.

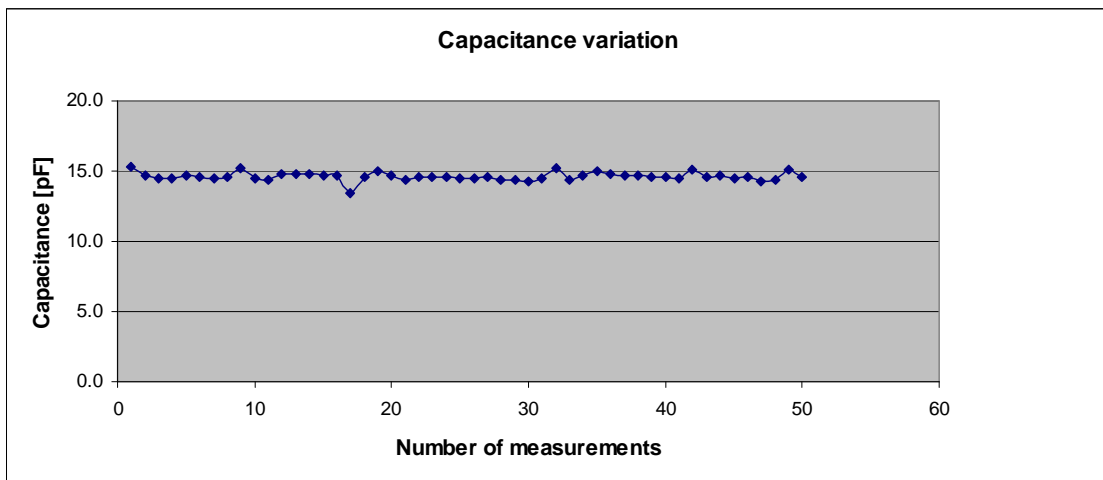
The DC level was set to zero, as no difference in measurements was observed when it was present.

The integration time was set to the minimum supplied by the impedance analyzer. Lower integration time results in a faster measurement (an almost instantaneous value grab). Figure 112 gives us a better understanding of the variation experienced when a measurement is taken. The final value registered for one measurement will be an average of these fifty. A higher number of points have been tried and no big difference in the average value was obtained.

Tests have been done using different impedance analyser setup for the AC level, DC level, frequency and integration time. After a number of tests a conclusion had been reached and the setup for the impedance analyser chosen. Table 8 shows the experimental setup for the impedance analyser.

Table 8

Frequency [kHz]	AC level [V]	DC level [V]	Integration time [s]
35	1	0	0.01

**Figure 112: Capacitance variation at constant frequency**

Before all tests were conducted a background capacitance was measured in order to eliminate the influence of different outside parameters (like electromagnetic fields coming from the motors, computers, and electrical resistance used to heat the rig) that could tamper with the EHD contact measurement. The background capacitance measurements imply measuring the capacitance of the entire system in testing conditions except for the contact (the ball is not loaded against the disc).

Background capacitance was measured for all tests regardless of the disc, lubricant, temperature, sliding condition used to measure capacitance. Additional value fluctuation resulted from temperature and sliding as well as the capacitance value from the electronic circuit that was connected to the measuring cables employed to capture results were also included in the background capacitance.

Figure 113 presents the measured background capacitance for the PAO 40 base oil at 40°C temperature, using a steel disc. From this graph it can clearly be observed that even the background capacitance varies with sliding. The difference in capacitance is ~0.8pF from pure rolling to sliding conditions. Value difference between the two sliding conditions is less than 0.2pF. This variation can be attributed to an increase in disc speed to facilitate the two sliding conditions, resulting in an increase in background capacitance.

As shown before, the signals from both disc and ball are collected through a brush. In the case of the disc, a graphite brush was employed and it is this researcher's opinion that the faster spin rate of the disc supplies this small, but significant variation, in background capacitance.

Figure 114 presents the way the background capacitance is influenced by the temperature; the results are for the base oil, in three different sliding conditions, for each temperature.

Even in this case the variation with temperature is not that large. In fact capacitance is influenced more by the sliding condition than by the temperature. Values wise, the gap between 40°C and 100°C in pure rolling conditions is ~0.3pF and increasing to ~0.6pF in sliding conditions. This variation can be explained by a slight fluctuation of resistance with temperature, the resistance can influence the capacitance variation with temperature.

This small variation with temperature and sliding can have quite an impact on the final results if it is not taken into account.

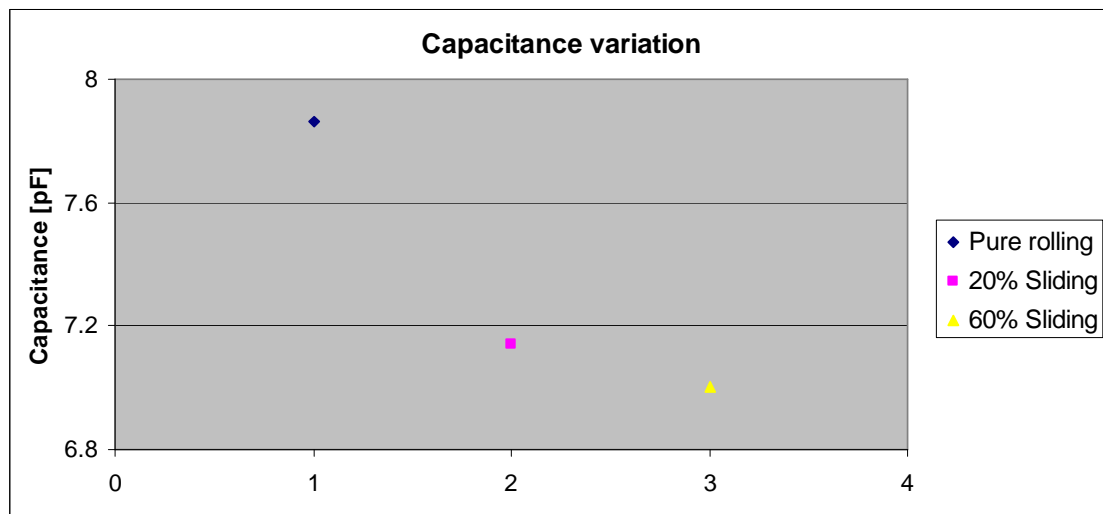


Figure 113: Background capacitance measurements in different rolling conditions

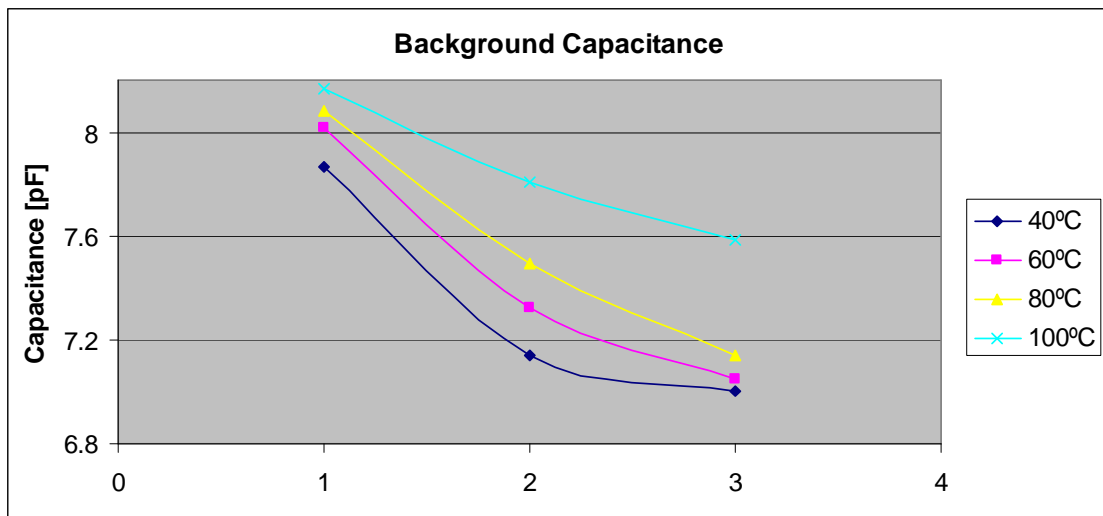


Figure 114: Background capacitance variation with temperature

5.5.2 Calibration of the Capacitance of EHD Contacts

The calibration of the capacitive method was done in two stages. The most important step was to measure the lubricant film using a well known optical method. This was a very important stage of the research, as all results obtained by the capacitive method were compared with results obtained using the optical method.

For the calibration, a Cr sputtered disc with a thickness of 15nm was used. The decision to use the disc with this particular Cr thickness has been explained in chapter 5.3.

All tests were done at the same speeds and temperatures used for the optical measurements.

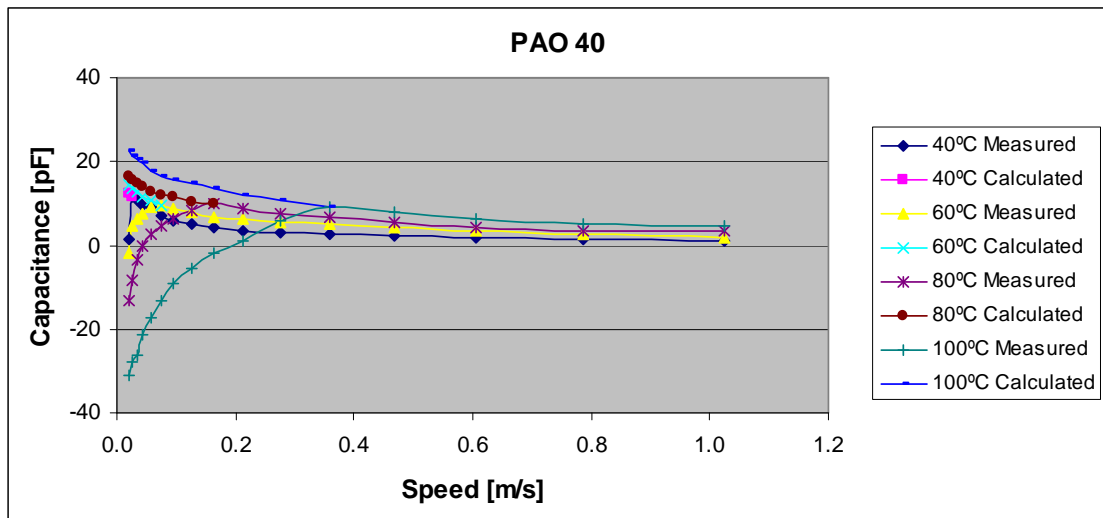


Figure 115: Capacitance measurements for PAO 40 at different temperatures using a Cr sputtered disc

Capacitive results using the Cr sputtered disc for a range of temperatures starting from 40°C up to 100°C is showed in Figure 115. It can clearly be observed that with a raise in temperature, the film thickness decreases and the capacitance values increase, phenomenon observed by previous researchers [66]. The difference in capacitance value at high speeds when the film thickness is the highest is very small, maximum 3pF; implicitly for low speeds and low film thicknesses, the capacitance is higher and the difference in value is obvious it almost doubles from 40°C to 100°C.

Figure 116 represents the film thickness variation with temperature. The graphs were made in such a way to eliminate the influence viscosity (η) might have on the oil film thickness thus showing that the capacitance method is precise enough to accurately measure lubricant gap over a range of temperatures and speeds.

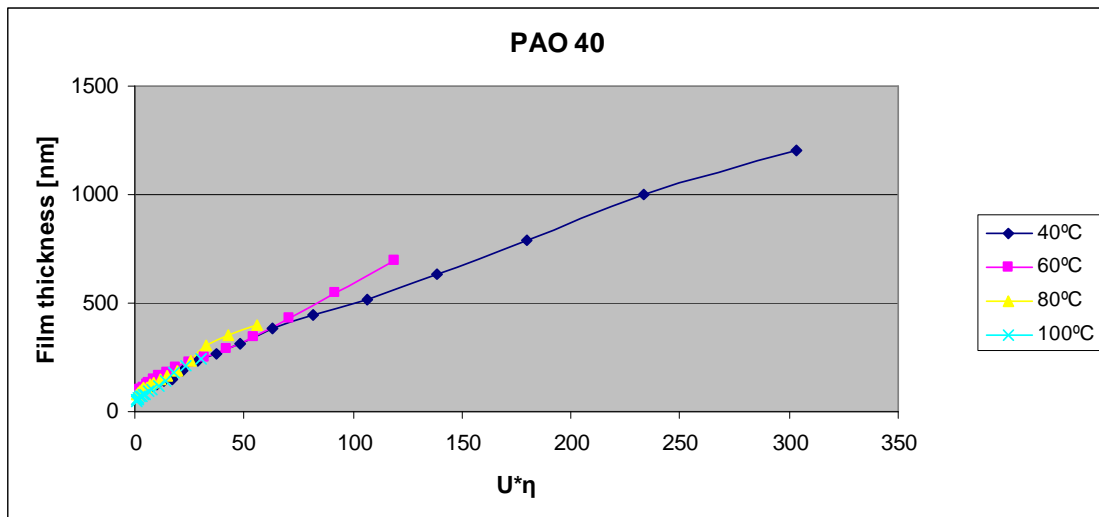


Figure 116: Film thickness measurements using the capacitive method

Figures 117–120 present the film thickness obtained using a Cr sputtered disc with a thickness of 15nm and the film thickness measured using the classical optical interferometry technique. The capacitance measurements were taken and using data from [93] and correlating the EHD contact with a parallel plate capacitor employing Equation 104 film thickness was extracted. From the graphs a conclusion can be drawn, that optical and electrical film thicknesses follow the same trend and are close in value therefore it is safe to say that the electrical method developed in this project is precise enough to measure film thicknesses without any further calibration.

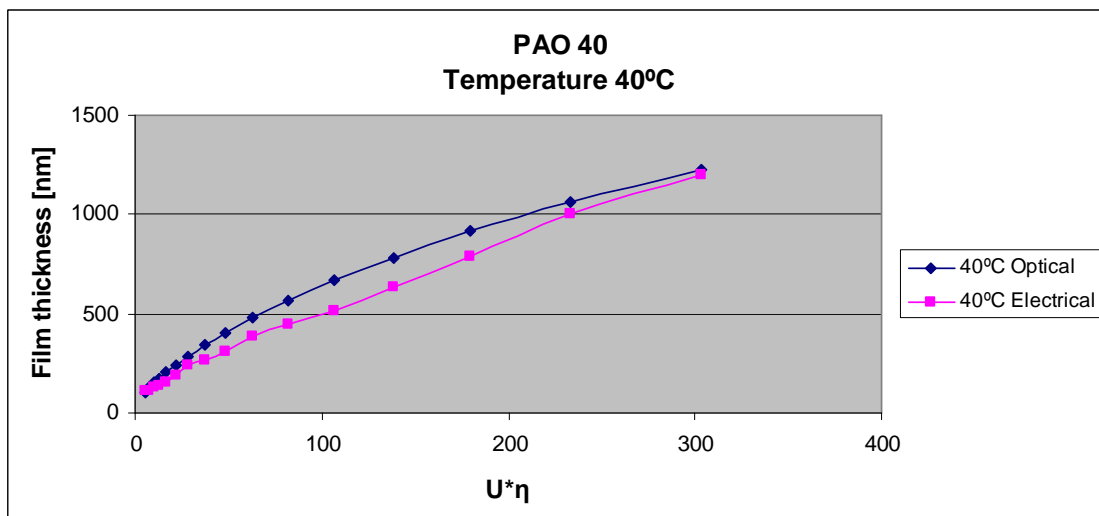


Figure 117: Film thickness measurements for PAO 40 at 40°C using a Chromium sputtered disc

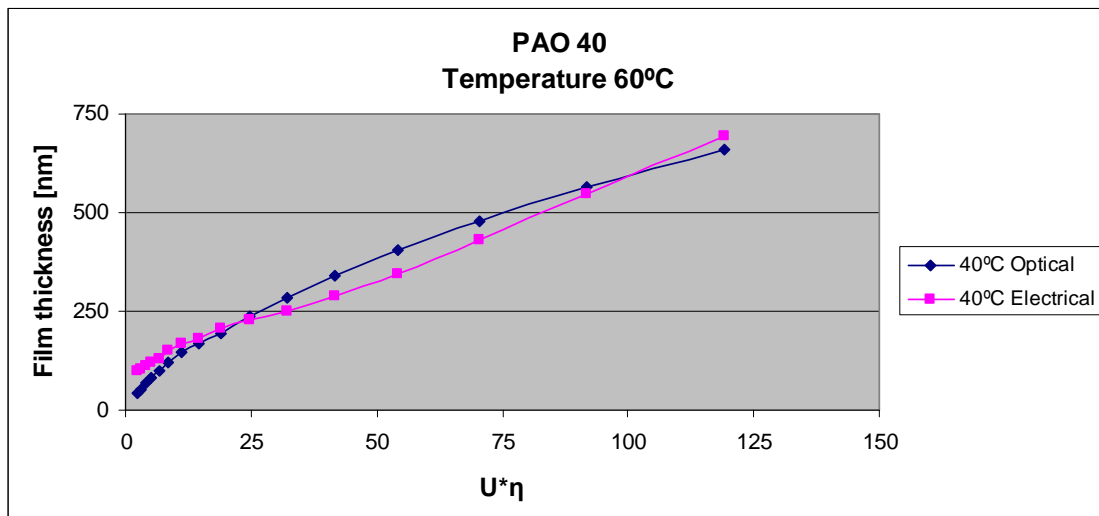


Figure 118: Film thickness measurements for PAO 40 at 60°C using a Chromium sputtered disc

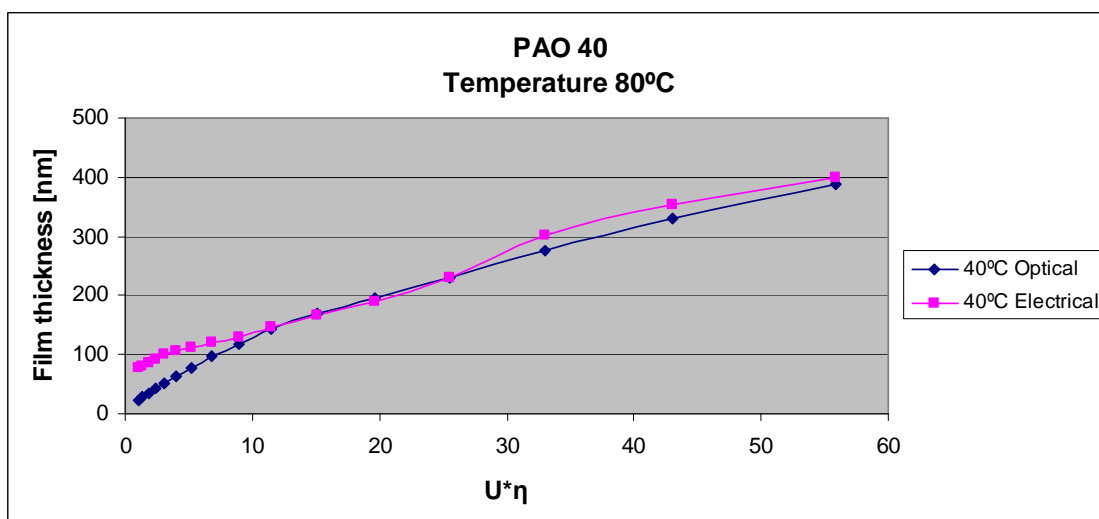


Figure 119: Film thickness measurements for PAO 40 at 80°C using a Chromium sputtered disc

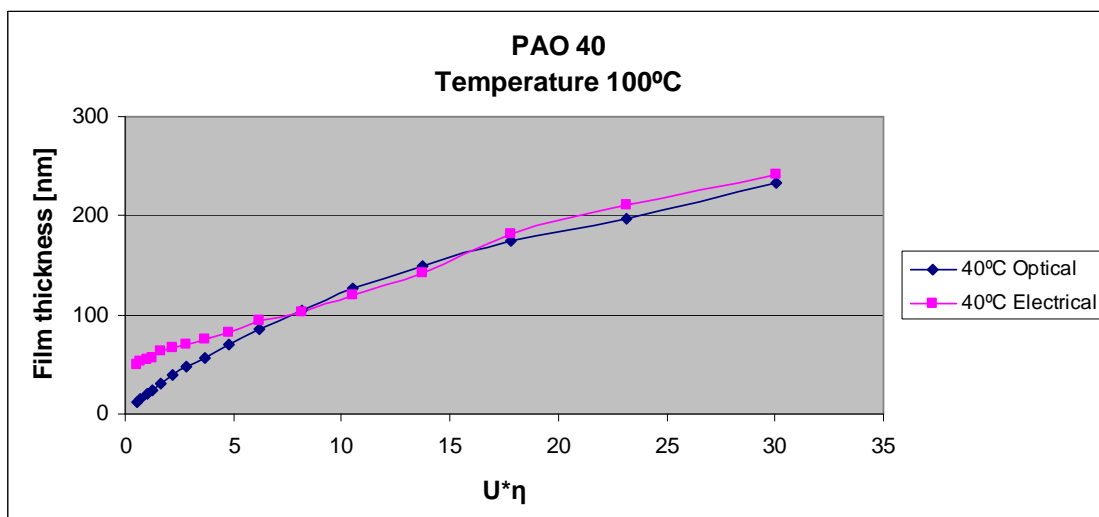


Figure 120: Film thickness measurements for PAO 40 at 100°C using a Chromium sputtered disc

6 RESULTS AND DISCUSSION

6.1 Film Thickness Measurement by the Optical Method

The Chromium thickness that gives a better image of the contact has been chosen and the calibration of the capacitive method against the optical method has been done using a disc with a Cr thickness of 15nm. Before optical measurements were done, the lubricants viscosity was analyzed over a range of temperatures.

VII's are effective at large temperatures, when the viscosity of the base oil has dropped significantly and the film thickness is very low. In the case of the lubrication in mixed or boundary regime the VII (a polymer) [42] is adsorbed at the surfaces, increasing the viscosity at the inlet of the contact, resulting in an increase film thickness (Figures 143–146). When the temperature is lower, the measured film thickness is larger and the adsorbed layer does not influence the general film thickness.

The data obtained in Figure 121 is from a rotational viscometer, where the gap between the surfaces is fixed and quite large in comparison to measured film thicknesses at high temperatures, thus the viscosity index does not appear to change in comparison to base oil at higher temperatures.

Figure 121 presents the measured viscosities for the lubricant mixes used in this project.

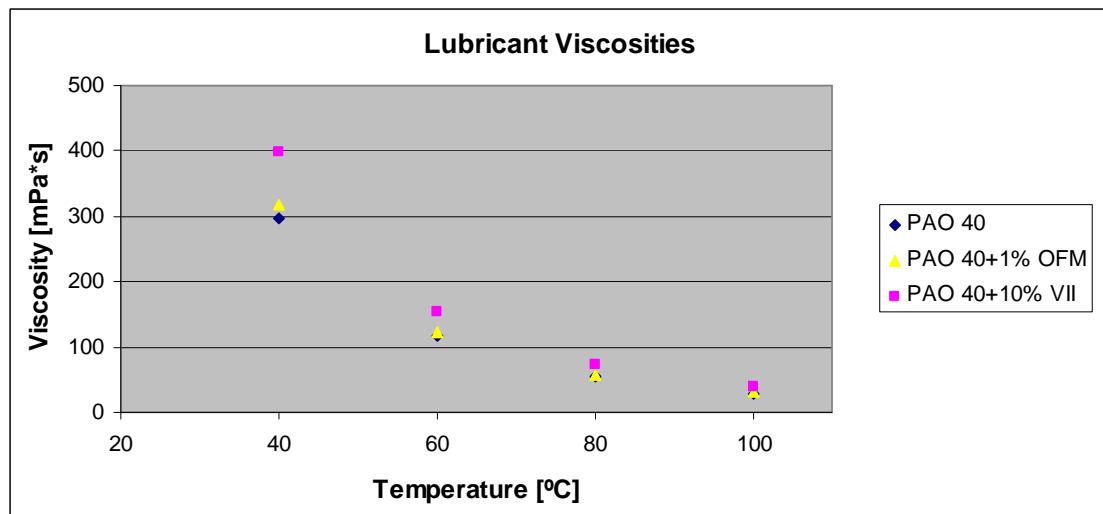


Figure 121: Lubricant viscosities at different temperatures

A clear influence of the two additives can be observed on lubricant viscosities; higher influence is seen at low temperatures. The OFM (organic friction modifier) additive supplies a slightly larger viscosity at low temperature and the values obtained for higher temperatures overlap with the values obtained for the base oil. The VII (viscosity index improver) mix gives a bigger difference in viscosity compared to the base oil, but this influence diminishes with an increase in temperature.

6.1.1 Base Oil

Film thickness measurements were measured for a number of speeds and different slide/roll conditions and the resulting graphs are presented below.

Figures 122–124 present the log/log graphs obtained for the chosen base oil at temperatures varying from 40°C to 100°C, using pure rolling conditions for Figure 122 and introducing two different slide to roll ratios for the other two graphs.

A clear difference can be seen between the temperatures used, an increase in temperature supplies a significant decrease in film thickness, caused by a lubricant viscosity drop.

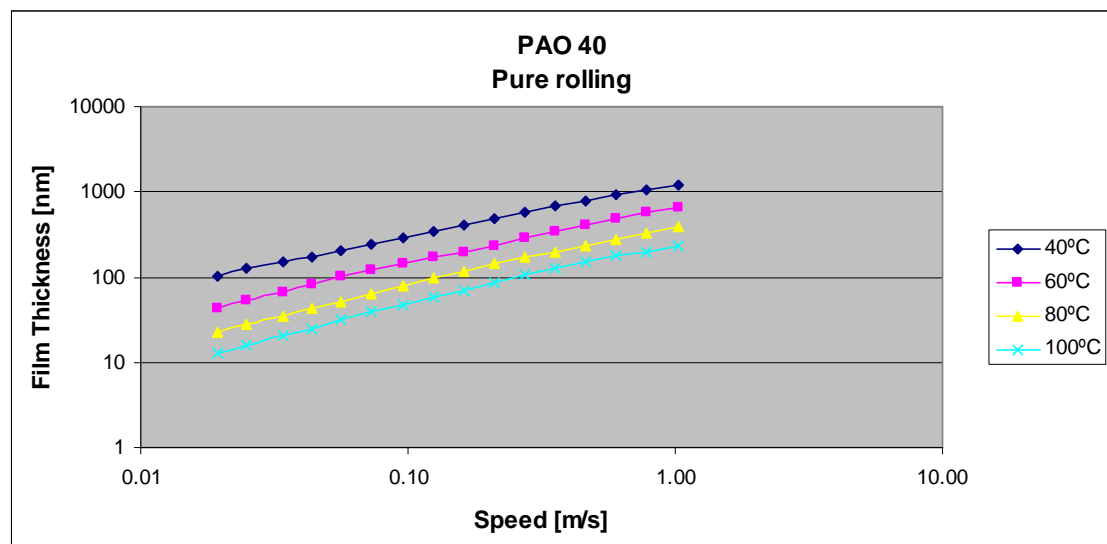


Figure 122: Film thickness measurements for a PAO 40 lubricant at different temperatures in pure rolling conditions

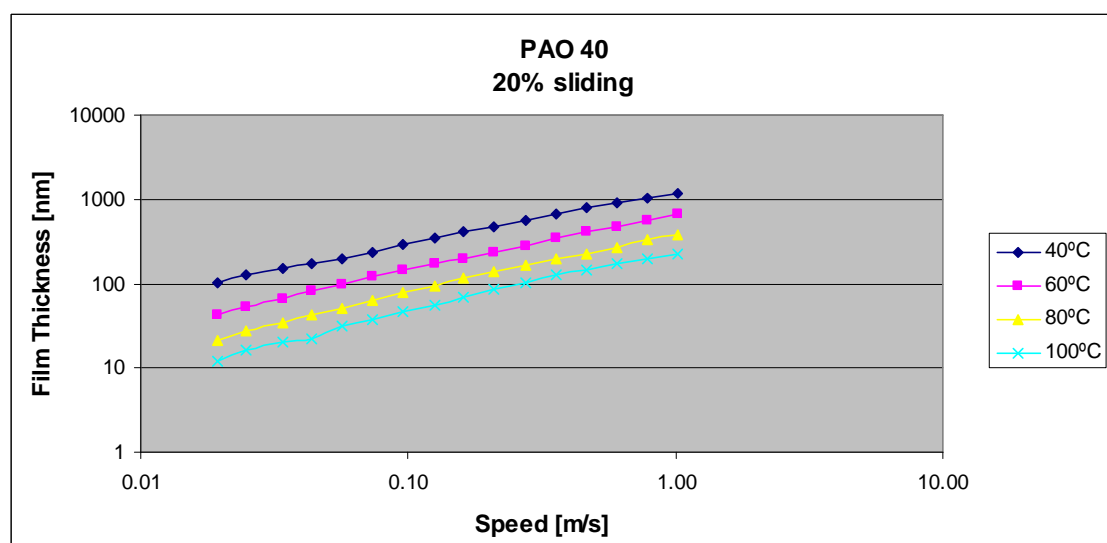


Figure 123: Film thickness measurements for a PAO 40 lubricant at different temperatures in a 20% slide/roll condition

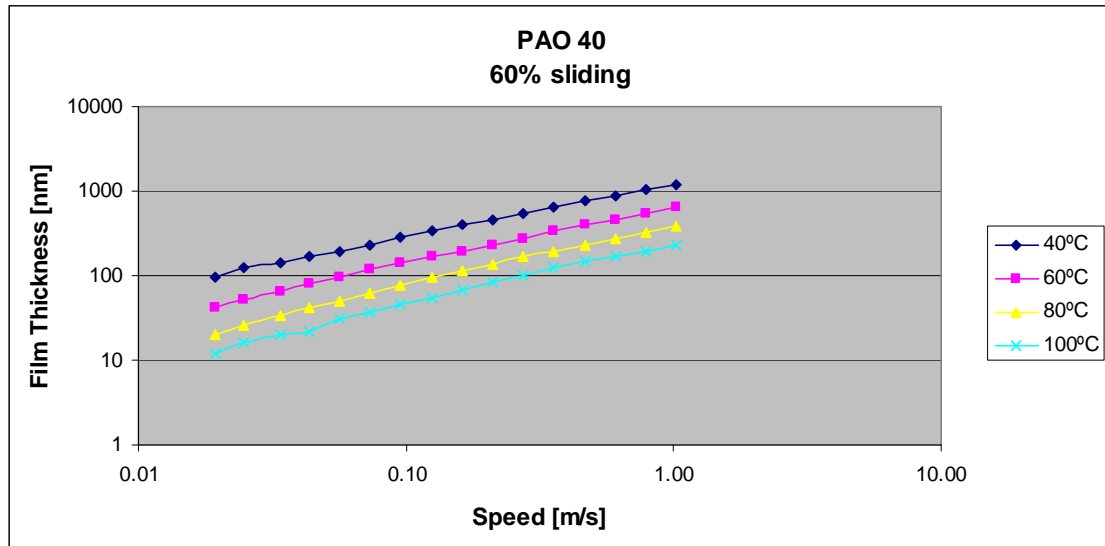


Figure 124: Film thickness measurements for a PAO 40 lubricant at different temperatures in a 60% slide/roll condition

Figures 125–128 give a better understanding of the film thicknesses variation, when different slide/roll lubricating conditions are applied to the same oil.

It can be stated that film thickness varies quite a lot with temperature. On the other hand, a big variation of film thickness with slide/roll conditions cannot be observed.

As found by previous researchers [101] positive sliding results in a decrease in central film thickness more so than negative sliding. The explication for this phenomenon is that the temperature increases in the contact influencing the local lubricant viscosity resulting in a smaller film thickness.

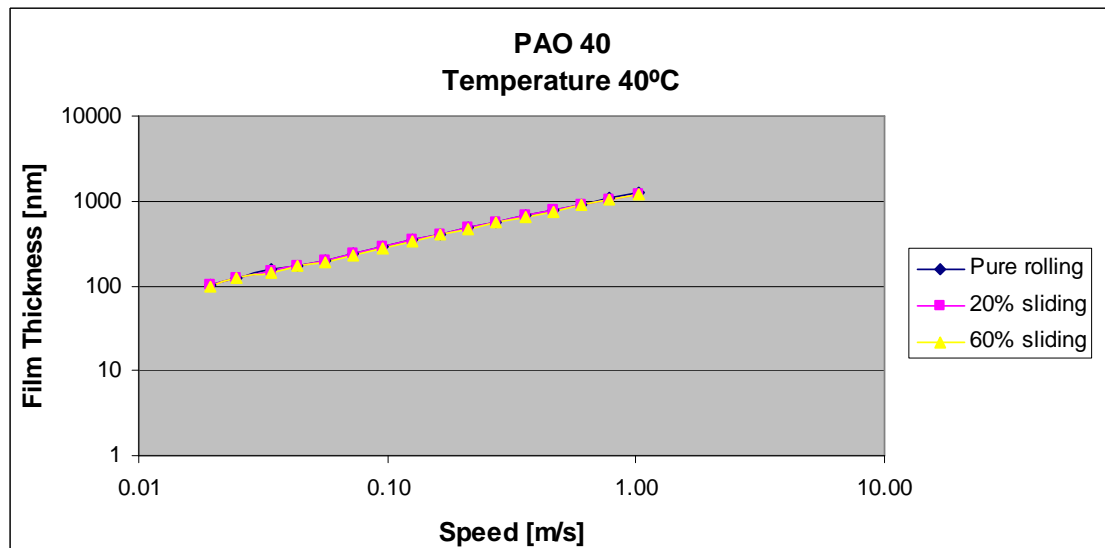


Figure 125: Film thickness comparison for a PAO 40 at 40°C in different slide/roll conditions

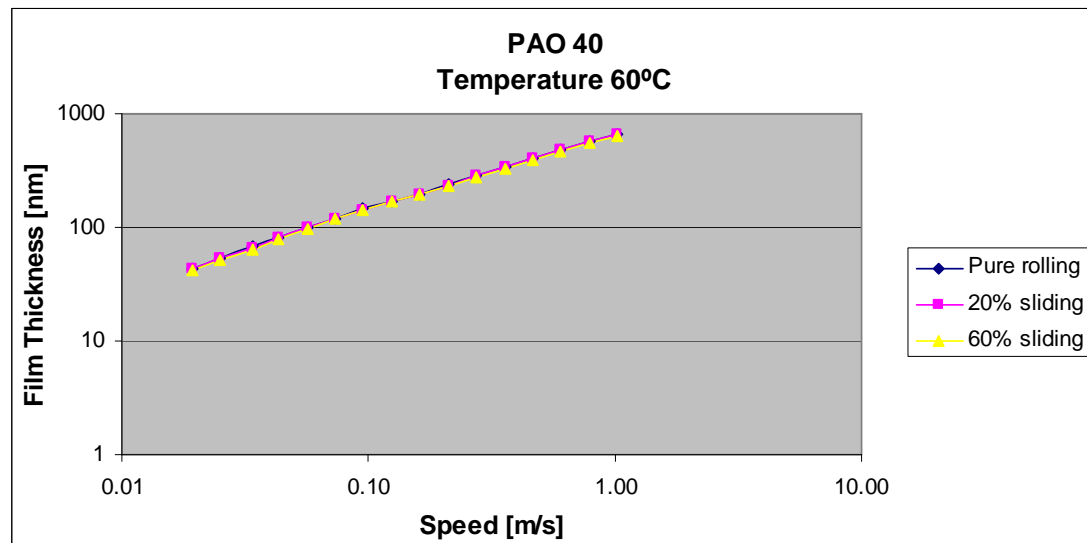


Figure 126: Film thickness comparison for a PAO 40 at 60°C in different slide/roll conditions

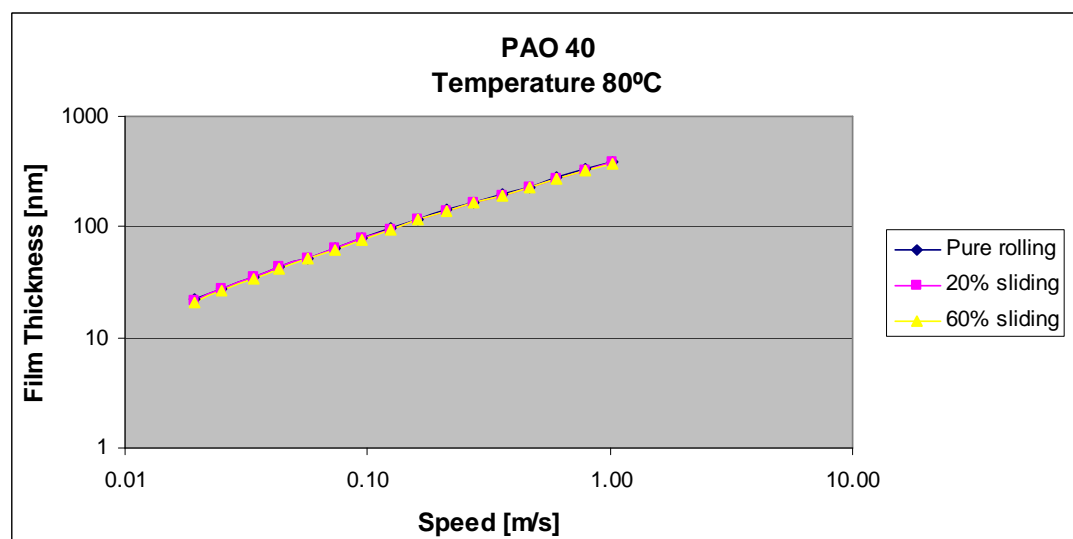


Figure 127: Film thickness comparison for a PAO 40 at 80°C in different slide/roll conditions

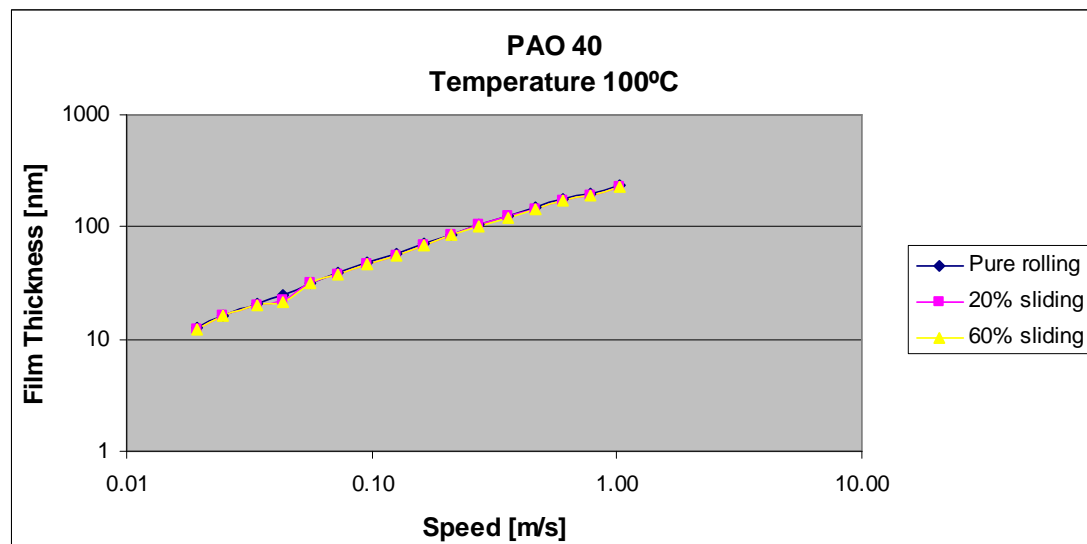


Figure 128: Film thickness comparison for a PAO 40 at 100°C in different slide/roll conditions

The difference in film thickness between the contacting surfaces is not observable when different rolling/sliding conditions are employed. In numbers, the variation in gap between the two contacting surfaces starts at 1nm, for low lubricant film thicknesses, and going up to 20nm, when the lubricant gap is close or over one micrometer thick.

Two different types of additives have been chosen to observe the influence of the additive presence in the lubricant mixture. From an optical point of view things are pretty clear, as this combination has been studied thoroughly by previous researchers [41, 42]. To see the influence of the additive on the capacitive method, at first optical measurements of the lubricant mixture have been done, in order to produce values against which the capacitive method can be calibrated.

6.1.2 Film Thickness of Organic Friction Modifier Solution

Two types of additives were utilized to see the influence they have on the film thickness measured by optical interferometry and on the measured capacitance.

The first type of additive used is an organic friction modifier (OFM). This additive influences the lubrication process only when the elastohydrodynamic and hydrodynamic lubrication fails and boundary conditions apply.

As stated before, even when additives are introduced to the lubricant, there is no noticeable difference in film thicknesses when slide/role ratios are employed.

When sliding is introduced in the testing conditions the lubricant mixture behaves in the same way as the bulk oil, the actual film thickness of the contact decreases.

Film thicknesses have been measured and the results are presented in Figures 129–131.

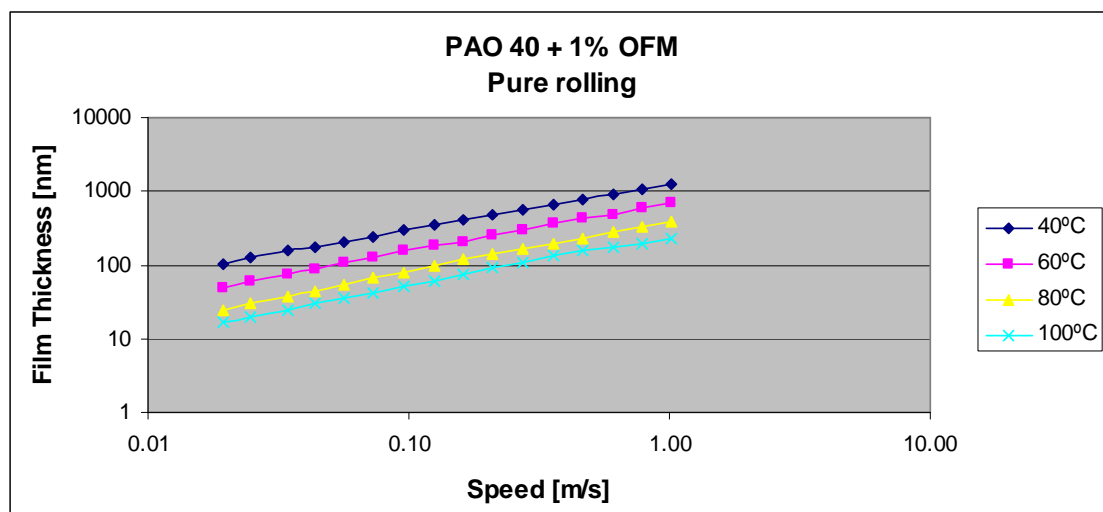


Figure 129: Film thickness measurements for a PAO 40 lubricant with a 1% organic friction modifier [OFM] present in the mixture at different temperatures in pure rolling conditions

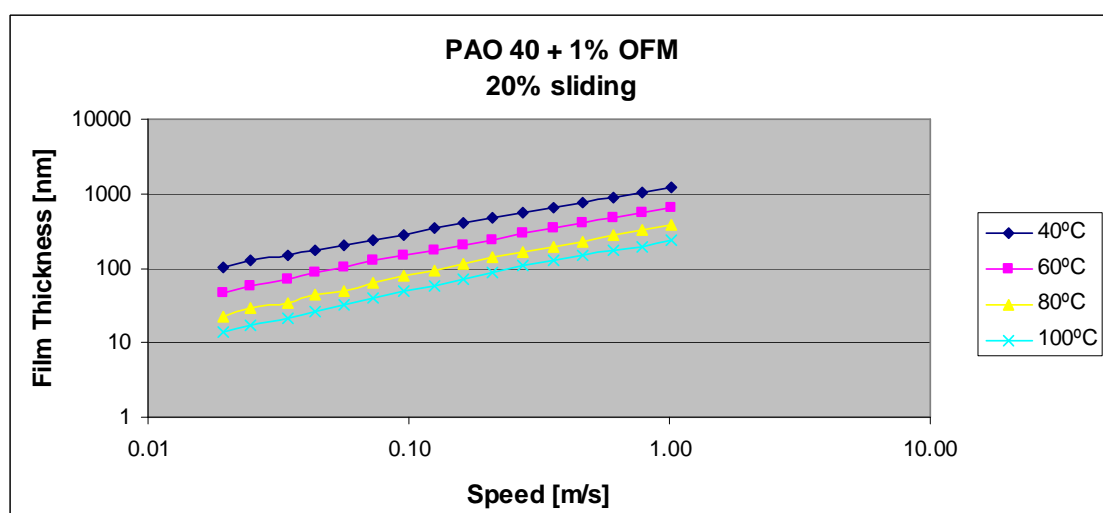


Figure 130: Film thickness measurements for a PAO 40 lubricant with a 1% OFM present in the mixture at different temperatures in 20 % slide/roll condition

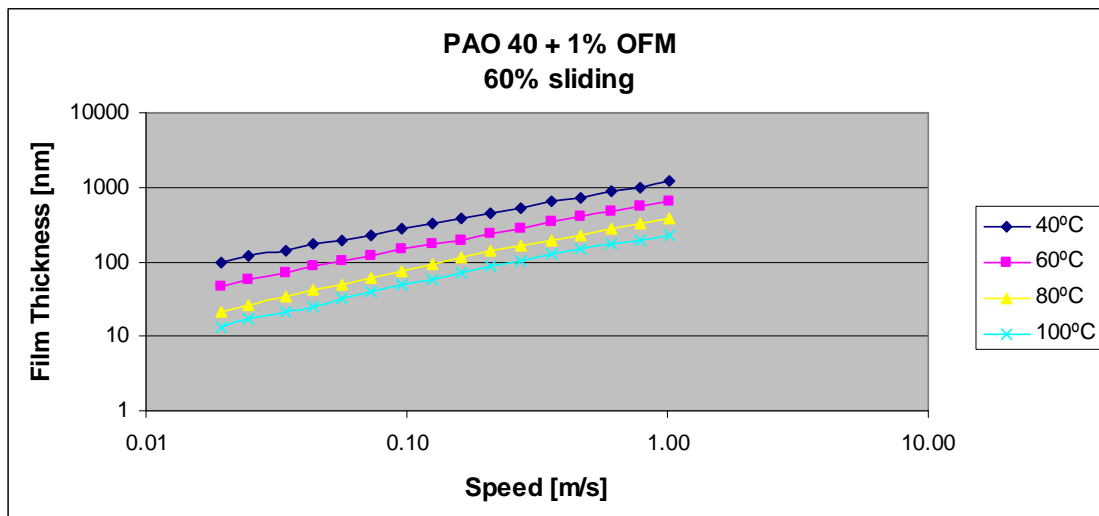


Figure 131: Film thickness measurements for a PAO 40 lubricant with a 1% OFM present in the mixture at different temperatures in 60 % slide/roll condition

A comparison between the lubricants in pure form and when additives are introduced has been done and the results are presented later on. The biggest influence on the film thickness is given by the viscosity index improver [VII], which will be discussed in the next chapter.

The next stage is to see if the introduction of different slide/roll ratios has the same effect as it does for the base oil employed, i.e. no significant increase or decrease in film thickness was observed. Figures 132–135 present the graphs extracted from the conducted tests on the 1% OFM lubricant mix.

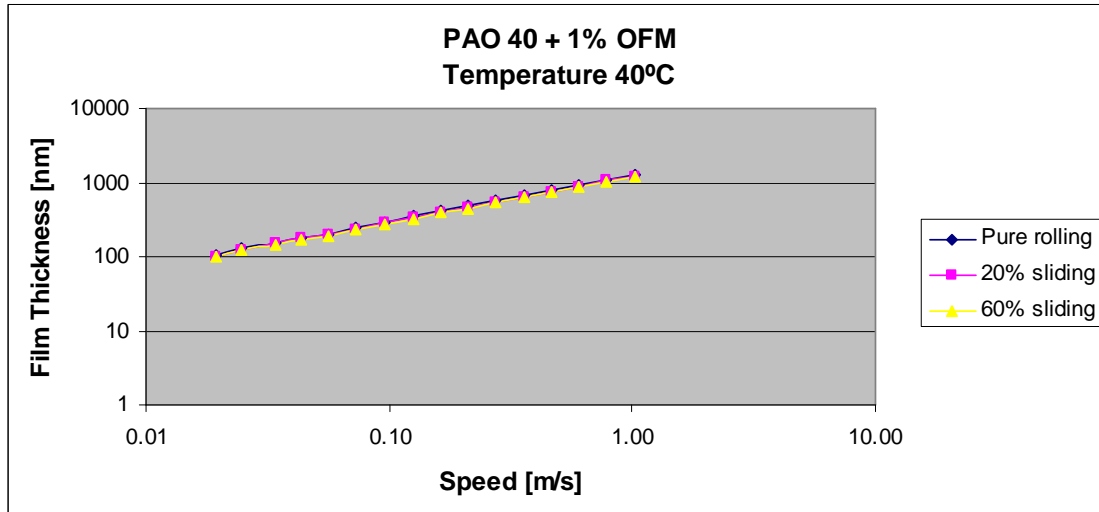


Figure 132: Comparison of film thickness measurements for a PAO 40 lubricant with a 1% OFM present in the mixture at 40°C in different slide/roll conditions

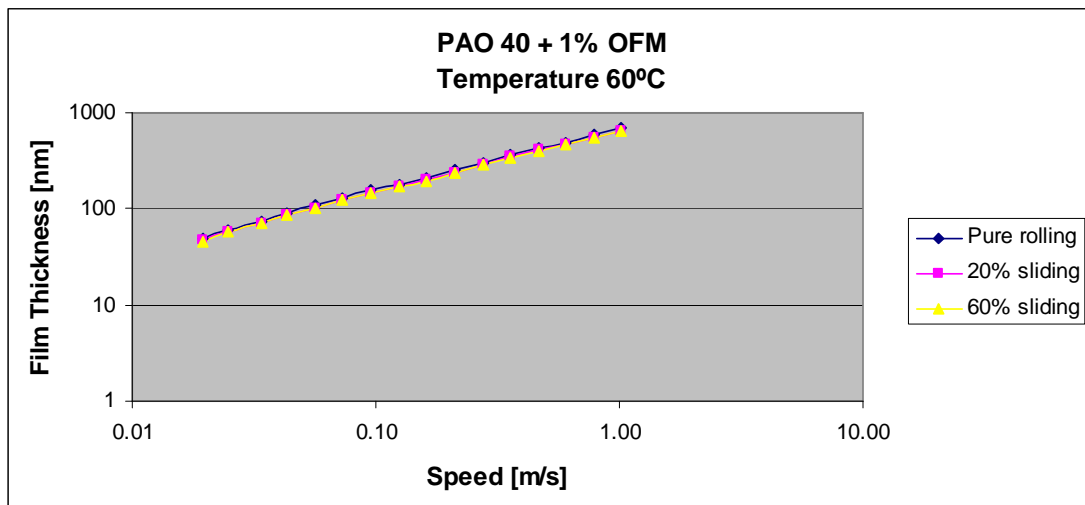


Figure 133: Comparison of film thickness measurements for a PAO 40 lubricant with a 1% OFM present in the mixture at 60°C in different slide/roll conditions

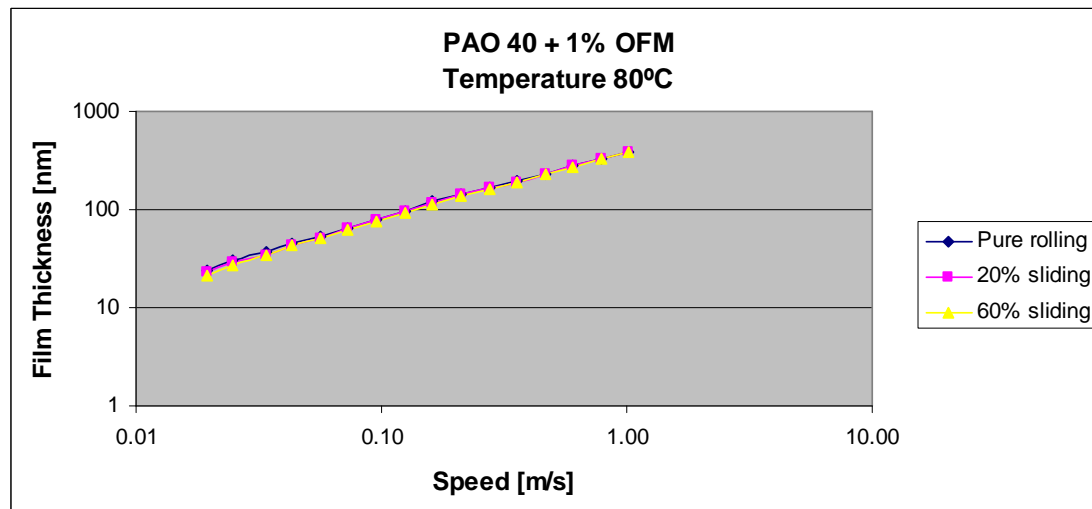


Figure 134: Comparison of film thickness measurements for a PAO 40 lubricant with a 1% OFM present in the mixture at 80°C in different slide/roll conditions

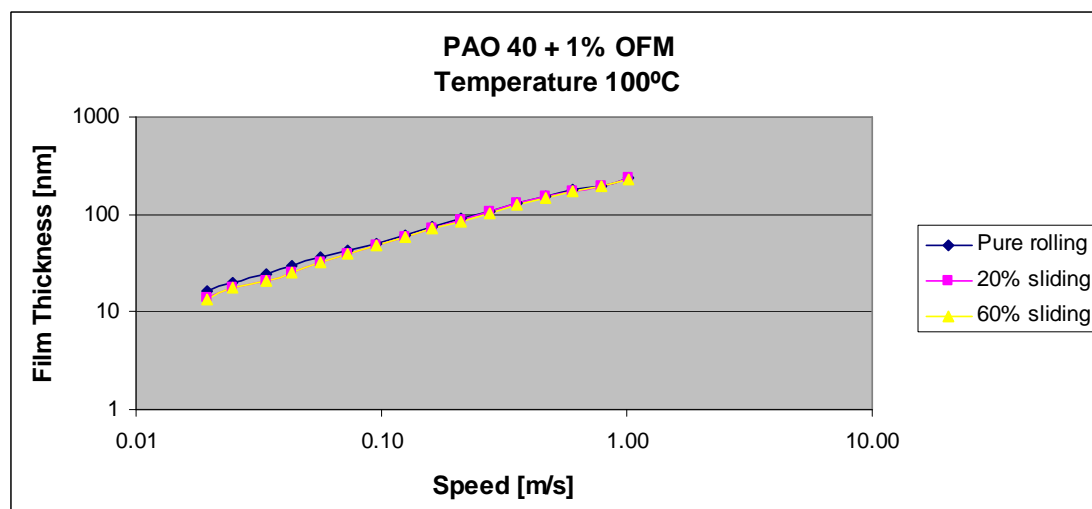


Figure 135: Comparison of film thickness measurements for a PAO 40 lubricant with a 1% OFM present in the mixture at 100°C in different slide/roll conditions

6.1.3 Film Thickness of Viscosity Index Improver Solution

The second additive used is a viscosity index improver (VII), this type of additive has been used for a long period of time in order to supply multigrade lubricants mineral based oils.

VII's are polymeric compounds (in the present thesis a polymethylacrylate type VII was used) which becomes more soluble and, thus, adopts a more open molecular conformation in the solution as the temperature is raised. In consequence they make a proportionately greater contribution to the viscosity of the blend at high rather than at low temperatures, thereby raising the viscosity index [42].

In the case of the viscosity index improver, a higher influence can be observed on the optically measured film thickness and as shown in the next chapter, Figures 143–146 the same influence can be seen on the capacitive measurements.

Figures 136–138 represent the graphs resulted from the conducted tests at different temperatures, employing different rolling conditions.

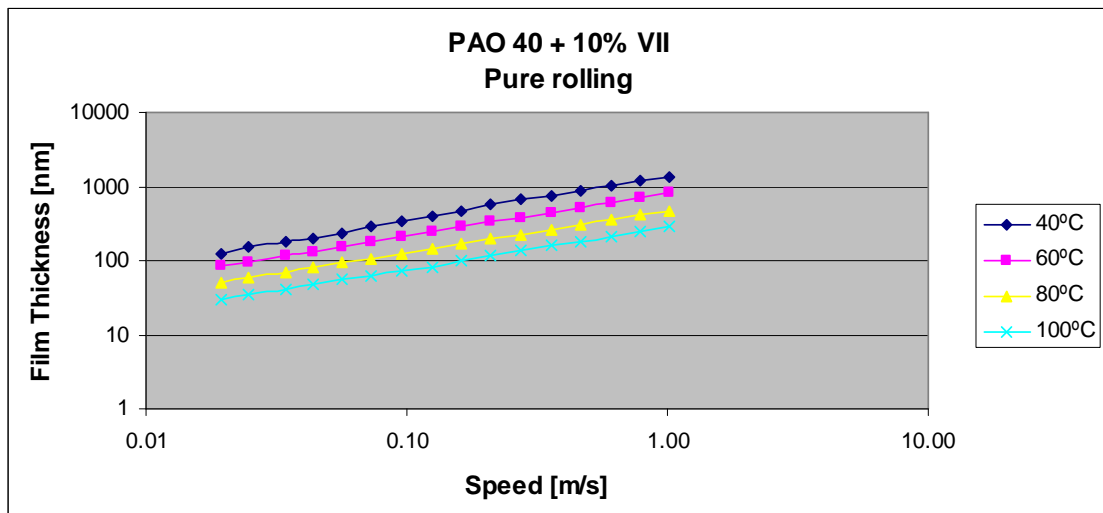


Figure 136: Film thickness measurements for a PAO 40 lubricant with a 10 % viscosity index improver [VII] present in the mixture at different temperatures in pure rolling conditions

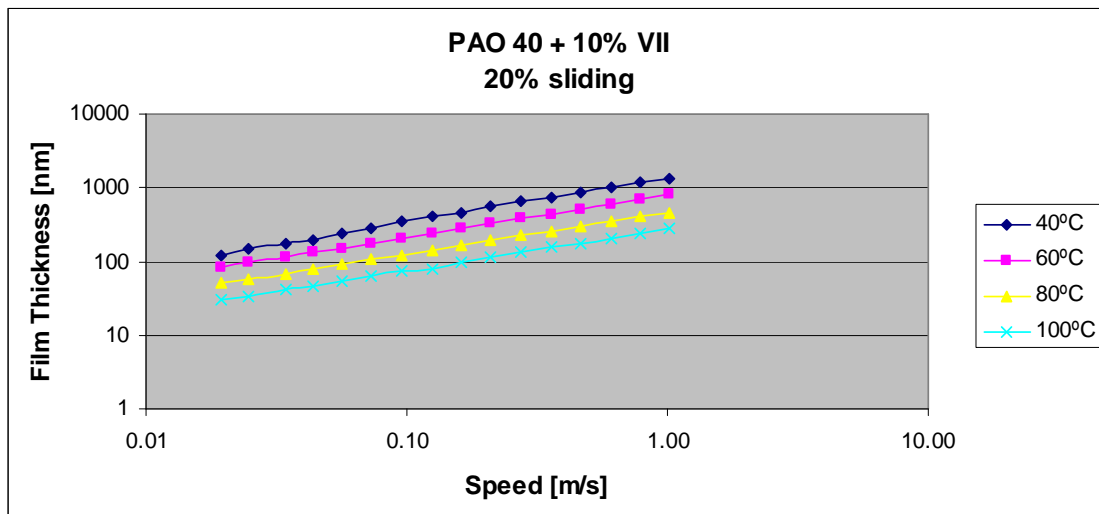


Figure 137: Film thickness measurements for a PAO 40 lubricant with a 10 % [VII] present in the mixture at different temperatures in 20 % slide/roll condition

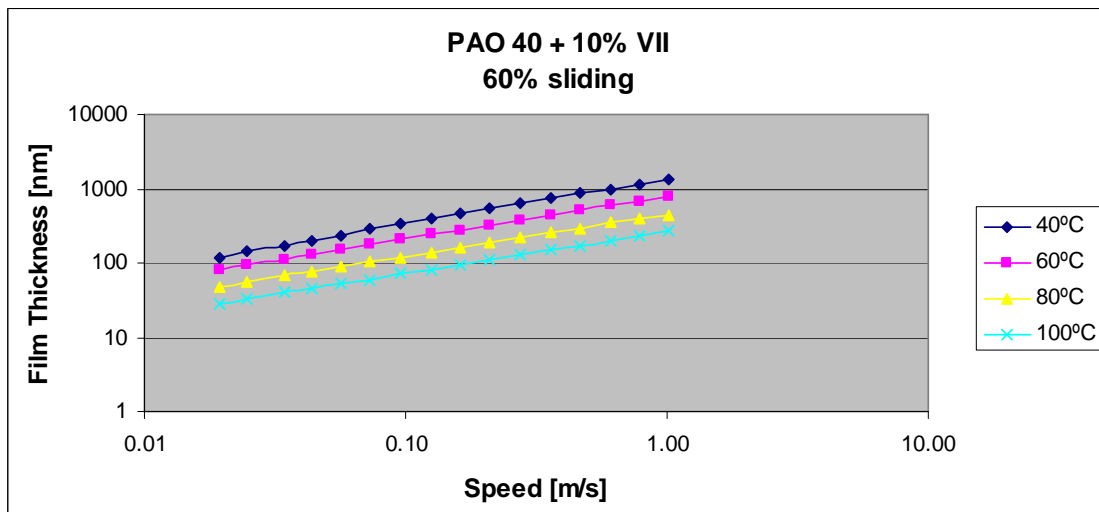


Figure 138: Film thickness measurements for a PAO 40 lubricant with a 10 % [VII] present in the mixture at different temperatures in 60 % slide/roll condition

Base oil and oil mixture with a viscosity index improver tests employing different rolling conditions have been carried out. As in previous tests, results are no different in this case (as for the two previous lubricants used) and no big variations can be observed when sliding is introduced.

Figure 139–142 present the resulting graphs from the comparison of the pure rolling and two different sliding conditions.

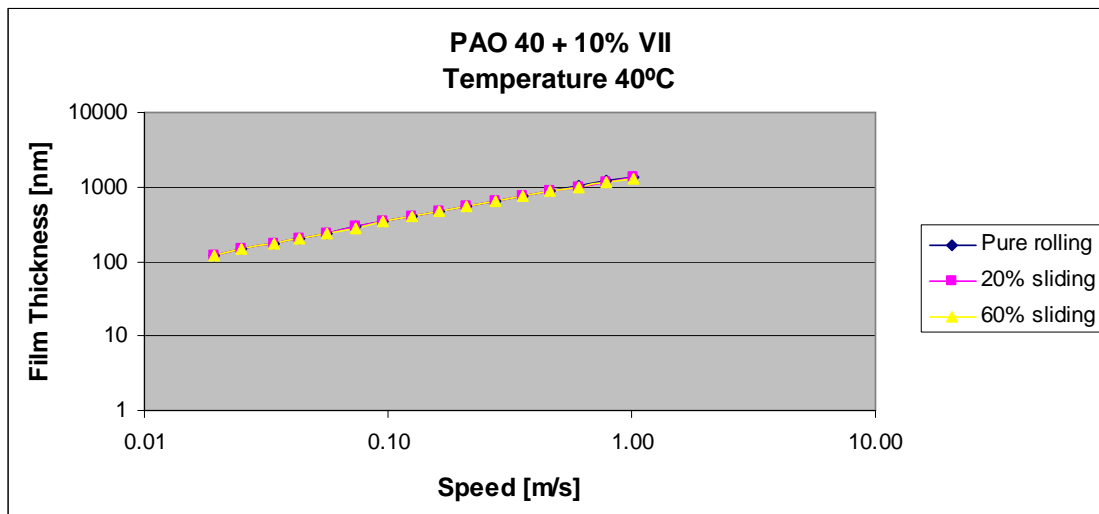


Figure 139: Comparison of film thickness measurements for a PAO 40 lubricant with a 10% VII present in the mixture at 40°C in different slide/roll conditions

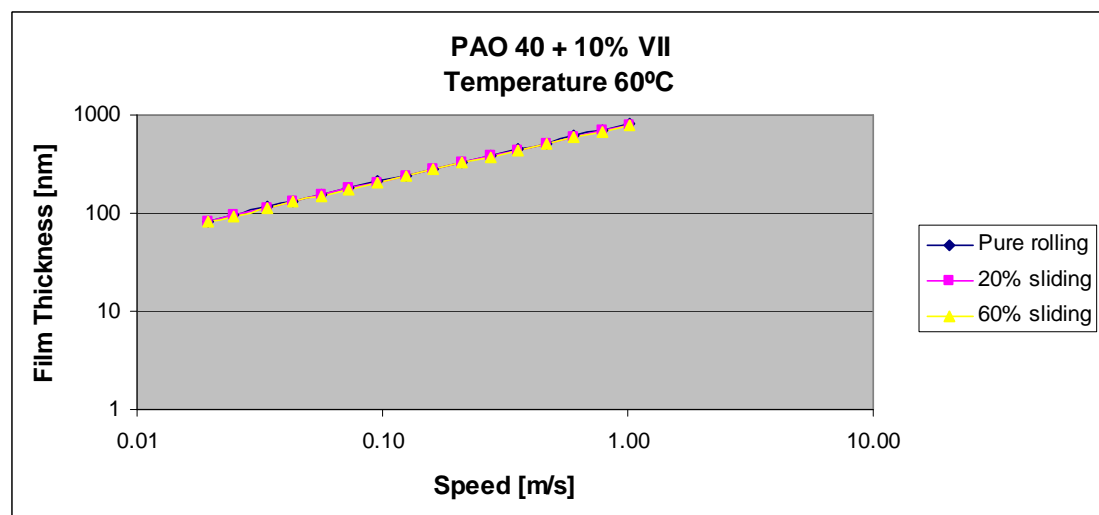


Figure 140: Comparison of film thickness measurements for a PAO 40 lubricant with a 10% VII present in the mixture at 60°C in different slide/roll conditions

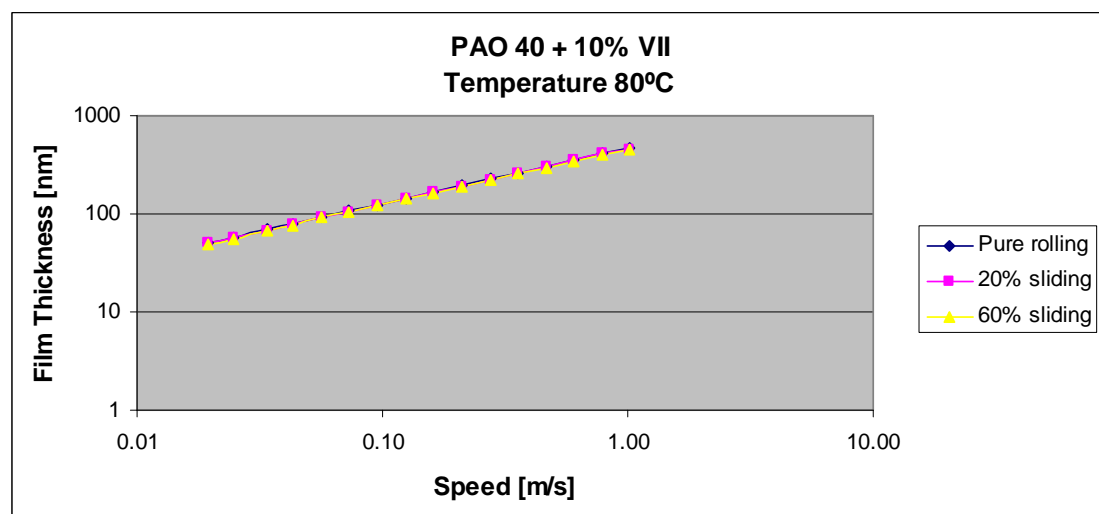


Figure 141: Comparison of film thickness measurements for a PAO 40 lubricant with a 10% VII present in the mixture at 80°C in different slide/roll conditions

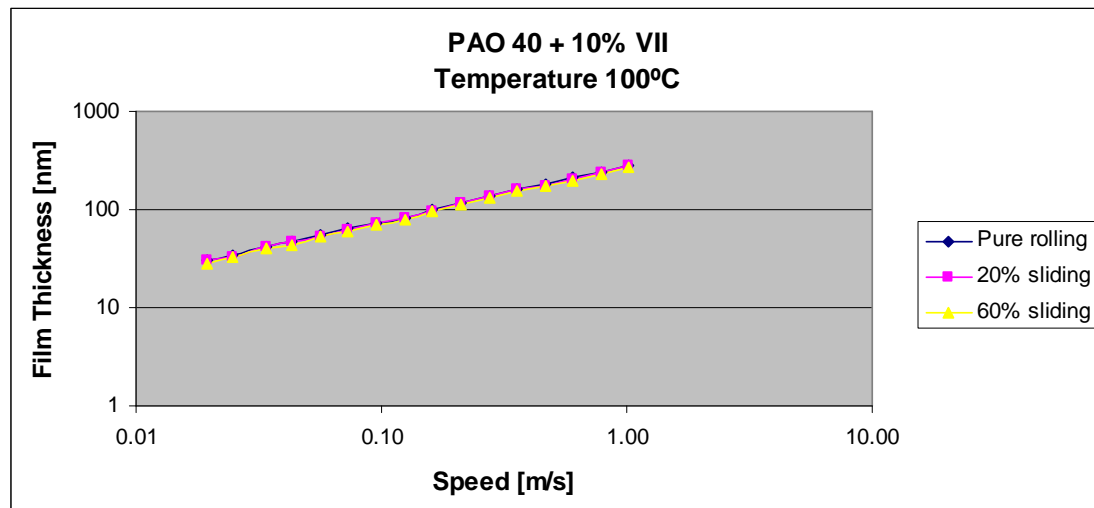


Figure 142: Comparison of film thickness measurements for a PAO 40 lubricant with a 10% VII present in the mixture at 100°C in different slide/roll conditions

6.1.4 Thickness Measurements Comparison Film Using Different Lubricant Solutions

A comparison between the base oil and the oil solutions employed has been conducted and is presented in this chapter.

One percent OFM gives the accepted boundary film formation on the two surfaces in contact; ten percent VII provides the typical viscosity raise in the lubrication process of the contact.

Figures 143–146 present a comparison between the base oil and the two lubricant solutions resulted from a mixture of 1% organic friction modifier [OFM] and 10 % viscosity index improver [VII]. The mixtures were chosen in such a way that each additive will give the expected enhancement to the lubricant mixture.

As the graphs show, the main influence on the film thickness is generated by the viscosity index improver [VII]. At low temperature and speeds, the film thickness between the two measurements is twenty nanometres thicker when the additive is present. At higher temperatures the surfaces gap doubles for low speeds and is one third higher at high speeds than the film thickness given by the lubricant in pure state.

In the case of the organic friction modifier the difference in film thickness is more difficult to see, as this additive will give larger film thicknesses only when a boundary film condition is introduced. The highest film thickness variation provided by this additive is given at very high temperatures. In our case, the boundary condition cannot be used because in boundary condition we have mixed lubrication, i.e. the asperities of the contacting surfaces touch. This phenomenon translates into a short circuit and negative values in the case of the capacitive method. A bigger influence of the OFM will be observed in the next chapter.

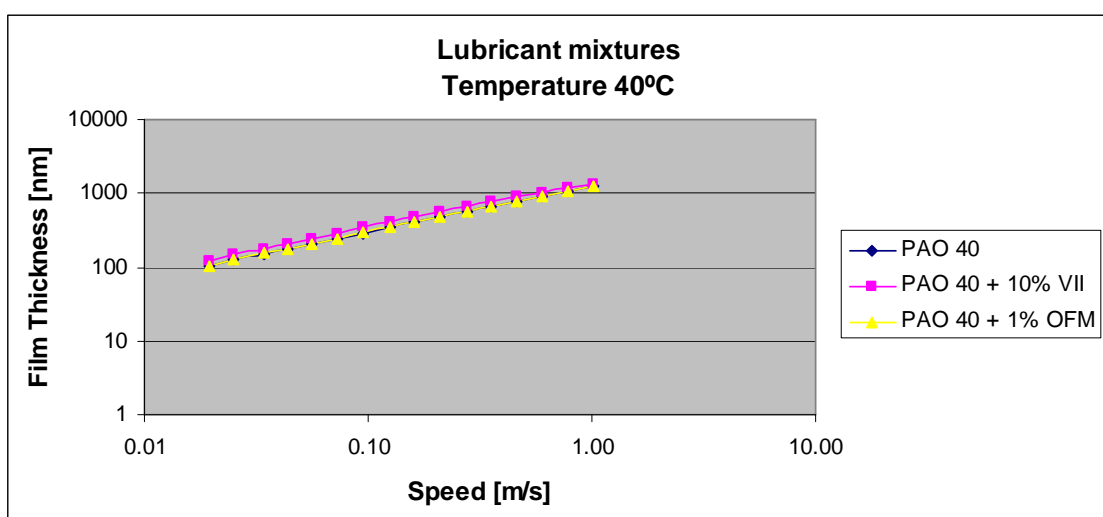


Figure 143: Film thickness comparison for a PAO 40 lubricant with different additives in the mixture at 40°C in pure rolling conditions

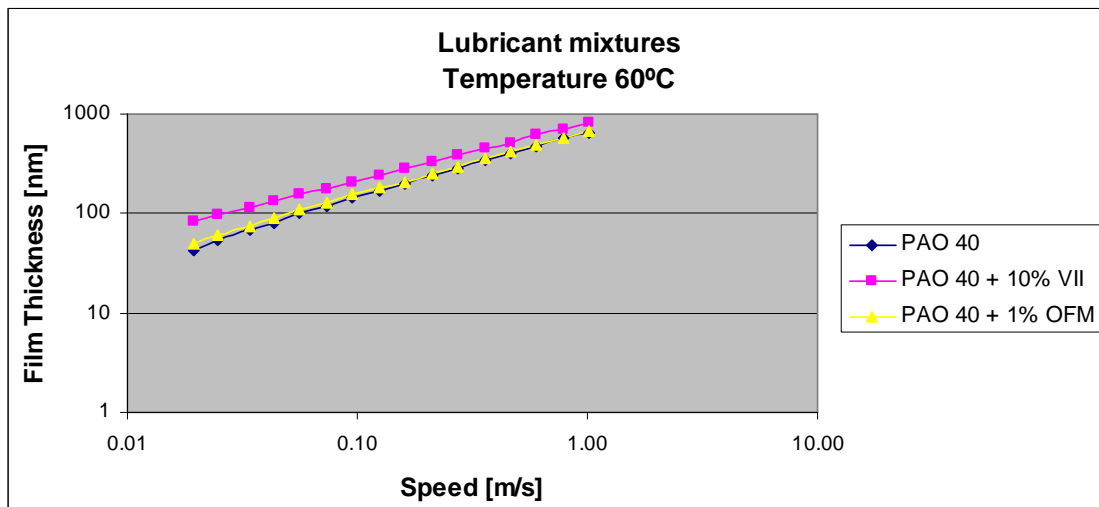


Figure 144: Film thickness comparison for a PAO 40 lubricant with different additives in the mixture at 60°C in pure rolling conditions

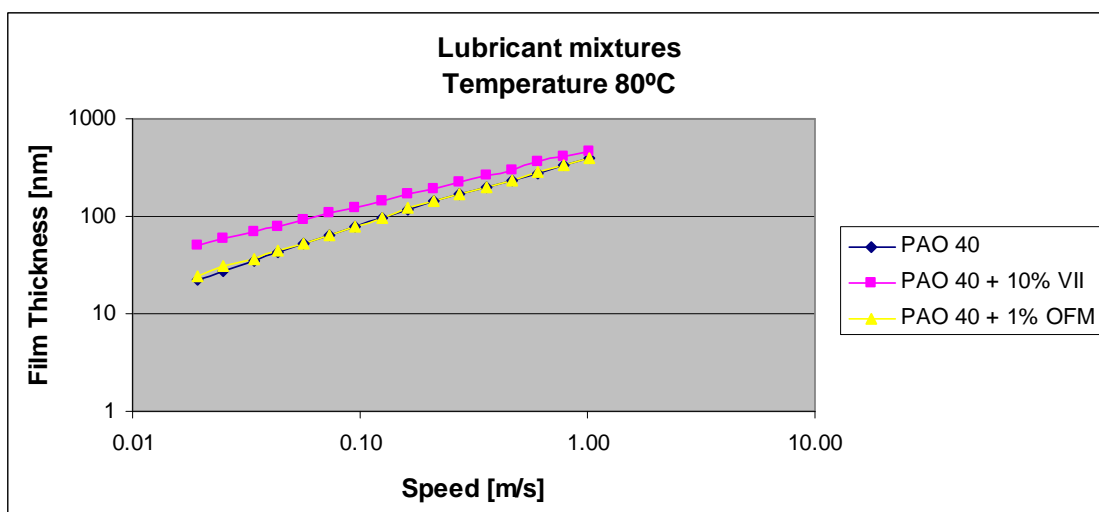


Figure 145: Film thickness comparison for a PAO 40 lubricant with different additives in the mixture at 80°C in pure rolling conditions

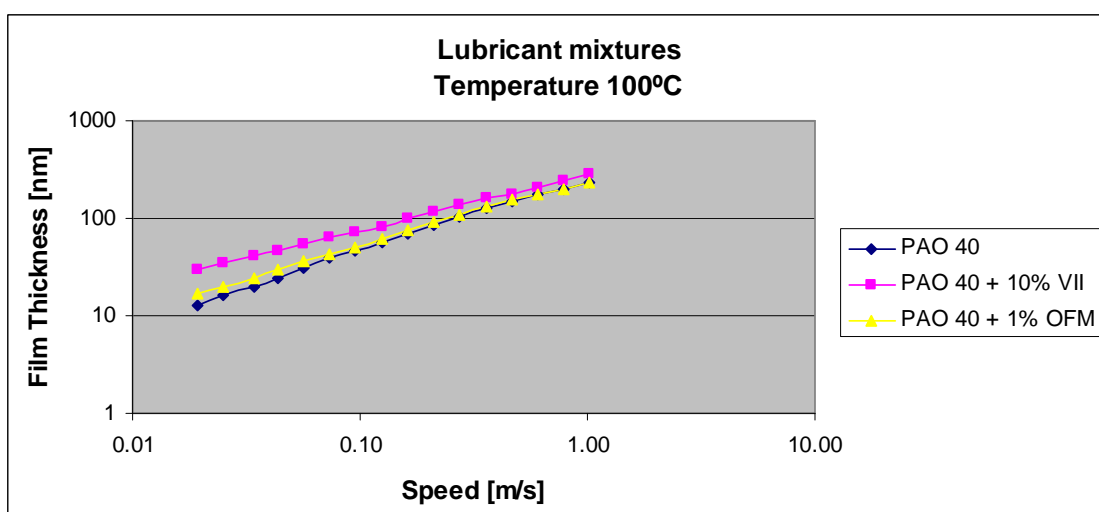


Figure 146: Film thickness comparison for a PAO 40 lubricant with different additives in the mixture at 100°C in pure rolling conditions

6.2 Limitations of the Capacitive Method

During the experiments an interesting phenomenon was observed. Accurate measurements below an optically measured film thickness of around one hundred nanometres could not be measured using the capacitive method. This incapability of measurement is thought to be attributed to a short circuit between the plates of the capacitor i.e. the ball asperities touched the disc asperities, resulting in a short circuit. The capacitive values decrease significantly with a decline in gap between the capacitor plates, going as far as negative values.

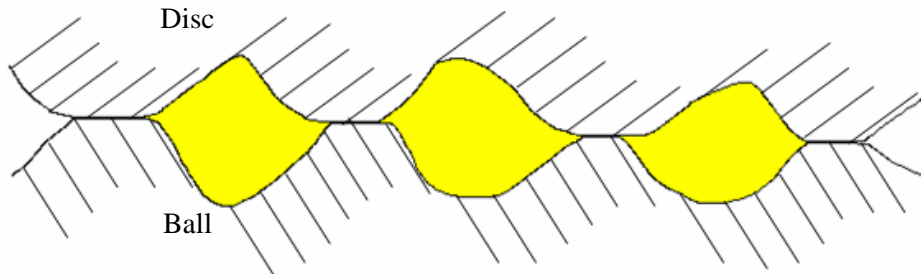


Figure 147: Contacting capacitor plates

Figure 147 illustrates, on an enlarged scale, the two capacitive plates touching. Only the highest peaks of the surface roughness touch initially; as the gap between the two surfaces decreases, the contact patch increases and the capacitive values goes in the range of negative values.

To overcome this problem with the capacitive method, a curve has been employed using the values that provide a predicted trend from the measured values. A formula has been extracted from this curve and using speed as an extension, values were extracted to continue the set of values that was measured. Figure 148 shows a comparison between the measured values and the calculated ones, for a lubricant mix consistent of a PAO 40 base oil with a 10% viscosity index improver additive, at a temperature of 80°C, using a Chromium sputtered disc with a metal film thickness of 15nm.

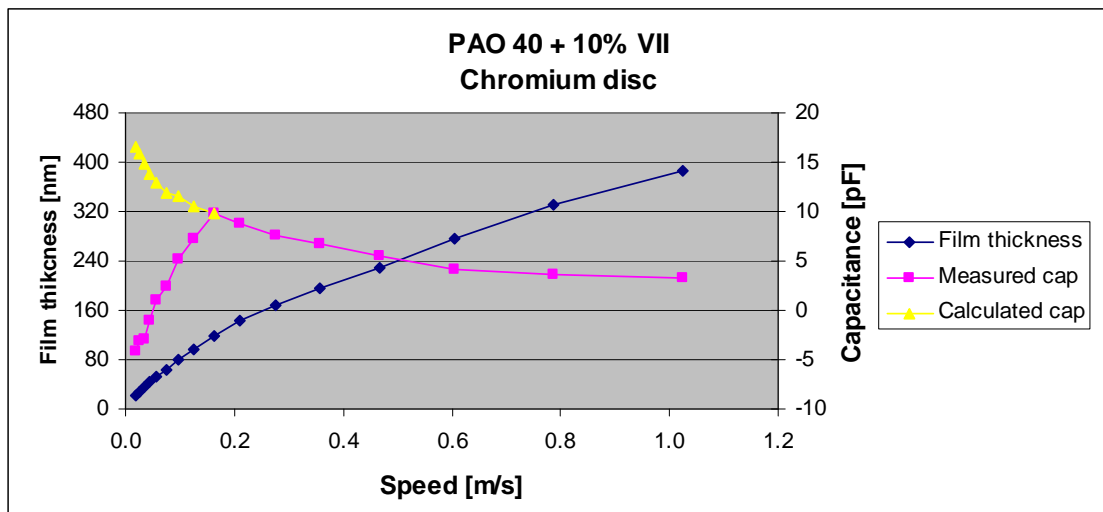


Figure 148: Capacity measured values compared with the calculated values at 80°C

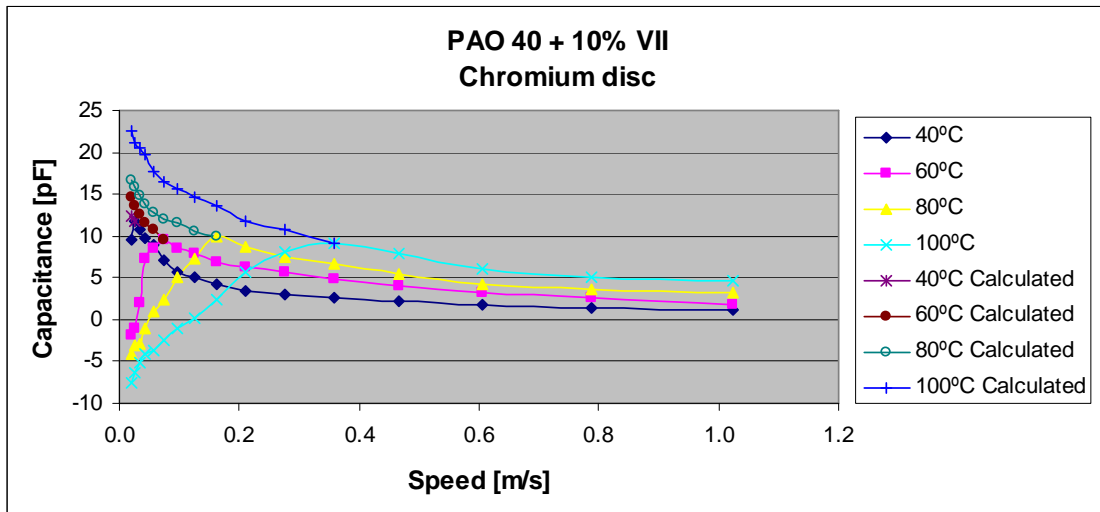


Figure 149: Capacitance measured values compared with the calculated ones for a range of temperatures

Figure 149 provides an insight in the behaviour of the capacitive values with a variation in temperature and implicitly, a variation of film thickness. The main trend to be observed here is the decrease in value for the measured capacitance, with an increase in temperature. On the other hand, this phenomenon can be predicted, as the film thickness decreases with an increase in temperature.

The measured capacitance values after this analysis, is limited to a lubricant film thickness of 100nm. Below this value, the surface roughness starts touching, resulting in negative values for the capacitance. On the other hand, if a careful analysis of the results is done, it can be seen that out of the 50 values measured for each test at a capacitor plate gap of 100nm, the values are quite close to each other.

A number of speeds were used to observe this phenomenon for the PAO 40 base oil at 80°C in pure rolling conditions using the Cr sputtered disc.

Figure 150 presents a graphical representation of the capacitance variation when film thickness is lower than 100nm. The measured film thickness at 0.163m/s is 118nm. As the lubricant gap decreases with the entrainment speed going down, we can clearly see a higher variation in capacitance measurements. When the speed is 0.056m/s the lubricant film thickness is 52nm, resulting in an increase in capacitance variation over the range of the 50 measured values per test. When the speed decreases even further, at 0.02m/s and a capacitor plate gap of 22nm, the measured capacitive values are experiencing a very high variation from -34pF at the lowest point and going up to 10pF as the highest point.

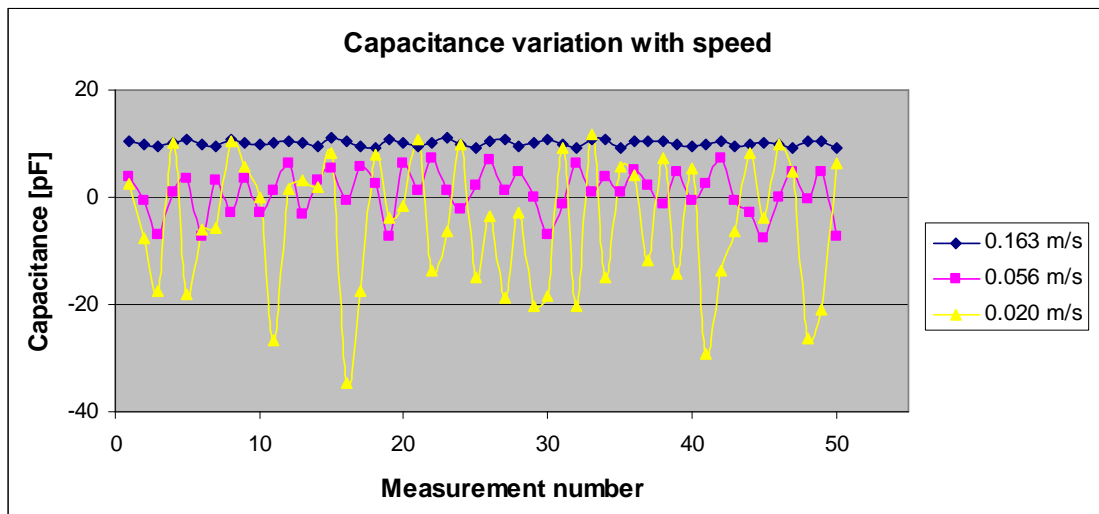


Figure 150: Capacitance variation at different speeds

6.3 Capacitance Measurements Results for EHD Point Contacts

6.3.1 Base Oil

Capacitance measurements using the base oil were done in two configuration settings, the first one was to calibrate the capacitive method against the optical method using a Cr sputtered disc with a Cr thickness of 15nm; the second one was done on a steel disc to see the influence of the steel disc on the capacitance. Apart from the two different types of discs that were used, the tests were conducted under three slide/roll conditions, pure rolling, 20% sliding and 60% sliding.

Figures 151–153 present the resulting graphs from the tests carried out on the base oil, using a steel disc, over a wide range of temperatures and sliding conditions.

As found by previous researchers, a decrease in film thickness i.e. capacitor plates distance, results in a significant increase in capacitance.

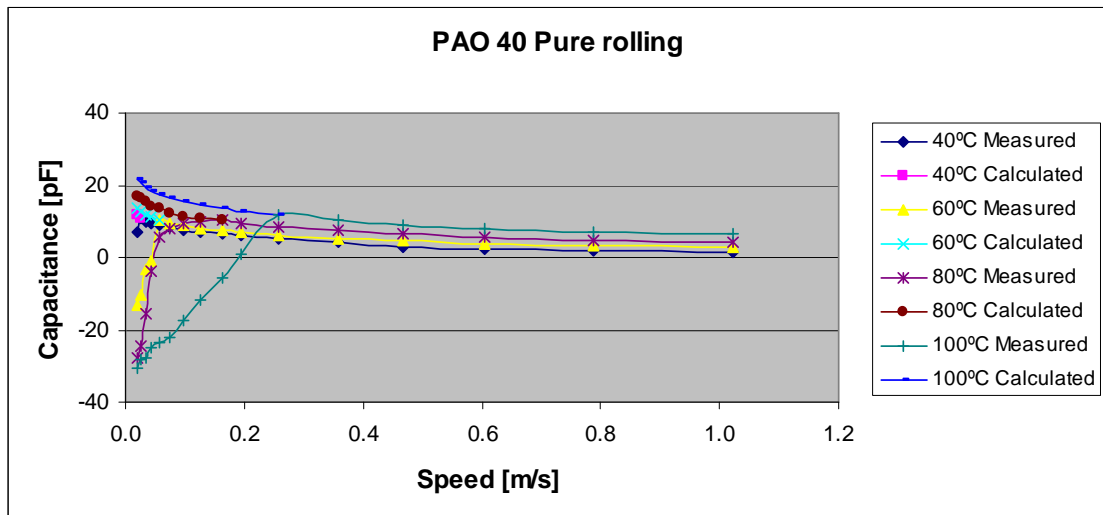


Figure 151: Capacitance measurements for the base oil in pure rolling conditions

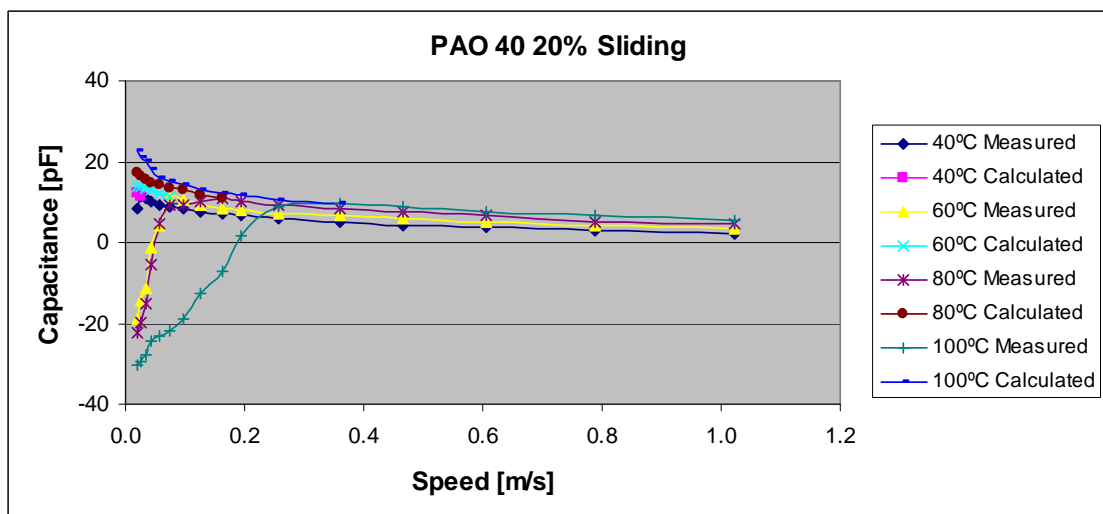


Figure 152: Capacitance measurements for the base oil when 20% sliding is present

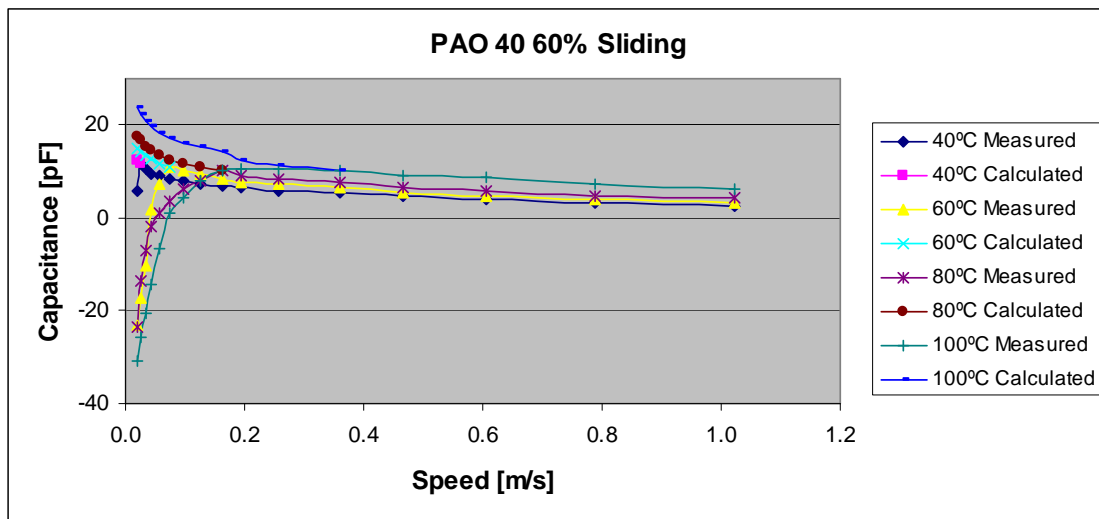


Figure 153: Capacitance measurements for the base oil when 60% sliding is present

Figures 154–157 present the log/log graphs for film thickness over a range of temperatures obtained from the optical and the electrical measurements. Film thicknesses for the capacitive measurements were obtained using Equation 104 and considering that the contact is a parallel plate capacitor.

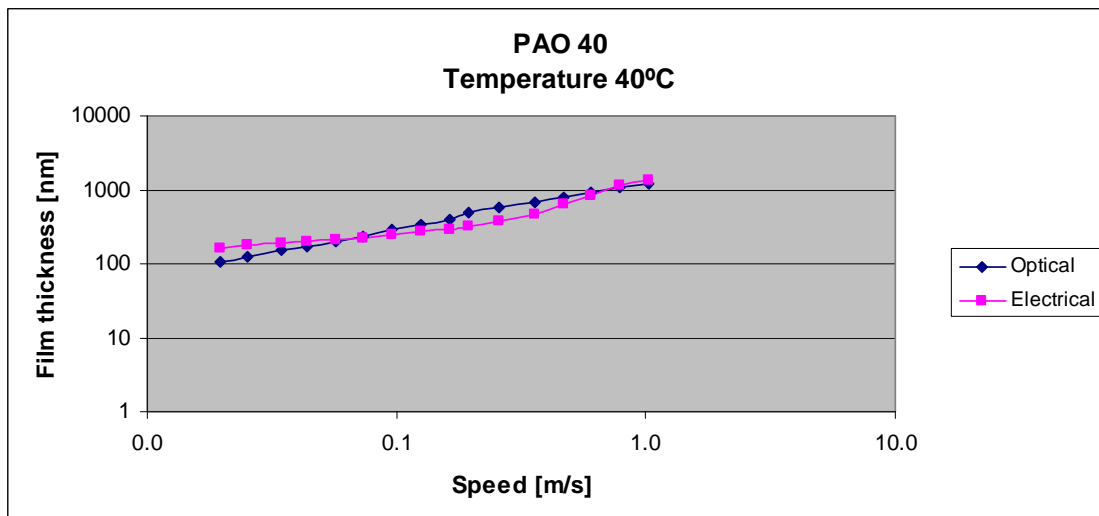


Figure 154: Film thickness measurements comparison between the optical and electrical method at a temperature of 40°C

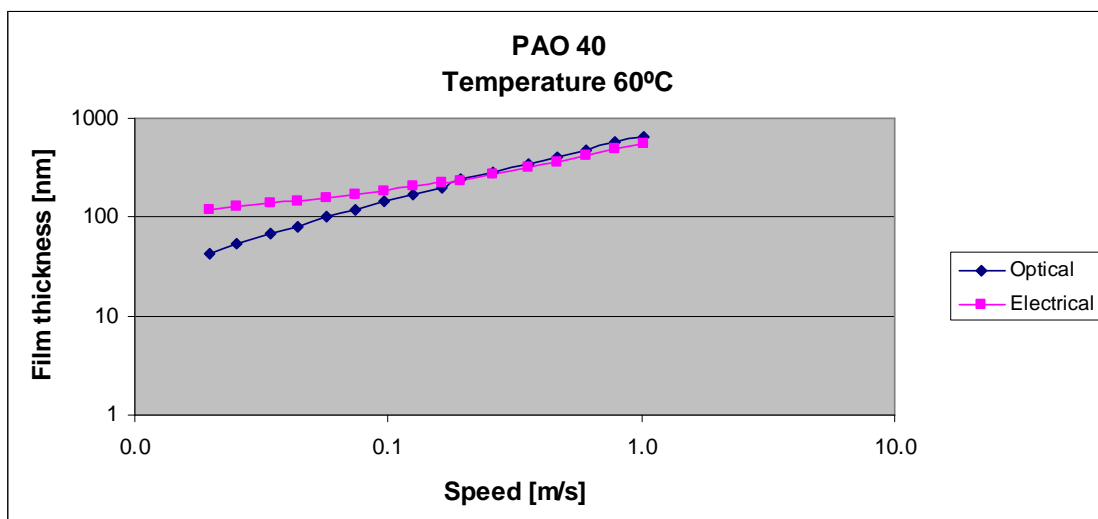


Figure 155: Film thickness measurements comparison between the optical and electrical method at a temperature of 60°C

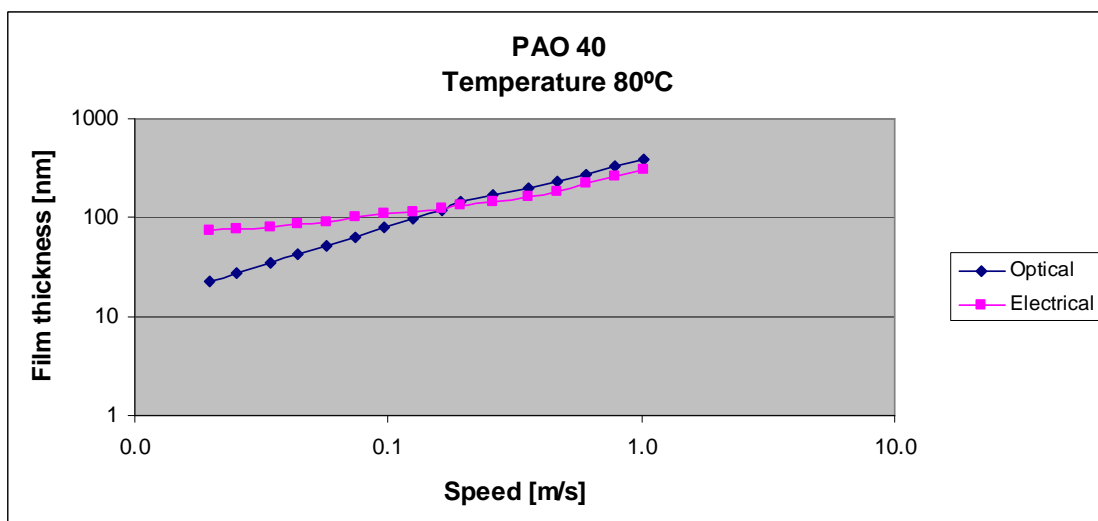


Figure 156: Film thickness measurements comparison between the optical and electrical method at a temperature of 80°C

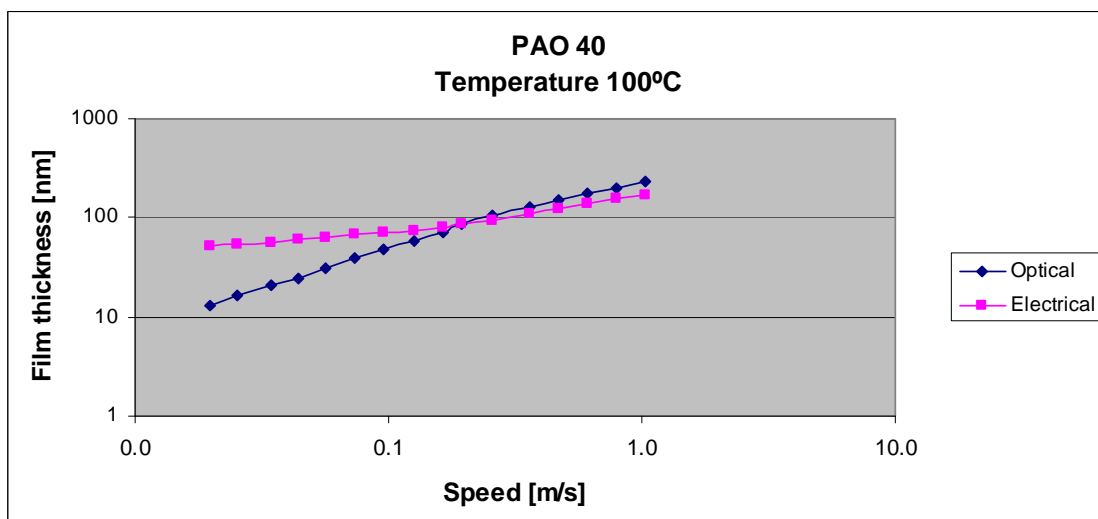


Figure 157: Film thickness measurements comparison between the optical and electrical method at a temperature of 100°C

Figures 158–161 present a comparison between the film thickness measurements done using the classical optical interferometry method and the capacitive results obtained.

The trend discovered by previous researchers applies here. As the capacitance values increase, the lubricant film thickness decreases.

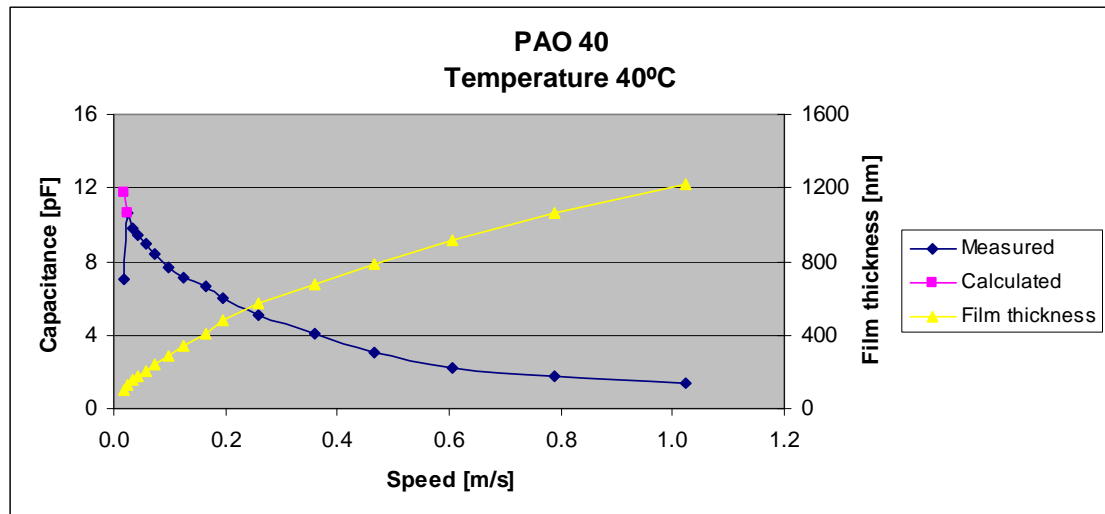


Figure 158: Film thickness comparison with capacitance measurements for the base oil at 40°C

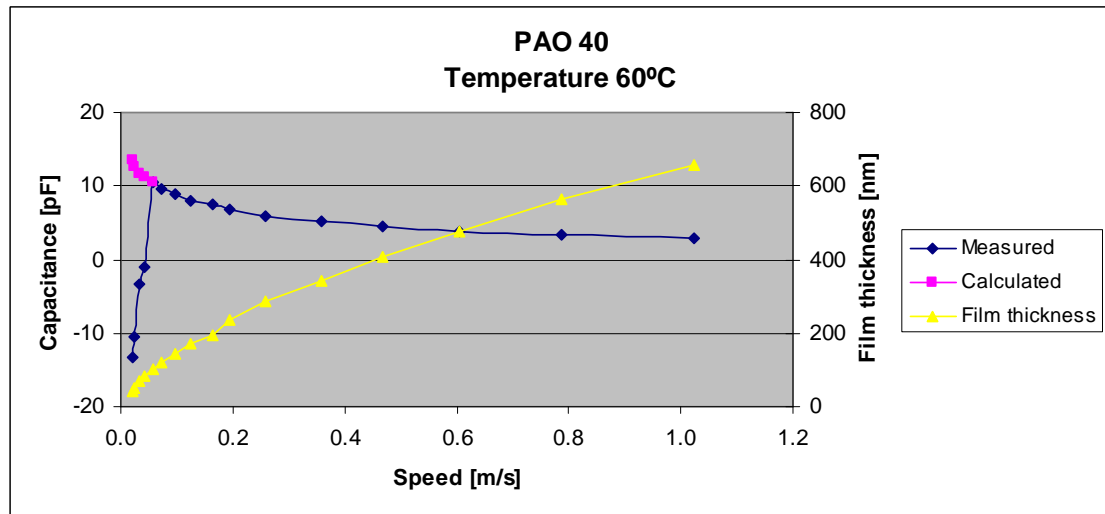


Figure 159: Film thickness comparison with capacitance measurements for the base oil at 60°C

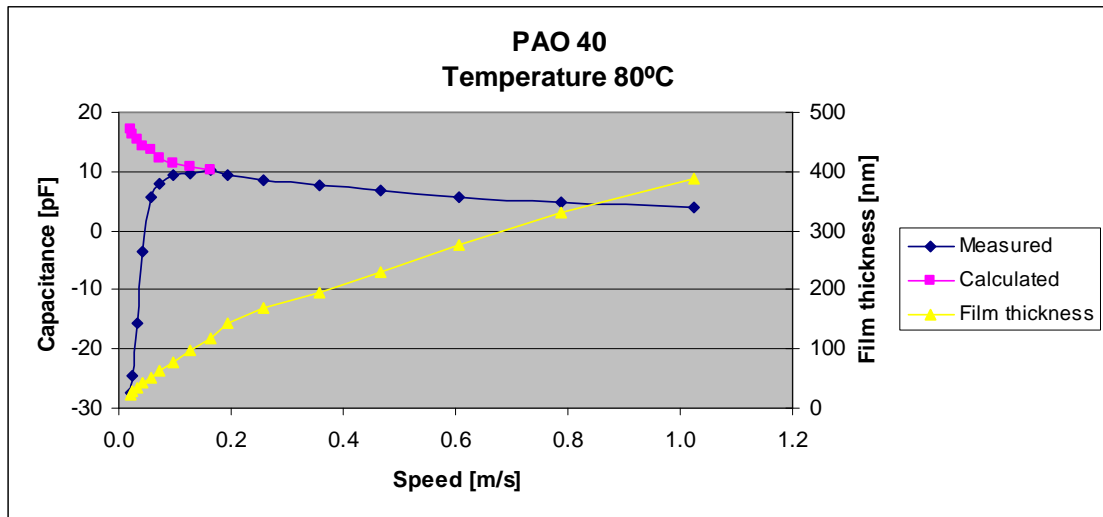


Figure 160: Film thickness comparison with capacitance measurements for the base oil at 80°C

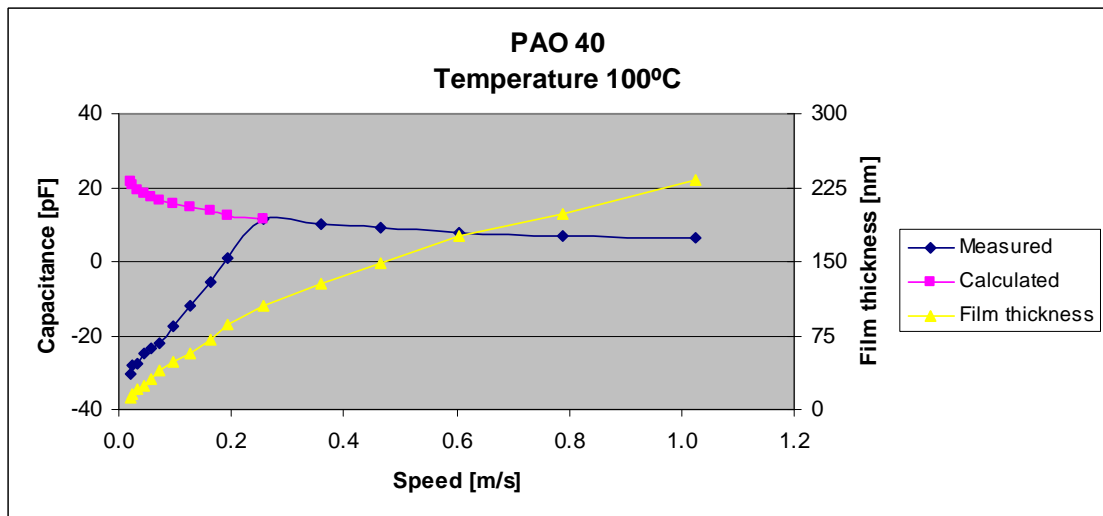


Figure 161: Film thickness comparison with capacitance measurements for the base oil at 100°C

When sliding is introduced, the capacitance values do not change drastically. However as seen for the optical measurements, a small difference can be observed at low speeds; low lubricant film thicknesses and a higher influence of the sliding condition can be observed at higher speeds, especially for low temperatures. At high temperatures, the capacitance measurements are almost imposing on each other, phenomenon explained by a low film thickness.

Figures 162–165 present a comparison done for the PAO 40 base oil in three different sliding conditions, for a number of temperatures.

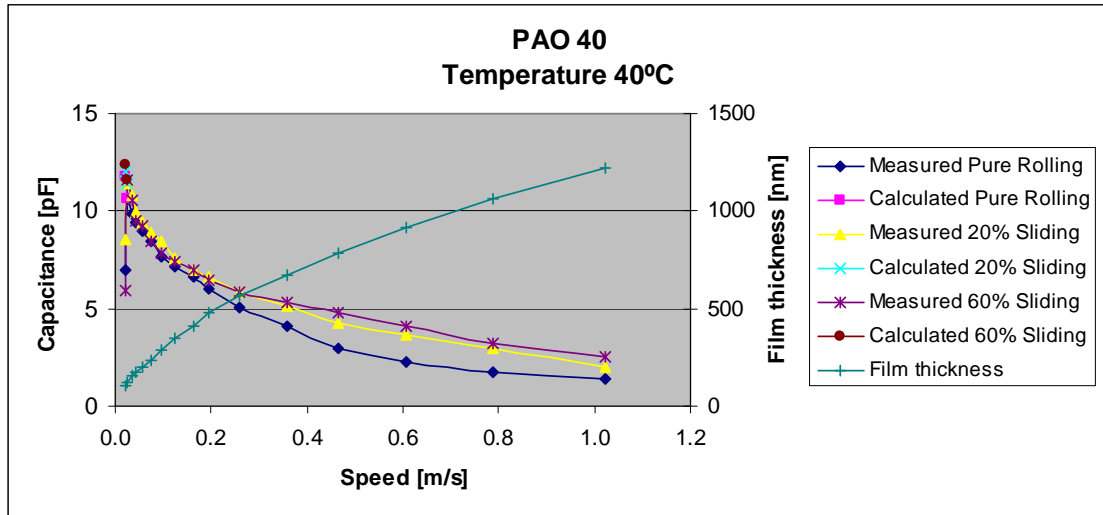


Figure 162: Capacitive measurements comparison in different sliding conditions at 40°C

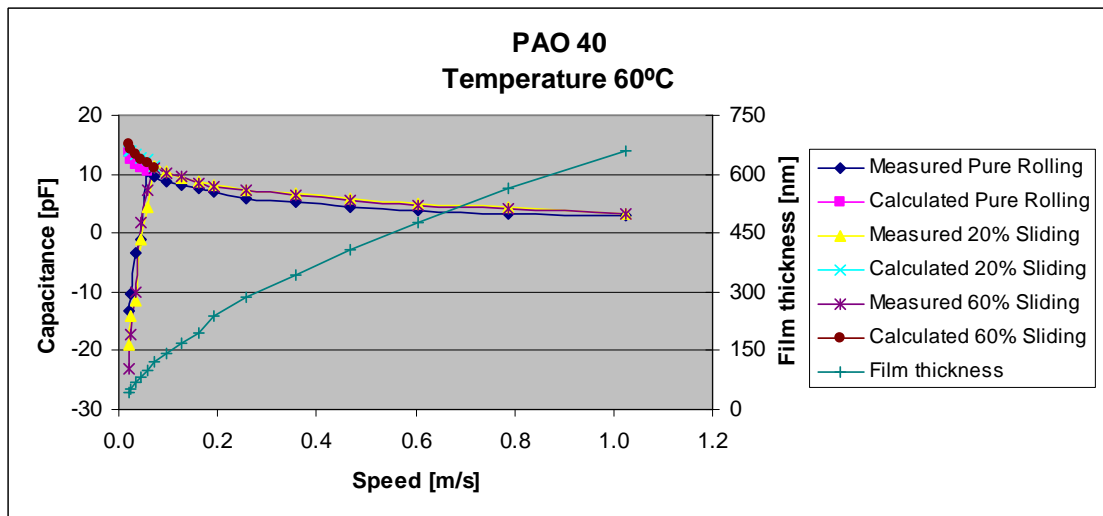


Figure 163: Capacitive measurements comparison in different sliding conditions at 60°C

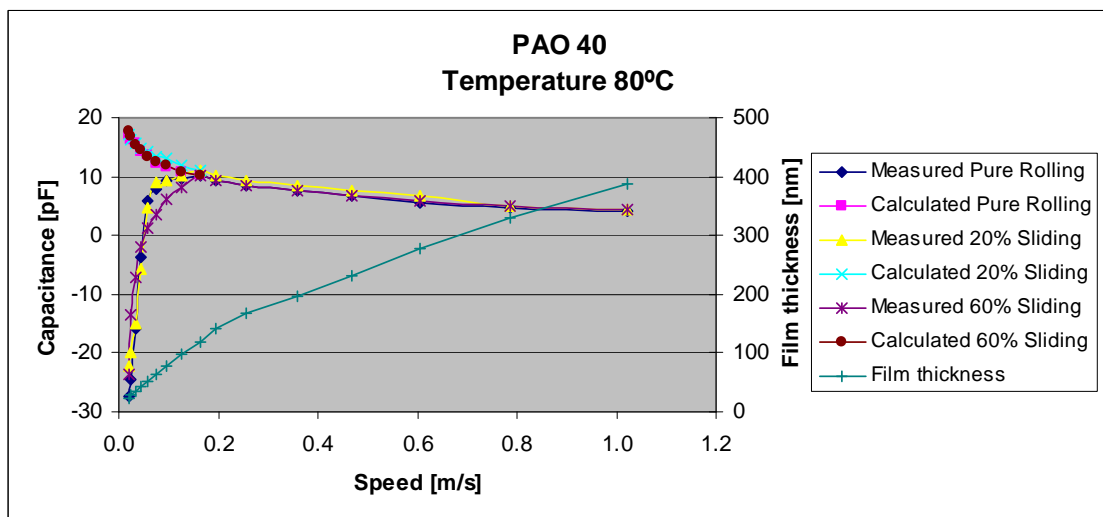


Figure 164: Capacitive measurements comparison in different sliding conditions at 80°C

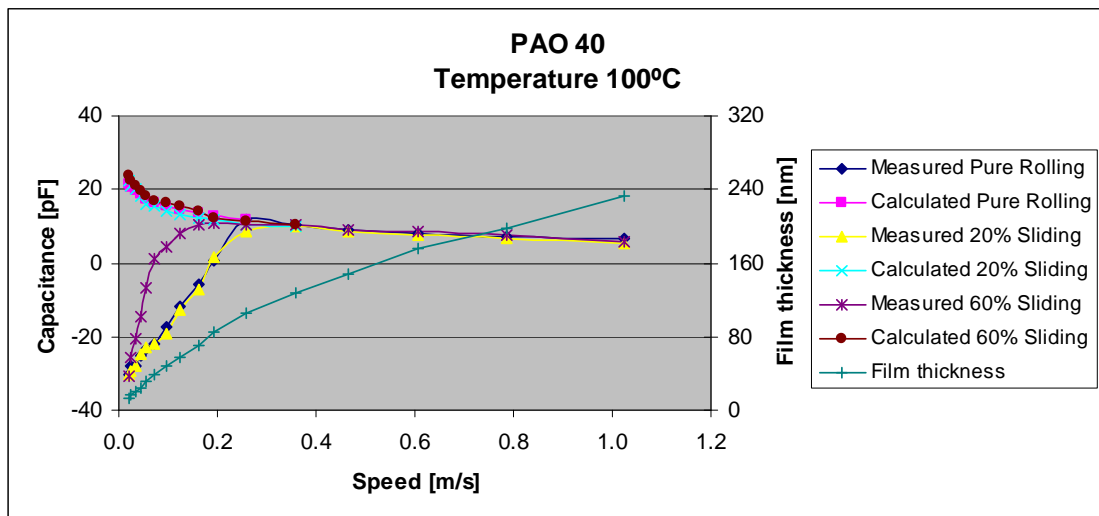


Figure 165: Capacitive measurements comparison in different sliding conditions at 100°C

6.3.2 Organic Friction Modifier Solution

The first additive that was used in capacitive measurements is an organic friction modifier (OFM) in a base oil combination of 1% weight. As explained in previous chapters, the variation in film thickness and implicitly in capacitance was not prominent when the OFM is used.

Figures 166–168 present the results obtained for the PAO 40 base oil mixed with a 1% weight OFM additive, using a steel disc over a range of temperatures and in different sliding conditions.

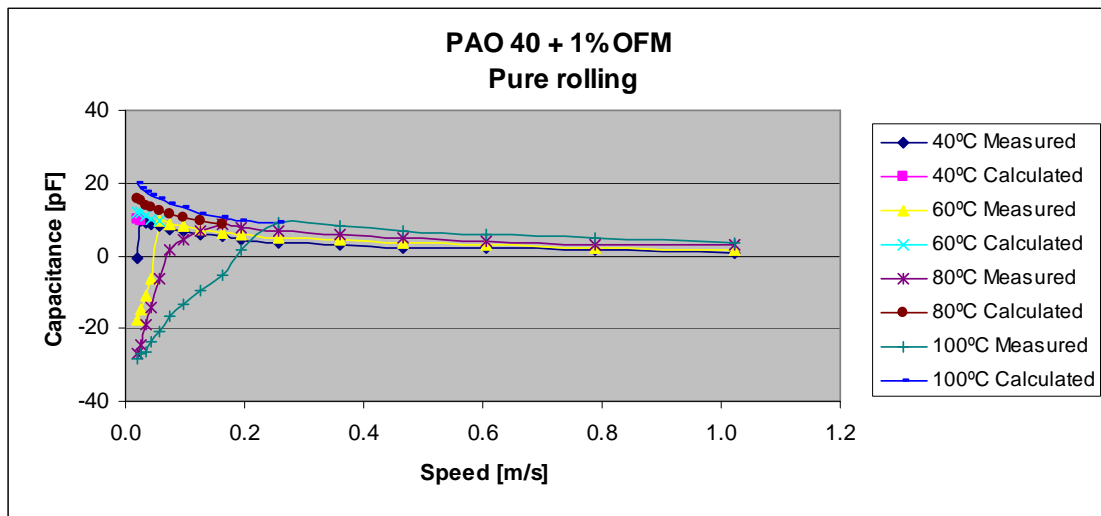


Figure 166: Capacitance measurements for the base oil mixed with 1% OFM in pure rolling conditions

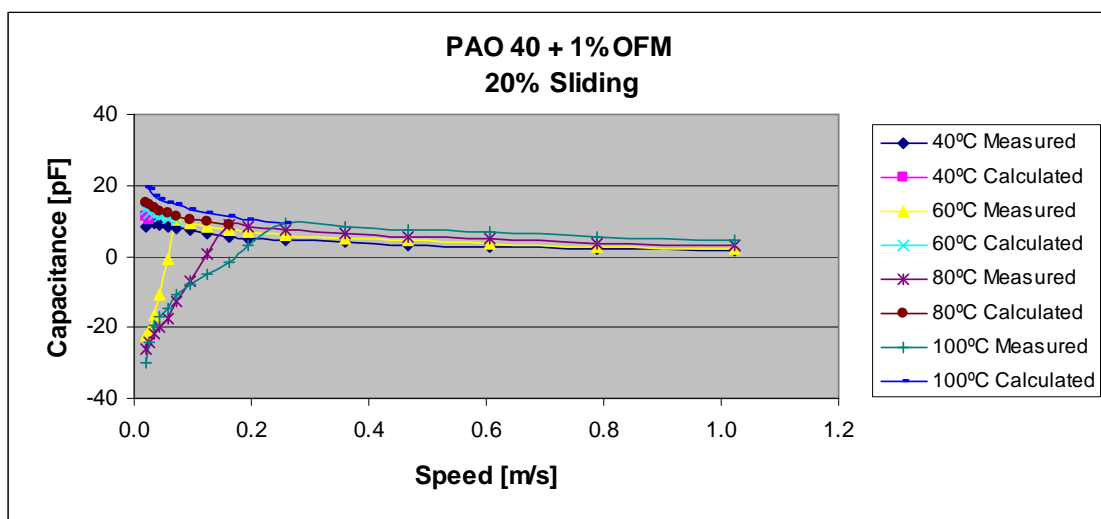


Figure 167: Capacitance measurements for the base oil mixed with 1% OFM in a 20% sliding condition

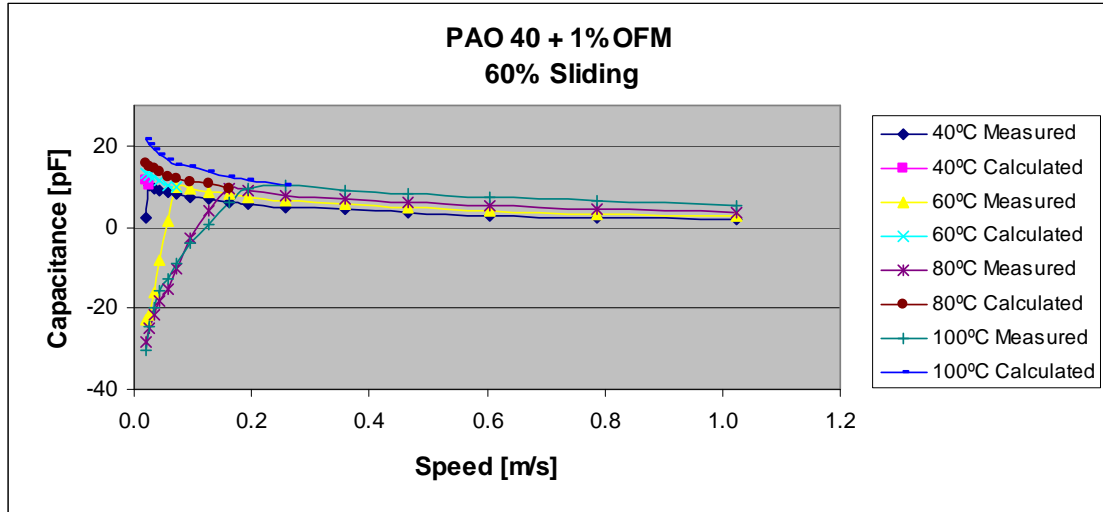


Figure 168: Capacitance measurements for the base oil mixed with 1% OFM in a 60% sliding condition

As specified before, the variation with the distance between the two capacitive plates is clearly shown by the boost in measured capacitive value; with a decline in capacitor plates distance i.e. film thickness.

Figures 169–172 present a comparison between the film thickness measured optically and the film thickness obtained from the capacitance measurements over a range of temperatures, as explained in the previous chapter the lubricant gap for the electrical measurements was obtained using data from [96] and considering that the contact is a parallel plate capacitor.

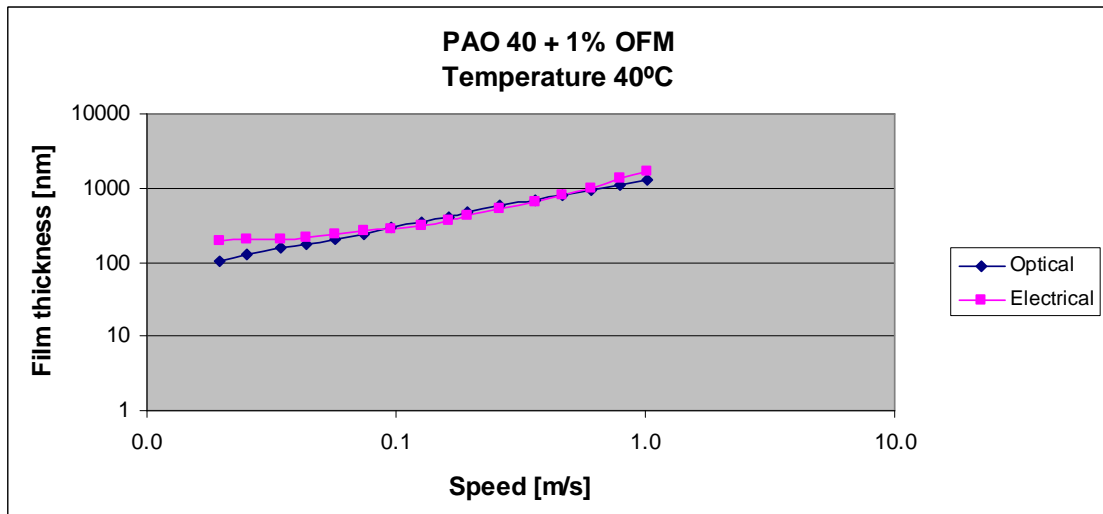


Figure 169: Film thickness measurements comparison between the optical and electrical method at a temperature of 40°C for a base oil mixed with 1% OFM

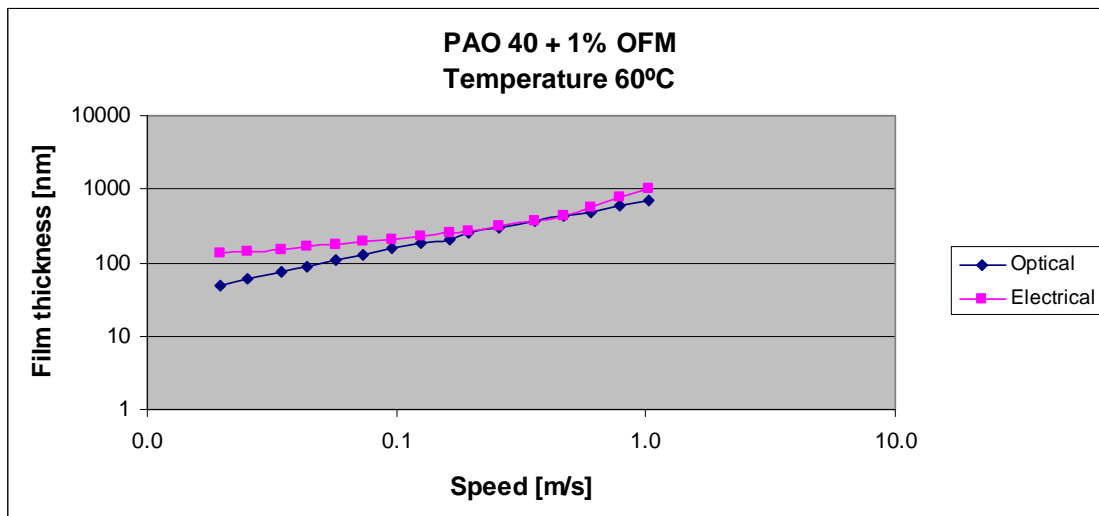


Figure 170: Film thickness measurements comparison between the optical and electrical method at a temperature of 60°C for a base oil mixed with 1% OFM

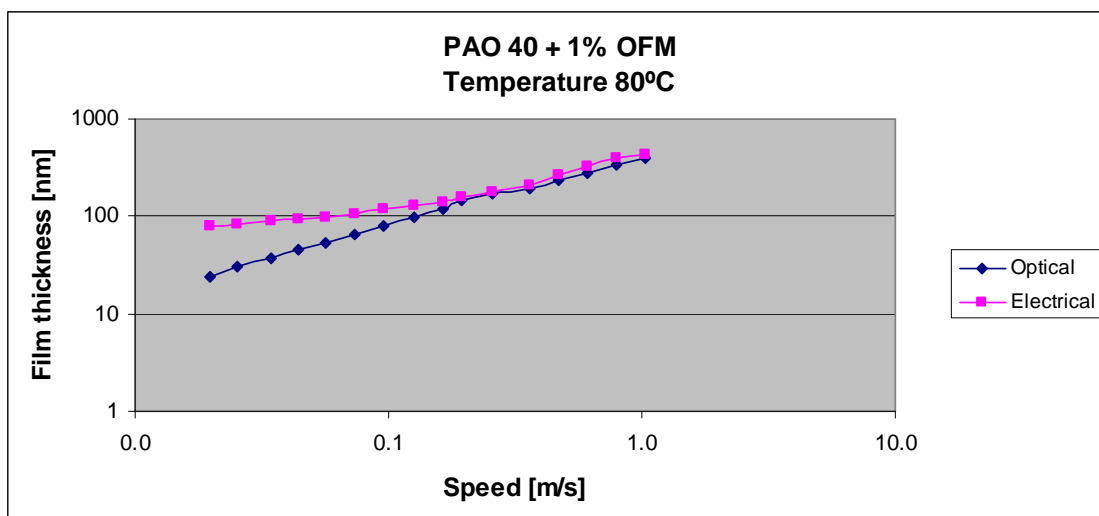


Figure 171: Film thickness measurements comparison between the optical and electrical method at a temperature of 80°C for a base oil mixed with 1% OFM

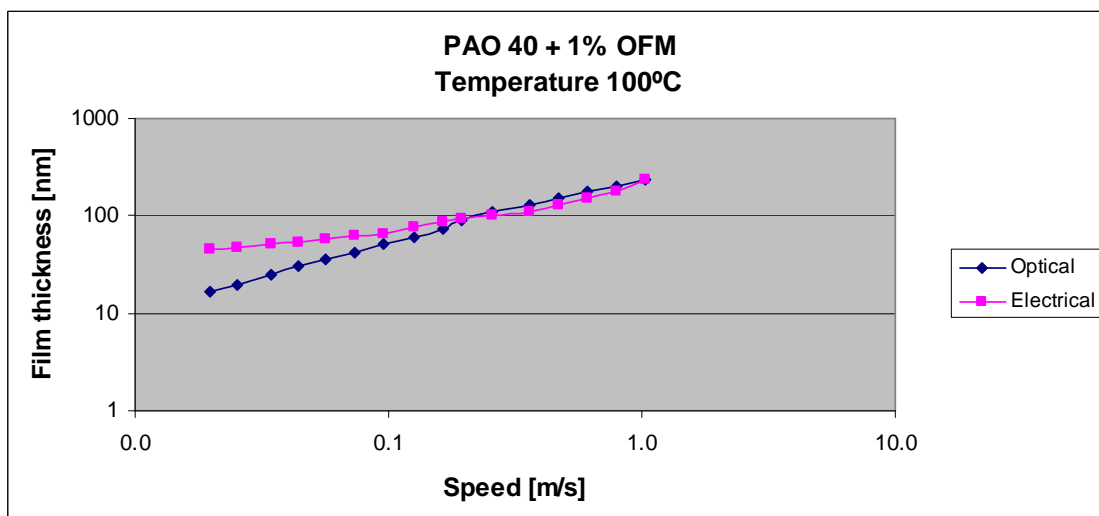


Figure 172: Film thickness measurements comparison between the optical and electrical method at a temperature of 100°C for a base oil mixed with 1% OFM

A comparison was made for the film thickness values obtained, using the classical optical interferometry technique and the obtained measurements from the capacitive method.

Figures 173–176 offer a better understanding on the phenomenon that takes place in the EHD studied contact. For these set of tests a steel disc was employed, accompanied by a lubricant mix with 1% wt. OFM.

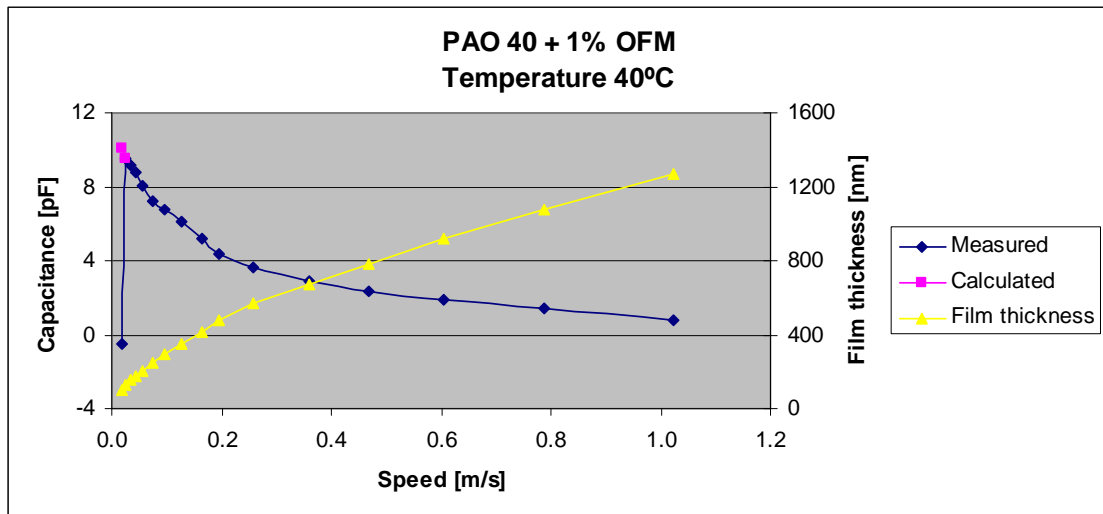


Figure 173: Capacitance values compared with film thickness for the base oil mixed with 1% OFM at a temperature of 40°C

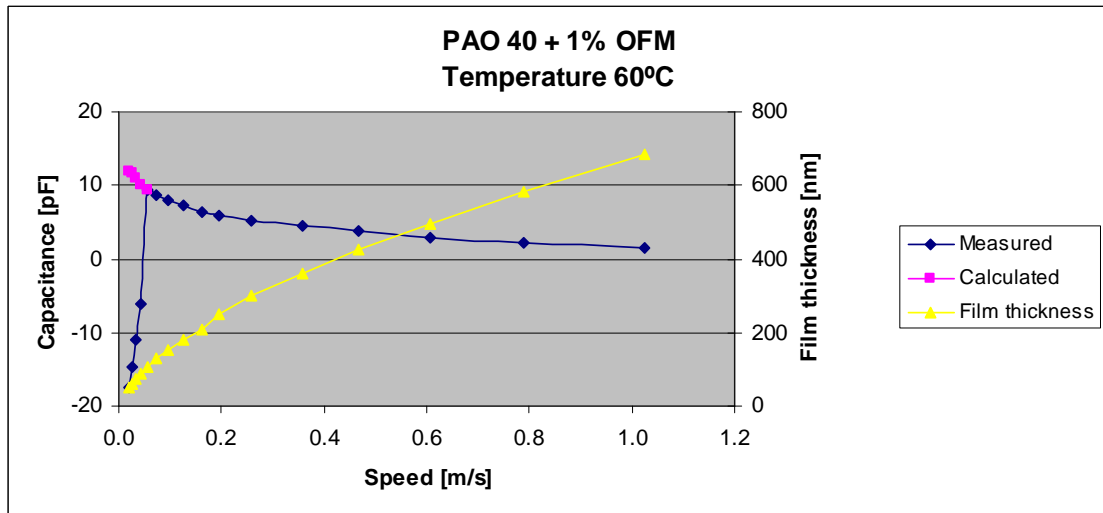


Figure 174: Capacitance values compared with film thickness for the base oil mixed with 1% OFM at a temperature of 60°C

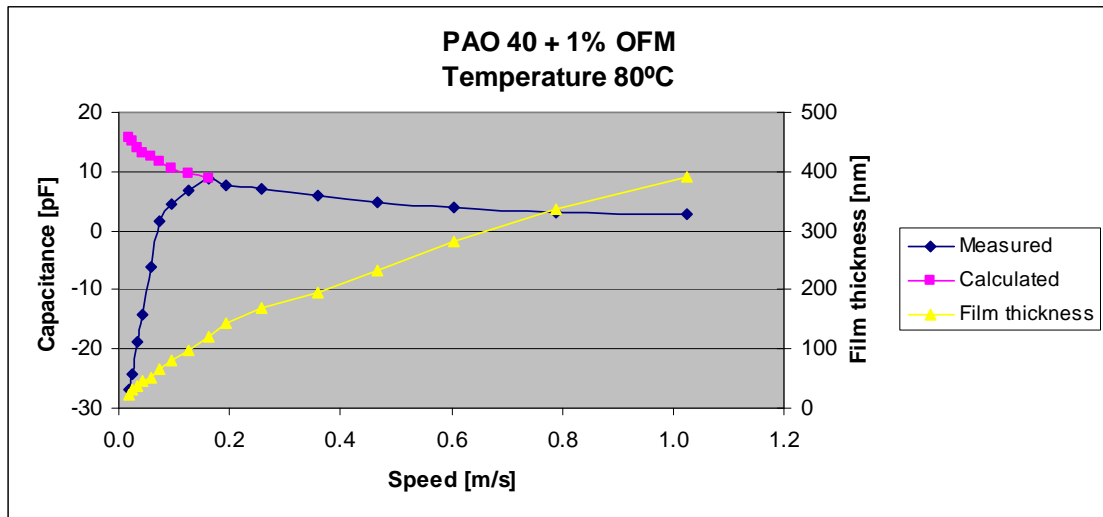


Figure 175: Capacitance values compared with film thickness for the base oil mixed with 1% OFM at a temperature of 80°C

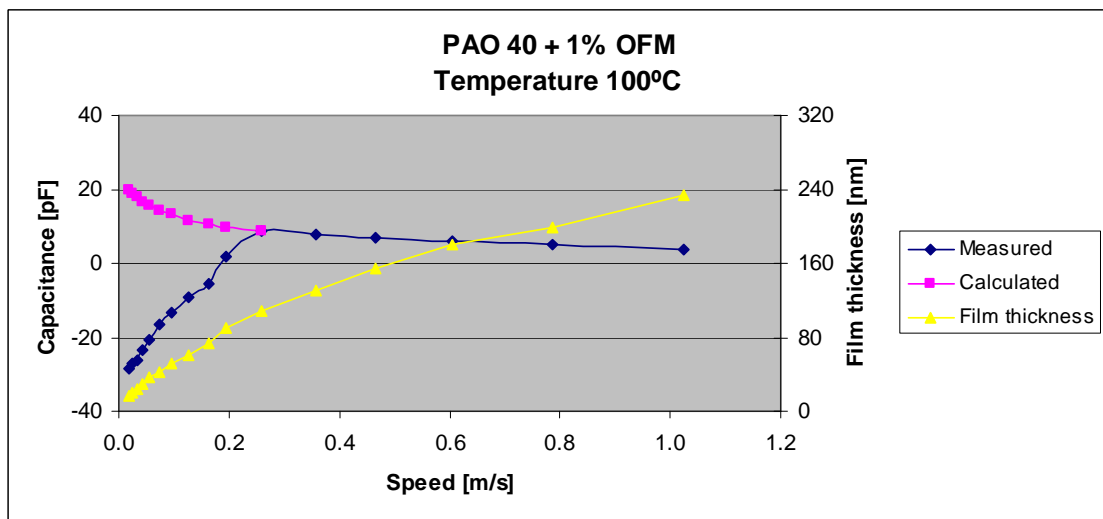


Figure 176: Capacitance values compared with film thickness for the base oil mixed with 1% OFM at a temperature of 100°C

Sliding tests were repeated for the lubricant mix that includes 1% OFM. The results obtained do not show a significant difference for the capacitance measurements. As explained for the base oil, there is a small difference in value at low temperatures and low speeds; the highest influence can be seen at higher speeds, where a bigger difference in capacitive value was measured. At high temperatures, unlike the phenomenon seen for the base oil, here, the capacitance values do not superimpose on each other: a clear difference can be observed even all be it small. This can be explained by the fact that the organic friction modifier forms a boundary film on the steel disc surface.

Figures 177–180 present the resulting graphs from the capacitive tests for the PAO 40 base oil with a 1% OFM mixture, over a range of temperatures and sliding conditions.

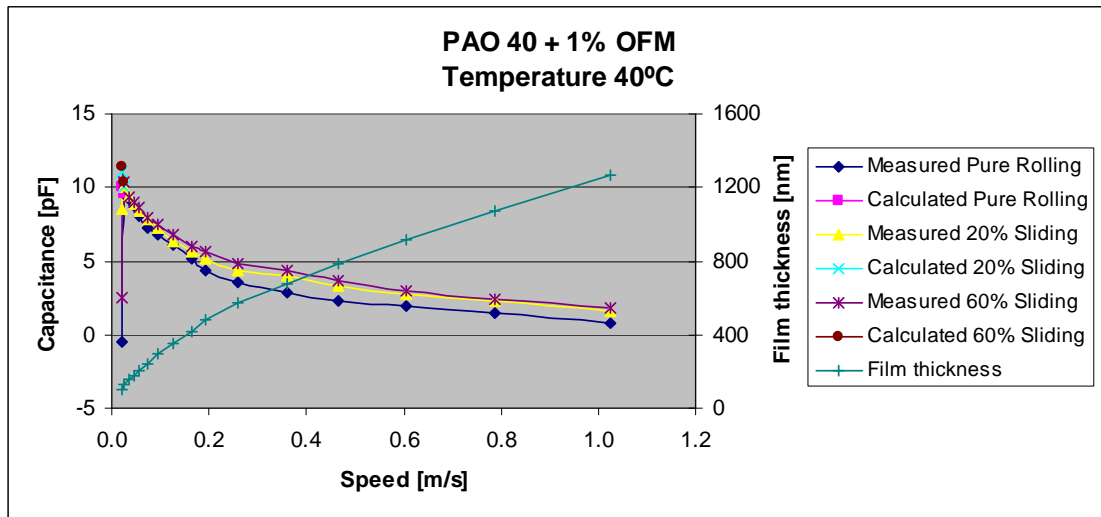


Figure 177: Capacitive measurements comparison in different sliding conditions at 40°C

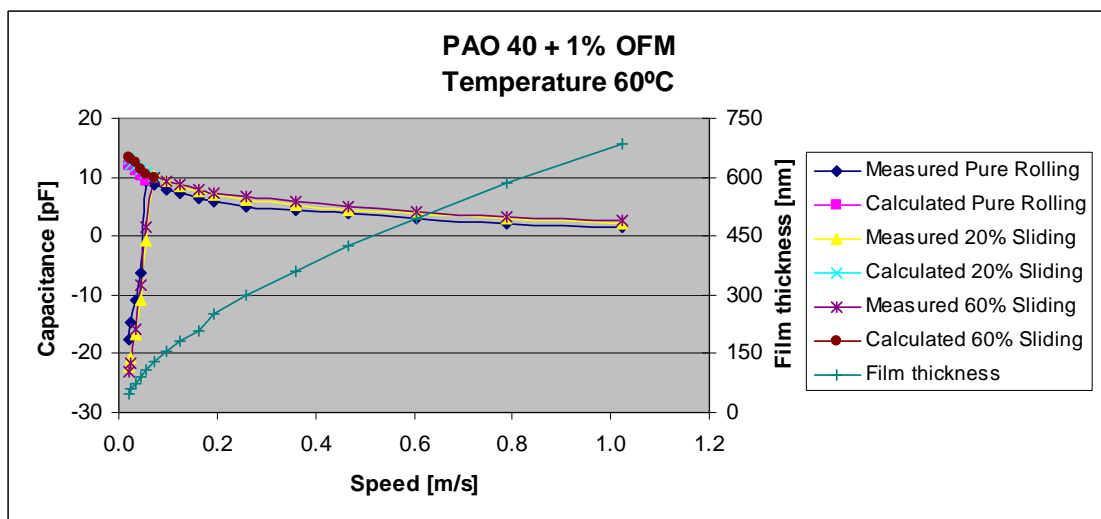


Figure 178: Capacitive measurements comparison in different sliding conditions at 60°C

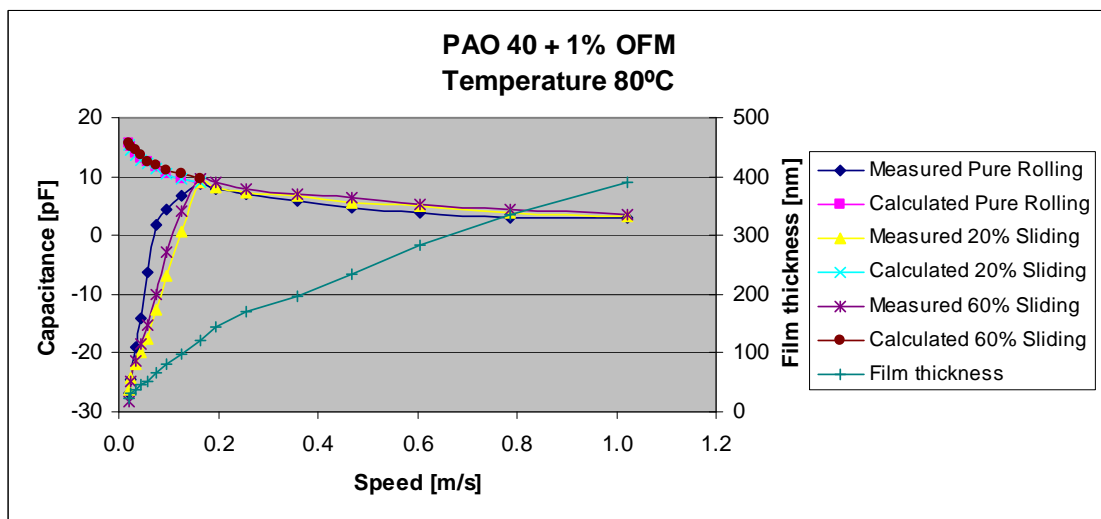


Figure 179: Capacitive measurements comparison in different sliding conditions at 80°C

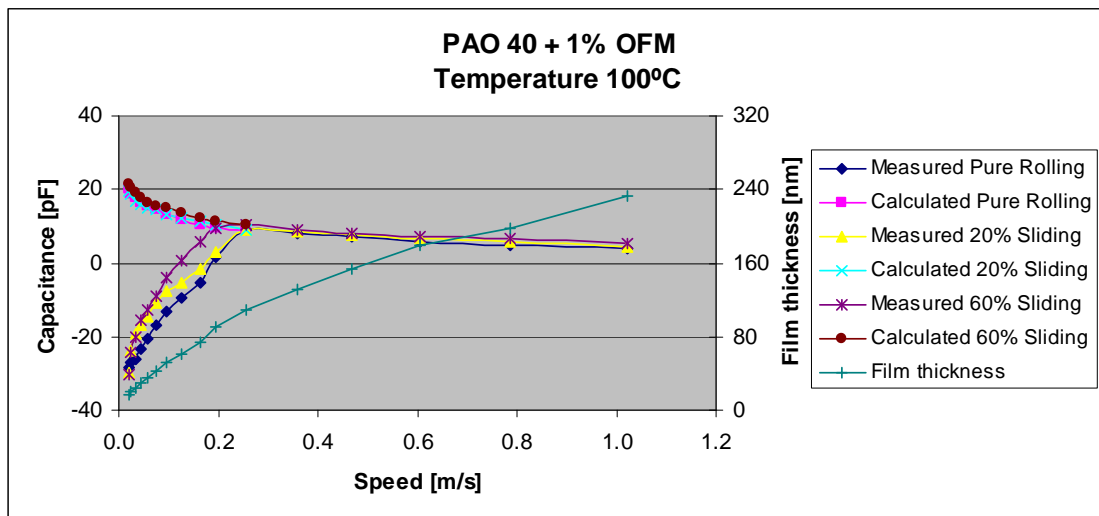


Figure 180: Capacitive measurements comparison in different sliding conditions at 100°C

6.3.3 Viscosity Index Improver Solution

The second additive that was used in the capacitance measurements was a viscosity index improver (VII) tested in a base oil mix of 10% weight. This additive has a higher influence on the film thickness measured by the optical technique; phenomenon that transfers in the capacitance measurements as well.

Figures 181–183 present the graphic representation of the results obtained using a steel disc at four different temperatures, over a wide number of speeds in different rolling conditions.

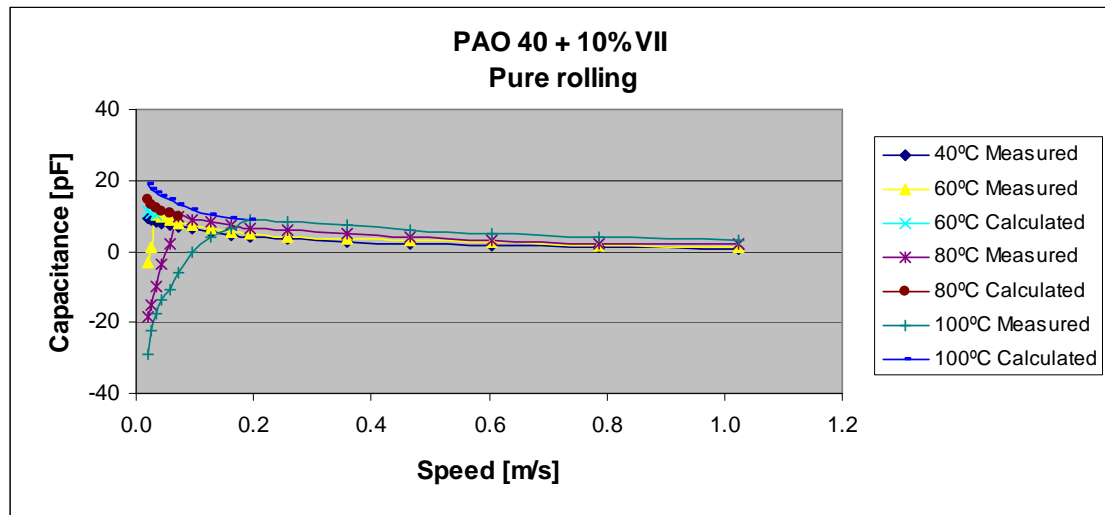


Figure 181: Capacitance measurements for the base oil mixed with 10% VII in pure rolling conditions

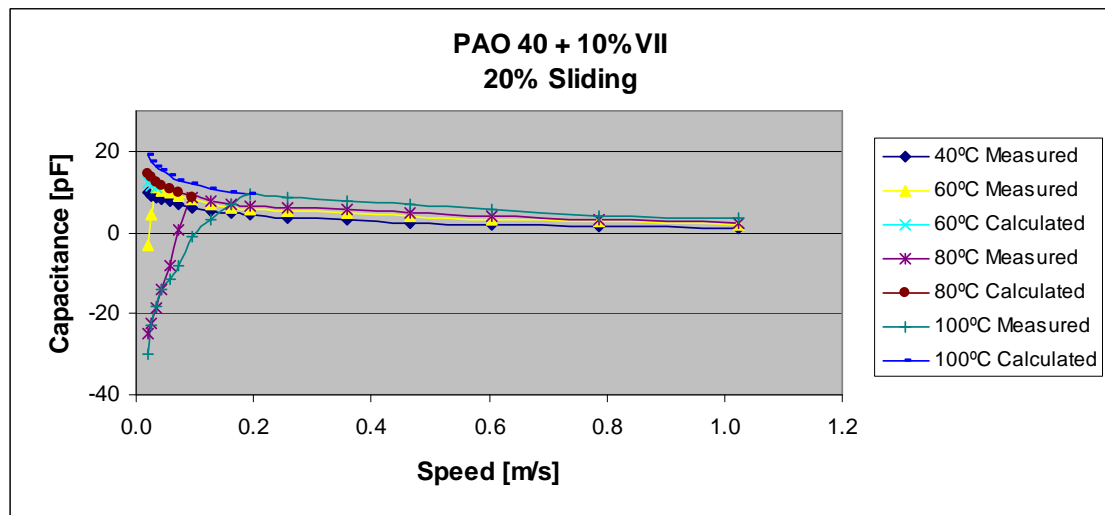


Figure 182: Capacitance measurements for the base oil mixed with 10% VII when 20% sliding is present

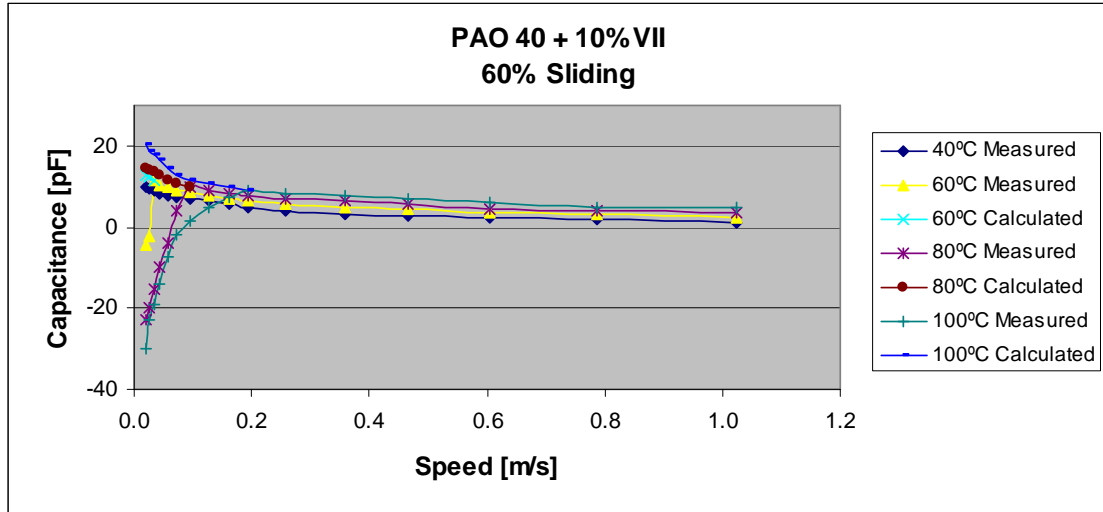


Figure 183: Capacitance measurements for the base oil mixed with 10% VII when 20% sliding is present

The expected phenomenon does not change, even in this case. A shrinking gap between the capacitor plates results in an increase in measured capacitance.

Figures 184–187 present a comparison between the film thickness measured optically and the film thickness obtained from the capacitance measurements over a range of temperatures. Comparison made possible by considering that the contact is a parallel plate capacitor employing Equation 104.

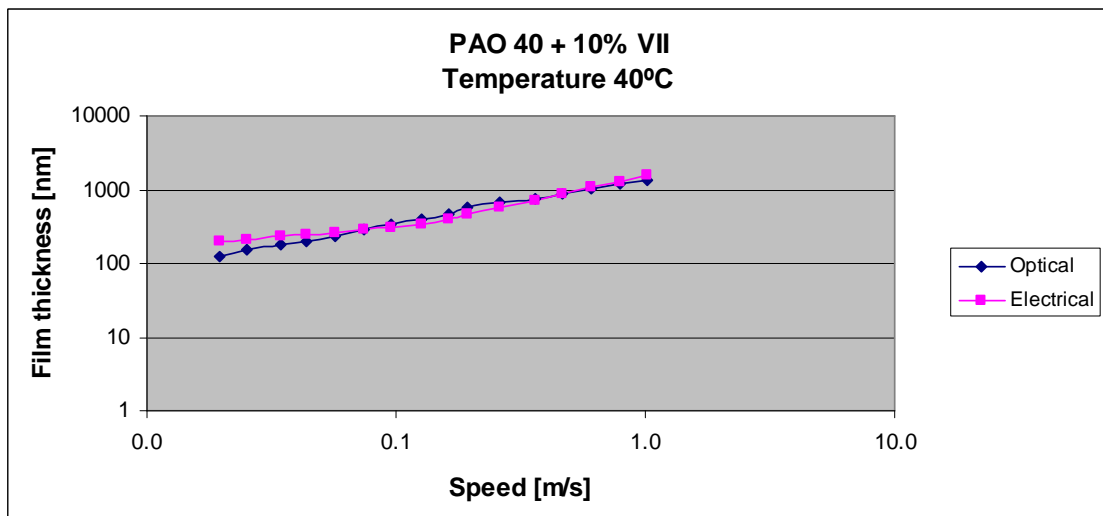


Figure 184: Film thickness measurements comparison between the optical and electrical method at a temperature of 40°C for a base oil mixed with 10% VII

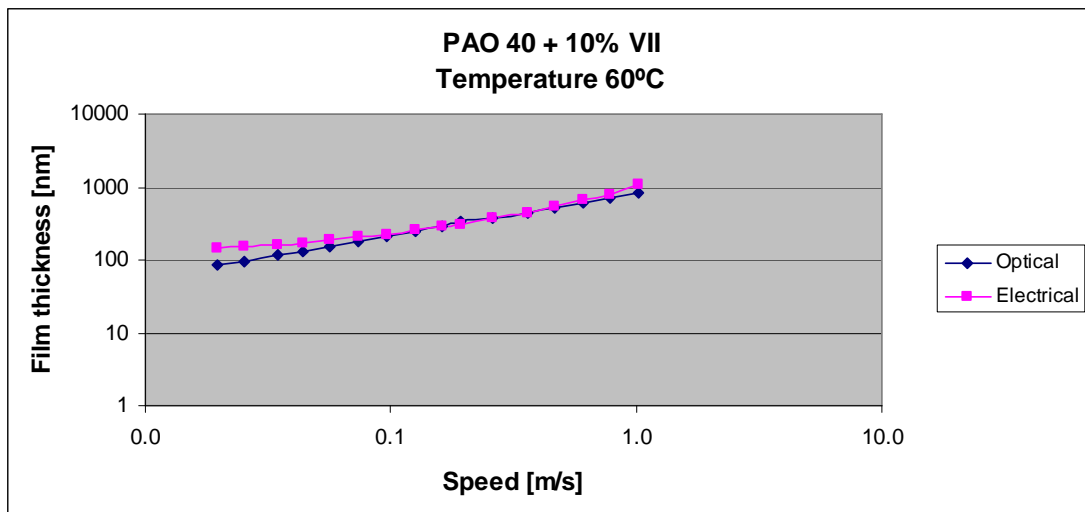


Figure 185: Film thickness measurements comparison between the optical and electrical method at a temperature of 60°C for a base oil mixed with 10% VII

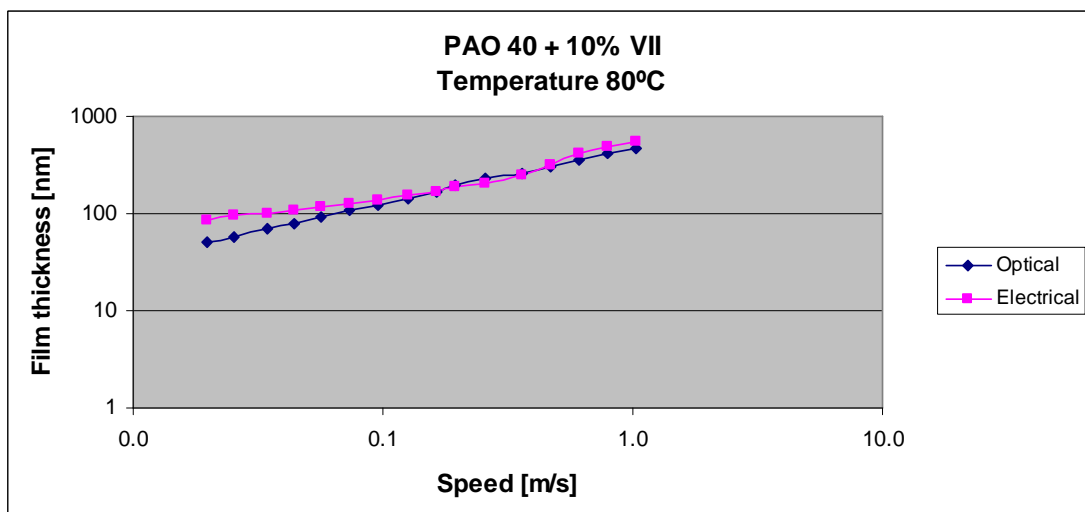


Figure 186: Film thickness measurements comparison between the optical and electrical method at a temperature of 80°C for a base oil mixed with 10% VII

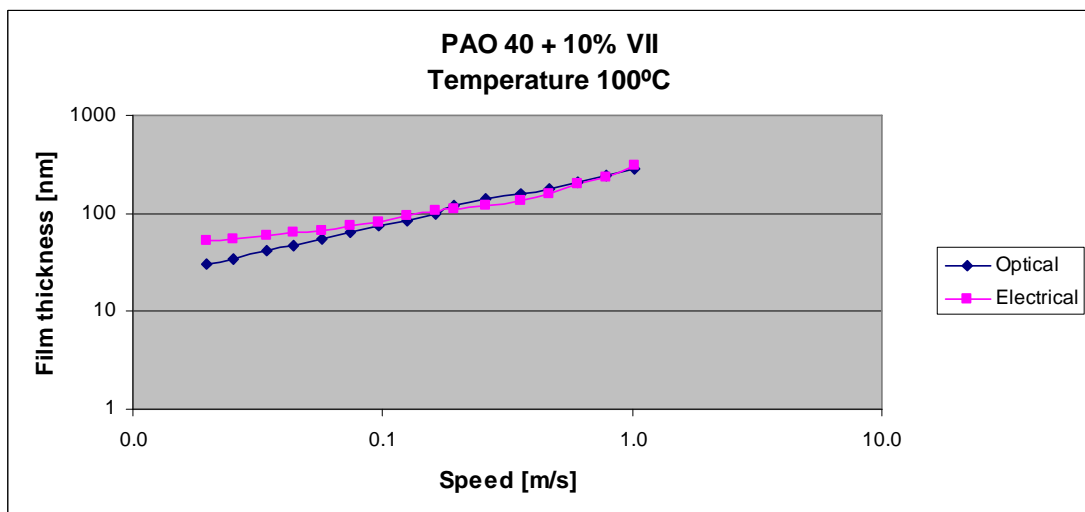


Figure 187: Film thickness measurements comparison between the optical and electrical method at a temperature of 100°C for a base oil mixed with 10% VII

A comparison between the film thickness measurements and the capacitive values obtained using the capacitive method has been done and are presented in Figures 188–191. For these tests, a steel disc was used in combination with a lubricant mix of 10% VII and base oil in three sliding conditions and four different temperatures.

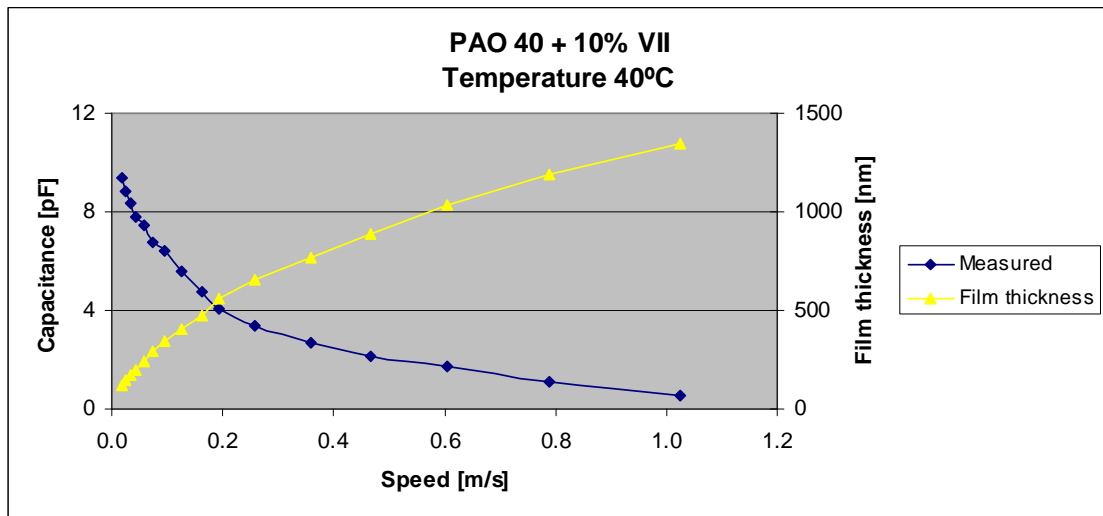


Figure 188: Capacitance values compared with film thickness for the base oil mixed with 10% VII at 40°C

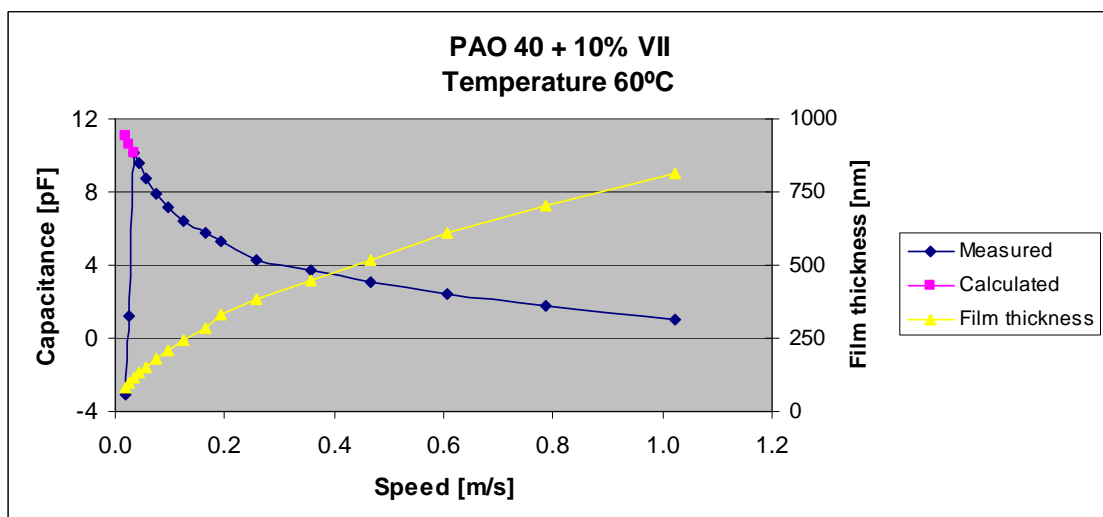


Figure 189: Capacitance values compared with film thickness for the base oil mixed with 10% VII at 60°C

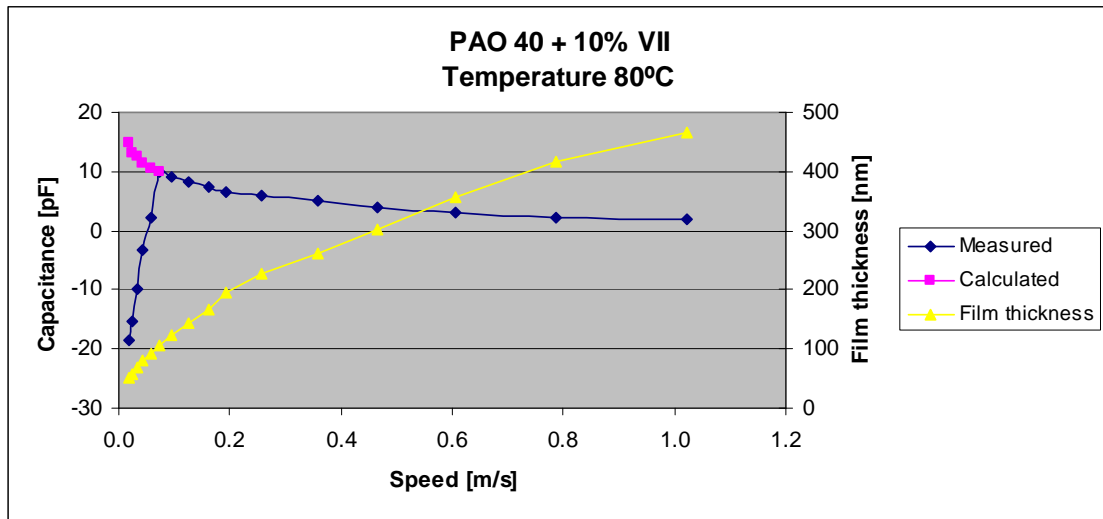


Figure 190: Capacitance values compared with film thickness for the base oil mixed with 10% VII at 80°C

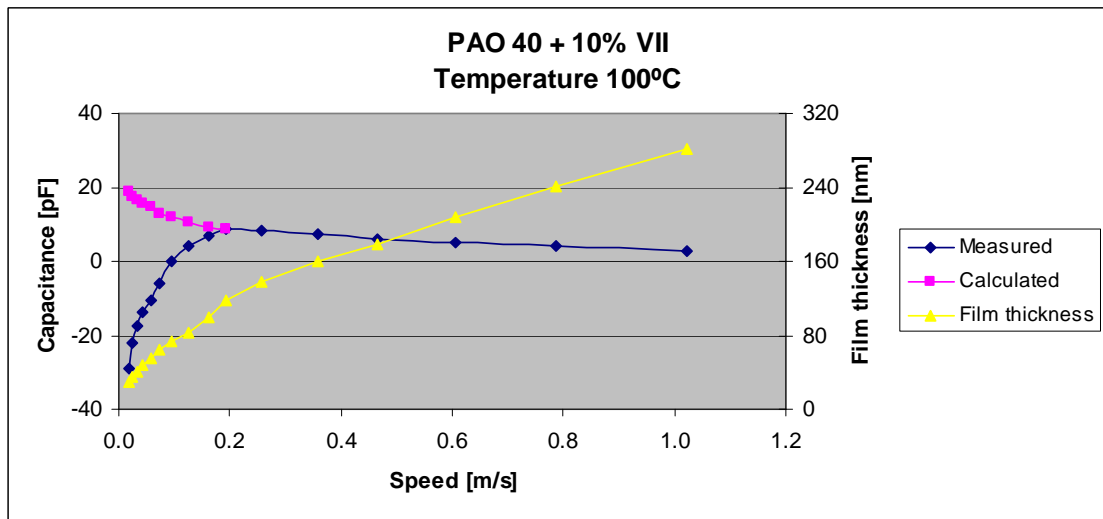


Figure 191: Capacitance values compared with film thickness for the base oil mixed with 10% VII at 100°C

The same sliding conditions were employed for the lubricant mix with the PAO 40 base oil mixed with 10% VII. As shown for the other two cases studied, so far no big difference in capacitive values can be extracted from the results. At a low speed and low temperature, the influence of sliding is barely observable. At higher speeds, a small difference in capacitive values can be seen. For this lubricant mix, at the higher temperature, the capacitive values clearly overlap on each other, phenomenon experienced for the base oil. This means that this additive behaves differently at high temperatures, as compared with the previous one.

Figures 192–195 provide a better understanding of the way the different sliding conditions influence the capacitive values, over a range of temperatures.

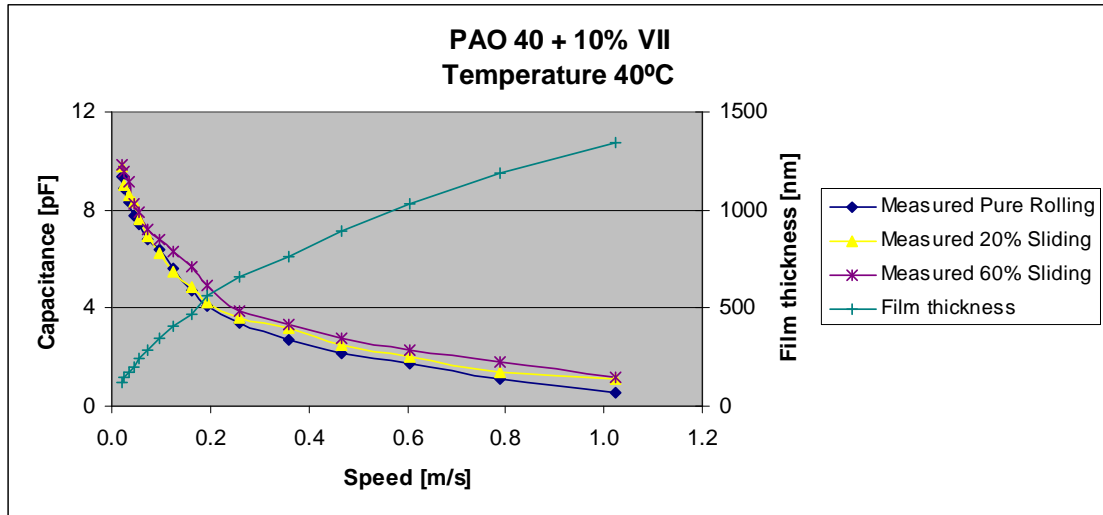


Figure 192: Capacitive measurements comparison in different sliding conditions at 40°C

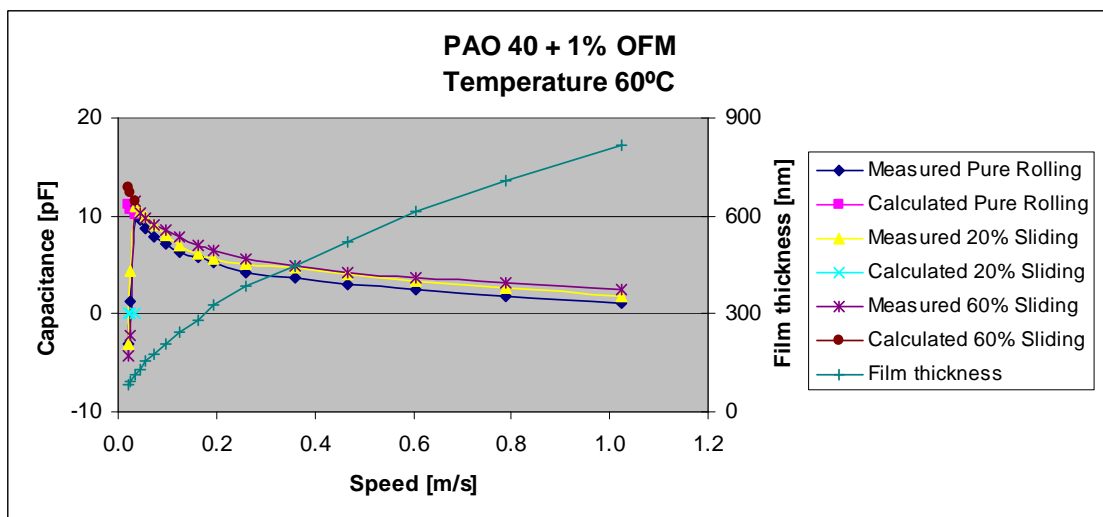


Figure 193: Capacitive measurements comparison in different sliding conditions at 60°C

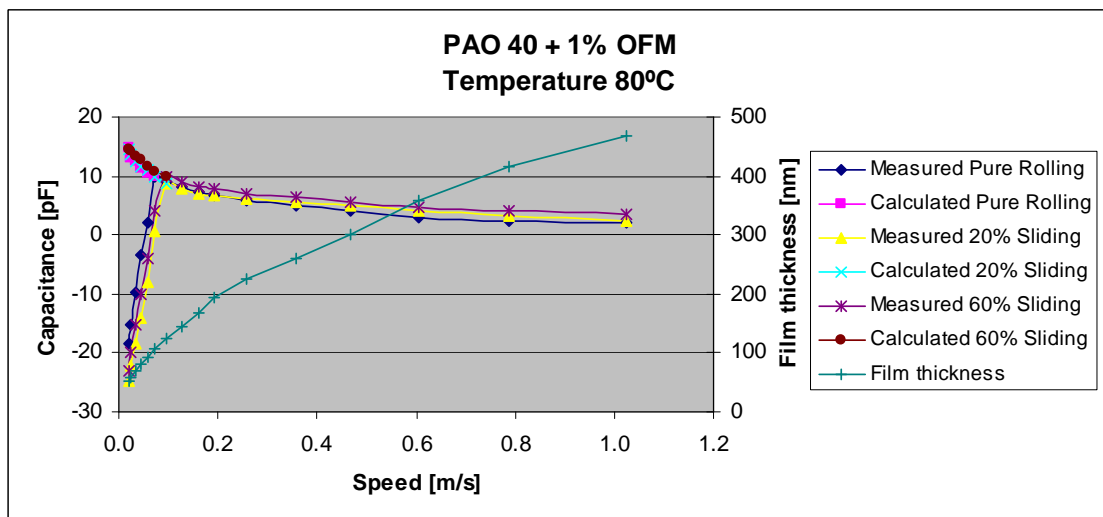


Figure 194: Capacitive measurements comparison in different sliding conditions at 80°C

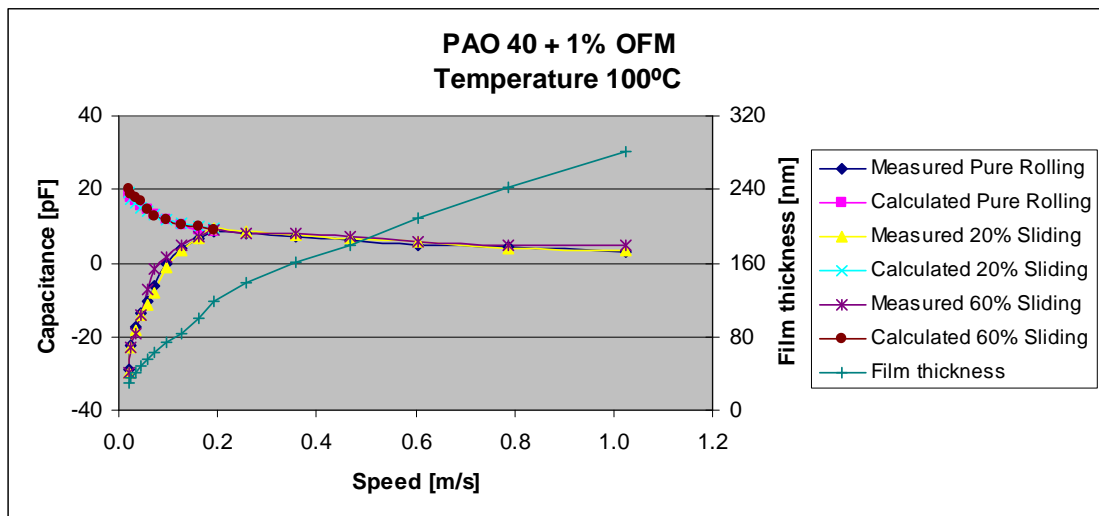


Figure 195: Capacitive measurements comparison in different sliding conditions at 100°C

6.4 Capacitance Measurements Comparison for Base Oil and Different Oil Mixtures

A comparison between the base oil and the two different oil solutions has been done to see the influence of the additives used on the capacitance results.

First tests to be analyzed were carried out in pure rolling conditions.

Figures 196–199 present the results obtained for the three lubricants in pure rolling conditions, over a range of temperatures.

As it can be seen from the resulting graphs, the capacitance measured for each lubricant is different from one another; as shown for the optical film thickness measurements, the lubricant mix with the viscosity index improver has the higher film thickness. This implies that in the case of the capacitive measurement, the resulting values are the lowest of all lubricants; the organic friction modifier behaves similar to the VII.

The higher the temperature used in the tests, the bigger the difference in the measured capacitance. The reason why the capacitance difference intensifies with a raise in temperature is that as seen for the optical measurements as the temperature increases so does the difference between the measured film thicknesses for the lubricant mixtures with additives.

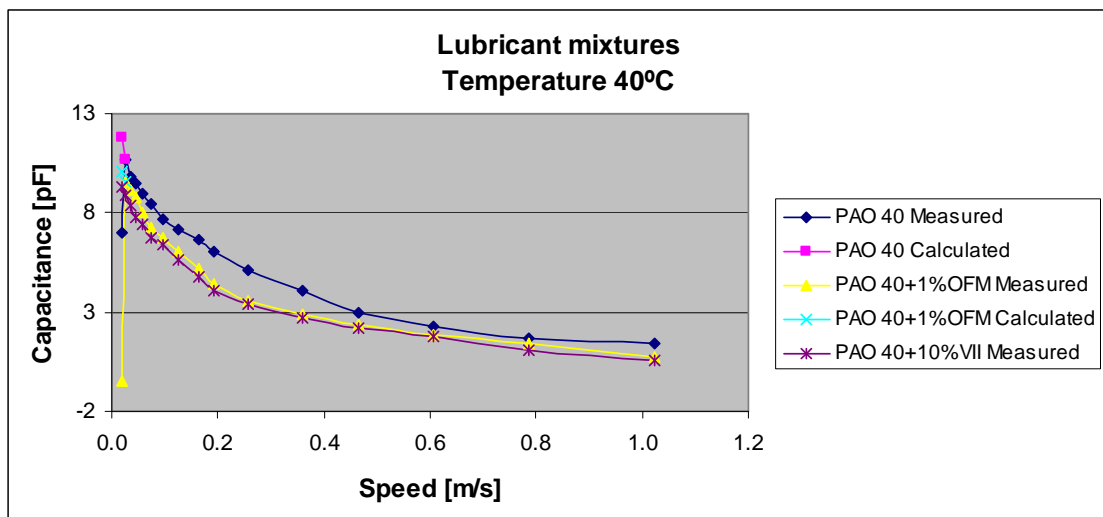


Figure 196: Capacitance measurements comparison for different lubricant mixtures at 40°C pure rolling

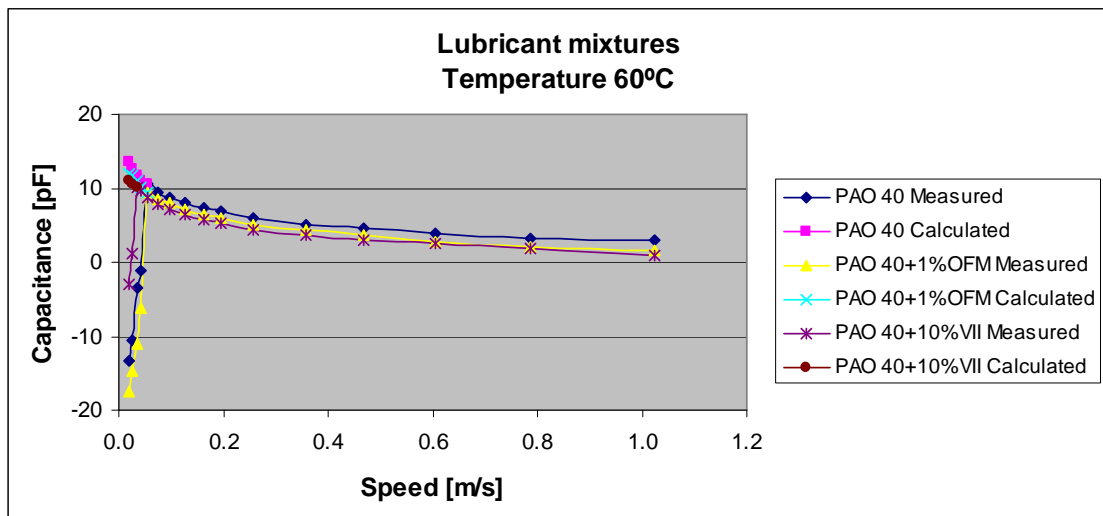


Figure 197: Capacitance measurements comparison for different lubricant mixtures at 60°C pure rolling

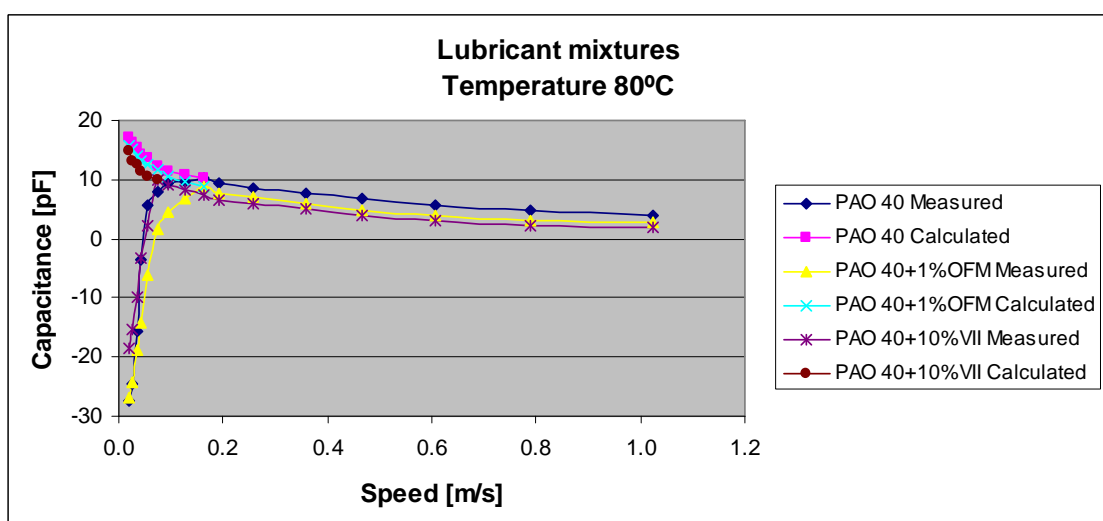


Figure 198: Capacitance measurements comparison for different lubricant mixtures at 80°C pure rolling

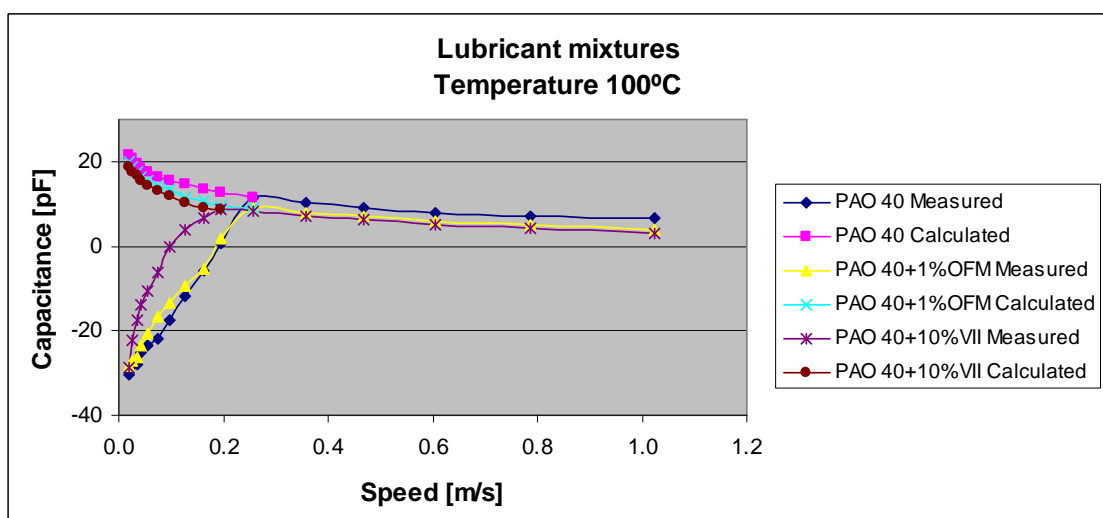


Figure 199: Capacitance measurements comparison for different lubricant mixtures at 100°C pure rolling

When sliding is introduced, the resulting graphs do not change significantly. In the case of the tests carried out in a 20% sliding environment for the three lubricants used, the results show the same trend as for the pure rolling conditions i.e. higher capacitive values for the base oil, due to a lower optically measured film thickness.

Figures 200–203 present the results obtained in a 20% sliding condition for all three lubricants used in four different temperatures.

A more visible difference in capacitance values can be seen for the lowest temperature, meaning that even a small change in experimental setting can have a significant influence on the outcome of the tests.

At higher temperatures, the measured difference tends to be constant over the range of speeds for which capacitive measurements were done.

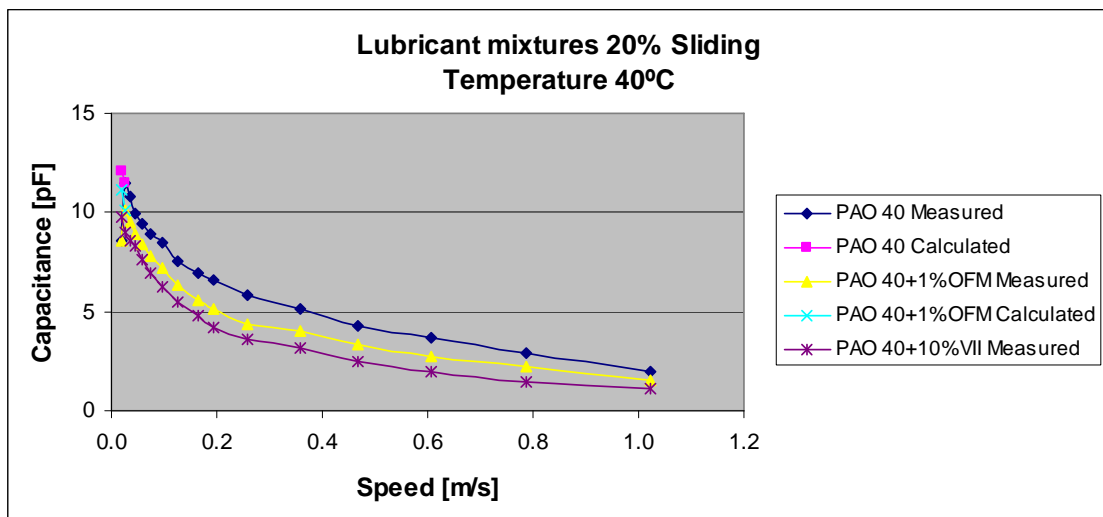


Figure 200: Capacitance measurements comparison for different lubricant mixtures at 40°C 20% sliding

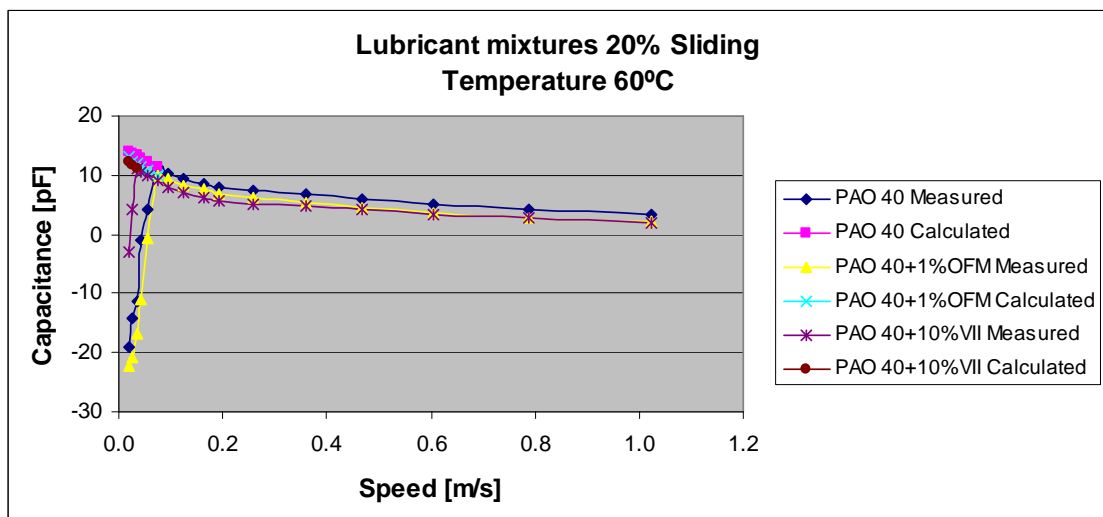


Figure 201: Capacitance measurements comparison for different lubricant mixtures at 60°C 20% sliding

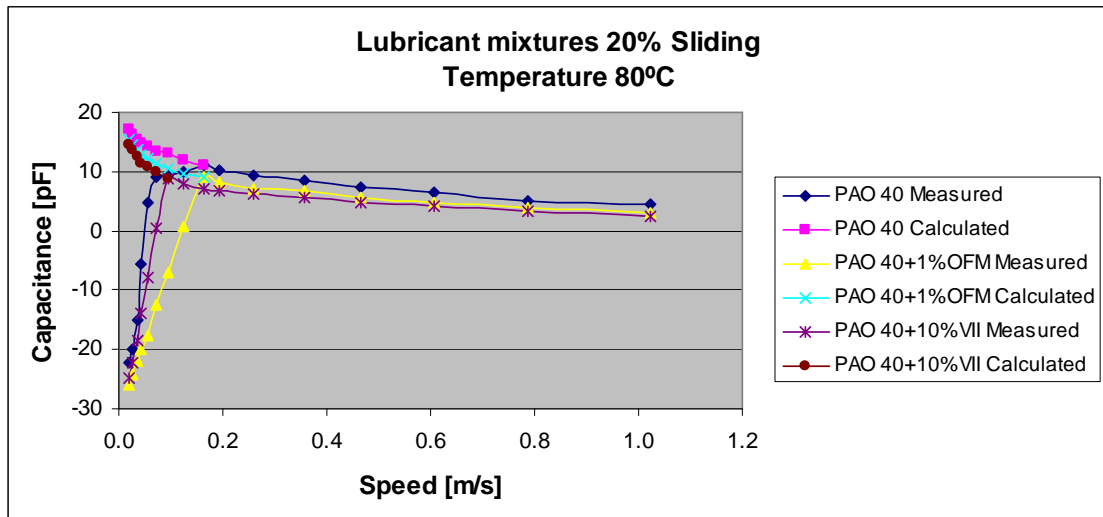


Figure 202: Capacitance measurements comparison for different lubricant mixtures at 80°C 20% sliding

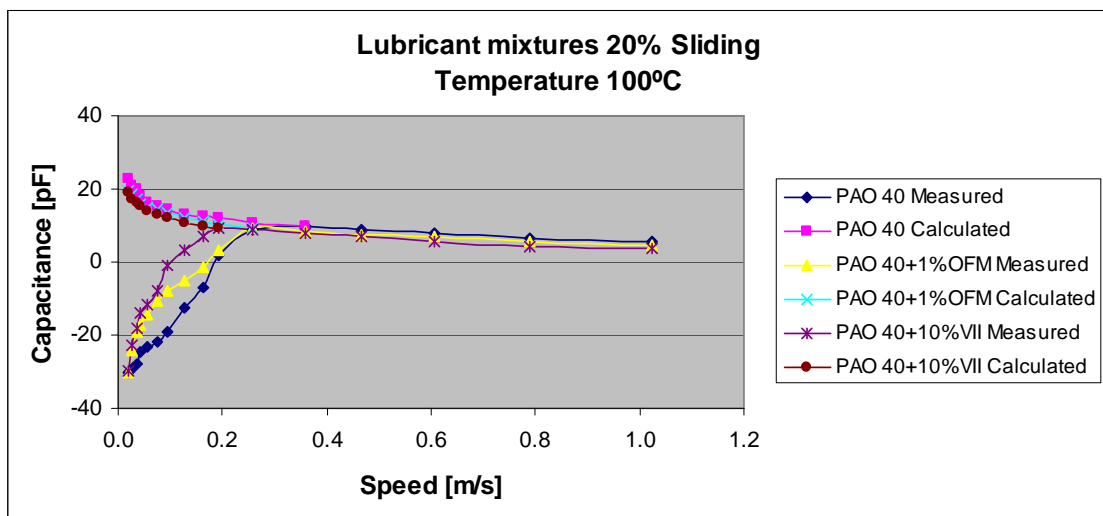


Figure 203: Capacitance measurements comparison for different lubricant mixtures at 100°C 20% sliding

The same trend was observed for a 60% slide/roll ratio as for the pure rolling condition and the 20% sliding one.

Again, it can be seen that the lubricant with the highest measured capacitance is the base oil, which has, in fact, the smallest registered film thickness.

Figures 204–207 show the graphs for the measured capacitive values in a 60% sliding condition in a range of speeds and temperatures.

As seen for the 20% sliding condition, a good value distinction can be made at a low temperature.

For all tests, in all conditions, a definite difference between base oil and the other two lubricant mixtures can clearly be seen, especially for low speeds.

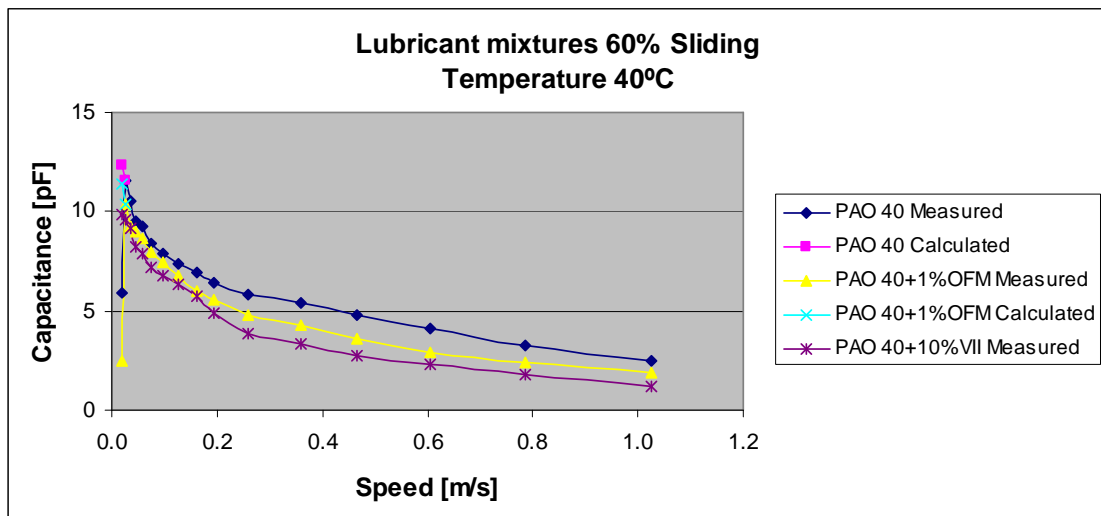


Figure 204: Capacitance measurements comparison for different lubricant mixtures at 40°C at 60% sliding

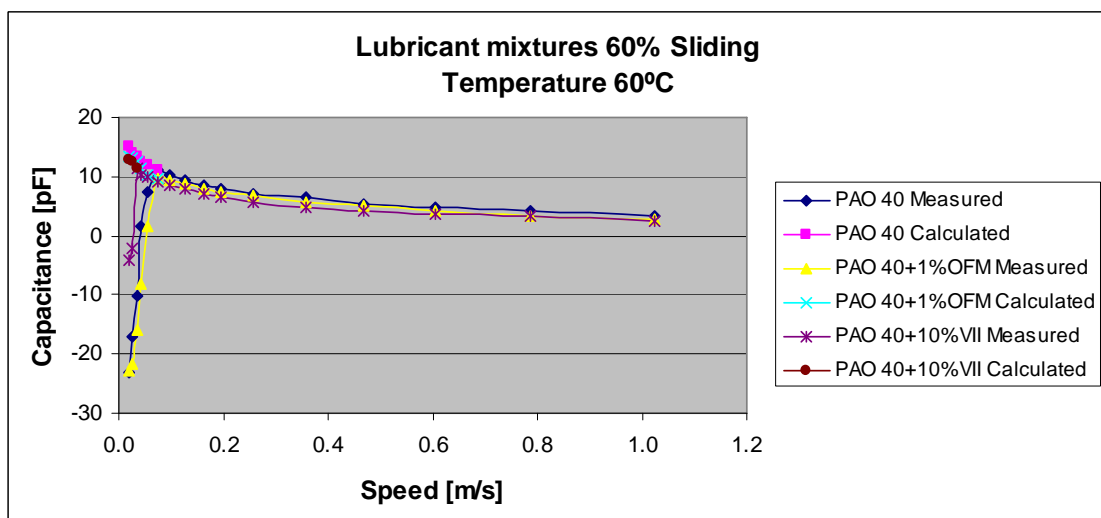


Figure 205: Capacitance measurements comparison for different lubricant mixtures at 60°C at 60% sliding

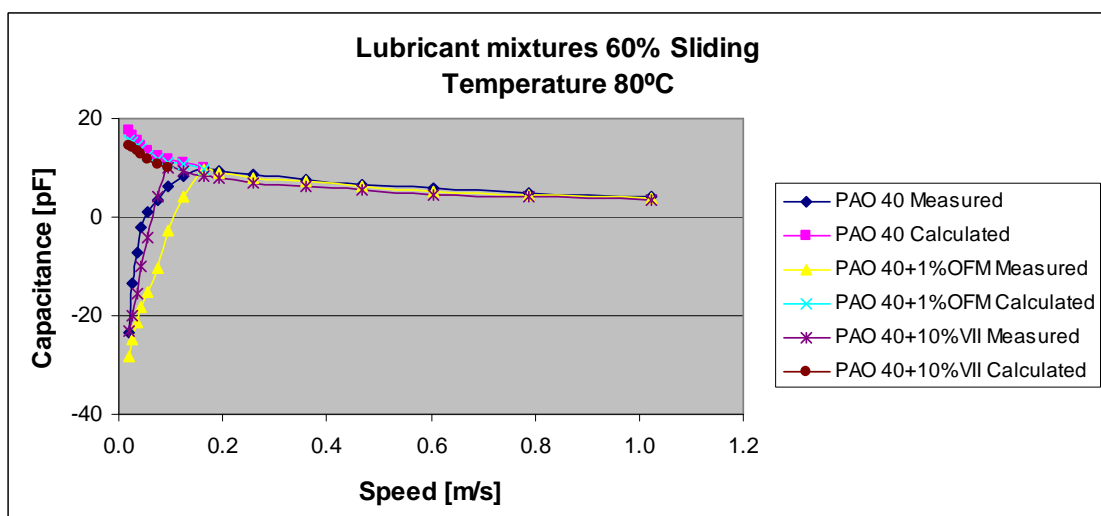


Figure 206: Capacitance measurements comparison for different lubricant mixtures at 80°C at 60% sliding

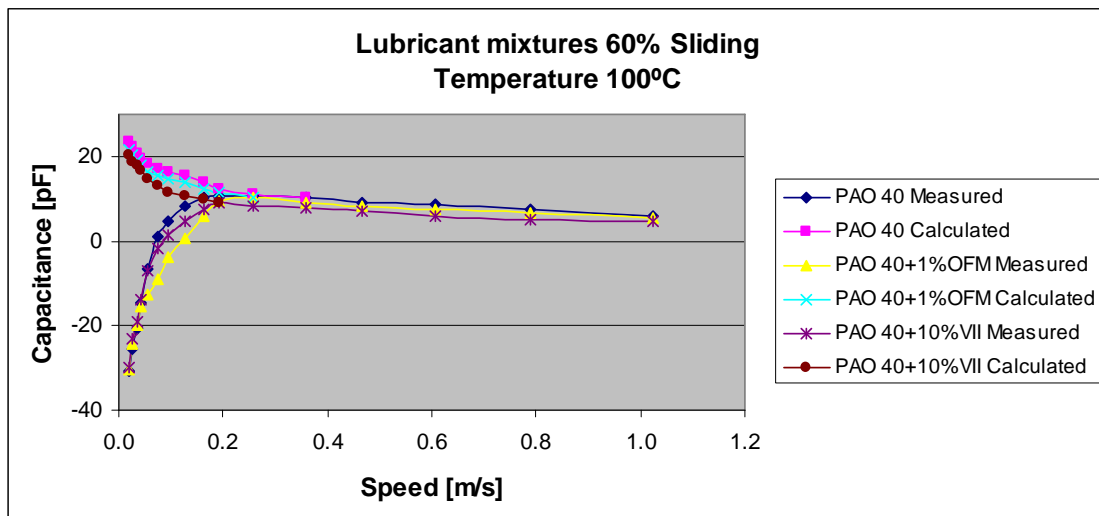


Figure 207: Capacitance measurements comparison for different lubricant mixtures at 100°C 60% sliding

6.5 Comparison between Chromium-coated glass and Steel discs Capacitive Measurements

A comparison between the measurements obtained using a Cr disc and the results from the steel disc were made, to assess the influence of the roughness and resistance on contact capacitance.

All tests presented in this chapter were conducted under pure rolling conditions.

The measured resistance for the two discs is zero for the steel disc and $110\text{k}\Omega$ for the Chromium disc.

The roughness of the two discs was measured using an optical profilometer, with the resulting measurements presented in Table 9.

For the steel disc the measured roughness value is $\sim 4\text{nm}$; this is an average taken for three different measurements, on three different positions on the disc.

For the Cr disc the measured roughness value is $\sim 1.5\text{nm}$, representing an average for the three points on the disc where measurements were taken.

Same measurements were carried out for the steel ball that was used in these tests, with a resulting roughness of $\sim 7\text{nm}$.

Table 9

	Steel disc	CR 15nm	Ball
Ra [nm]	3.26	1.38	7.07
	4.3	1.33	7.28
	3.82	1.47	7.09

Figures 208–211 present the optically measured film thickness against the electrically measured film thickness graphs extracted from tests done using the PAO 40 base oil, using a Cr sputtered disc and a steel equivalent.

The results clearly show slightly higher measured values for the steel disc, phenomenon explained by a lower contact resistance in the case of the steel disc. This trend can be especially observed for higher speeds where the two curves start to be clearly distinguishable from one another.

From these measurements we can draw the conclusion that the resistance has a much higher influence on the measured capacitance than the actual roughness of the disc used.

At low speeds, the capacitance measurements are similar for all temperatures resulting in a close similarity for the extracted film thickness values. The higher variation is observed for the higher speeds and it is more accentuated for the elevated temperatures, where as shown before, the film thickness is smaller.

For the higher temperatures, the values measured at low speeds are almost imposing on each other.

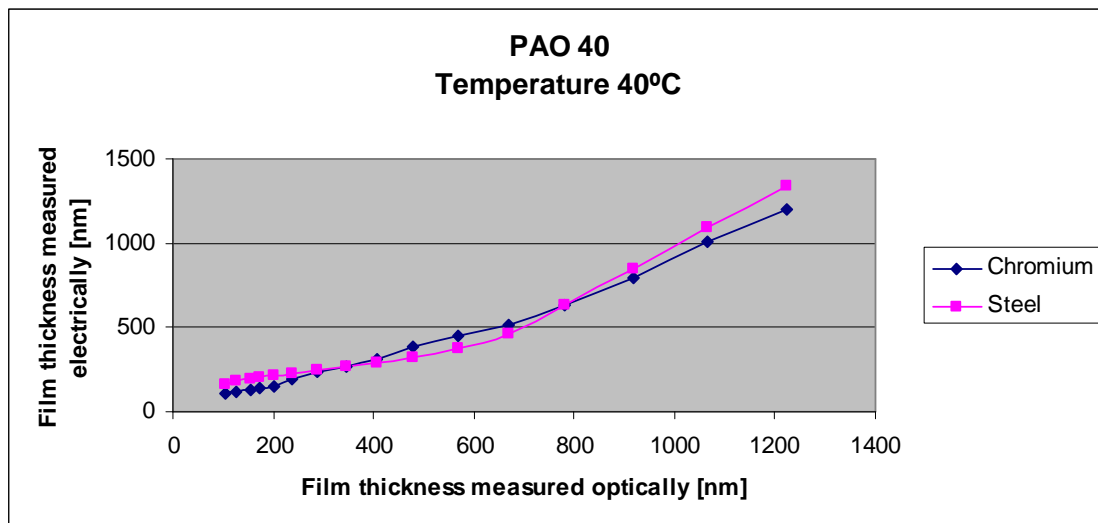


Figure 208: Film thickness measurements comparison between Cr and Steel at 40°C for PAO 40

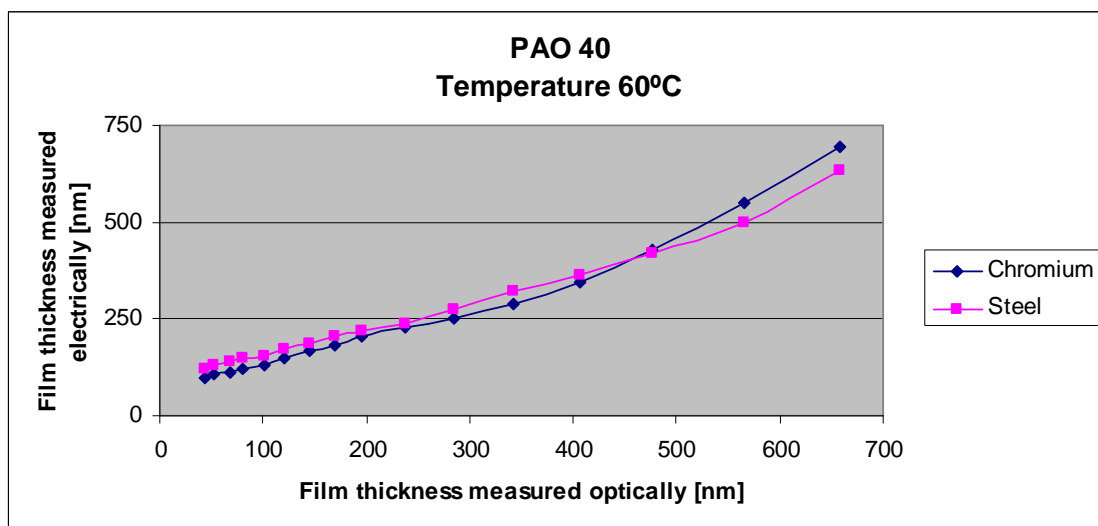


Figure 209: Film thickness measurements comparison between Cr and Steel at 60°C for PAO 40

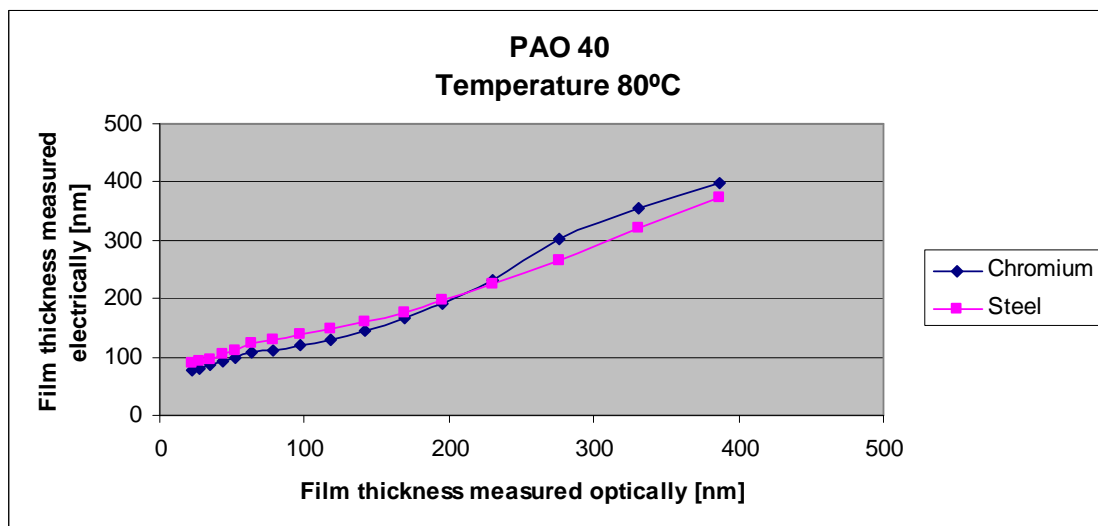


Figure 210: Film thickness measurements comparison between Cr and Steel at 80°C for PAO 40

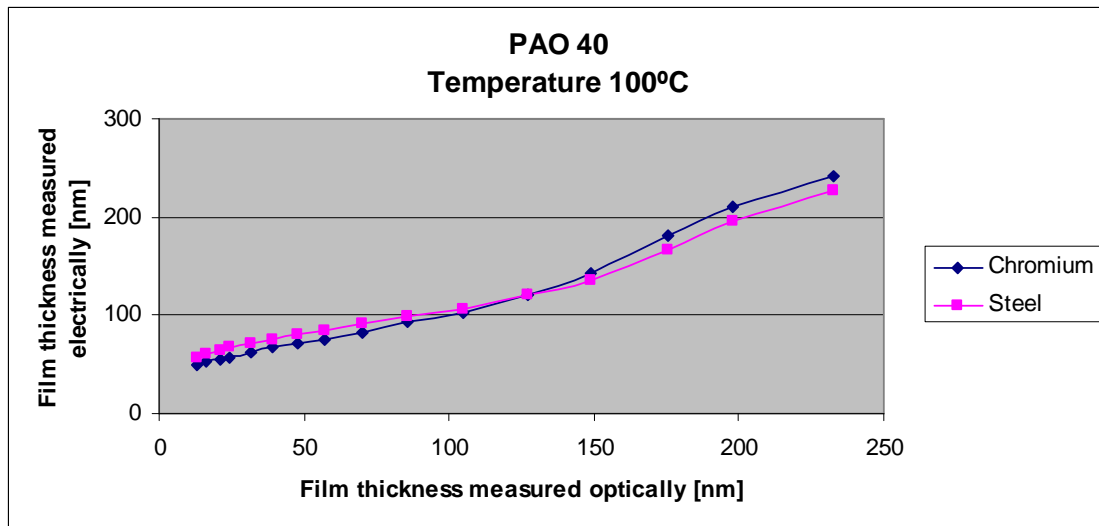


Figure 211: Film thickness measurements comparison between Cr and Steel at 100°C for PAO 40

Figures 212–215 present the film thickness results between the Cr disc and the steel disc using a lubricant mix that has 1% OFM over a range of temperatures.

In this case it can clearly be observed that the higher recorded film thickness is measured for the steel disc, not for the Cr one.

Although this behaviour is not the expected one, influenced by the difference in resistance, for the two discs in this case the higher influence is given by the boundary layer formed on the steel disc surface by the employed additive.

A small difference can be observed for all temperatures used for these tests. At low speeds and high temperatures the determined values are almost similar from one disc to another, and the most noticeable dissimilarity comes at high speeds and high temperatures.

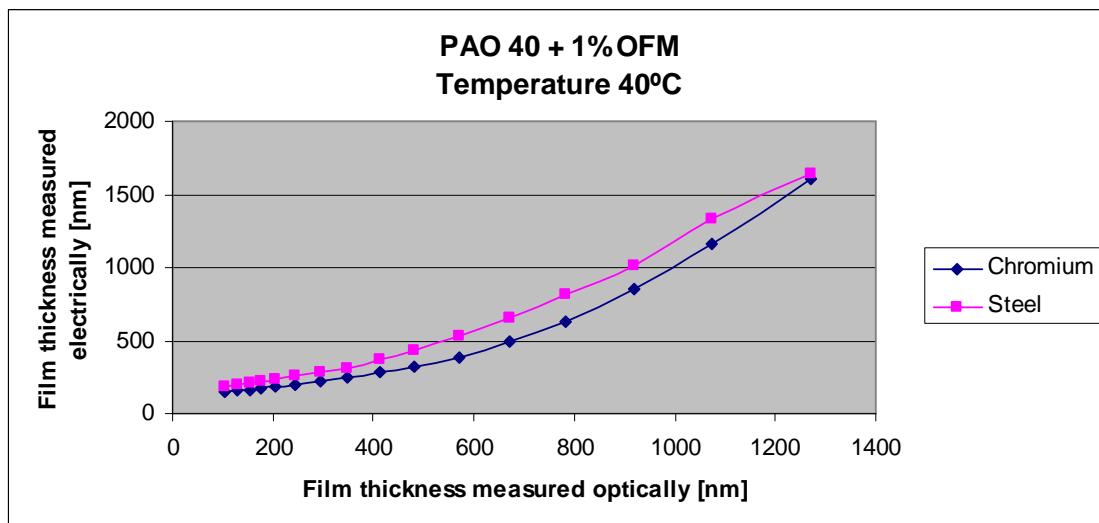


Figure 212: Film thickness measurements comparison between Cr and Steel at 40°C 1% OFM mix

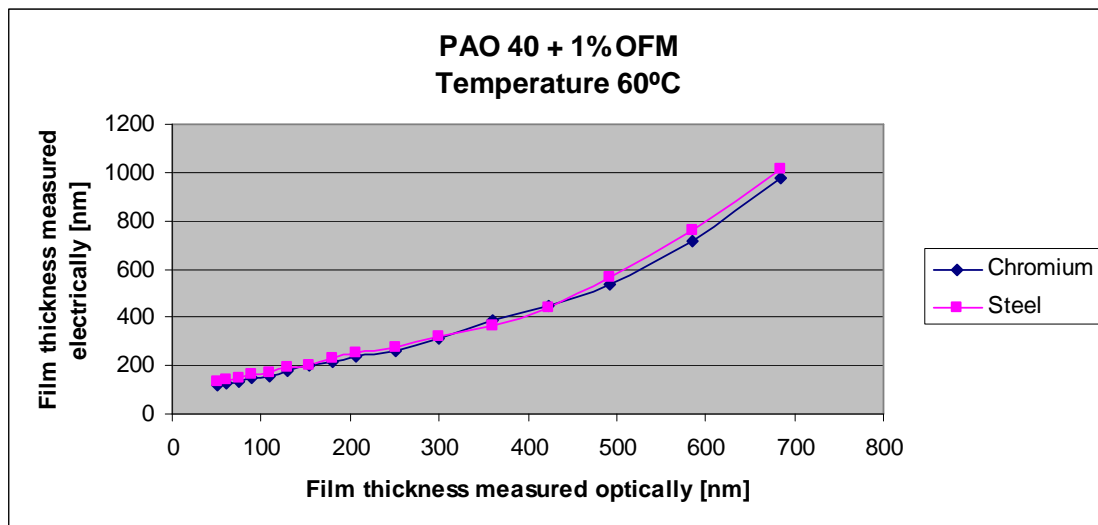


Figure 213: Film thickness measurements comparison between Cr and Steel at 60°C 1% OFM mix

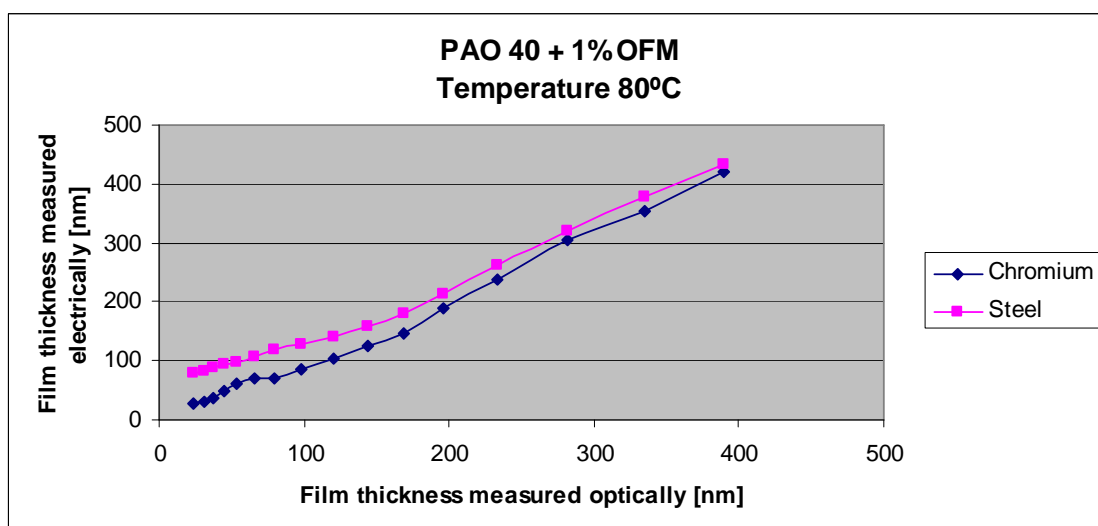


Figure 214: Film thickness measurements comparison between Cr and Steel at 80°C 1% OFM mix

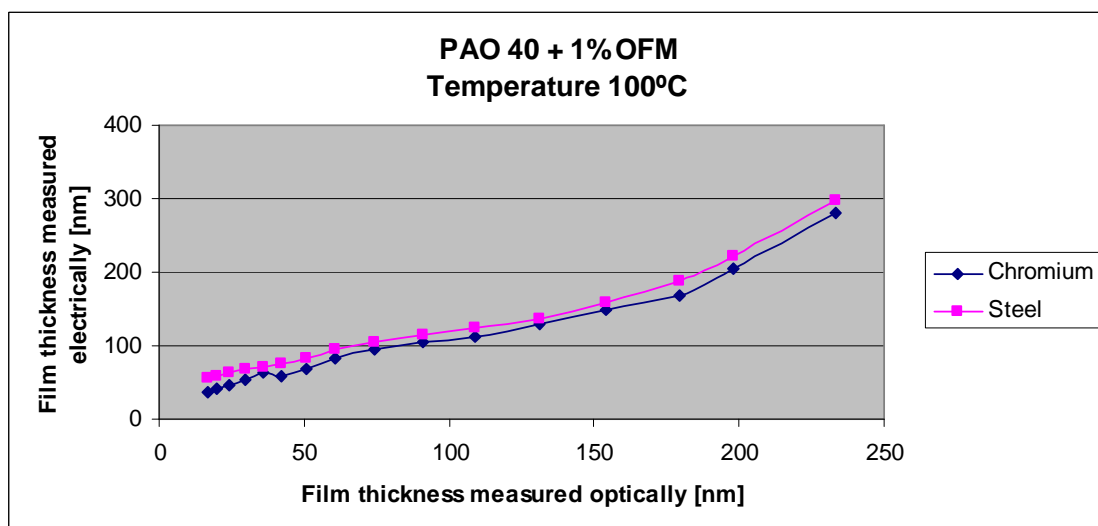


Figure 215: Film thickness measurements comparison between Cr and Steel at 100°C 1% OFM mix

Figures 216–219 present a comparison between the results obtained using a Cr disc and those obtained for the steel disc utilizing a lubricant mix that has 10% VII over a range of temperatures and speeds.

As shown for the other lubricant mix that uses 1% OFM, the film thickness measurements obtained using the Cr disc are lower than the ones obtained using the steel disc.

In this case, a small differentiation can be observed at all temperatures. At low speeds and high temperatures, the achieved values are almost similar from one disc to another; however the more noticeable distinction comes at high speeds and high temperatures.

In contrast to the other additive, the most highlighted variation in capacitance over the whole range of speeds is given at higher temperatures, resulting in a much higher adsorbed boundary layer produced by the VII additive on the steel disc surface.

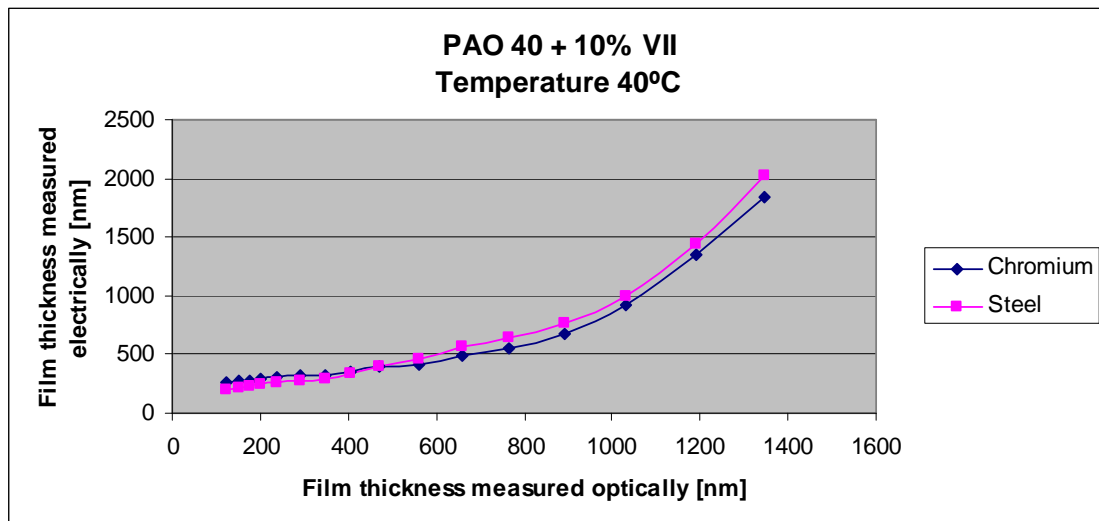


Figure 216: Film thickness measurements comparison between Cr and Steel at 40°C 10% VII mix

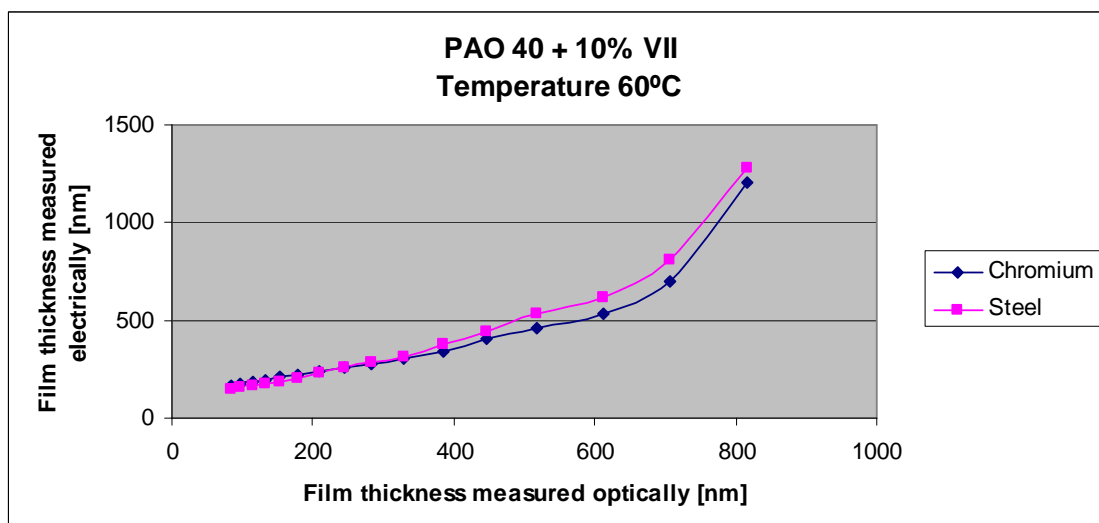


Figure 217: Film thickness measurements comparison between Cr and Steel at 60°C 10% VII mix

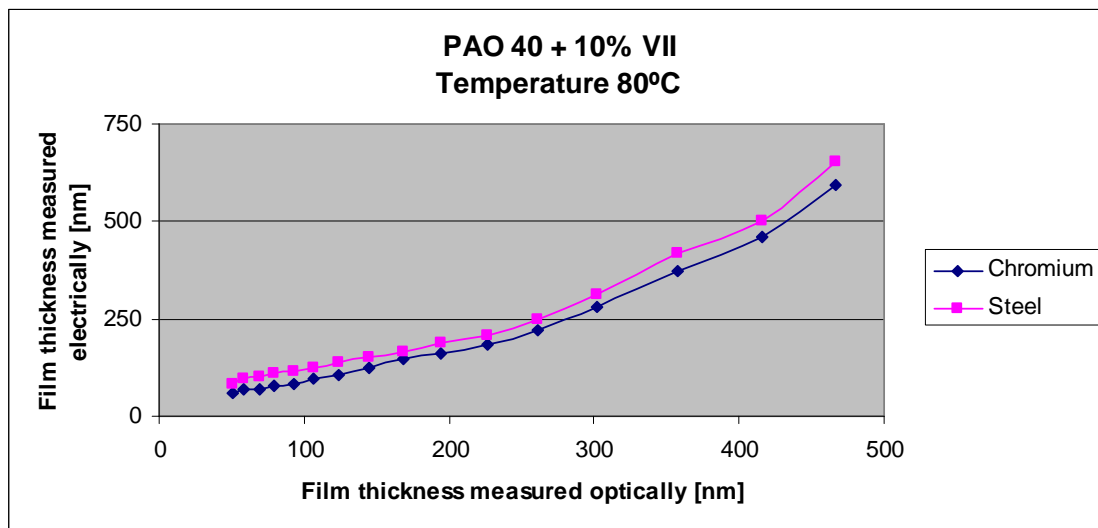


Figure 218: Film thickness measurements comparison between Cr and Steel at 80°C 10% VII mix

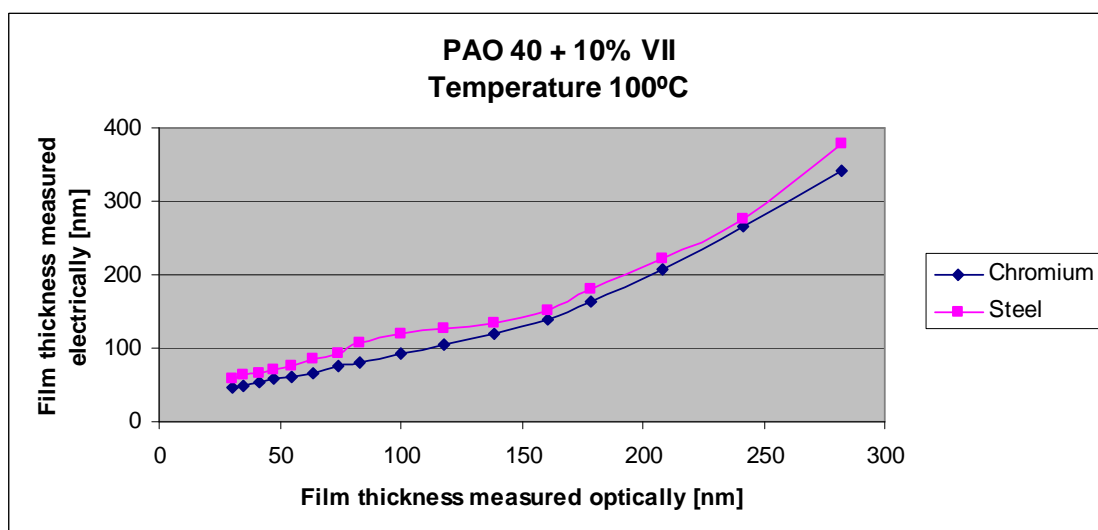


Figure 219: Film thickness measurements comparison between Cr and Steel at 100°C 10% VII mix

7 CONCLUSIONS

A novel method to measure elastohydrodynamic contact film thickness based on electrical capacitance has been developed and presented. Capacitance measurements have been used for some time, but a successful precise calibration has not been achieved yet. This project has attempted to overcome some of the difficult issues regarding the application of the capacitive method for the study of thin elastohydrodynamic films, with the hope that this method could ultimately be used to monitor and measure film thickness during machine operation.

Optical methods, which are currently more popular, have the disadvantage that they require one of the contacting surface materials to be transparent (typically glass or sapphire). These methods are generally accepted as providing accurate results and hence have been used for calibration. In order to achieve this, the widely exploited Ultra Thin Film Interferometry technique (UTFI) was modified to use a chromium layer as a contacting surface instead of a silica layer, thus simulating a metal-on-metal tribopair as encountered in real life machinery, and potentially allowing simultaneous capacitance and optical measurements.

The experimental rig used in the tests was based on an existing EHL (Elastohydrodynamic Lubrication) rig capable of measuring lubricant films as thin as few nanometres. Changes were made to the experimental setup to allow an electrical signal to be applied and collected from the two contacting bodies. Conditions employed for the optical method were successfully replicated for the electrical method (capacitance) as well.

This study started with the premise that a thicker chromium layer applied to a glass/sapphire disc will provide the necessary phase change for the normally fragile silica layer to be eliminated. This would potentially allow very thin films to be measured, even when sliding conditions are applied, which would normally destroy the silica layer very quickly. Theoretical analysis showed an increase in phase change caused by an increase in Cr thickness. After a detailed investigation and multiple attempts with different chromium thicknesses it was shown that an increase in metal thickness results in a strong reflection of the metal/glass interface. This makes it very difficult to use optical interferometry method without the silica layer. It was concluded that for test conditions used, an increase in chromium thickness does not supply the necessary phase change required for the accurate measurement of lubricant film thicknesses.

The first stage of the project was to obtain a benchmark (accurately measured lubricant film thickness) for the capacitance values to be calibrated against. Film thickness measurements were carried out using the classical UTFI method and the calibration values determined. First,

a base-oil was used to obtain film thickness values for a range of entrainment speeds, temperatures and sliding conditions. The results obtained for the base-oil were compared with results obtained for oil mixtures using two different additives: an organic friction modifier (OFM) and a viscosity index improver (VII). The use of these additives had a significant affect on the observed results:

- ▲ The OFM additive provided a boundary film when hydrodynamic (HD) and elasto-hydrodynamic (EHD) lubrication failed, whilst it did not influence the overall film thickness as significantly as the VII additive.
- ▲ The VII additive provided a good overall improvement on the film thickness, especially at higher temperatures, providing more protection against film failure due to vibration or surface asperities.

Overall, the biggest variation in film thickness was observed as a result of an increase in entrainment speed, as predicted by a number of existing models. As the entrainment speed increases there is a corresponding and predictable increase in the amount of lubricant pushed into the contact, which results in a significant increase in the film thickness.

Lubricant temperature was also shown to influence film thickness. This effect was found to have inverse effect of speed, with film thickness decreasing as the lubricant temperature increased. This is largely due to the effect of temperature on the lubricant viscosity. As the lubricant temperature increases, its viscosity decreases resulting in a rapid drop in lubricant film thickness.

The introduction of sliding (surface velocity difference) showed no significant effect on film thickness, as has been predicted in previous optical interferometry studies. Whilst positive sliding tends to reduce the film thickness, this effect is small in comparison to the effect of temperature and entrainment speed. This outcome is almost certainly due to a small increase in temperature of the contact region that occurs with the introduction of sliding, which influences the local viscosity of the lubricant resulting in a drop in oil film thickness.

In order to calibrate the capacitance method, a number of capacitance tests were carried out under identical experimental conditions to those used for the optical method. The largest variation in capacitance measurement was found to occur as a result of changes in temperature, with increasing lubricant temperature resulting in a corresponding increase in measured capacitance. From the results of the optical measurements, increases in lubricant temperature result in a noticeably decreased film thickness.

Using the analogy of a parallel plate capacitor, decreasing the plate separation increases the capacitance, hence this result is to be expected.

As found using optical methods, the introduction of sliding had little effect on the measured contact capacitance, however, a small variation was still observed. This could either be attributed to a small variation in background capacitance or that the capacitance method used is accurate enough to measure the minor changes in film thickness that result from the introduction of sliding. A small increase in contact capacitance was measured over a range of speeds; probably as a result of a slight decrease in film thickness due to the small localised temperature increase that occurs because of sliding.

The introduction of the two additives had a similar effect on the capacitance measurements as was found for the optical method, with the highest influence resulting from the addition of a VII. The optical methodology showed that the introduction of a VII resulted in an increase in the film thickness, which was indicated by a decrease in the measured capacitance. The OFM behaved similarly to the VII, albeit with a smaller decrease in measured capacitance value. The reason why the OFM does not have the same influence on the capacitance as the VII is that the OFM additive has an influence on the lubrication process only when the HD or EHD film fails and is replaced by boundary lubrication.

Further capacitance tests were conducted to show the effect of replacing the steel disc with the various chromium-layered discs. The results of these tests highlighted the importance of the electrical resistance of the disc and the surface roughness. For tests conducted using the base oil alone the disc resistance played an important role in influencing measured capacitance, resulting in a higher value for the steel disc that had zero resistance as compared to the chromium disc that has a measured resistance of $110\text{k}\Omega$ between the contact and the point of signal collection.

The capacitance method developed in this project allowed accurate measurements for EHD film thicknesses larger than 100nm. Attempts made to measure the capacitance of films with lower thicknesses failed, likely as a consequence of contacting asperities between the two surfaces, which resulted in a short circuit of the two capacitor plates. Theoretical capacitance values for film thickness lower than 100nm were determined by the use of curve-fitting of the measured values. A formula was extracted from the curve and using the speed values the capacitive results for lubricant film thicknesses lower than 100nm were extrapolated.

Achievements in this thesis in the study of EHD lubricant films are listed below:

- ▲ The existing experimental rig was successfully modified to allow the use of a modified optical method as well as an electrical method based on the theory of parallel-plate capacitance.

- ▲ It has been shown that the optical interferometry method which employs relatively thick chromium layer did not provide the expected precision required for capacitance calibration due to the strong reflection of the metal/glass interface; hence a more traditional optical method was employed for calibration.
- ▲ The new capacitive method developed in this project was capable of accurate measurements for EHD film thicknesses conditions as low as 100nm. A model was proposed for thinner film thickness based on extrapolation of the measured results.
- ▲ Results obtained from optical and capacitance measurements were compared and a good correlation was found between the results. This indicates that the capacitance method can potentially be used as a reliable method of film thickness measurements, including in real metal–metal machine elements without the need for further calibration.

RECOMMENDATIONS FOR FUTURE WORK

A paper [92] has been written to observe the influence of different lubricants on artificial roughness features. This paper concentrated on the effect of two lubricants with different pressure/viscosity coefficients and two discs (one glass and one sapphire at different loads), on the artificially deposited bumps as they pass through the contact.

Figure 220 shows a schematic representation of a ball with an artificial roughness feature on the surface passing through a lubricated contact.

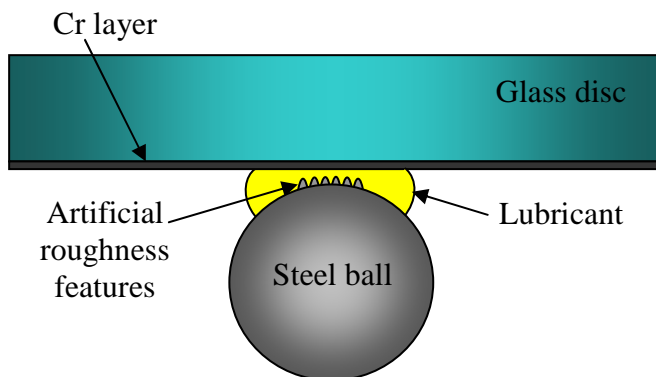


Figure 220: Ball with artificial roughness features passing through a lubricated contact

The next step was to repeat the same measurements and observe the influence the bumps have on the capacitance. It is the authors' opinion that the capacitance method developed in this project is sensitive enough to detect the passing of these Cr bumps across the lubricated contact.

As shown in the next chapter the capacitive method is limited to measuring film thicknesses not smaller than 100nm. This is perfect for the artificial roughness setup, as the longitudinal bumps have a height of 85nm.

A special disc will have to be made to enable the measurement of capacitance and optical film thickness in the same time. Figure 221 shows a graphical representation of the disc that was designed to be used.

The gap in silica will permit wires to be connected to the Cr layer allowing measurement of the EHD film thickness optically and electrically (using capacitance) simultaneously, permitting a calibration with a higher level of accuracy even for thicknesses lower than 100nm.

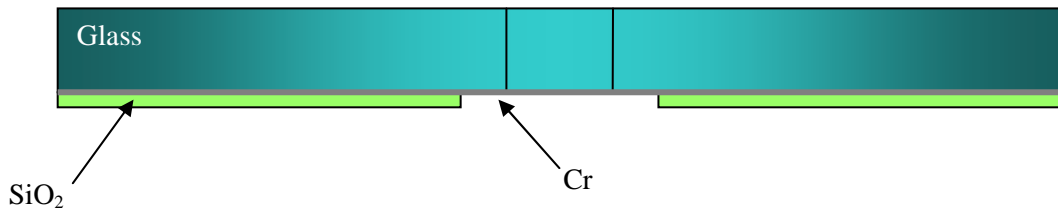


Figure 221: Schematic representation of the specially designed glass disc

A new method for capturing the signal from both the Cr/steel disc and steel ball has to be designed and used in order to eliminate the background noise introduced by the configuration used at the moment.

A number of tests have to be carried out to assess the variation of capacitance in these conditions by taking into account the variation of the lubricant dielectric constant at different pressures [different loads].

A study on the effect of the pressure on the dielectric properties of lubricants (by high pressure viscometry) would provide data which lead to a better evaluation of the capacitance in EHD conditions.

The effect of the polarity of the fluid may also play a role in the capacitance measurements, thus a study on this phenomenon may also be desirable.

APPENDIX

LIST OF PUBLISHED PAPERS

M. D. Furtuna, R. P. Glovnea “*An Experimental Investigation into the Effect of Lubricant on the Local Film Thickness of Artificial Roughness Features*” Proceedings of the STLE/ASME I.J.T.C. 2008, Miami, Florida.

Y. Nagata, M. D. Furtuna, C. Bell and R. P. Glovnea “*Evaluation of Electric Permittivity of Lubricating Oils in EHD Conditions*” 2nd International Conference on Advanced Tribology, 3–5 December 2008, Singapore, also submitted to Tribology International (under review).

R. Glovnea, M. D. Furtuna, Y. Nagata and J. Sugimura “*Electrical Methods for the Evaluation of Lubrication in Elastohydrodynamic Contacts*” the paper was submitted to the Japanese Journal of Tribology and is currently under revision.

MODIFICATION TO THE EXISTING EXPERIMENTAL RIG

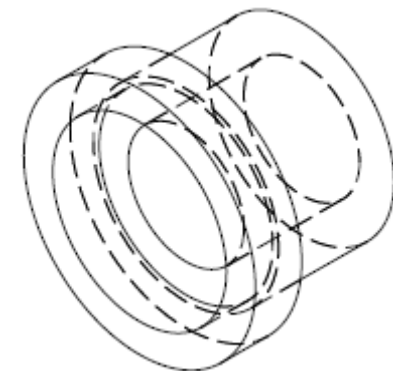
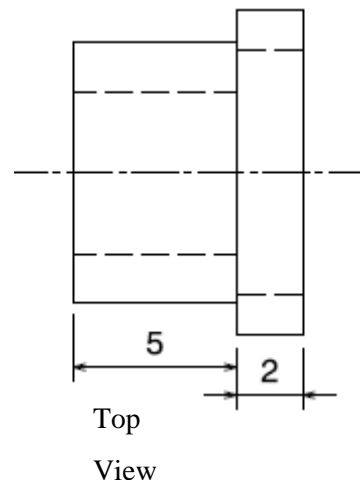
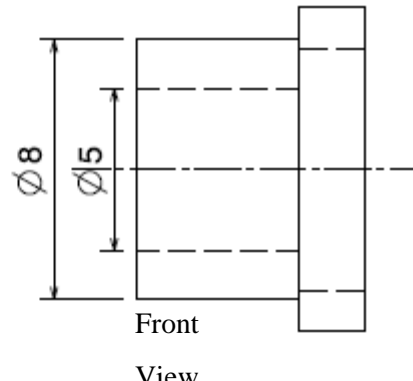
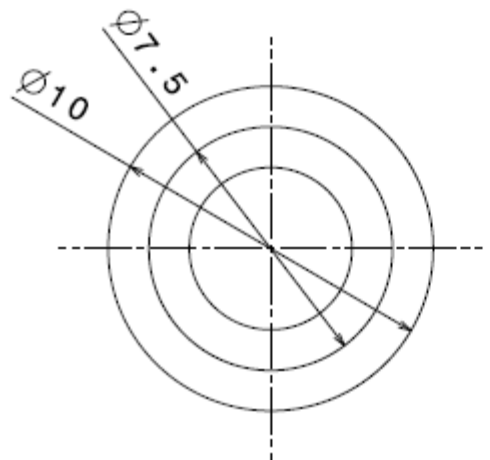
Modifications to the PCS Instruments rig were done and in this chapter the design of the additional parts needed to collect the electrical signal from both the ball and the disc are presented.

The first stage was to electrically insulate disc and the ball from the rest of the experimental rig, this was resolved by using a plastic spacer introduced between the screw that holds the bearing on the carriage. The disc solution was to use a plastic spacer between the shaft and the disc surface.

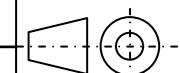
The next problem approached was to collect the signal from the disc, to solve this problem the existing disc shaft spacer was redesigned to allow two wires to pass from the bottom of the disc to the copper nut holding the disc in place.

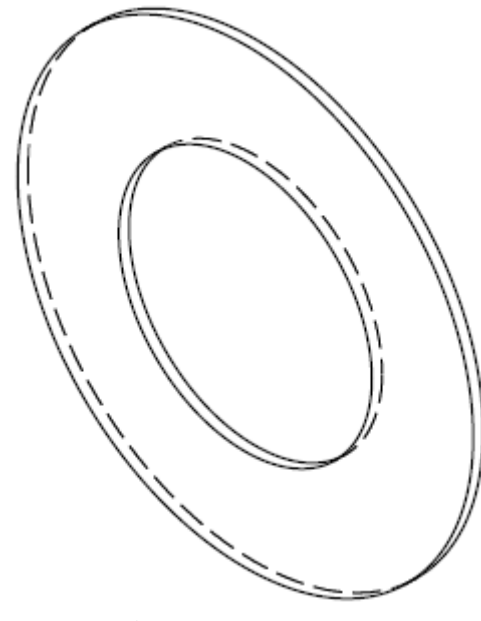
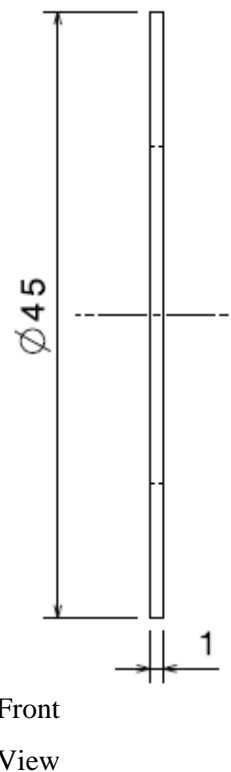
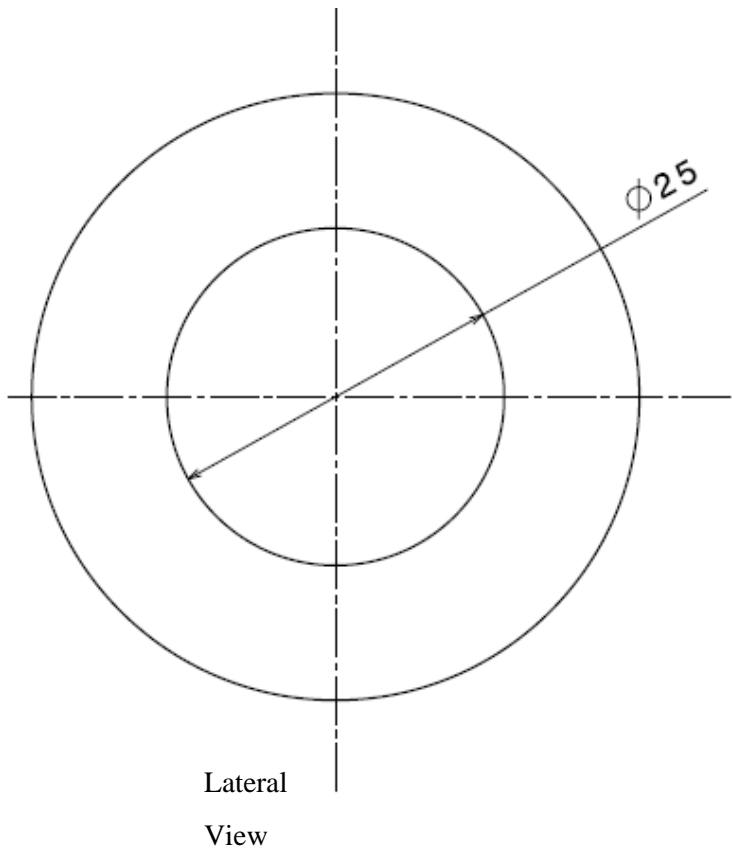
Brushes used to collect the signal from the disc and the ball were designed, the brush used for the disc was straight forward as the solution employed uses one of the oldest methods used to apply/collect electrical signals from rotating elements. For the disc the brush was made from graphite and the rotating element made from copper. For the ball the signal collection was very difficult to deal with due to the fact that the ball and the shaft were submerged in lubricant and it is believed that an oil film is formed between the brush and the shaft when they are in contact. Several combinations of brushes and were tried and the one that gave the best results was chosen.

Drawings of all parts employed to collect and electrically insulate the glass/steel disc and the ball are presented below.

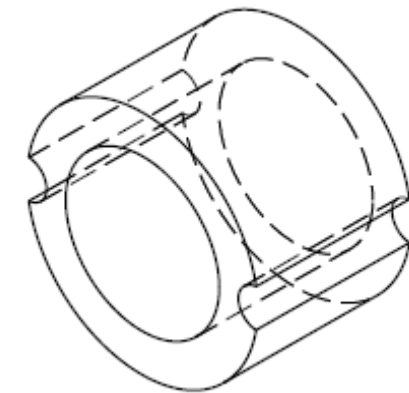
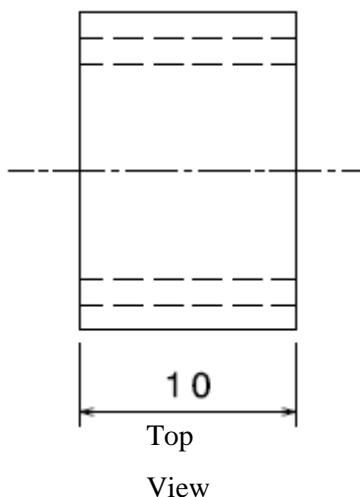
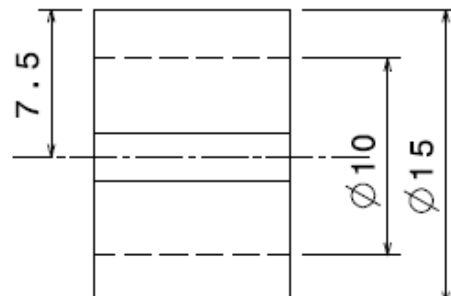
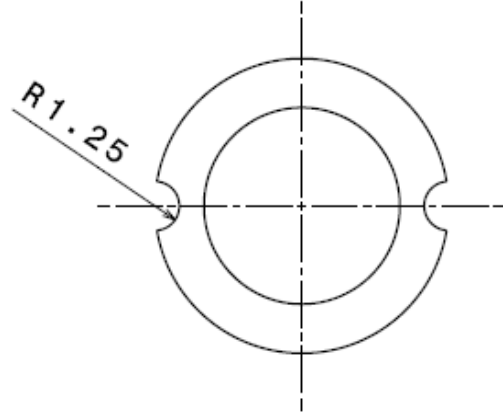


Bearing insulator		Date: 8/09/2010
Marian Furtuna	Scale: 5:1	All dimensions in mm

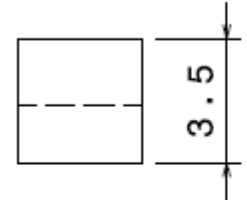




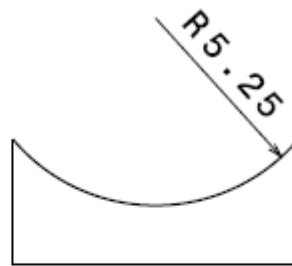
Disc insulator		Date: 8/09/2010	
Marian Furtuna	Scale: 2:1	All dimensions in mm	



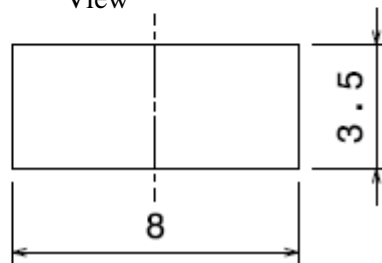
Disc shaft spacer		Date: 8/09/2010	All dimensions in mm
Marian Furtuna	Scale: 3:1		



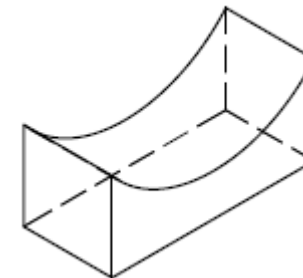
Lateral
View



Front
View

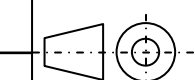


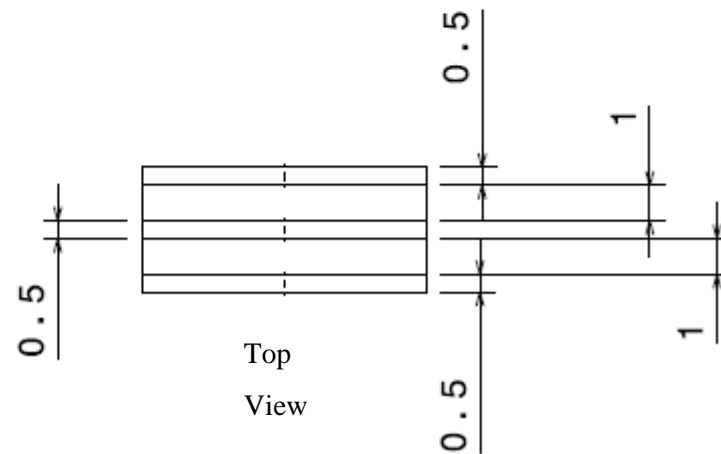
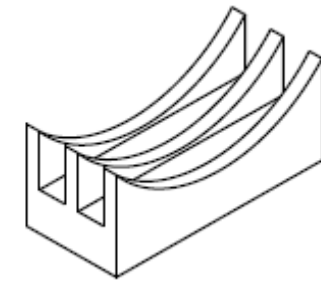
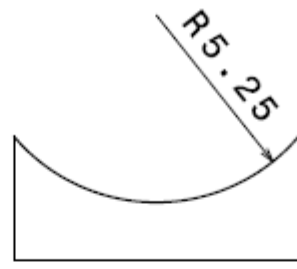
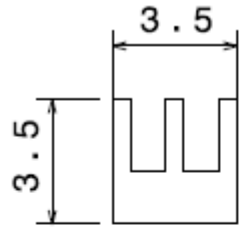
Top
View



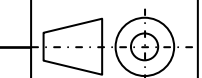
Isometric
View

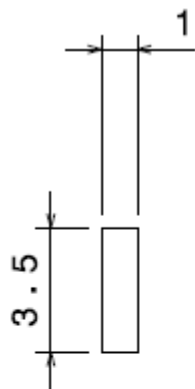
Brush 1	Date: 8/09/2010	
Marian Furtuna	Scale: 5:1	All dimensions in mm



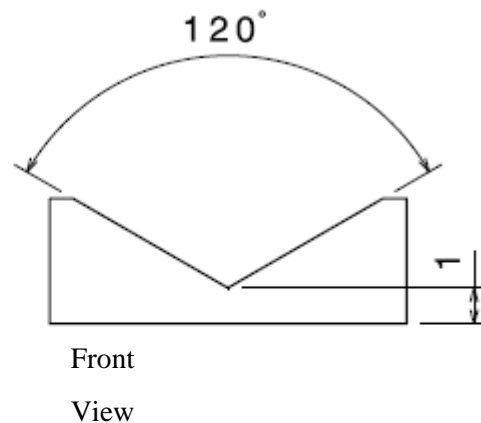


Brush 2		Date: 8/09/2010
Marian Furtuna	Scale: 5:1	All dimensions in mm

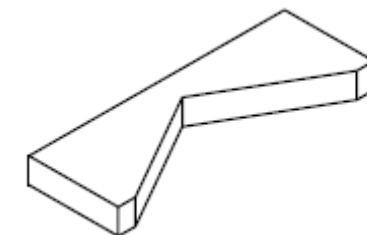




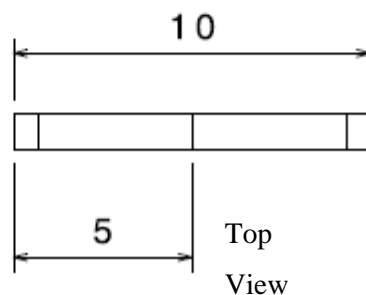
Lateral
View



Front
View

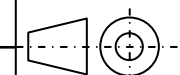


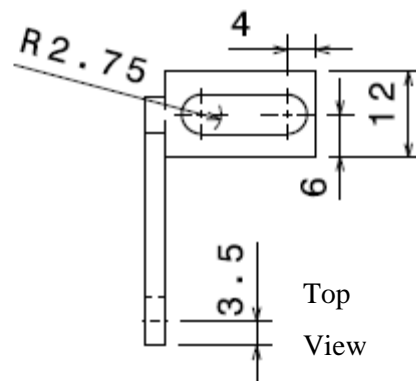
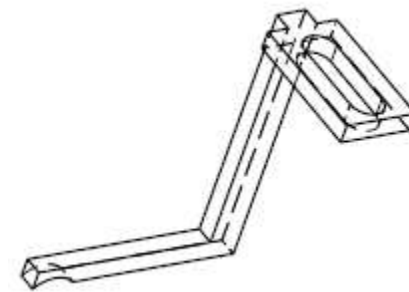
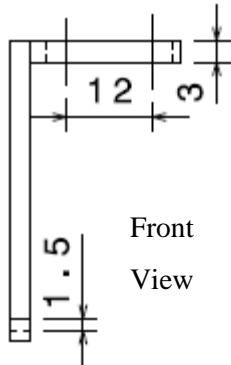
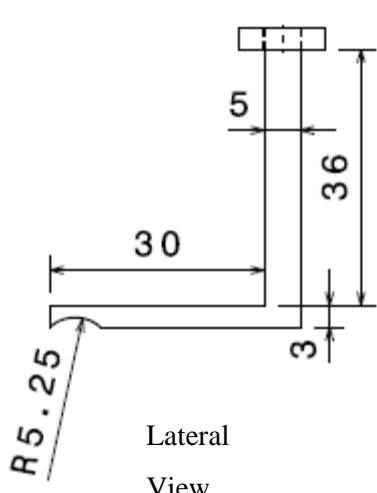
Isometric
View



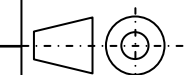
Top
View

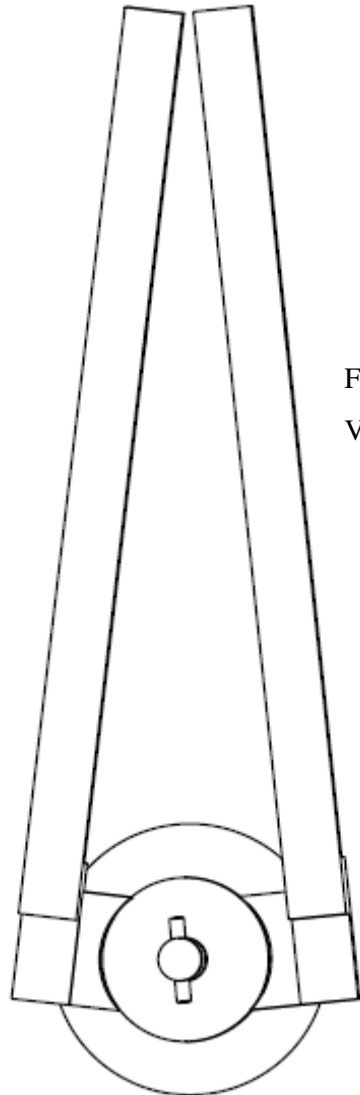
Brush 3		Date: 8/09/2010
Marian Furtuna	Scale: 5:1	All dimensions in mm



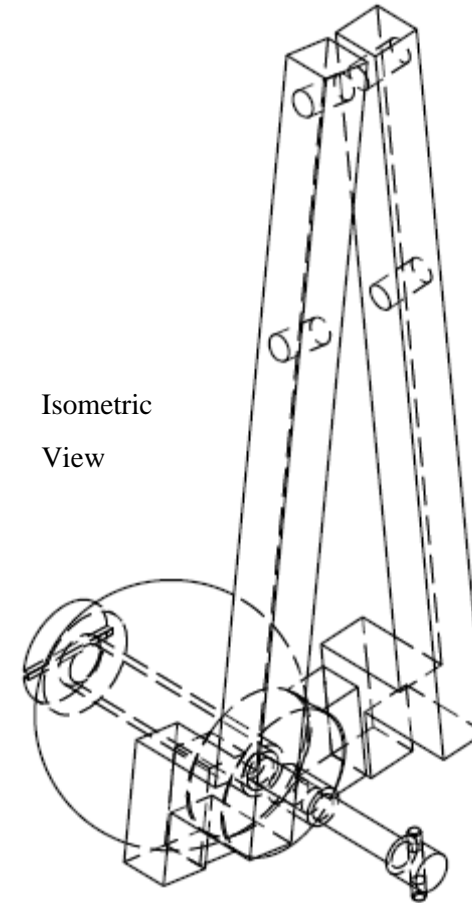


Brush 4		Date: 8/09/2010
Marian Furtuna	Scale: 1:1	All dimensions in mm



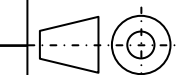


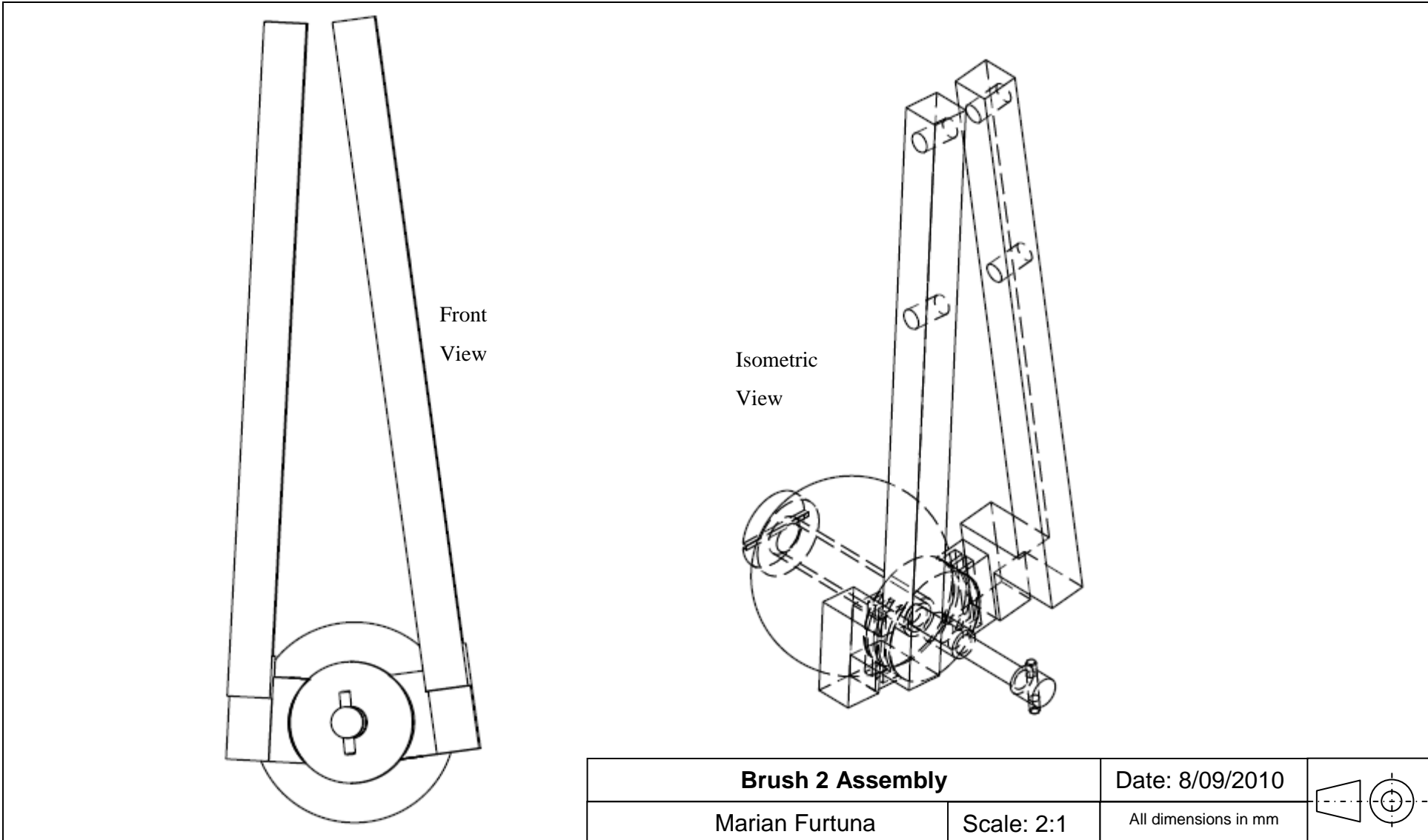
Front
View

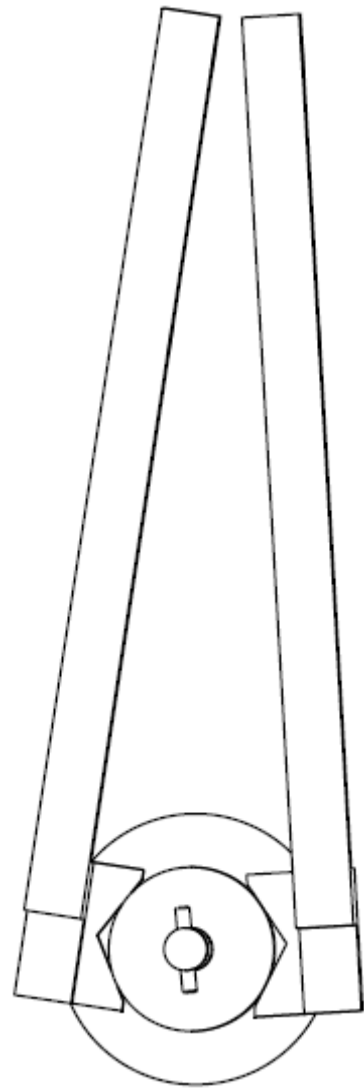


Isometric
View

Brush 1 Assembly		Date: 8/09/2010
Marian Furtuna	Scale: 2:1	All dimensions in mm

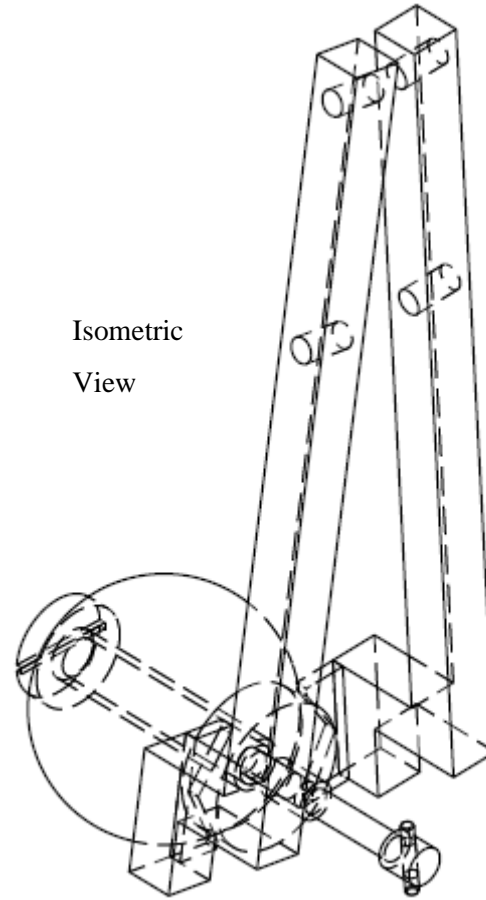






Front
View

Isometric
View



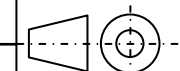
Brush 3 Assembly

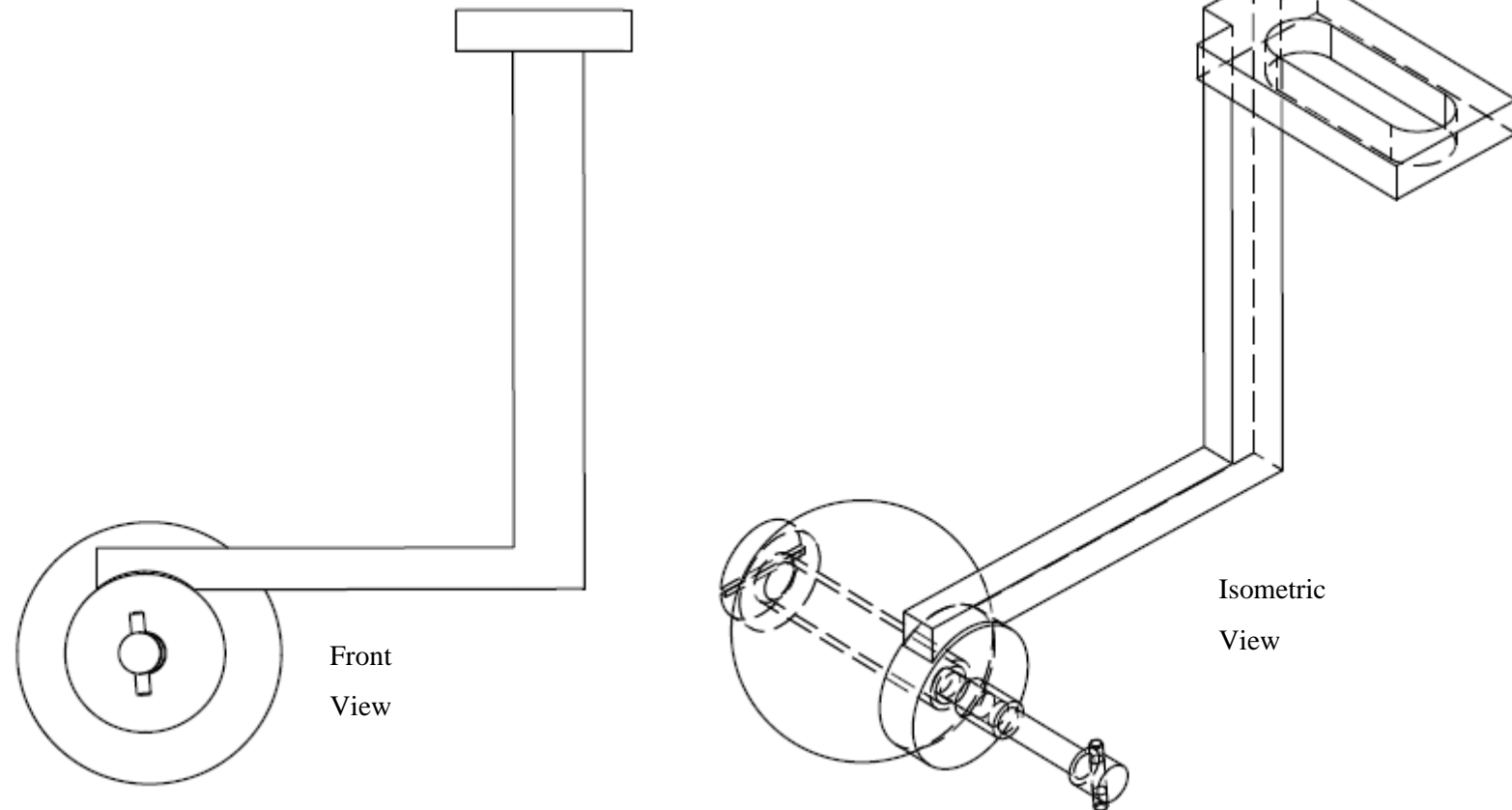
Date: 8/09/2010

Marian Furtuna

Scale: 2:1

All dimensions in mm





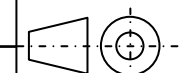
Brush 4 Assembly

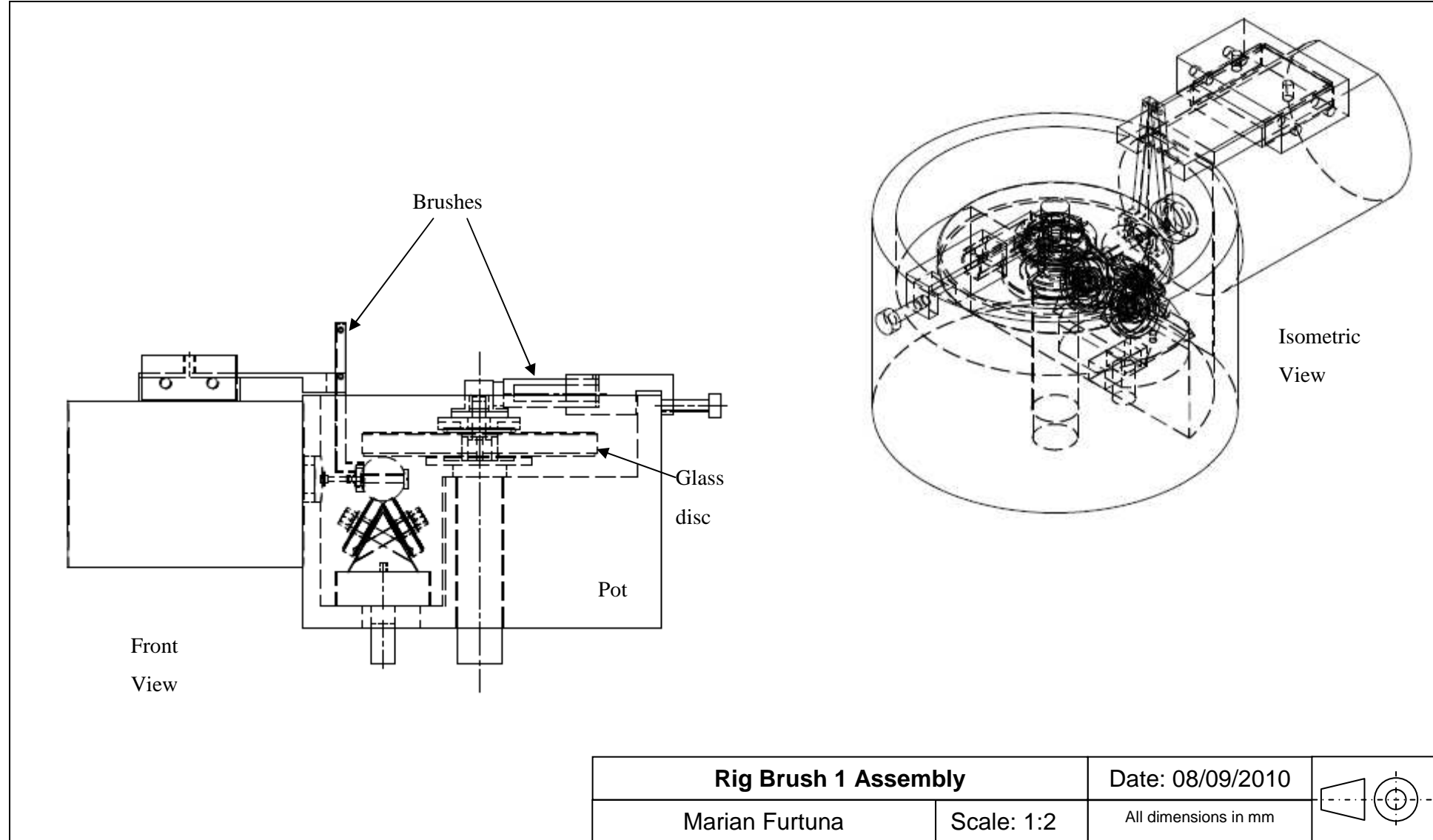
Date: 8/09/2010

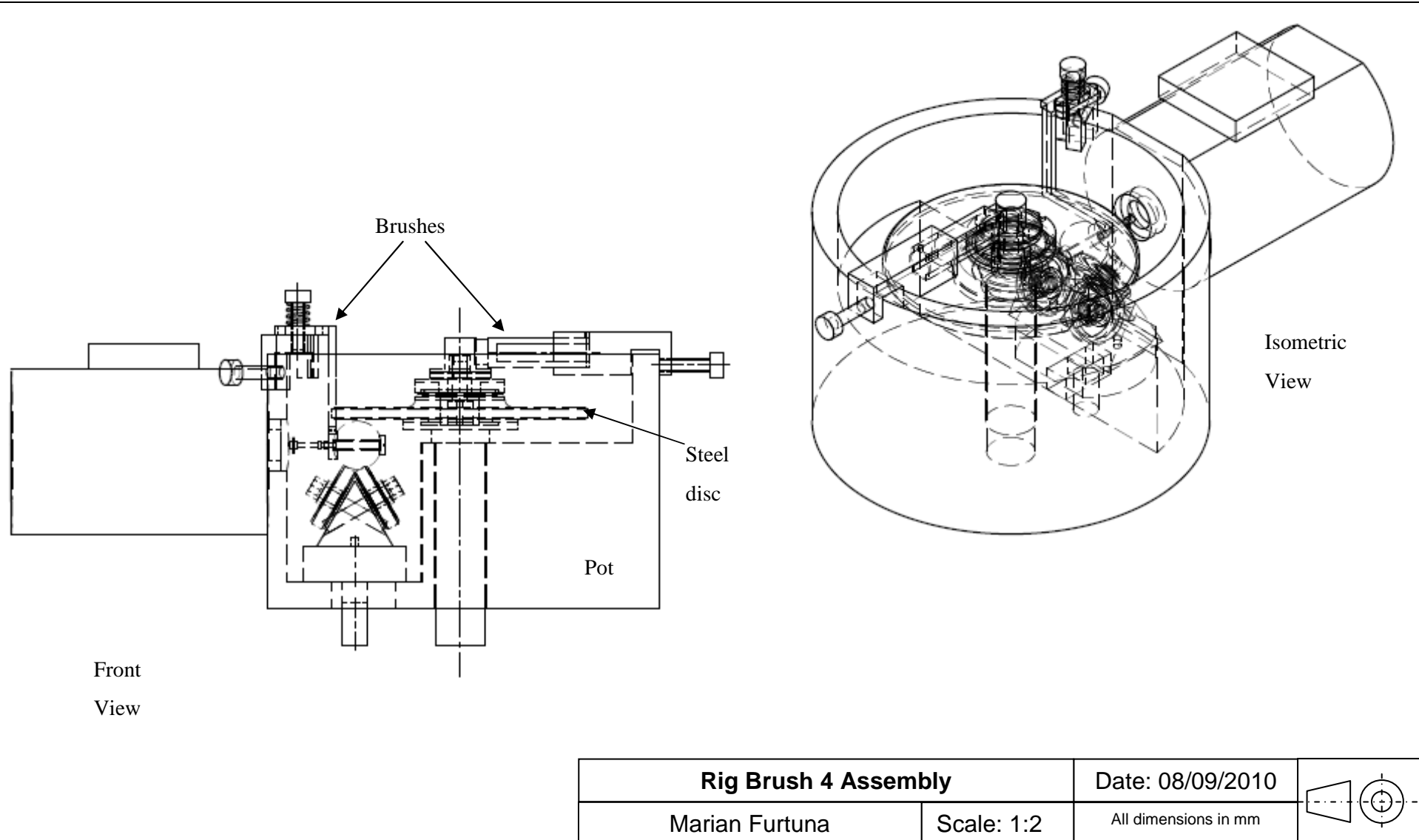
Marian Furtuna

Scale: 2:1

All dimensions in mm







Rig Brush 4 Assembly		Date: 08/09/2010
Marian Furtuna	Scale: 1:2	All dimensions in mm

BIBLIOGRAPHY

- [1] A. Z. Szeri “*Fluid Film Lubrication Theory and Design*”, 1998
- [2] R. Gohar “*Elastohydrodynamics*” Ellis Horwood Series in Mechanical Engineering, 2001
- [3] G. W. Stachowiak and A. W. Batchelor “*Engineering Tribology*” (3rd Edition), 2006, Elsevier Inc.
- [4] K.L. Johnson, 1985, “*Contact Mechanics*”, Publ. Cambridge University Press, Cambridge
- [5] A. Cameron, “*The Principles of Lubrication*”, 1966
- [6] D. Dowson, G.R. Higginson “*The Fundamentals of Roller Gear Lubrication Elasto-Hydrodynamic Lubrication*” 1966
- [7] M. Kaneta, T. Shigeta, P. Yang “*Film Pressure Distributions in Point Contacts Predicted by Thermal EHL Analyses*” Tribology International 39 (2006) 812–819
- [8] K. Stadler, N. Izumi, T. Morita, J. Sugimura, B. Piccigallo “*Estimation of Cavity Length in EHL Rolling Point Contact*” Journal of Tribology July 2008, Vol. 130
- [9] A.N. Grubin and I.E. Vinogradova “*Fundamentals of the Hydrodynamic Theory of Lubrication of Heavily Loaded Cylindrical Surfaces*”, (in Russian) Central Scientific Research Institute for Technology and Mechanical Engineering, Book No. 30, Moscow, 1949. D.S.I.R Trans. No. 337
- [10] A.M. Ertel “*Hydrodynamic Lubrication Based on New Principles*” Akad. Nauk. SSSR Prirod. Math. I Mekh., 1939, Vol. 3, pp. 41-52
- [11] D. Dowson and G.R. Higginson “*A Numerical Solution to the Elastohydrodynamic Problem*” J. Mech. Eng. Sci., 1959, Vol. 1, pp. 6-15
- [12] J. A. Greenwood “*An Extension of the Grubin Theory of Elastohydrodynamic Lubrication*” J. Phys. D, Appl. Phys., Vol. 5, 1972
- [13] Francis A. Jenkins and Harvey E. White “*Fundamentals of optics*”, 1957
- [14] M Francon, JM Stone “*Optical interferometry*” American Journal of Physics, 1968
- [15] F. J. Westlake and A. Cameron, “*A Study of Ultra-Thin Lubricant Films Using an Optical Technique*”, Proc. Instn. Mech. Engrs. 1967–1968, Vol. 182, Pt. 3G
- [16] L. D. Wedeven and A. Cameron, “*A Study of Elastohydrodynamic Lubrication in Rolling Bearings Using Optical Interference*”, Proc. Instn. Mech. Engrs. 1967–1968, Vol. 182, Pt. 3G
- [17] F. J. Westlake and A. Cameron, “*Fluid Film Interferometry in Lubrication Studies*”, Applied science, Nature, Vol. 214, May 6, 1967
- [18] A. Cameron and R. Gohar, “*Theoretical and Experimental Studies of the Oil Film in Lubricated Point Contact*” Proc. Royal Soc. London, A291, pp.520–536
- [19] R. Gohar and A. Cameron, “*The Mapping of Elastohydrodynamic Contacts*”, ASLE Transactions 10, 215–225, 1967
- [20] C. A. Foord, W. C. Hammann and A. Cameron, “*Evaluation of Lubricants Using Optical Elastohydrodynamics*”, ASLE Transactions 11, 31–43, 1968

- [21] M. Kaneta, P. Yang, “*Formation Mechanism of Steady Multi-Dimples in Thermal EHL Point Contacts*”, Journal of Tribology, April 2003, Vol. 125, 241–251
- [22] L. D. Wedeven and A. Cameron, “*Fluid Film Interferometry in Lubrication Studies*” Proc. Instn. Mech. Engrs. 1967–1968, Vol. 182, Pt. 3G
- [23] C. G. Johnston, R. Wayte and H. A. Spikes, “*The Measurement and Study of Very Thin Lubricant Films in Concentrated Contacts*” Tribology Transactions, Volume 34 1991, 2, 187–194
- [24] J. Molimard, M. Querry, P. Vergne, I. Křupka, M. Hartl, “*Calculation of Pressure Distribution in EHD Point Contacts from Experimentally Determinated Film Thickness*”, Tribology International, Vol. 38, 2005, 391–401
- [25] R. P. Glovnea, A. K. Forrest, A. V. Olver and A. H. Spikes, “*Measurement of Sub-Nanometer Lubricant Films Using Ultra-Thin Film Interferometry*”, Tribology Letters, Vol. 15, No. 3, October 2003
- [26] R. Wang and P. L. Wong, “*Optical Characteristics of Thin Film Coating and Measurement of its Thickness*”, Tribology International, Volume 30, No. 11, pp. 801–806, 1997
- [27] M. Hartl, I. Křupka, R. Poliščuk, and M. Liška, “*An Automatic System for Real-Time Evaluation of EHD Film Thickness and Shape Based on the Colorimetric Interferometry*”, Tribology Transactions, Vol. 42, 1992, 2, 303–309
- [28] I. Křupka, M. Hartl, M. Liška, “*Thin Lubricating Films Behaviour at Very High Contact Pressure*”, Tribology International, Vol. 39, 2006, 1726–1731
- [29] F. Guo and P. L. Wong, “*A Wide Range Measurement System for Thin Lubricating Film: From Nano to Micro Thickness*”, Tribology Letters, Vol. 17, No. 3, October 2004, 521–531
- [30] A. D. Chapkov, S. Bair, P. Cann, A. A. Lubrecht, “*Film Thickness in Point Contacts under Generalized Newtonian EHL Conditions: Numerical and Experimental Analysis*”, Tribology International, 2007
- [31] G. Guangteng, P. M. Cann, A. V. Olver, H. A. Spikes “*Lubricant Film Thickness in Rough Surface, Mixed Elastohydrodynamic Contact*” Journal of Tribology, 2000, Vol. 122 / 65
- [32] R. P. Glovnea, A. V. Olver and A. H. Spikes, “*Lubrication of Rough Surfaces by a Boundary Film-Forming Viscosity Modifier Additive*”, Journal of Tribology, January 2005, Vol. 127, 223–229
- [33] Choo, J.W., Olver, A.V., Spikes, H.A., 2007, “*The Influence of Transverse Roughness in Thin Film, Mixed Elastohydrodynamic Lubrication*”, Tribology International, 40, pp. 220–232
- [34] J. W. Choo, R. P. Glovnea, A. V. Olver, H. A. Spikes “*The Effects of Three-Dimensional Model Surface Roughness Features on Lubricant Film Thickness in EHL Contacts*” Journal of Tribology, ASME, 2003, Vol. 125
- [35] A. V. Olver L. K. Tiew, S. Medina, J. W. Choo “*Direct Observations of a Micropit in an Elastohydrodynamic Contact*“ Wear, Volume 256, Issues 1–2 , January 2004, Pages 168–175

- [36] M. Kaneta and H. Nishikawa “*Experimental Study on EHD Lubrication*” Proc. Inst. Mech. Engrs., Vol. 213, Part J, 1999
- [37] I. Křupka, M. Hartl, “*The Influence of Thin Boundary Film on Real Surface Roughness in Thin Film, Mixed EHD Contact*”, Tribology International, 2006
- [38] I. Krupka, M. Hartl, “*The Effect of Surface Texturing on the EHD Lubrication Films*” Tribology International, Vol. 40, 2007, 1100–1110
- [39] R. P. Glovnea, J. W. Choo, A. V. Olver, H. A. Spikes “*Compression of a Single Transverse Ridge in a Circular Elastohydrodynamic Contact*”, Journal of Tribology, 2003 by ASME, 2003, Vol. 125/275–282
- [40] H. Nishikawa, K. Ueda, M. Kaneta, J. Wang, P. Yang “*Effects of Longitudinal Roughness on Fluid Temperature in Point Elastohydrodynamic Lubrication Contacts*” Proc. IMechE, Part J:J, Engineering Tribology, Vol. 212, 2007, 793–799
- [41] M. Smeeth, H. A. Spikes, S. Gunsel “*The Formation of Viscous Surface Films by Polymer Solutions: Boundary or Elastohydrodynamic Lubrication*” Tribology Transactions, 1996, Vol. 39, 726–734
- [42] M. Smeeth, H. A. Spikes, S. Gunsel “*Boundary Film Formation by Viscosity Index Improvers*” Tribology Transactions, 1996, Vol. 39, 726–734
- [43] H.M. Martin, “*Lubrication of Gear Teeth*”, Engineering (London), 1916, Vol. 102, p. 119–121 and p.527
- [44] C. Siripongse, P.R. Rogers and A. Cameron, “*Discharge through Oil Films*”, Engineering, 1958, 186, p. 146–147
- [45] C. Siripongse and A. Cameron, “*Lubrication of the Four Ball Machine*”, Engineering, 1958, 186, p. 147–149
- [46] A.W. Crook, “*Simulated gear-tooth contacts: some experiments upon their lubrication and sub-surfaces deformation*“ Rev. Proc. Inst. Mech. Engrs. Vol.171, pag 187, 1957
- [47] A.W. Crook, “*Lubrication of Rollers*”, Phil. Trans. Roy. Soc. Lon. Series A, 1958, Vol. 250, 981, 387–409
- [48] A. Dyson, H. Naylor and A.R. Wilson, “*The Measurement of Oil Film Thickness in Elastohydrodynamic Contacts*”, Proc. Inst. Mech. Engrs., 1965, 180, p. 119–134
- [49] J.F. Archard and M.T. Kirk, “*Lubrication at Point Contacts*” Phil. Trans. Roy. Soc. Lon. Series A, 1960, Vol. 261, 1307, 532-550
- [50] I.O. MacConochie and A. Cameron, “*The Measurement of Oil Film Thickness in Gear Teeth.*” ASME Trans. 1960, J. Basic Eng., 82D, 29–34
- [51] M. Ibrahim and A. Cameron, “*Oil Film Thickness and Mechanisms of Scuffing in Gear Teeth*”, Inst. Mech. Engrs Lubrication and Wear Convention, 1963, p. 228–238
- [52] P. S. Y. Chu and A. Cameron “*Flow of Electric Current through Lubricated Contacts*” ASTLE Transactions 10, 226 – 234, 1967

- [53] J.P. Vichard, “*Transient Effects in the Lubrication of Hertzian Contacts*” *J. Mech. Eng. Sci.*, 1971, Vol. 13, pp. 173–189
- [54] H. van Leeuwen, H. Meijer, H., M. Schouten, “*Elastohydrodynamic Film Thickness And Temperature Measurements In Dynamically Loaded Concentrated Contacts: Eccentric Cam–Flat Follower*”, Fluid film lubrication–Osborne Reynolds Centenary, ed. Dowson, Taylor, Godet, Berthe, Elsevier, 1987
- [55] S. Furakama, and T. Sumi, “*A Dynamic Theory of Piston–Ring Lubrication*”, *Bull. of JSME*, 1961, Vol. 4, 16, 744–752
- [56] G.M. Hamilton and S.L. Moore, “*Measurement of the Oil Film Thickness between the Piston Rings and Liner of a Small Diesel Engine*”, *Proc. Inst. Mech. Engrs.*, 1974, Vol. 188, p 253–261
- [57] G.M. Hamilton and S.L. Moore, “*Comparison between Measured and Calculated Thickness of the Oil–Film Lubricating Piston Rings*”, *Proc. Inst. Mech. Engrs.*, 1974, Vol. 188, p 262–268
- [58] I. Sherrington, N. Grice, and J. C. Jackson, “*A Capacitance Based Transducer to Detect Oil Leakage from the Turbine End of a Turbocharger*”, SAE Technical Papers Series 930191, International Congress and Exposition, Detroit, Michigan, March 1–5, 1993
- [59] I. Sherrington, E. H. Smith, “*Experimental Methods For Measuring The Oil Film Thickness Between The Piston Rings And Cylinder Wall Of Internal Combustion Engines*” *Tribology International* Vol. 18, No. 6, December 1985, p315–320
- [60] N. Grice, I. Sherrington, E. H. Smith, S. G. O’Donnell, J. F. Stringfellow, “*A Capacitance Based System For High Resolution Measurement of Lubricant Film Thickness*” Proc. of “Nordtrib ‘90”. 4th Nordic Symposium on Tribology, Lubrication, Friction and Wear (10–3 June 1990)
- [61] I. Sherrington, “*A Review of the Development of Oil Film Thickness Measurement Technology and Its Significance to the Understanding and Control of Lubrication in the Piston–Ring Packs of Internal Combustion Engines*” Proc. of “Nordtrib 2010”. Nordic Symposium on Tribology, Lubrication, Friction and Wear (8–11 June 2010)
- [62] D. O. Ducu, R. J. Donahue, J. B. Ghandhi “*Design of Capacitance Probes for Oil Film Thickness Measurements between the Piston Ring and Liner in Internal Combustion Engine*” *Journal of Engineering for Gas Turbines and Power*, Vol. 123, 633, 2001
- [63] B. Ya. Karastelev, V. V. Permyakov, A. M. Podushnyi, V. F. Yukhimenko, Yu. V. Yakubovskii “*Comparison of Methods of Measuring the Thickness of a Liquid Film*” Vladivostok, Translated from *Zhurnal Prikladnoi Mekhaniki i Tekhnicheskoi Fiziki*, No. 4, pp. 161–164, 1974
- [64] R. J. Severens, H. J. M. Verhoeven, M. Schaepkens, M. C. M. van de Sanden, D. C. Schram “*Electrodeless Thin Film Conductance Measurements Using the Sommer–Tanner Method*” *Rev. Sci. Instrum.* 67 (10), 1996

- [65] W. Zheng, Z. Zhang, S. Sun “*The New Development of Measuring EHL Oil Film Thickness for Thrust Bearing*” 2000
- [66] K. Nakano and Y. Akiyama “*Simultaneous Measurement of Film Thickness and Coverage of Loaded Boundary Films with Complex Impedance Analysis*” Tribology Letters, Vol. 22, No. 1, 2006
- [67] A. R. Wilson, “*The Relative Thickness of Grease and Oil Films in Rolling Bearings*” Proc. Instn. Mech. Engrs. Vol. 193, IMechE 1979
- [68] P. Iulius, I. Dusulita “*The Experimental Determination of the Oil Layer Thickness Variation from the Antifriction Bearings*” Ananlele Universitatii “Eftimie Murgu” Resita No. 1, 2008, ISSN 1453–7394
- [69] M.J. Furey, “*Surface Roughness Effect on Metallic Contact and Friction*”, ASLE Trans., 4, 1–11, 1961
- [70] P.S.Y. Chu and A. Cameron, “*Flow of Electrical Current through Lubricated Contacts*”, ASLE Trans., 10, p. 226–234, 1967
- [71] T.E. Tallian, Y.P. Chiu, D.F. Huttenlocher, J.A. Kamenshine, L.B. Sibley and N.E. Sindlinger, “*Lubricant Films in Rolling Contact of Rough Surfaces*”, ASLE Trans., 7, 109–126, 1964
- [72] J.M. Palacios, “*Elastohydrodynamic Films in Mixed Lubrication: An Experimental Investigation*”, Wear, 89, p.203–213, 1983
- [73] W.E. ten Napel, and R. Bosma, “*The Influence of Surface Roughness on the Capacitive Measurement of Film Thickness in Elastohydrodynamic Contacts*”, Proc. Inst. Mech. Engrs., vol. 185, 37, p. 635–939, 1971
- [74] G. Guanteng, A.V. Olver and H.A. Spikes, “*Contact Resistance Measurement in Mixed Lubrication*”, The advancing frontier of engineering tribology, STLE/ASME, ed.: Q. Wang, J. Nethzel and F. Sadeghi, p.64–71, 1999
- [75] J. Lord and R. Larsson, “*Film Forming Capability in Rough Surface EHL Investigated Using Contact Resistance*”, Trib. Intn., 41, p.831–838, 2008
- [76] F.E. Simpson and W.I.J. Crump, “*Effects of Electric Currents on the Life of Rolling Contact Bearings*”, Proc. Lubr. Wear. Conv., Inst. Mech. Engrs., p. 296–304, 1963
- [77] A. W. Morgan and D. Wyllie, “*A Survey of Rolling Bearing Failures*”, Proc. Inst. Mech. Engrs., 184, p. 48–56, 1969
- [78] G. Kure and Palmethofer, “*Electrically–Insulated Bearings*”, SKF Evolution online, 3, 96, 1996
- [79] H. Prashad, “*Diagnosis of Rolling-Element Bearings Failure by Localized Electrical Current between Track Surfaces of Races and Rolling–Elements*”, J. Trib., 124, p. 468–473, 2002
- [80] Y. Yamamoto, B. Ono. and A. Ura, “*Effect of Applied Voltage in Friction and Wear Characteristics in Mixed Lubrication*”, Lubrication Science, 8–2, p. 199–207, 1996

- [81] J. B. Luo, M. W. Shen, and S. Z. Wen J. “*Tribological Properties of Nanoliquid Film Under an External Electric Field*” Appl. Phys. 96, 6733, 2004
- [82] G X Xie , J B Luo , S H Liu , D Guo , G Li and C H Zhang “*Effect of Liquid Properties on the Growth and Motion Characteristics of Micro–Bubbles Induced by Electric Fields in Confined Liquid Films*” Journal of Physics, Applied Physics, 2009, Vol 23, No. 11
- [83] A. A. Carey “*The Dielectric Constant of Lubrication Oils*” Computational Systems Inc. Knoxville, TN 37932, 1998
- [84] C. Rococea, C. Rococea, I. Nacu “*Angular Contact Ball Bearings Passed by Electric Current*” 6th International Multidisciplinary Conference, Technical University of “Gh. Asachi” Iasi, Romania;
- [85] R. S. Dwyer–Joyce, B.W. Drinkwather, C. J. Donohoe, “*The Measurement of Lubricant–Film Thickness Using Ultrasound*” Proc. R. Soc. Lond. A (2003) 459, 957–976
- [86] J. Zhang; B. W. Drinkwather; R. S. Dwyer–Joyce “*Monitoring of Lubricant Film Failure in a Ball Bearing Using Ultrasound*” ASME 612 / Vol. 128, July 206
- [87] J. Zhang; B. W. Drinkwather; R. S. Dwyer–Joyce “*Calibration of the Ultrasonic Lubricant–Film Thickness Measurement Technique*” Meas. Sci. Technol. 16, 2005, 1784–1791
- [88] T. Reddyhoff, R. Dwyer–Joyce and P. Harper “*Ultrasonic Measurement of Film Thickness in Mechanical Seals*” Sealing Technology July 2006
- [89] F. E. Hoge “*Laser Measurement of the Spectral Extinction Coefficients of Fluorescent, Highly Absorbing Liquids*”, Applied Optics, 1982, Vol. 21, No. 10
- [90] A. C. Jones; M. Millington; J. Muhl; J. M. De Feritas; J.S. Barton; G. Gregory “*Calibration of an Optical Fluorescence Method for Film Thickness Measurement*” Meas. Sci. technol. 12 (2001) N23–N27
- [91] G.M. Ostroski; J.B. Ghandhi “*Laser–Induced Fluorescence Measurements of the Oil Film Thickness in an Internal Combustion Engine*” Society of Photo–Optical Instrumentation Engineers Vol. 3172
- [92] M. D. Furtuna, R. P. Glovnea “*An Experimental Investigation into the Effect of Lubricant on the Local Film Thickness of Artificial Roughness Features*” Proceedings of the STLE/ASME IJTC 2008, Miami, Florida
- [93] A.R., LaFountain, 1999, “*The Behaviour of Lubricant Blends in Elastohydrodynamic Contacts*” PhD thesis, University of London
- [94] J. Sugimura, M. Hashimoto and Y. Yamamoto “*Study of Elastohydrodynamic Contacts with Fluorescence Microscope*” Leeds–Lyon Symposium on Tribology 14–17 Sept, 1999
- [95] J. Sugimura and M. Akiyama “*Study of Non–Steady State Grease Lubrication with Fluorescence Microscope*” Leeds–Lyon Symposium on Tribology 5–8 Sept, 2000
- [96] Y. Nagata, M. Furtuna, C. Bell and R. Glovnea “*Evaluation of Electric Permittivity of Lubricating Oils in EHD Conditions*” 2nd International conference on Advanced Tribology, 3–5 Dec 2008, Singapore

- [97] J.K. Vij, W.G. Scaife, J.H. Calderwood, “*The Pressure and Temperature Dependence of the Complex Permittivity of Haptanol Isomers*”, J. Phys. D: Appl. Phys., Vol. 11, 545, 1978
- [98] A. Gilchrist, J.E. Earley, R.H. Cole, “*Effect of Pressure on Dielectric Properties and Volume of 1-Propanol and Glycerol*”, J. Chem. Phys., Vol. 26, 1, 1957
- [99] S. Hudlet, M. Saint-Jean, C. Guthmann, J. Berger, “*Evaluation of the Capacitive Force between an Atomic Force Microscopy Tip and a Metallic Surface*”, Eur. Phys. J. B. 2, 5–10, 1998
- [100] <http://www.solartronanalytical.com/Pages/1260AFRAPage.htm>
- [101] E. Ciulli, K. Stadler, T. Draexl, “*The Influence of the Slide-to-Roll Ratio on the Friction Coefficient and Film Thickness of EHD Point Contacts under Steady State and Transient Conditions*” Tribology International, Vol. 42, 526–536, 2009